ROBOT-ASSISTED EAR SURGERY

EDITED BY: Paul Van De Heyning, Olivier Sterkers, Vincent Van Rompaey and Vedat Topsakal
PUBLISHED IN: Frontiers in Surgery and Frontiers in Neurology

frontiers Research Topics

ISSN 1664-8714
ISBN 978-2-88976-317-7
DOI 10.3389/978-2-88976-317-7

About Frontiers

Frontiers is more than just an open-access publisher of scholarly articles: it is a pioneering approach to the world of academia, radically improving the way scholarly research is managed. The grand vision of Frontiers is a world where all people have an equal opportunity to seek, share and generate knowledge. Frontiers provides immediate and permanent online open access to all its publications, but this alone is not enough to realize our grand goals.

Frontiers Journal Series

The Frontiers Journal Series is a multi-tier and interdisciplinary set of open-access, online journals, promising a paradigm shift from the current review, selection and dissemination processes in academic publishing. All Frontiers journals are driven by researchers for researchers; therefore, they constitute a service to the scholarly community. At the same time, the Frontiers Journal Series operates on a revolutionary invention, the tiered publishing system, initially addressing specific communities of scholars, and gradually climbing up to broader public understanding, thus serving the interests of the lay society, too.

Dedication to Quality

Each Frontiers article is a landmark of the highest quality, thanks to genuinely collaborative interactions between authors and review editors, who include some of the world's best academicians. Research must be certified by peers before entering a stream of knowledge that may eventually reach the public - and shape society; therefore, Frontiers only applies the most rigorous and unbiased reviews.
Frontiers revolutionizes research publishing by freely delivering the most outstanding research, evaluated with no bias from both the academic and social point of view. By applying the most advanced information technologies, Frontiers is catapulting scholarly publishing into a new generation.

What are Frontiers Research Topics?

Frontiers Research Topics are very popular trademarks of the Frontiers Journals Series: they are collections of at least ten articles, all centered on a particular subject. With their unique mix of varied contributions from Original Research to Review Articles, Frontiers Research Topics unify the most influential researchers, the latest key findings and historical advances in a hot research area! Find out more on how to host your own Frontiers Research Topic or contribute to one as an author by contacting the Frontiers Editorial Office: frontiersin.org/about/contact

ROBOT-ASSISTED EAR SURGERY

Topic Editors:
Paul Van De Heyning, University of Antwerp, Belgium
Olivier Sterkers, Sorbonne Universités, France
Vincent Van Rompaey, University of Antwerp, Belgium
Vedat Topsakal, Vrije University Brussel, Belgium

Citation: Van De Heyning, P., Sterkers, O., Van Rompaey, V., Topsakal, V., eds. (2022). Robot-Assisted Ear Surgery. Lausanne: Frontiers Media SA.
doi: 10.3389/978-2-88976-317-7

Table of Contents

frontiers in Surgery

ORIGINAL RESEARCH
published: 14 May 2021
doi: 10.3389/fsurg.2021.659688

Thermal Safety of Endoscopic Usage in Robot-Assisted Middle Ear Surgery: An Experimental Study

Jinxi Pan[1,2,3†], *Haoyue Tan*[1,2,3†], *Jun Shi*[1,2,3†], *Zhaoyan Wang*[1,2,3], *Olivier Sterkers*[1,4], *Huan Jia*[1,2,3*] and *Hao Wu*[1,2,3*]

[1] Department of Otolaryngology-Head and Neck Surgery, Shanghai Ninth People's Hospital, Shanghai Jiao Tong University School of Medicine, Shanghai, China, [2] Ear Institute, Shanghai Jiao Tong University School of Medicine, Shanghai, China, [3] Shanghai Key Laboratory of Translational Medicine on Ear and Nose Diseases, Shanghai, China, [4] APHP, Groupe Hospitalo-Universitaire Pitié Salpêtrière, Otorhinolaryngology Department, Unit of Otology, Auditory Implants and Skull Base Surgery, Paris, France

OPEN ACCESS

Edited by:
Akira Ishiyama,
University of California, Los Angeles,
United States

Reviewed by:
Holger Sudhoff,
Bielefeld University, Germany
Hans Thomeer,
University Medical Center
Utrecht, Netherlands

***Correspondence:**
Hao Wu
wuhao@shsmu.edu.cn
Huan Jia
huan.jia.orl@shsmu.edu.cn

[†]These authors have contributed equally to this work and share first authorship

Specialty section:
This article was submitted to Otorhinolaryngology - Head and Neck Surgery,
a section of the journal Frontiers in Surgery

Received: 28 January 2021
Accepted: 16 April 2021
Published: 14 May 2021

Citation:
Pan J, Tan H, Shi J, Wang Z, Sterkers O, Jia H and Wu H (2021) Thermal Safety of Endoscopic Usage in Robot-Assisted Middle Ear Surgery: An Experimental Study. Front. Surg. 8:659688. doi: 10.3389/fsurg.2021.659688

Objectives: The widespread application of endoscopic ear surgery (EES), performed through the external auditory canal, has revealed the limitations of the one-handed technique. The RobOtol® (Collin ORL, Bagneux, France) otological robotic system has been introduced to enable two-handed procedures; however, the thermal properties of dedicated endoscopes, which are usually used in neurosurgery, called "neuro-endoscopes," have not yet been clarified for the robotic systems. In this study, we aimed to profile the thermal characteristics of two dedicated neuro-endoscopes, as compared to endoscopes used routinely in manual EES, called "oto-endoscopes," and defined by a smaller diameter and shorter length, and to discuss the safe application of robotic assistance in EES.

Methods: Two neuro-endoscopes (3.3 mm, 25 cm, 0°/30°) were studied using two routine light sources (LED/xenon), and two routine oto-endoscopes (3 mm, 14 cm, 0°/30°) were initially measured to provide a comprehensive comparison. Light intensities and temperatures were measured at different power settings. The thermal distributions were measured in an open environment and a human temporal bone model of EES. The cooling measures were also studied.

Results: Light intensity was correlated with stabilized tip temperatures ($P < 0.01$, $R^2 = 0.8719$). Under 100% xenon power, the stabilized temperatures at the tips of 0°, 30° neuro-endoscopes, and 0°, 30° oto-endoscopes were 96.1, 60.1, 67.8, and 56.4°C, respectively. With 100% LED power, the temperatures decreased by about 10°C, respectively. For the 0° neuro-endoscope, the illuminated area far away 1cm from the tip was below 37°C when using more than 50% both power, while this distance for 30° neuro-endoscope was 0.5 cm. In the EES temporal bone model, the round window area could reach 59.3°C with the 0° neuro-endoscope under 100% xenon power. Suction resulted in a ∼1–2°C temperature drop, while a 10 mL saline rinse gave a baseline temperature which lasted for 2.5 min.

Conclusion: Neuro-endoscope causes higher thermal releasing in the surgical cavity of ESS, which should be especially cautious in the robotic system usage. Applying submaximal light intensity, a LED source and intermittent rinsing should be considered for the safer robot-assisted EES using a neuro-endoscope that allows a two-handed surgical procedure.

Keywords: endoscopic ear surgery, robot-assisted, thermal damage, endoscope, robotic

INTRODUCTION

Endoscopic ear surgery (EES) has become a popular technique in recent years as a result of its better exposure and closer view of micro-anatomic structures in the middle ear (1, 2). However, the broad clinical applicability of EES has revealed some limitations, and one of the most frequently mentioned is the one-handed technique, which makes complex operations more challenging especially when hemorrhage occurs (1, 3, 4). Therefore, endoscope holders for endoscopic surgery (5–8) and robotic arms such as RobOtol® (Collin ORL, Bagneux, France) (9) have been introduced to enable two-handed procedures. To adapt these devices, longer endoscopes (10, 11) had to be applied in order to avoid the interference between surgeon's hands and robotic arm/ endoscopic holder. For RobOtol®, the specific endoscopes were routinely used in neurosurgical procedures (neuro-endoscopes). The usage of endoscopic holder or robotic system also changes the surgical mode for endoscope, that the endoscope stays longer and more statically in EAC. These factors might potentially bring out thermal damage to local tissue.

Several studies have reported thermal injuries caused by endoscopic application in the nasal (12–14) and abdominal cavities (15, 16). Others have investigated the thermal risk associated with the use of oto-endoscopes (17–23), such as deterioration of inner ear function (18) and facial palsy (23). Up to now, the thermal effects of neuro-endoscopes have not been investigated or published, and the RobOtol® system works with these endoscopes. Taking into consideration the thermal effects of the light source, endoscope size, power settings, and cooling mechanisms (17–22), the safety of neuro-endoscopes in EES should be thoroughly and precisely investigated, particularly those devices adapted for robotic assistance, which is considered to represent the future tendency for EES.

This study aimed to investigate the thermal effects of neuro-endoscopes, in an open environment and with EES in a human temporal bone model, as compared to usual endoscopes for manual EES, named oto-endoscopes. The effects of cooling by clinical suction and rinsing were also investigated. The aim was to provide safety information and optimum configuration for robot-assisted EES techniques.

MATERIALS AND METHODS

Endoscope Systems

Four regular Karl Storz endoscopes were investigated: the Hopkins 28007AA (3.3 mm diameter, 0° tip, 25 cm length) and Hopkins 28007BA (3.3 mm, 30°, 25 cm), which are conventionally used in neurosurgery (named neuro-endoscopes either Neuro-0 and Neuro-30 in this study), and are now used with a robotic system dedicated for ear surgery (RobOtol®, Collin ORL, Bagneux, France), and the Hopkins 7220AA (3 mm, 0°, 14 cm) and Hopkins 7220BA (3 mm, 30°, 14 cm), which are conventionally used in otology (named oto-endoscopes either Oto-0 and Oto-30 in this study). Two endoscope systems were used: a 300 W xenon light source (Model 20133120, Karl Storz Endoskope, Tuttlingen, Germany) and a 175 W LED light source (Model 20161420, Karl Storz Endoskope), connected to the endoscope being tested using the same standard fiber optic cable (Model 495NA, Karl Storz Endoskope).

Light Intensity and Temperature Measurements

The light intensity was measured with a lux meter (TES 1332A, TES Electrical Electronic Corp, Taiwan, PRC) with an accuracy of ±4% rdg ± 10 dgts (>10,000 lux). The temperature was measured with a JK808 eight-channel temperature tester and accessory JK80x data acquisition software (Changzhou Jin'ailian Electronic Technology Co., Ltd., Changzhou, PRC), with a measurement accuracy of 0.2% ± 1°C.

Light Intensity and Thermal Distribution in an Open Environment

The tip of the endoscope was firmly placed in close contact with the light detector of the lux meter. Light intensity was recorded when the source output was stable. The initial power was set at 5% and then tested to 100% in 5% increments. Both light sources were studied with each of the four endoscopes.

Seven thermocouple sensors were used to measure the axial thermal distributions for each of the endoscopes. Three sensors were placed 0.5, 1, and 2 cm in front of the tip of the endoscope along the light axis, and the remaining four were placed at the tip of the endoscope, 1 cm to the rear of the tip, 1/4 shaft length rear of the tip, and 1/2 shaft length rear of the tip (**Figure 1A**). The sensors' data collection cycle was adjusted to 1 s. After the baseline (ambient) temperature had been recorded for 30 s, the light source for the endoscope was turned on for 600 s, then the subsequent 180 s was recorded as a cooling period after the light source had been turned off. According to the light intensity results and clinical requirements, the power was set at 20, 45, 46, 47, 48, 49, 50, 51, 52, 53, 54, 55, and 100% for the xenon light source, and at 5, 10, 15, 20, 25, 50, and 100% for the LED light source.

Seven thermocouple sensors were used to record the thermal distribution in the illuminated area. They were placed at the tip,

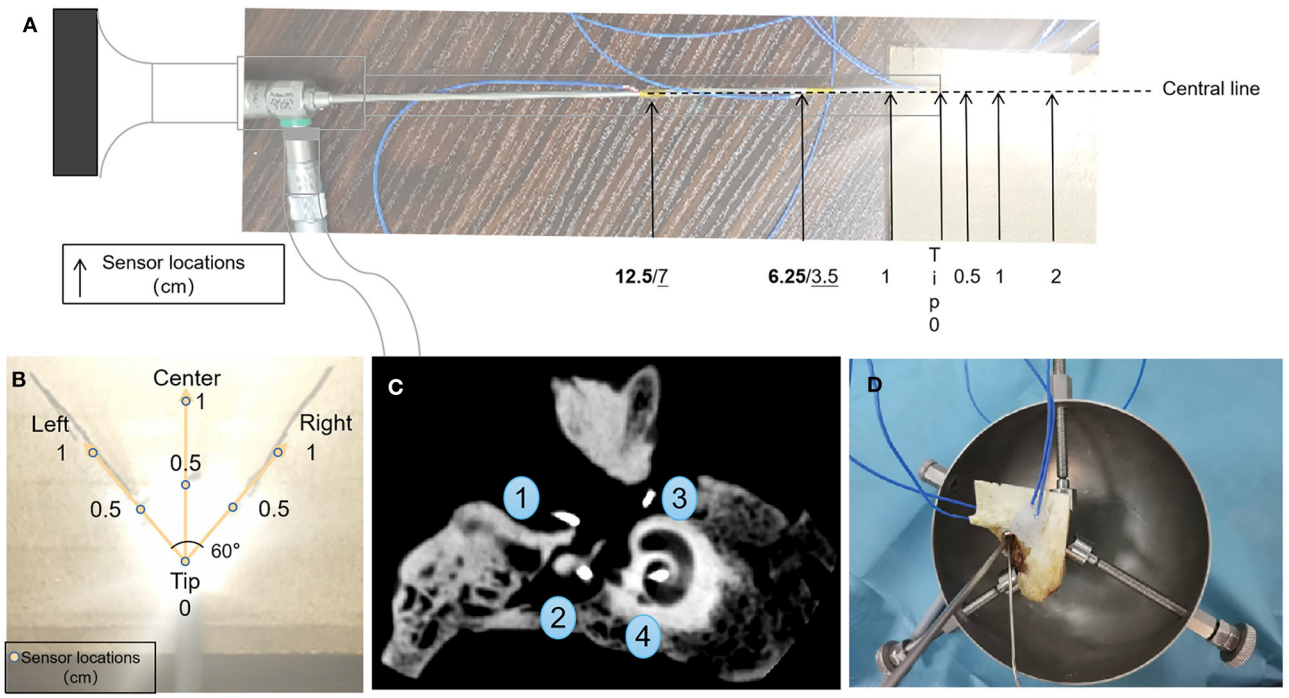

FIGURE 1 | Configurations for sensors in the open environment **(A,B)** and temporal bone **(C)**, and transcanal endoscopic ear surgery settings **(D)**. **(A)** Temperature sensors placement relating to the tip of the endoscope. Boldface indicates the 1/2 shaft length and 1/4 shaft length distances (cm) of the sensors to the rear of the tip of the neuroscope, and underline indicates their placement to the rear of the tip of the oto-endoscope. **(B)** Temperature sensors placement according to the illuminated area. **(C)** Representative cone-beam computed tomography images of sensor positions in temporal bone 4R. ① Fundus of the external auditory canal, ② aditus ad antrum, ③ round window/niche, and ④ modiolus/fundus of the inner auditory canal.

and 0.5 cm (left, center, right), and 1 cm (left, center, right) in front of the tip. Left and right sensors were placed at an angle of 60° centered on the tip as this is the edge of the illuminated area (**Figure 1B**). The power settings were 50% or 100% for both light sources.

Thermal Distribution With EES Using a Human Temporal Bone Model

Two left sides (1L; 2L) and two right sides (3R; 4R) of temporal bones (Henan Haizhirun Biotechnology Co., Ltd., Henan, PRC) were studied. Four sensors were firmly fixed at four anatomic landmarks: the fundus of the external auditory canal, the aditus ad antrum (after a canal wall-up mastoidectomy had been drilled), the round window/niche, and the modiolus/fundus of the inner auditory canal. The mastoidectomy cavity and the orifice of the internal auditory canal were sealed by bone wax (Knochenwachs; B. Braun Surgical, S.A., Barcelona, Spain) to prevent heat dissipation. Cone-beam computed tomography scans were performed to verify the correct location of these sensors (**Figure 1C**).

The Neuro-0 and Oto-0 endoscopes were used in this experiment, and were firmly placed at the level of the tympanic annulus (**Figure 1D**) via the external auditory canal (EAC), without contacting the skin. After the baseline (ambient) temperature had been recorded for 30 s, the LED or xenon light source was turned on at 100 or 50% power settings for 10 min, and subsequently, the local temperature was recorded for 3 min after turning off the light source.

The effect of cooling measures was studied by applying suction or rinsing, which are the general procedures used in routine EES, and using a xenon light source which produces more heat than the LED source. A #3 French (∼1 mm) suction tube (Chong Ning Medical Co., Ltd, Shanghai, PRC) with a negative pressure of 0.04–0.05 MPa, which is regularly used in middle ear surgery, was placed close to the endoscope tip. For the continuous suction cooling test, after an initial 60 s period, suction was turned on. For the discontinuous suction cooling test, after an initial 60 s period, two cooling periods of 30 and 60 s were performed separated by a 30 s interval. The effect of rinsing measures was studied by injecting ambient temperature saline (10 mL) into the middle ear cavity through the EAC and which was immediately sucked out.

Statistical Analysis

Light intensity (lux), power setting (%), time (s), and temperature (°C) were measured. The ambient temperature during the experiments was 25 ± 3°C. Values are presented as means and standard deviation or ratios. Statistical analyses were conducted with WPS Office (Kingsoft Office Corp., Beijing, PRC) and GraphPad Prism8 (GraphPad Prism Software, San Diego, CA, USA), with a significance level represented as $^*P < 0.01$.

This work did not contain animal/human studies. No IRB (institutional review board) approval was required.

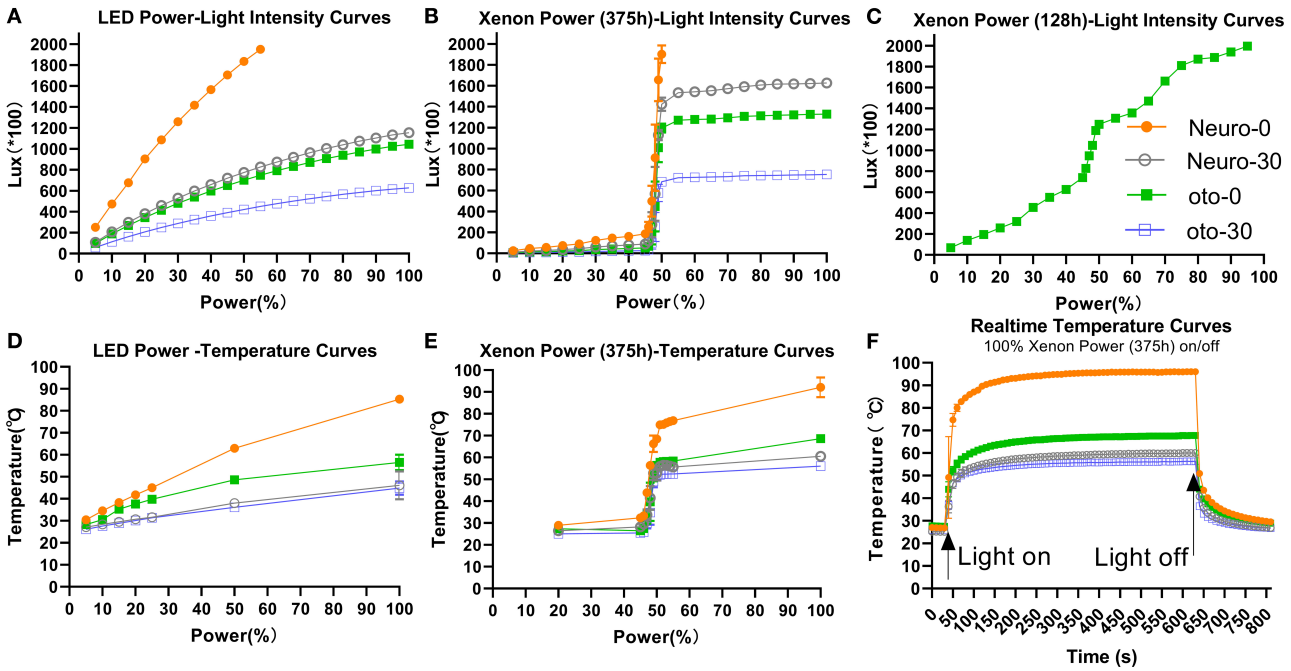

FIGURE 2 | Light intensity **(A–C)** and temperature **(D–F)** changes with various endoscopes using different LED or xenon light source power settings. **(A)** The fitting equations of the power-light intensity curves are as follows: Neuro-0: $y = -0.2533x^2 + 49.16x + 9.507$, $R^2 = 0.9999$; Neuro-30: $y = -0.07455x^2 + 18.61x + 31.53$, $R^2 = 0.9996$; Oto-0: $y = -0.06736x^2 + 16.83x + 28.61$, $R^2 = 0.9996$; Oto-30: $y = -0.04046x^2 + 10.11x + 17.65$, $R^2 = 0.9996$. **(D)** The fitting equations of the power-temperature curves are as follows: Neuro-0: $y = -0.002671x^2 + 0.8610x + 25.94$, $R^2 = 0.9980$; Neuro-30: $y = -0.0007388x^2 + 0.2805x + 25.52$, $R^2 = 0.8607$; Oto-0: $y = -0.003346x^2 + 0.6454x + 25.42$, $R^2 = 0.9732$; Oto-30: $y = -0.0005655x^2 + 0.2537x + 25.13$, $R^2 = 0.9626$.

RESULTS

Light Intensity

Light intensity increased with power setting (**Figures 2A–C**) and differed among the four endoscopes. The larger diameter and 0° endoscope had the highest light intensity. The light intensities at 5% xenon power were 25 ± 1 (*100 lux), 11 ± 0 (*100 lux), 7 ± 1 (*100 lux), and 4 ± 0 (*100 lux) for Neuro-0, Neuro-30, Oto-0, and Oto-30, respectively. The light intensities at 100% xenon power were >2,000 (* 100 lux), 1,627 ± 3 (*100 lux), 1,330 ± 12 (*100 lux), and 753±6 (*100 lux) for corresponding endoscopes. With the LED light source (**Figure 2A**), the curves could be described using quadratic equations; however, with the xenon light source (with 375 h registered), the light intensity increased sharply between 45 and 50% power (**Figure 2B**). This phenomenon could also be observed with a newer xenon light source (with 128 h registered) (**Figure 2C**), but less sharply.

Temperature at Endoscope Tips

Temperatures at the endoscope tips increased with power (**Figures 2D,E**) and changed rapidly over time when switching on/off power (**Figure 2F**). Under 100% xenon power, the stabilized temperatures of Neuro-0, Neuro-30, Oto-0, and Oto-30 endoscopes were 96.1, 60.1, 67.8, and 56.4°C, respectively (**Figure 2E**). Under 50% xenon power, the stabilized tip temperatures of the corresponding endoscopes were 68.5, 52.8, 56.4, and 51.1°C, respectively. But there was a sharp increase in temperature from 45 to 50% xenon power, similar to the power–light intensity curves.

The LED light source showed a more stable output than the xenon light source with increasing power. Adopting 100% LED power, the stabilized temperatures of Neuro-0, Neuro-30, Oto-0, and Oto-30 endoscopes were 86.9, 51.9, 53.3, and 47.6°C, respectively (**Figure 2D**). Adopting 50% LED power, the stabilized temperatures of the corresponding endoscopes were 62.9, 38.1, 48.6, and 36.1°C, respectively.

Overall, the stabilized endoscope tip temperatures and light intensities were correlated among all combinations (temperature = 0.02282*light intensity + 27.01, $p < 0.01$, $R^2 = 0.8719$).

Thermal Distribution on the Endoscope Shaft and in an Open Environment

The temperature was highest at the tip of the endoscope and gradually decreased with distance in front of or behind the tip (**Tables 1**, **2**). At 100% xenon or LED power, the temperatures of all endoscope shafts were below 37°C, as was the temperature 0.5 cm in front of the tip of the Oto-0 and Oto-30 endoscopes. But for Neuro-0, at 50% xenon or LED power, the maximum temperature at 0.5 cm in front of the tip might still be higher than 37°C (45.4 and 38.5°C, respectively).

TABLE 1 | Thermal spread with distance in front of or behind the tip and with the xenon light source.

Distance to tip (cm)[a]		Neuro-0		Neuro-30
		100% power	50% power	100% power
0		92.1 ± 4.5	62.9 ± 6.7	60.5 ± 1.4
−1		31.9 ± 0.8	31.1 ± 0.1	30.2 ± 0.2
+0.5	Center	46.9 ± 1.5	45.4 ± 2.0	37.4 ± 0.4
	Left	38.9 ± 1.4	38.5 ± 1.3	34.9 ± 0.5
	Right	42.5 ± 0.2	39.5 ± 1.7	35.7 ± 0.2
+1	Center	31.5 ± 0.9	32.4 ± 0.5	30.3 ± 0.2
	Left	29.0 ± 0.3	29.7 ± 0.3	28.2 ± 0.1
	Right	30.6 ± 0.2	31.5 ± 0.4	30.1 ± 0.3

[a]*Negative values in cm indicate measurements made on the endoscope shaft; Positive values in cm indicate those made in front of the tip in an open environment (see* ***Figure 1****). Temperature (°C, means ± standard deviation).*

TABLE 2 | Thermal spread with distance in front of or behind the tip and with the LED light source.

Distance to tip (cm)[a]		Neuro-0		Neuro-30
		100% power	50% power	100% power
0		85.3 ± 1.8	52.3 ± 0.3	46.2 ± 6.4
−1		34.2 ± 0.3	32.3 ± 0.1	30.7 ± 0.2
+0.5	Center	48.6 ± 1.2	38.5 ± 0.2	32.8 ± 1.2
	Left	42.0 ± 0.9	37.8 ± 1.1	32.2 ± 0.2
	Right	46.5 ± 0.1	35.5 ± 0.8	32.7 ± 0.5
+1	Center	33.4 ± 3.0	30.7 ± 0.2	28.2 ± 0.3
	Left	32.3 ± 0.3	29.9 ± 0.4	26.7 ± 0.2
	Right	34.6 ± 0.3	30.7 ± 0.5	28.2 ± 0.4

[a]*Negative values in cm indicate measurements made on the endoscope shaft; Positive values in cm indicate those made in front of the tip in an open environment (see* ***Figure 1****). Temperature (°C, means ± standard deviation).*

Characteristics of Temperature Elevation in Temporal Bone

Temperature elevation in temporal bone was similar between xenon (**Figures 3A,C**) and LED (**Figures 3B,D**) light source power settings. In the temporal bone, with the Neuro-0 endoscope under 100% light source power (**Figures 3C,D**), the temperature increased slightly at the EAC fundus (xenon: 26.1–33.7°C; LED: 29.2–32.2°C), aditus ad antrum (xenon: 28.4–37.4°C; LED: 32.7–36°C), and modiolus/fundus of the inner auditory canal (xenon: 28–38.1°C; LED: 28.2–36.4°C), except at the round window (xenon: 54.1–59.3°C; LED: 52.4–57°C), a critical location between the middle and inner ears. For the Neuro-0 endoscope, the temperature at the round window was still elevated above 37°C using the two light sources at 50% power (**Figures 3A,B**).

When applying suction or rinsing, with the maximum temperature settings (100% power, xenon, Neuro-0) (**Figure 4A**), a slight temperature drop (∼1–2°C) occurred after suction was initiated when the light remained on, while continuous suction (**Figure 4B**) demonstrated a more robust cooling effect than discontinuous suction (**Figure 4C**). The 10 mL saline rinsing at ambient temperature caused a precipitous temperature drop within 10 s, resulting in a temperature close to the baseline, and it took at least 2.5 min for the temperature to rise to about 37°C (**Figure 4D**).

DISCUSSION

In the EES, two-handed surgery might be useful depending on the surgery. Although the one-handed technique could be feasible in middle ear ossicular chain reconstruction, the two-handed technique might result in better exposure and control of the bleeding while resection of a glomus tympanicum or bleeding lesions. The surgeons also have to make a balance among exposure, workspace, and surgery safety in EES, though smaller diameter (e.g., 3 mm) endoscopes lead to less heat, larger diameter (e.g., 4 mm) endoscopes might lead to better exposure. A good vision of anatomical structures is mandatory for otological surgery. Therefore, the choice of endoscope diameter is guided by the external auditory canal size allowing one to work with one tool in one-handed EES or two tools with a two-handed EES. Then, a compromise of 3.3 mm endoscope was selected, and its 25 cm in length (neuro-endoscope) happens to meet the design and need of RobOtol®, as reported recently (9). It is reasonable to presume that with the progress in camera and image processing technology, the endoscope in the future will be even thinner with a preserved excellent image quality.

In the present study, we focused on the thermal safety of neuro-endoscopes for robot-assisted EES, to address concerns about heat issues among doctors who have not yet used the RobOtol® or will use the RobOtol® to assist in complex surgery. In EES, Bottrill et al. (22) first reported a temperature rise in the lateral semicircular canal with oto-endoscope applying. They recorded a maximum temperature of 55°C 2 mm in front of the tip of the endoscope, which could result in burns and charring. MacKeith et al. (14) reported that the tip temperature rose to 67.4°C, indicating the importance of avoiding the tip directly touching tissue. Previous similar reports did not investigate the effects of a range of power settings, and temperature measurements were usually limited to the endoscope tip (3, 17–22). Routine oto-endoscopes were introduced in first part of this study to provide a comprehensive comparison.

As expected, neuro-endoscopes, which have a larger diameter, result in more heat and light being applied to the illuminated area than oto-endoscopes with a similar light source and power settings. These findings strongly suggest that attention should be paid to the power settings and heat diffusion of neuro-endoscopes used with robotic assistance. Although the full range of output settings are rarely applied in the clinic, even at <50% power setting, which might be applied in many centers (12, 17, 19), there would be thermal damage to the inner ear. Under 50% power setting, Das et al. reported (24) that merely converting the type of light source from LED to xenon will cause a higher temperature rise and significantly deteriorate the higher-frequency hearing. Therefore, based on our results, it can be reasonably inferred that an endoscope with a larger diameter

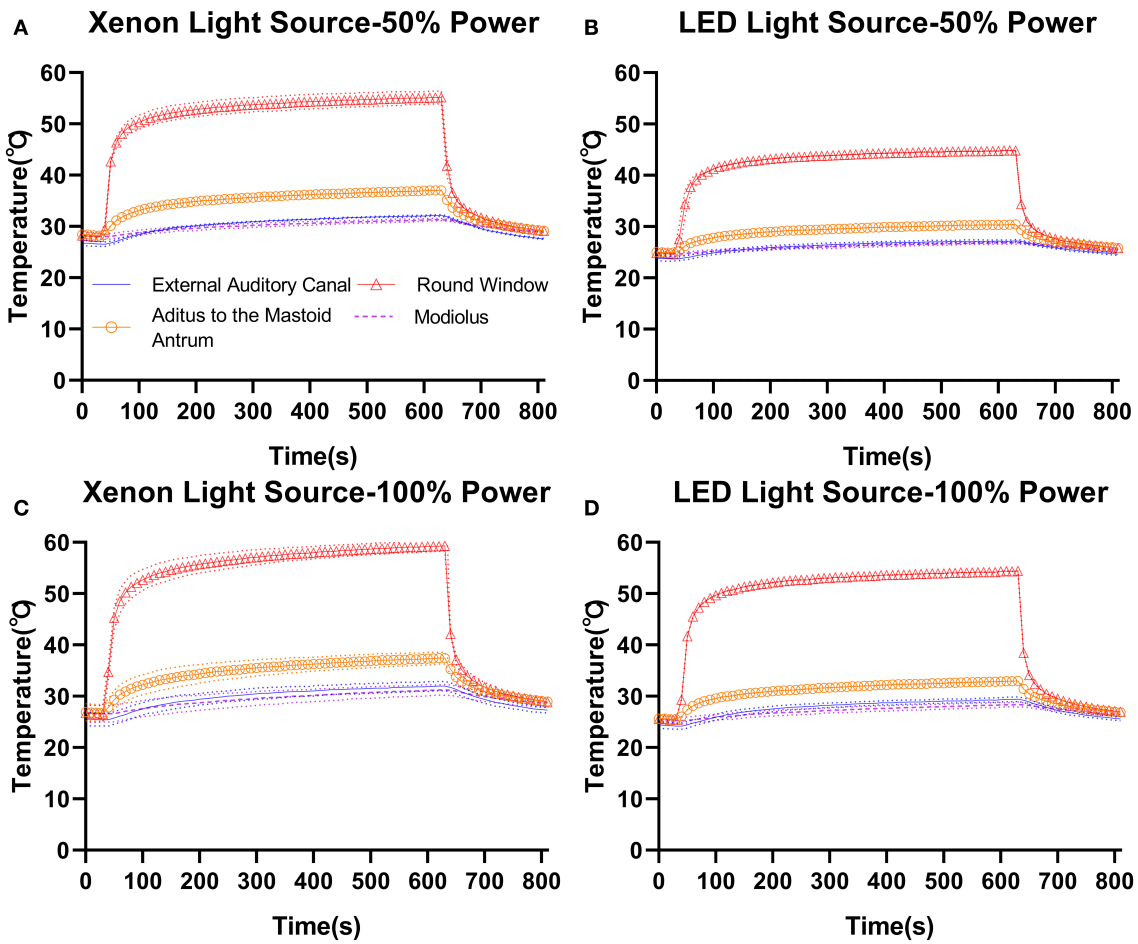

FIGURE 3 | Temperature elevation in temporal bone (4R) with the Neuro-0 endoscope under different xenon **(A,C)** and LED **(B,D)** light source power settings.

transmits more heat, which will inevitably increase the severity of damage to delicate structures such as the inner ear. We also further explored the safe working distance. The suggested safe working distance for these neuro-endoscopes was 1 cm in front of the tip. Only for Neuro-30, the distance could be 0.5 cm in front of the tip when using LED power. Future *in vivo* studies or clinical experience with robotic system might be helpful and valuable to confirm this distance. Through the application of navigation and robot system software optimization, safe distances that are difficult to maintain by manual operation can be easily achieved with robot assistance. Unexpectedly, a rapidly increasing output was observed with increasing power using a xenon light with 375 h usage times between 45 and 50% power, and a less sharply increasing output was observed when using a xenon light with 128 h usage times. This phenomenon could be attributed to the way that light intensity is adjusted using the shading plate. The LED source showed a more stable output with power and may be a better choice than a xenon source in clinical practice (12, 24).

For the same endoscope, the profiles of light intensity and endoscope tip temperature were similar over the entire light source power settings, and light intensity was correlated with endoscope tip peak temperature. This correlation makes it possible to predict the maximum endoscope tip temperature and evaluate the functional status of the light sources over the entire power range in a short time by measuring the light intensity, which could be used as a routine self-check process for robot-assisted EES. In addition, the power setting of a given temperature could be estimated, while future research should be performed to investigate which maximal temperature at the tip is safe, for EES. Furthermore, the correlation could be used to establish a temperature estimation model to predict the stabilized temperatures of other combinations of endoscopes, light sources, and fiber optic cables under certain conditions.

White balance adjustment is generally applied before surgical manipulation. This will decrease the brightness on the screen but not in the surgical cavity. As each surgeon has his own preference for power setting in EES, the surgeon or operation room nurse should reduce the power setting when using larger and longer endoscopes, not just when adjusting white balance.

Suction and rinsing, which are regularly used in clinical practice, could give varying degrees of cooling effects. Rinsing was found to be much more effective. In cadaveric human temporal bone (36°C chamber, xenon and LED, 100 or 50% power), Kozin observed the maximum temperature at the round

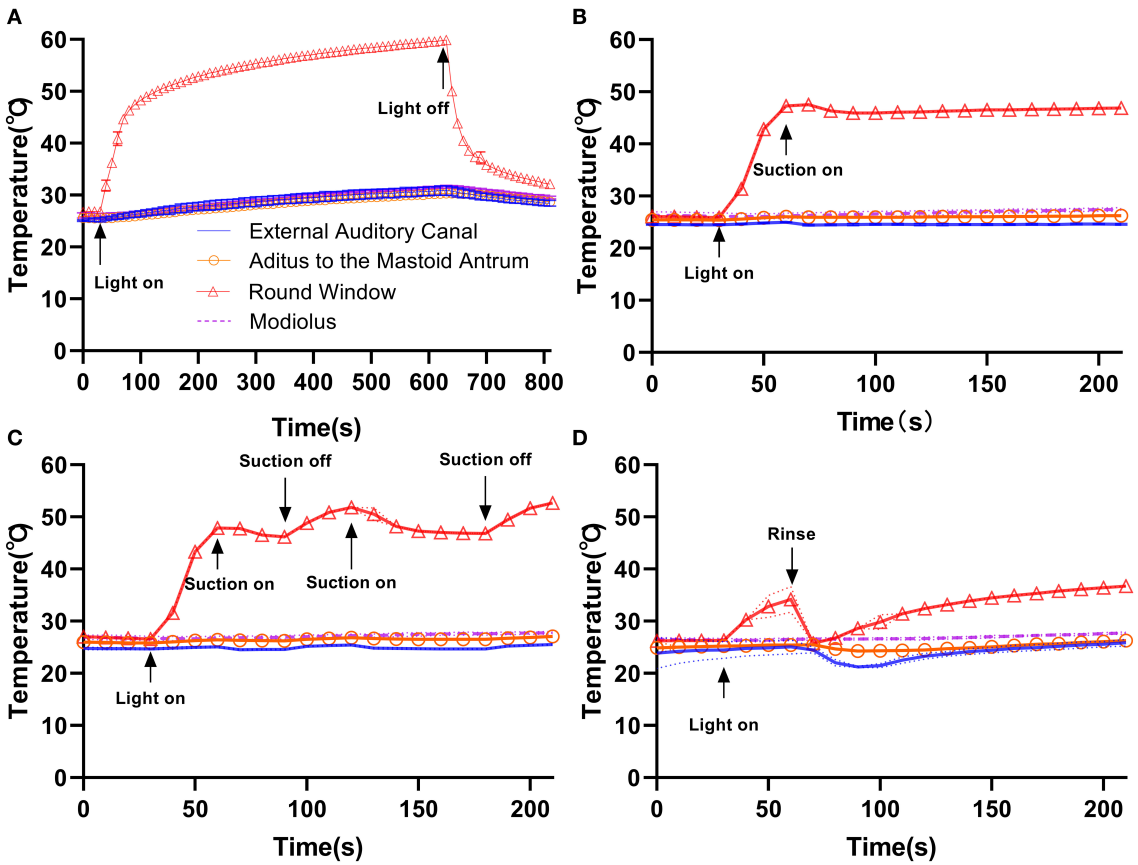

FIGURE 4 | Compared with the control group **(A)**, continuous suction **(B)**, discontinuous suction **(C)**, and rinsing **(D)** resulted in different cooling effects in temporal bone with the Neuro-0 endoscope under 100% xenon light source power. Rinsing resulted in a better cooling effect.

window membrane and rose by 8–10°C relative to the chamber temperature, and the cooling effect while applying a #20 French suction resulting in an 11°C temperature drop. However, #20 French suction (nearly ∼6.7 mm in diameter) was not applicable to routine EES, which led to the choice of a #3 French suction (1 mm in diameter) in the present study. Accordingly, cooling measures such as continuous suction or intermittent rinsing (10 mL ambient temperature saline every 2.5 min or so) should be integrated into the robotic system applied in clinical practice to ensure safety during EES.

The main weakness of our study was *in vitro*. Thermal features are different *in vivo* (22). The lower temperature gradient *in vivo* may reduce the cooling rate because, *in vivo*, the surrounding temperature would be 37°C, or perhaps slightly lower, due to anesthesia and operating room temperature, but obviously not as low as 25°C as in this study. An active circulation system would dissipate some of the heat. In addition, the higher humidity and reflective properties of the tissue would mitigate temperature fluctuations.

Another disadvantage that should be noted is that the two-handed EES is not always feasible in a limited external auditory canal whose smallest maximum diameter range from 6.5 to 15.0 mm and the smallest minimum diameter range from 3.4 to 6.4 mm (25). In our clinical experience, a pure transcanal approach with two tools and a robot-held endoscope is difficult in external auditory canals narrower than 6 mm. This is because the endoscope is 3.3 mm wide and we use common otological tools. There may be no additional benefit from insisting on using the RobOtol® technique throughout the procedure under current technology. The steps that are easier with two tools are the tympano-meatal flap dissection (blood suction and flap pulling and tension), the tympanic membrane dissection from the malleus handle, the partial or total prosthesis placement, and the graft (cartilage or fascia placement). All other steps can be done with one hand for sure. We recommend starting using the robot-held endoscope with a large auditory canal during the learning curve. With a smaller endoscope or dedicated tool (in diameter and bayonet shape), we may be able to work in smaller canals but these tools are ready yet.

Yet despite these limitations, we believe our findings of light intensity and temperature changes with power, time, and cooling measures may be useful in clinical practice. Furthermore, the results for thermal spread from the tip of the endoscope and thermal distribution in human temporal bones may help in make EES practice as safe as possible. We might not need to use more power to obtain high-quality images as images

taken during surgery by routine oto-endoscope at lower light intensities have no loss of quality (26), and future studies should investigate the light intensity applied during surgery and verify the functional consequences of the corresponding temperatures in an animal model.

The clinical application of robotics is a general trend, and related technologies will develop rapidly in the foreseeable future. Similarly, endoscopic imaging technology will continue to improve. The advancement of endoscopy technology may be able to fundamentally solve the problem of excessive temperature elevation caused by endoscope application by reducing the heat generation of the light source with the next-generation cold light source and improving imaging quality at low light intensity. Meanwhile, the advancement of micro-sensing technology could make the robot's perception more sensitive, and realize the real-time monitoring of the ambient temperature under the endoscope application, which provides further safety guarantee for the robot-assisted EES. Further, inspired by the single-port transoral robotic surgical system (27), subsequent development of robotic EES could further miniaturize relative devices to make the utmost of the middle ear space. Then, in single-port trancanal robotic EES, almost all the middle ear cavity is visible, and multiple-manipulator-operation could be achieved throughout the surgery. Before that, endoscope holder/robotic arm design should still take into account our findings of light intensity and temperature variations with light source power setting, and the temporal and spatial distribution of temperatures.

CONCLUSIONS

Under the same conditions of the light source and power setting, neuro-endoscopes produce more heat than oto-endoscopes. LED light sources are associated with less significant temperature rises and have a more stable output with increasing power than xenon light sources. The light intensity at the endoscope tip could predict local temperature for a given endoscope and light source. Suction results in a slight temperature drop, while local rinsing is more effective in cooling. Applying submaximal light intensity, a LED source and intermittent rinsing should be considered for safer robot-assisted EES using a neuro-endoscope which allows a two-handed surgical procedure.

DATA AVAILABILITY STATEMENT

The raw data supporting the conclusions of this article will be made available by the authors, without undue reservation.

AUTHOR'S NOTE

This study was independent of the clinical trial of RobOtol®. Partially results of preliminary study were previously presented as a poster presentation at the 17th National Scientific Congress of Chinese Society of Otolaryngology-Head and Neck Surgery on November 27–29, 2020, online.

AUTHOR CONTRIBUTIONS

JS, ZW, OS, HJ, and HW: conceptualization. JP and HT: methodology. JP, HT, OS, and HJ: formal analysis. HW and OS: resources. JP: writing/original draft preparation. JS, ZW, OS, and HJ: writing/review and editing. ZW and HJ: funding acquisition. All authors contributed to the article and approved the submitted version.

FUNDING

This work was supported by the Shanghai Scientific and Technological Innovation Action Plan (grant number: 19441900100), by the Science & Technology Innovation Fund of Shanghai Ninth People's Hospital, Shanghai Jiaotong University School of Medicine (grant number: CK2018004), and by Shanghai Key Laboratory of Translational Medicine on Ear and Nose Diseases (grant number: 14DZ2260300). The funders had no role in study design, data collection and analysis, decision to publish, or preparation of the manuscript.

REFERENCES

1. Kozin ED, Gulati S, Kaplan AB, Lehmann AE, Remenschneider AK, Landegger LD, et al. Systematic review of outcomes following observational and operative endoscopic middle ear surgery. *Laryngoscope.* (2015) 125:1205–14. doi: 10.1002/lary.25048
2. Kozin ED, Kiringoda R, Lee DJ. Incorporating endoscopic ear surgery into your clinical practice. *Otolaryngol Clin North Am.* (2016) 49:1237–51. doi: 10.1016/j.otc.2016.05.005
3. Mitchell S, Coulson C. Endoscopic ear surgery: a hot topic? *J Laryngol Otol.* (2017) 131:117–22. doi: 10.1017/S0022215116009828
4. Bae MR, Kang WS, Chung JW. Comparison of the clinical results of attic cholesteatoma treatment: endoscopic versus microscopic ear surgery. *Clin Exp Otorhinolaryngol.* (2019) 12:156–62. doi: 10.21053/ceo.2018.00507
5. Khan MM, Parab SR. Endoscopic cartilage tympanoplasty: a two-handed technique using an endoscope holder. *Laryngoscope.* (2016) 126:1893–8. doi: 10.1002/lary.25760
6. Khan MM, Parab SR. Concept, design and development of innovative endoscope holder system for endoscopic otolaryngological surgeries. *Indian J Otolaryngol Head Neck Surg.* (2015) 67:113–9. doi: 10.1007/s12070-014-0738-y
7. Ozturan O, Yenigun A, Aksoy F, Ertas B. Proposal of a budget-friendly camera holder for endoscopic ear surgery. *J Craniofac Surg.* (2018) 29:e47–9. doi: 10.1097/SCS.0000000000004022
8. Zhong F, Li P, Shi J, Wang Z, Wu J, Chan JY, et al. Foot-Controlled Robot-Enabled EnDOscope Manipulator (FREEDOM) for sinus surgery: design, control, and evaluation. *IEEE Trans Biomed Eng.* (2020) 67:1530–41. doi: 10.1109/TBME.2019.2939557
9. Vittoria S, Lahlou G, Torres R, Daoudi H, Mosnier I, Mazalaigue S, et al. Robot-based assistance in middle ear surgery and cochlear implantation: first clinical report. *Eur Arch Otorhinolaryngol.* (2020) 278:77–85. doi: 10.1007/s00405-020-06070-z
10. Ozturan O, Dogan R, Eren SB, Aksoy F. Intraoperative thermal safety of endoscopic ear surgery utilizing a holder. *Am J Otolaryngol.* (2018) 39:585–91. doi: 10.1016/j.amjoto.2018.07.001
11. Miroir M, Nguyen Y, Szewczyk J, Mazalaigue S, Ferrary E, Sterkers O, et al. RobOtol: from design to evaluation of a robot for middle ear surgery. In:

IEEE/RSJ International Conference on Intelligent Robots and Systems. Taipei (2010). p. 850–6.
12. Tomazic PV, Hammer GP, Gerstenberger C, Koele W, Stammberger H. Heat development at nasal endoscopes' tips: danger of tissue damage? A laboratory study. *Laryngoscope.* (2012) 122:1670–3. doi: 10.1002/lary.23339
13. Nelson JJ, Goyal P. Temperature variations of nasal endoscopes. *Laryngoscope.* (2011) 121:273–8. doi: 10.1002/lary.21367
14. MacKeith SA, Frampton S, Pothier DD. Thermal properties of operative endoscopes used in otorhinolaryngology. *J Laryngol Otol.* (2008) 122:711–4. doi: 10.1017/S0022215107000734
15. Hensman C, Hanna GB, Drew T, Moseley H, Cuschieri A. Total radiated power, infrared output, and heat generation by cold light sources at the distal end of endoscopes and fiber optic bundle of light cables. *Surg Endosc.* (1998) 12:335–7. doi: 10.1007/s004649900665
16. Yavuz Y, Skogås JG, Güllüoglu MG, Langø T, Mårvik R. Are cold light sources really cold? *Surg Laparosc Endosc Percutan Tech.* (2006) 16:370–6. doi: 10.1097/01.sle.0000213711.32805.15
17. Kozin ED, Lehmann A, Carter M, Hight E, Cohen M, Nakajima HH, et al. Thermal effects of endoscopy in a human temporal bone model: implications for endoscopic ear surgery. *Laryngoscope.* (2014) 124:E332–9. doi: 10.1002/lary.24666
18. Aksoy F, Dogan R, Ozturan O, Eren SB, Veyseller B, Gedik O. Thermal effects of cold light sources used in otologic surgery. *Eur Arch Otorhinolaryngol.* (2015) 272:2679–87. doi: 10.1007/s00405-014-3202-4
19. Ito T, Kubota T, Takagi A, Watanabe T, Futai K, Furukawa T, et al. Safety of heat generated by endoscope light sources in simulated transcanal endoscopic ear surgery. *Auris Nasus Larynx.* (2016) 43:501–6. doi: 10.1016/j.anl.2015.12.014
20. Dundar R, Bulut H, Güler OK, Yükkaldiran A, Demirtas Y, Iynen I, et al. Oval window temperature changes in an endoscopic stapedectomy. *J Craniofac Surg.* (2015) 26:1704–8. doi: 10.1097/SCS.0000000000001934
21. Dundar RI, Bulut H, Yükkaldiran A, Güler OK, Demirtaş Y, Iynen I, et al. Temperature rises in the round window caused by various light sources during insertion of rigid endoscopes: an experimental animal study. *Clin Otolaryngol.* (2016) 41:44–50. doi: 10.1111/coa.12468
22. Bottrill I, Perrault DF Jr, Poe D. In vitro and in vivo determination of the thermal effect of middle ear endoscopy. *Laryngoscope.* (1996) 106:213–6. doi: 10.1097/00005537-199602000-00020
23. Li KH, Chan LP, Chen CK, Kuo SH, Wang LF, Chang NC, et al. Comparative study of endoscopic and microscopic type I tympanoplasty in terms of delayed facial palsy. *Otolaryngol Head Neck Surg.* (2020) 164:645–51. doi: 10.1177/0194599820945634
24. Das A, Mitra S, Agarwal P, Sengupta A. Prolonged intra-operative thermal exposure in endoscopic ear surgery: is it really safe? *J Laryngol Otol.* (2020) 134:727–31. doi: 10.1017/S0022215120001449
25. Ito T, Kubota T, Furukawa T, Kakehata S. Measurement of the pediatric and adult osseous external auditory canal: implications for transcanal endoscopic ear surgery. *Otol Neurotol.* (2020) 41:e712–9. doi: 10.1097/MAO.0000000000002653
26. McCallum R, McColl J, Iyer A. The effect of light intensity on image quality in endoscopic ear surgery. *Clin Otolaryngol.* (2018) 43:1266–72. doi: 10.1111/coa.13139
27. Holsinger FC, Magnuson JS, Weinstein GS, Chan JY, Starmer HM, Tsang RK, et al. A next-generation single-port robotic surgical system for transoral robotic surgery: results from prospective nonrandomized clinical trials. *JAMA Otolaryngol Head Neck Surg.* (2019) 145:1027–34. doi: 10.1001/jamaoto.2019.2654

Conflict of Interest: The authors declare that the research was conducted in the absence of any commercial or financial relationships that could be construed as a potential conflict of interest.

frontiers in Surgery

ORIGINAL RESEARCH
published: 07 July 2021
doi: 10.3389/fsurg.2021.695728

Robot-Assisted Electrode Array Insertion Becomes Available in Pediatric Cochlear Implant Recipients: First Report and an Intra-Individual Study

Huan Jia[1,2,3†], *Jinxi Pan*[1,2,3†], *Wenxi Gu*[1,2,3†], *Haoyue Tan*[1,2,3], *Ying Chen*[1,2,3], *Zhihua Zhang*[1,2,3], *Mengda Jiang*[4], *Yun Li*[1,2,3], *Olivier Sterkers*[1,5] *and Hao Wu*[1,2,3*]

[1] *Department of Otorhinolaryngology Head and Neck Surgery, Shanghai Ninth People's Hospital, Shanghai Jiaotong University School of Medicine, Shanghai, China,* [2] *Ear Institute, Shanghai Jiaotong University School of Medicine, Shanghai, China,* [3] *Shanghai Key Laboratory of Translational Medicine on Ear and Nose Diseases, Shanghai, China,* [4] *Department of Radiology, Shanghai Ninth People's Hospital, Shanghai Jiao Tong University School of Medicine, Shanghai, China,* [5] *APHP, Groupe hospitalo-Universitaire Pitié Salpêtrière, Otorhinolaryngology Department, Unit of Otology, Auditory Implants and Skull Base Surgery, Paris, France*

OPEN ACCESS

Edited by:
Paul Van De Heyning, University of Antwerp, Belgium

Reviewed by:
Angel Ramos De Miguel, University of Las Palmas de Gran Canaria, Spain
Neil Donnelly, University of Cambridge, United Kingdom

***Correspondence:**
Hao Wu
wuhao@shsmu.edu.cn

†These authors have contributed equally to this work and share first authorship

Specialty section:
This article was submitted to Otorhinolaryngology - Head and Neck Surgery, a section of the journal Frontiers in Surgery

Received: *15 April 2021*
Accepted: *02 June 2021*
Published: *07 July 2021*

Citation:
Jia H, Pan J, Gu W, Tan H, Chen Y, Zhang Z, Jiang M, Li Y, Sterkers O and Wu H (2021) Robot-Assisted Electrode Array Insertion Becomes Available in Pediatric Cochlear Implant Recipients: First Report and an Intra-Individual Study. Front. Surg. 8:695728. doi: 10.3389/fsurg.2021.695728

Background: As an advanced surgical technique to reduce trauma to the inner ear, robot-assisted electrode array (EA) insertion has been applied in adult cochlear implantation (CI) and was approved as a safe surgical procedure that could result in better outcomes. As the mastoid and temporal bones are generally smaller in children, which would increase the difficulty for robot-assisted manipulation, the clinical application of these systems for CI in children has not been reported. Given that the pediatric candidate is the main population, we aim to investigate the safety and reliability of robot-assisted techniques in pediatric cochlear implantation.

Methods: Retrospective cohort study at a referral center in Shanghai including all patients of simultaneous bilateral CI with robotic assistance on one side (RobOtol® system, Collin ORL, Bagneux, France), and manual insertion on the other (same brand of EA and CI in both side), from December 2019 to June 2020. The surgical outcomes, radiological measurements (EA positioning, EA insertion depth, mastoidectomy size), and audiological outcomes (Behavior pure-tone audiometry) were evaluated.

Results: Five infants (17.8 ± 13.5 months, ranging from 10 to 42 months) and an adult (39 years old) were enrolled in this study. Both perimodiolar and lateral wall EAs were included. The robot-assisted EA insertion was successfully performed in all cases, although the surgical zone in infants was about half the size in adults, and no difference was observed in mastoidectomy size between robot-assisted and manual insertion sides ($p = 0.219$). The insertion depths of EA with two techniques were similar ($P = 0.583$). The robot-assisted technique showed no scalar deviation, but scalar deviation occurred for one manually inserted pre-curved EA (16%). Early auditory performance was similar to both techniques.

Conclusion: Robot-assisted technique for EA insertion is approved to be used safely and reliably in children, which is possible and potential for better scalar positioning and might improve long-term auditory outcome. Standard mastoidectomy size was enough for robot-assisted technique. This first study marks the arrival of the era of robotic CI for all ages.

Keywords: cochlear implant, robot-assisted, robotic, hearing loss, scalar position

INTRODUCTION

Minimizing intracochlear trauma is an essential consideration in cochlear implantation (CI), particularly the preservation of residual hearing, by applying soft surgery and derivative techniques (1–5). As a key procedure in CI, the electrode array (EA) should be placed in the scala tympani and avoid damaging the intracochlear structures. Positioning the EA in the scala tympani leads to better postoperative speech recognition compared to the outcomes with scala vestibuli insertion. Because scalar deviation or translocation can increase the distance between the electrode and the ganglion cells, decreasing the electrical stimulation efficiency, and damage the basilar membrane, inducing residual hearing loss (6, 7). Despite the improvements in EA design and surgical approach, the incidence of EA deviation or translocation is very common, especially with perimodiolar arrays (8). Besides the experience of the surgeon, the natural limitations of the human hand, such as tremor, drift, or jerk, appear to be the main factors leading to intracochlear damage (9, 10).

To overcome the bottleneck in manual micro-manipulation, several otological robots have been designed and applied in CI, the main ones being RobOtol® (Collin ORL, Bagneux, France) by Sorbonne University/AP-HP (11), HEARO® (CAScination AG, Bern, Switzerland) by Bern University (12), and micro-stereotactic frames by Vanderbilt University (13). Among them, RobOtol® focuses on minimally invasive insertion of the EA, and previous studies in temporal bones and animal models have shown that semi-automated robot-assisted insertion was more accurate and less traumatic than manual insertion with a higher number of electrodes correctly positioned in the scala tympani (14, 15).

As the first device to obtain European certification for clinical use (CE mark), the RobOtol® system has been used in France and China since 2019 for robotic-assisted CI in profoundly deaf adults (16–18). Both teams reported that robot-assisted EA insertion was a safe surgical procedure. As the mastoid and temporal bones are generally smaller in children, which would increase the difficulty for robot-assisted EA insertion, the clinical application of these systems for CI in children has not been reported.

After successful use of RobOtol® in adult CI recipients and with safety verification in pediatric temporal bone models (PHACON Temporal Bone Patient "Klein," GA, USA), our center has performed robotic-assisted EA insertion in children since December 2019. Here we present the first series of pediatric CI with robotic assistance reporting the efficacy of robot-assisted insertion in children and clarifying the surgical safety issues of RobOtol® in pediatric patients.

MATERIALS AND METHODS

Study Design and Participants

We conducted a retrospective cohort study of simultaneous bilateral CI recipients from December 2019 to June 2020 at our department (SH9H-2020-T166-1). Inclusion criteria were: (1) same brand of CI and EA on both sides; (2) unilateral robotic and contralateral manual EA insertion. Five infants and an adult were enrolled in this study.

Patient demographics, information on the cochlear implant, medical records, radiological data, and audiological outcomes were collected. All parents of infants and adult patient gave their written informed consent to permit the use of their medical data.

Cochlear Implants

Three types of cochlear implants were used: (i) Cochlear CI512 with a perimodiolar array of 22 electrodes, 19/15.6 mm length (total/active), 0.4 mm diameter in the distal part, and 0.8 mm in the proximal portion (Cochlear AG, Lane Cove, Australia); (ii) Concerto FLEXsoft with a lateral wall array of 19 electrodes, 31.5/26.4 mm length (total/active), 0.5 × 0.4 mm diameter in the distal part and 1.3 mm in the proximal portion (MED-EL, Vienna, Austria); (iii) CS-10A TM with a lateral wall array of 24 electrodes, 22/20 mm length (total/active), 0.4 mm diameter in the distal part and 0.8 mm in the proximal portion (Nurotron, Hangzhou, China) (19).

Surgical Techniques

In all cases, the CI followed the soft surgery protocol (1) and was performed by two senior otologists (manual insertions by H.W.; robot-assisted insertions by H.J.). The same standard surgical approach was used for both insertion techniques: a retro-auricular approach, mastoidectomy, posterior tympanotomy, and exposure of the round window. After opening the round window, either manual or robot-assisted insertion was applied by one right-handed senior otologist via a round window approach. The manual insertion was slowly and carefully performed according to the minimally invasive protocol (20–23).

Robot-assisted EA insertion was performed using the RobOtol® system as a platform, and a specific custom-made micro-forceps (Nurotron, Hangzhou, China) as an actuator (**Figure 1**). The speed of the robotic arm could be switched between three gears (high speed: 10 mm/s max; medium speed: 2 mm/s max; low speed: 1 mm/s max). Before the robot-assisted

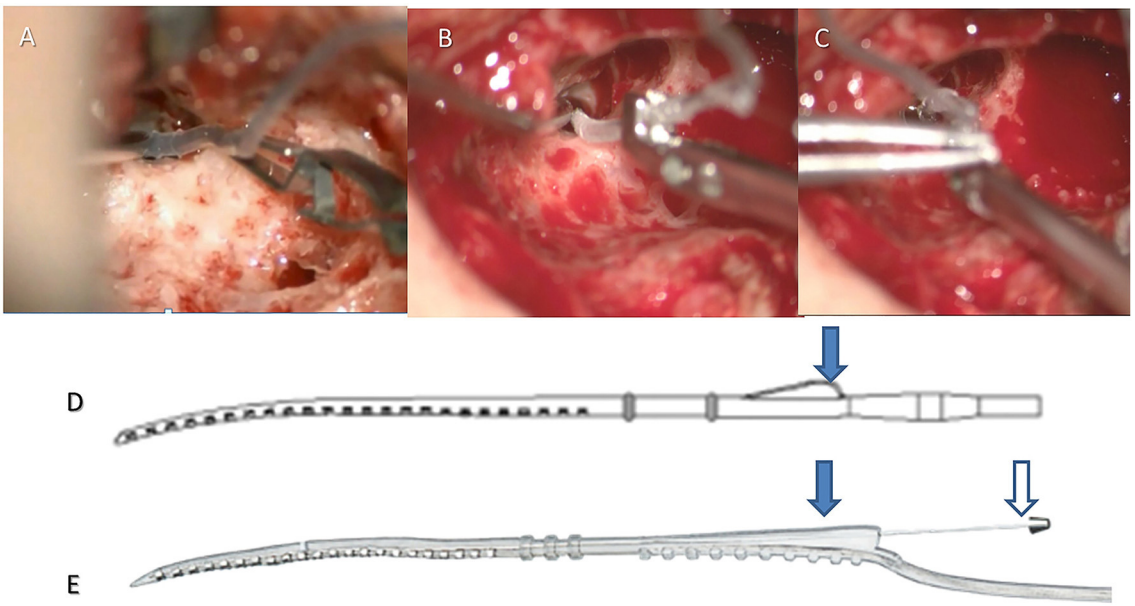

FIGURE 1 | Robot-assisted insertion with a lateral wall or perimodiolar electrode array. For the lateral wall EA (e.g., CS-10A TM), the crest of the EA (arrow in **D**) was clamped by the robotic tool **(A)**, the EA was robotically advanced until the round window marker reached the round window, then the EA was released. For the perimodiolar EA, the crest was clamped by the robotic tool (arrow on the left in **E**), the EA was robotically advanced until the first marker reached the round window **(B)**, then the stylet was held manually (arrow on the right in **E**). The EA was then robotically advanced until the round window marker reached the round window **(C)**, then the stylet was manually retracted, and finally, the EA was robotically released (Robot-assisted AOS technique).

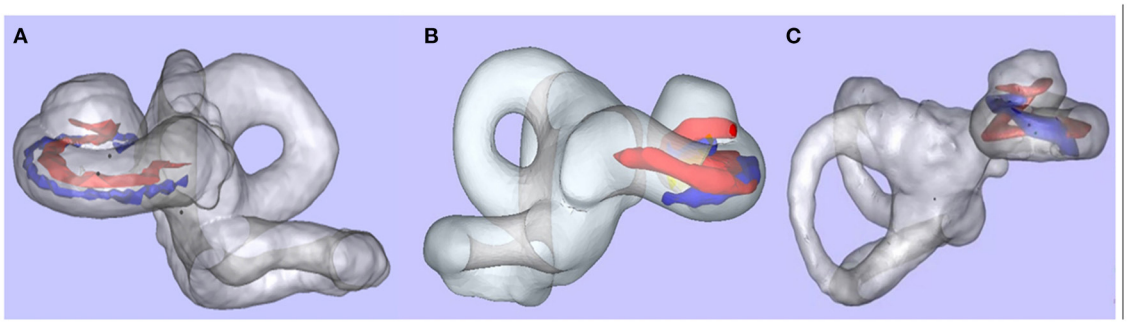

FIGURE 2 | Scalar positioning of the electrode array. After 3D merged reconstruction, the cochlea (membrane labyrinth, gray), the basilar membrane (red), and the EA (blue) could be observed clearly. **(A)** Full scala tympani positioning of EA. **(B)** Scalar deviation at 180°. **(C)** Scalar translocation from 180° (data from other patient, not in this study).

procedure, RobOtol® was draped with a sterile cover, moved into the optimal surgical position, and then the sterilized micro-forceps was mounted on the arm (16–18). The surgeon controlled the robot-assisted arm with the SpaceMouse (3D-connection, Waltham, MA, USA) mounted on the rail of the operating table. The closing and opening of the micro-forceps were controlled by two buttons on the SpaceMouse. After adjusting the robotic arm to the optimum position and aiming it at the ideal insertion axis, the EA was introduced slowly into the cochlear through the round window (low-speed mode), advancing to the target position without interruption, and then released carefully (**Figure 1**). For the perimodiolar EA, the stylet was manually held and later extracted using the Advance Off-Stylet (AOS) technique (**Figures 1B,C,E**) (24). The same standard technique for closure of the surgical cavity was applied on both sides. The duration of the following procedures was recorded:

1) Robotic arm preparation time: moving the robotic system into place and adjusting its arm to the surgical field (additional time required compared to classic manual surgery);
2) EA preparation time for robotic assistance: mounting the EA on the robotic tool, opening the round window, and aiming the robotic arm along the insertion axis;
3) EA insertion (either manual or robotic).

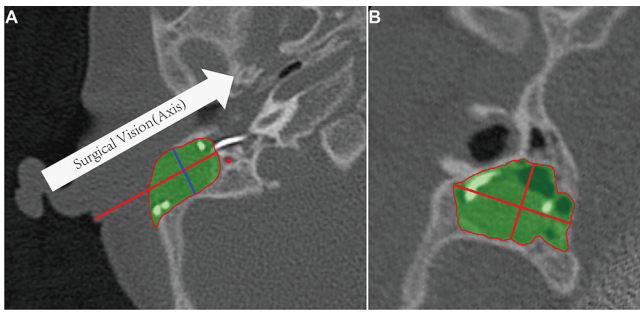

FIGURE 3 | Mastoidectomy size and related anatomic parameters. **(A)** Definition of surgical vision (axis) on the axial plane. The green portion is the volume of the mastoidectomy, the red line is the distance from skin to posterior tympanotomy. **(B)** The area, transverse length, and longitudinal width of the maximum cross-section (blue line in **A**) in the direction of surgical vision.

Radiological Analysis

All patients underwent preoperative high-resolution spiral computed tomography (CT), magnetic resonance imaging (MRI), and a post-implantation (spiral or cone-beam) CT. The cochlear length (distance A), width (distance B), and height (distance H) were measured by Otoplan (CAScination AG, Bern, Switzerland) on the preoperative CT image and completed by the audiologist (Y.C.) independently. The insertion depth and the number of extracochlear electrodes were measured, and the scalar positioning of the EA was assessed by 3D fusion reconstruction of pre-and post-implantation CT with itk-SNAP, CloudCompare, and Blender, as previously described (25). This evaluation was performed by an otologist (H.T.) and a neuroradiologist (M.J.), blinded to the treatment allocation. Full scala tympani positioning of EA was shown in **Figure 2A**. "Scalar deviation" (**Figure 2B**) was defined as the presence of at least one electrode located above the basilar membrane although the distal electrode returned into the scala tympani. "Scalar translocation" (**Figure 2C**) was defined as the presence of one or several electrodes located above the basilar membrane from the penetration site to the tip of the EA.

The measurement of mastoidectomy size parameters was realized using Mimics 17.0 (The Materialise Group, Leuven, Belgium) by removing the postoperative 3D temporal bone volume from the preoperative volume (Boolean operation). The direction of the surgeon's sight, which is parallel to the posterior wall of the external auditory canal on the axial plane, was defined as the axis of surgery. The cross-section of the mastoidectomy was vertical to this axis. The maximum cross-section along this axis was defined as the surgical vision plane, and its transverse length, longitudinal width, and area were measured (**Figure 3**). The distance from skin to facial recess on this axis was also measured as the depth. Two researchers from the hospital cross-checked the measured data for quality control.

Audiological Evaluations

The preoperative audiological evaluation included the click and tone-burst auditory brainstem response (ABR) in pediatric cases to estimate the corresponding audiometry thresholds in children (26), and additionally, pure-tone audiometry and speech discrimination score (SDS) with Mandarin speech test materials (MSTMs) in a soundproof room for the adult case. The mean threshold of audiometry was calculated at 0.5, 1, 2, and 4 kHz. The first mapping of CIs was performed 1 month after surgery, and subsequent mapping was performed regularly at our center. Postoperative auditory outcomes were collected at 6 months after first mapping. Behavioral audiometry for the infants and aided hearing thresholds for the adult at 0.5, 1, 2, and 4 kHz were recorded.

Statistical Analysis

SPSS statistical software, version 20 (IBM Corp., Armonk, NY, USA) was used for statistical analysis. No imputation was made for missing data. Values are presented as means ± standard deviation (SD). Auditory outcomes and anatomic measurements for the two sides were analyzed using a paired-samples *t*-test or Wilcoxon rank-sum test. A P-value < 0.05 was considered statistically significant.

RESULTS

In this study, the five infants were 17.8 ± 13.5 months old (10–42 months), and the adult was 39 years old at the time of surgery. All patients experienced severe or profound hearing loss (HL), and no syndromic deafness was found. The infants all had congenital HL, and the adult presented progressive HL for 17 years with profound HL for 2 years and with no benefit from hearing aids. No inner ear malformation was observed. The distances A, B, and H of the bilateral cochlea in these cases were similar. Two cases were bilaterally and simultaneously implanted with the FLEXsoft lateral wall EA, two cases with the CS-10A TM lateral wall EA, and two cases with the CI512 perimodiolar EA.

Both insertion techniques were successful without intraoperative complications. Intraoperative electrophysiological measurements such as the electrodes impedance and neural response telemetry (NRT) thresholds were normal in all ears. When using the RobOtol® system, the extra preparation time to position the robotic arm was 208.2 ± 105.6 s, and the additional preparation time to position the EA was 241.7 ± 123.5 s. The duration of insertion under robotic assistance was 197.8 ± 64.5 s, which was significantly slower than that by manual insertion (72.8 ± 10.1 s, $n = 6$, $t = 5.39181$, $p = 0.003$) (**Table 1**). With robotic assistance, the FLEXsoft EA seemed to require a longer preparation time which took an average of 386 s compared to an average of 191 and 148 s for the CS-10A TM and CI512 EAs, respectively. The insertion times were shorter with the perimodiolar EA, taking an average of 127 s compared to an average of 269.5 and 197 s for FLEXsoft and CS-10A TM EAs, respectively.

There were no postoperative complications such as local infection or facial palsy in these cases. Postoperative imaging showed full insertion of the EA in all cases. There was no difference in insertion depth between the robot-assisted and manual insertion sides ($t = 0.58692$, $p = 0.583$). The average

TABLE 1 | Cochlear implant type and surgical outcomes in the six cases in this study.

Sex	Age at surgery	Device		Side	Surgical technique			EA positioning		
		Model	EA type, total/active length (mm)		Robotic arm preparation time (s)	EA preparation time (s)	EA insertion time (s)	Insertion depth (°)		Scalar position
M	13 mo	Concerto FLEXsoft	Lateral wall, 31.5/26.4	**R**	**371**	**440**	**281**	**579**		**All in ST**
				M			87		583	All in ST
M	13 mo	Nurotron CS-10A TM	Lateral wall, 22/20	**R**	**145**	**241**	**188**	**406**		**All in ST**
				M			80		429	All in ST
F	10 mo	Concerto FLEXsoft	Lateral wall, 31.5/26.4	**R**	**306**	**332**	**258**	**588**		**All in ST**
				M			78		591	All in ST
F	42 mo	Cochlear CI512	Perimodiolar, 19/15.6	**R**	**105**	**125**	**132**	**387**		**All in ST**
				M			63		376	All in ST
M	12 mo	Cochlear CI512	Perimodiolar 19/15.6	**R**	**178**	**171**	**122**	**377**		**All in ST**
				M			65		349	In ST, except scalar deviation at 180–210°
F	39 yr	Nurotron CS-10A TM	Lateral wall, 22/20	***R***	***144***	***141***	***206***	***444***		***All in ST***
				M			*64*		*427*	*All in ST*

Sex column: M, male; F, female. Age column: mo, month; yr, year. Side column: R, inserted with robot assistance; M, inserted manually. EA, electrode array. ST, scala tympani. Boldface indicates the robot-assisted side. Italics indicates the adult case.

TABLE 2 | Anatomic parameters of cochlea and mastoidectomy in infant and adult recipients.

Age at surgery	Cochlea size (mm)			Surgical technique	Mastoidectomy size				
	Length	Width	Height		Maximum cross-sectional area (mm^2)	Anterior–posterior distance (mm)	Superior–inferior distance (mm)	Facial recess distance from skin (mm)	Mastoidectomy volume (mm^3)
13 mo	**9.3**	**6.5**	**3**	**R**	**163.3**	**18.1**	**11.3**	**23.0**	**1,542.0**
	8.9	5.9	3.1	M	171.2	19.2	11.3	22.7	1,938.0
13 mo	**8.7**	**6.5**	**3.3**	**R**	**118.7**	**14.8**	**10.3**	**25.8**	**1,325.0**
	8.8	6.7	3.3	M	169.5	17.3	12.4	24.2	1,892.0
10 mo	**9.5**	**6.9**	**4.0**	**R**	**164.4**	**18.8**	**9.9**	**25.3**	**1,612.0**
	9.1	6.8	3.8	M	190.9	20.1	11.6	23.0	1,929.0
42 mo	**9.1**	**6.6**	**3.3**	**R**	**179.0**	**17.2**	**11.7**	**26.5**	**2,587.0**
	10	6.8	3.2	M	169.2	20.2	10.1	25.7	2,699.0
12 mo	**10.4**	**7.3**	**2.9**	**R**	**172.6**	**17.6**	**13.0**	**23.6**	**2,031.0**
	9.9	6.7	3.3	M	169.7	18.6	11.5	22.2	1,701.0
Average in children	9.4 ± 0.6	6.7 ± 0.4	3.3 ± 0.3		166.9 ± 18.7	18.2 ± 1.6	11.3 ± 1.0	24.2 ± 1.5	1,925.6 ± 435.2
39 yr	***9.5***	***6.9***	***3.0***	***R***	***379.6***	***29.4***	***16.7***	***32.1***	***5,560.0***
	9.1	*7*	*2.8*	*M*	*287.5*	*25.0*	*14.1*	*31.7*	*5,608.0*

Age column: mo, month; yr, year. R, inserted with robot assistance. M, inserted manually. Boldface indicates the robot-assisted side. Italics indicates the adult case.

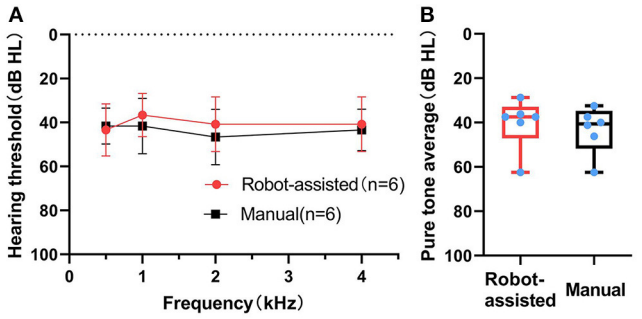

FIGURE 4 | (Behavior) Pure-tone audiometry with CI after 6–9 months. Pure tone audiometry (PTA) thresholds **(A)** and pure tone average **(B)** in the robot-assisted ($n = 6$) and manual insertion ($n = 6$) groups 6–9 months after first mapping.

insertion depth was 585.3 ± 5.3° for the Med-El lateral wall EA, 372.3 ± 16.3° for the Cochlear perimodiolar EA, and 426.5 ± 15.6° for the Nurotron lateral wall EA (**Table 1**). Among the 12 ears, 11 EAs realized full tympanic scalar positioning, only one ear (8%) with perimodiolar EA presented scalar deviation at 180–210° (**Figure 2B**).

The maximum cross-section and mastoidectomy sizes were not significantly different between the manual and the robotic-assisted insertion side in the five infants ($Z = -0.80904$, $p = 0.438$; $Z = -1.07872$, $p = 0.313$, respectively) or in all cases ($Z = 0$, $p = 1$; $Z = -1.25794$, $p = 0.219$, respectively) (**Table 2**). Furthermore, the average mastoidectomy size in the infants (1,925.6 ± 435.2 mm^3, $n = 10$) was about one-third of the size in the adult (5,584.0 ± 33.9 mm^3, $n = 2$). The surgical cross-sections in the infants (166.9 ± 18.7 mm^2, $n = 10$) were about half of the size in the adult (333.6 ± 65.1 mm^2, $n = 2$). The anterior-posterior and superior-inferior distances of the posterior tympanotomy, and the facial recess distance from the skin in the infants were about 70% of those in the adult.

All cases benefited from CI. The average aided pure-tone audiometry (PTA) with CI was 42 ± 10.6 dB HL about 6–9 months after implantation. The average aided PTA was not different between the manual and the robotic-assisted insertion side (40 ± 11.5 dB HL vs. 43 ± 10.4 dB HL, $n = 6$, $Z = -1.36083$, $p = 0.250$) (**Figure 4**). In the adult recipient, the monosyllabic word recognition score, disyllabic word recognition score, and sentence recognition score (SRS) were 48, 38, and 82% in the robotic-assisted insertion side, and 38, 36, and 88% in the manually inserted side, respectively.

DISCUSSION

Currently, the robotic assistance techniques in CI mainly focus on two surgical manipulations: the minimally invasive approach to the inner ear (called direct cochlea access) (12, 27, 28), and minimally invasive EA insertion (14, 15, 29, 30). Different application scenarios with surgical robots have led to various designs for the robotic systems. To gain middle ear access, HEARO® and micro-stereotactic systems use task-specific robotic techniques to perform high-precision automatic drilling procedures (12, 13). Subsequent EA insertion is carried out manually through the narrow tunnel, which might increase the occurrence of tip fold-over (31). Because the minimal invasive EA insertion and accurate scalar positioning attached more relevance to good audiological outcomes, RobOtol® is designed to replace manual insertion with robotic insertion while all other steps are the same as routine surgical procedures. This small change makes the learning curve shorter, and training for this device only takes a few hours for an experienced otologist.

From childhood to adulthood, the mastoid grows in terms of length, width, and depth, and growth and development reach an initial plateau by the age of 7 years for all dimensions (32). Smaller mastoidectomy size mainly limits the translation and inclination of the surgical tool and introduces challenges for robot-assisted manipulations. Therefore, all current reports of robotic systems for cochlear implantation were studied in adults. Because the children are the leading candidates for CI in most countries, the possible and safe application of robotic systems in pediatric CI needs to be thoroughly investigated.

In this series, as all children were younger than 4 years, their surgical zone (cross-sectional area of mastoidectomy) was about 18 × 11 mm, which was about half of the adult (27 × 15 mm). Under this anatomical limitation, RobOtol® was successfully applied in all children with one try of EA insertion, as no additional local trauma or complications occurred. The postoperative radiological image revealed no difference in the mastoidectomy size between the two sides, which means that routine mastoidectomy is sufficient to allow robotically realize EA insertion. These anatomical data could also inspire the development of related robotic tools.

While preparing for insertion of the EA, the Med-EL array required more time to reach the optimal axis. Its ultra-soft features and the clamping site, which is further from the tip, are considered to be the main causes. While inserting the EA, the duration for perimodiolar EA insertion was shorter because the AOS technique for this type of EA needs cooperation as the stylet is manually held and retracted, which could not well control speed as fully robotic manipulation. We had to apply manual-robotic cooperation mode for AOS technique because the fully automatic AOS procedure requires more degrees of freedom, which inevitably enlarges the instrument and requires further validation.

The insertion depth was no different on the two insertion technique sides with the same EA. Full tympanic scalar insertion was realized for all lateral wall EAs, under either manual or robotic technique. For the perimodiolar array, full tympanic scalar insertion was all realized with the robotic technique, but one scalar deviation was observed at 180–210° with the manual technique which might be caused by excessive force from the discordance of the two-handed AOS technique. It seems that robotic assistance could overcome this discordance with good mastery of this technology. However, some actions are not totally automatic, and enough and good training was indispensable.

Evaluation of audiological outcomes is more difficult in infants because the speech discrimination score, considered to be

the main auditory rehabilitation index, could not be evaluated. Alternatively, the aided behavioral audiometry was studied for these infants. The average threshold at 0.5, 1, 2, and 4 kHz at 6–9 months after first mapping was not different between the two sides. In the ear with scalar deviation, the threshold did not show an evident difference from the contralateral ear. The hearing preservation by robot-assisted EA insertions may be more significant. But the preoperative hearing of the patients in this series was poor (generally > 95 dB HL), which could not be applied for the study of residual hearing.

The introduction of the robotic system to CI changes some procedures. The micro-stereotactic system extended the average surgical duration (from incision to closure) to 3 h (31), HEARO® extended it to 4:05 h (33), while RobOtol® only increased duration by about 10–15 min. If for safety considerations, the minimally invasive approach is aborted, converting to a traditional approach might need more time. For RobOtol®, as the routine surgical workflow was barely disturbed, the additional surgical time required could be explained by the following three points. First, RobOtol® changes the regular surgical layout, as the lateral or front side of the surgeon is completely occupied, leading to interference with the microscope and nurse, and requiring repositioning, so that introducing an exoscope could solve part of the problem (34). Second, the high precision of the robotic arm limits its operating space to a 20 cm range thus the comfortable positioning of the robotic arm in the vicinity of the mastoidectomy is extended by ∼3.5 min. Lastly, the positioning of the EA at the entry point to the cochlea takes ∼4 min, and the subsequent insertion process is a slow and steady process lasting ∼3.3 min on average in our study.

Though following up for a longer period than previously reported studies (16, 17), the small case number and lacking more audiological outcomes in children are still the main limitations of the present investigation; however, the current preliminary results, that robotic-assisted insertion seems to lead to less scalar deviation, encouraged us to carry out a prospective, double-blind, randomized trial for robotic EA insertion (ChiCTR2000036534). Additionally, the realization of a fully robot-assisted AOS technique for the perimodiolar EA needs further development to reduce the influence of the biases from manual manipulation. The high-level evidence of the audiological benefits of this advanced technology will be presented soon. Anyway, this preliminary study might mean the arrival of the era of robot-assisted surgery in all ages of CI recipients.

CONCLUSION

The RobOtol® system can safely realize robot-assisted EA insertion for pediatric recipients and can deliver all types of the electrode array. Moreover, the robot-assisted insertion might lead to less intracochlear damage thus potentially improving the long-term audiological outcome, though more evidence needs to be gathered to clarify this. This study serves as a foundation for more research on robotic technology in pediatric cochlear implantation and marks the beginning of a new era in cochlear implantation.

DATA AVAILABILITY STATEMENT

The original contributions presented in the study are included in the article/supplementary material, further inquiries can be directed to the corresponding author/s.

ETHICS STATEMENT

The studies involving human participants were reviewed and approved by the ethics committee of Shanghai Ninth People's Hospital affiliating to Shanghai Jiaotong University School of Medicine (SH9H-2020-T166-1). Written informed consent to participate in this study was provided by the participants' legal guardian/next of kin.

AUTHOR CONTRIBUTIONS

JP, HJ, and YC designed the study. YL, OS, and HW validated the design. JP, HJ, HT, YC, ZZ, MJ, YL, and HW conducted experiments. JP, HT, and YC acquired data and visualized the results. JP and WG drafted the manuscript. OS, HJ, and HW analyzed data and reviewed the manuscript. All authors have read and approved the final version of the manuscript.

FUNDING

This work was supported by the Clinical Research Plan of SHDC (Grant Number: SHDC2020CR3010A); the Interdisciplinary Research of 9th People's Hospital Affiliated to Shanghai Jiao Tong University School of Medicine (Grant Number: JYJC201801); the Shanghai Collaborative Innovation Center for Translational Medicine (Grant Number: TM201813); and the Shanghai Key Laboratory of Translational Medicine on Ear and Nose Diseases (Grant Number: 14DZ2260300).

REFERENCES

1. Lehnhardt E. Intracochlear placement of cochlear implant electrodes in soft surgery technique. *HNO.* (1993) 41:356–9.
2. Wanna GB, Noble JH, Gifford RH, Dietrich MS, Sweeney AD, Zhang D, et al. Impact of intrascalar electrode location, electrode type, and angular insertion depth on residual hearing in cochlear implant patients: preliminary results. *Otol Neurotol.* (2015) 36:1343–8. doi: 10.1097/MAO.0000000000000829
3. Carlson ML, Driscoll CL, Gifford RH, Service GJ, Tombers NM, Hughes-Borst BJ, et al. Implications of minimizing trauma during conventional cochlear implantation. *Otol Neurotol.* (2011) 32:962–8. doi: 10.1097/MAO.0b013e3182204526
4. Cosetti MK, Friedmann DR, Zhu BZ, Heman-Ackah SE, Fang Y, Keller RG, et al. The effects of residual hearing in traditional cochlear implant candidates after implantation with a conventional electrode. *Otol Neurotol.* (2013) 34:516–21. doi: 10.1097/MAO.0b013e3182785210
5. Jia H, Venail F, Piron JP, Batrel C, Pelliccia P, Artières F, et al. Effect of surgical technique on electrode impedance after cochlear implantation. *Ann Otol Rhinol Laryngol.* (2011) 120:529–34. doi: 10.1177/000348941112000807

6. Aschendorff A, Kromeier J, Klenzner T, Laszig R. Quality control after insertion of the nucleus contour and contour advance electrode in adults. *Ear Hear*. (2007) 28:75S−9S. doi: 10.1097/AUD.0b013e318031542e
7. O'Connell BP, Hunter JB, Wanna GB. The importance of electrode location in cochlear implantation. *Laryngoscope Investig Otolaryngol.* (2016) 1:169–74. doi: 10.1002/lio2.42
8. Jwair S, Prins A, Wegner I, Stokroos RJ, Versnel H, Thomeer HGXM. Scalar translocation comparison between lateral wall and perimodiolar cochlear implant arrays - a meta-analysis. *Laryngoscope.* (2020) 131:1358–68. doi: 10.1002/lary.29224
9. Wanna GB, Noble JH, Carlson ML, Gifford RH, Dietrich MS, Haynes DS, et al. Impact of electrode design and surgical approach on scalar location and cochlear implant outcomes. *Laryngoscope.* (2014) 124:S1–7. doi: 10.1002/lary.24728
10. Mürbe D, Hüttenbrink KB, Zahnert T, Vogel U, Tassabehji M, Kuhlisch E, et al. Tremor in otosurgery: influence of physical strain on hand steadiness. *Otol Neurotol.* (2001) 22:672–7. doi: 10.1097/00129492-200109000-00019
11. Miroir M, Nguyen Y, Szewczyk J, Sterkers O, Bozorg Grayeli A. Design, kinematic optimization, and evaluation of a teleoperated system for middle ear microsurgery. *Sci World J.* (2012) 2012:907372. doi: 10.1100/2012/907372
12. Weber S, Gavaghan K, Wimmer W, Williamson T, Gerber N, Anso J, et al. Instrument flight to the inner ear. *Sci Robot.* (2017) 2:eaal4916. doi: 10.1126/scirobotics.aal4916
13. Kratchman LB, Blachon GS, Withrow TJ, Balachandran R, Labadie RF, Webster RJ 3rd. Design of a bone-attached parallel robot for percutaneous cochlear implantation. *IEEE Trans Biomed Eng.* (2011) 58:2904–10. doi: 10.1109/TBME.2011.2162512
14. Torres R, Jia H, Drouillard M, Bensimon JL, Sterkers O, Ferrary E, et al. An optimized robot-based technique for cochlear implantation to reduce array insertion trauma. *Otolaryngol Head Neck Surg.* (2018) 159:900–7. doi: 10.1177/0194599818792232
15. Drouillard M, Torres R, Mamelle E, De Seta D, Sterkers O, Ferrary E, et al. Influence of electrode array stiffness and diameter on hearing in cochlear implanted guinea pig. *PLoS ONE.* (2017) 12:e0183674. doi: 10.1371/journal.pone.0183674
16. Vittoria S, Lahlou G, Torres R, Daoudi H, Mosnier I, Mazalaigue S, et al. Robot-based assistance in middle ear surgery and cochlear implantation: first clinical report. *Eur Arch Otorhinolaryngol.* (2021) 278:77–85. doi: 10.1007/s00405-020-06070-z
17. Daoudi H, Lahlou G, Torres R, Sterkers O, Lefeuvre V, Ferrary E, et al. Robot-assisted cochlear implant electrode array insertion in adults: a comparative study with manual insertion. *Otol Neurotol.* (2021) 42:e438–44. doi: 10.1097/MAO.0000000000003002
18. Jia H, Pan JX, Li Y, Zhang ZH, Tan HY, Wang ZY, et al. Preliminary application of robot-assisted electrode insertion in cochlear implantation. *Zhonghua Er Bi Yan Hou Tou Jing Wai Ke Za Zhi.* (2020) 55:952–6. doi: 10.3760/cma.j.cn115330-20200228-00141
19. Rebscher S, Zhou DD, Zeng FG. Development and clinical introduction of the nurotron cochlear implant electrode array. *J Int Adv Otol.* (2018) 14:392–400. doi: 10.5152/iao.2018.6285
20. Mowry SE, Woodson E, Gantz BJ. New frontiers in cochlear implantation: acoustic plus electric hearing, hearing preservation, and more. *Otolaryngol Clin North Am.* (2012) 45:187–203. doi: 10.1016/j.otc.2011.09.001
21. Naderpour M, Aminzadeh Z, Jabbari Moghaddam Y, Pourshiri B, Ariafar A, Akhondi A. Comparison of the pediatric cochlear implantation using round window and cochleostomy. *Iran J Otorhinolaryngol.* (2020) 32:3–10. doi: 10.22038/ijorl.2019.37313.2219
22. Jang JH, Choo OS, Kim H, Yi Park H, Choung YH. Round window membrane visibility related to success of hearing preservation in cochlear implantation. *Acta Otolaryngol.* (2019) 139:618–24. doi: 10.1080/00016489.2019.1609701
23. Snels C, IntHout J, Mylanus E, Huinck W, Dhooge I. Hearing preservation in cochlear implant surgery: a meta-analysis. *Otol Neurotol.* (2019) 40:145–53. doi: 10.1097/MAO.0000000000002083
24. Stöver T, Issing P, Graurock G, Erfurt P, ElBeltagy Y, Paasche G, et al. Evaluation of the advance off-stylet insertion technique and the cochlear insertion tool in temporal bones. *Otol Neurotol.* (2005) 26:1161–70. doi: 10.1097/01.mao.0000179527.17285.85
25. Torres R, Drouillard M, De Seta D, et al. Cochlear Implant Insertion Axis Into the Basal Turn: A Critical Factor in Electrode Array Translocation. *Otol Neurotol.* (2018) 39:168–76. doi: 10.1097/MAO.0000000000001648
26. Lu TM, Wu FW, Chang H, Lin HC. Using click-evoked auditory brainstem response thresholds in infants to estimate the corresponding pure-tone audiometry thresholds in children referred from UNHS. *Int J Pediatr Otorhinolaryngol.* (2017) 95:57–62. doi: 10.1016/j.ijporl.2017.02.004
27. Bell B, Gerber N, Williamson T, Gavaghan K, Wimmer W, Caversaccio M, et al. *In vitro* accuracy evaluation of image-guided robot system for direct cochlear access. *Otol Neurotol.* (2013) 34:1284–90. doi: 10.1097/MAO.0b013e31829561b6
28. Balachandran R, Mitchell JE, Blachon G, Noble JH, Dawant BM, Fitzpatrick JM, et al. Percutaneous cochlear implant drilling via customized frames: an in vitro study. *Otolaryngol Head Neck Surg.* (2010) 142:421–6. doi: 10.1016/j.otohns.2009.11.029
29. Hussong A, Rau T, Eilers H, Baron S, Heimann B, Leinung M, et al. Conception and design of an automated insertion tool for cochlear implants. *Annu Int Conf IEEE Eng Med Biol Soc.* (2008) 2008:5593–6. doi: 10.1109/IEMBS.2008.4650482
30. Nguyen Y, Kazmitcheff G, De Seta D, Miroir M, Ferrary E, Sterkers O. Definition of metrics to evaluate cochlear array insertion forces performed with forceps, insertion tool, or motorized tool in temporal bone specimens. *Biomed Res Int.* (2014) 2014:532570. doi: 10.1155/2014/532570
31. Labadie RF, Balachandran R, Noble JH, Blachon GS, Mitchell JE, Reda FA, et al. Minimally invasive image-guided cochlear implantation surgery: first report of clinical implementation. *Laryngoscope.* (2014) 124:1915–22. doi: 10.1002/lary.24520
32. Eby TL, Nadol JB Jr. Postnatal growth of the human temporal bone. Implications for cochlear implants in children. *Ann Otol Rhinol Laryngol.* (1986) 95:356–64. doi: 10.1177/000348948609500407
33. Caversaccio M, Wimmer W, Anso J, Mantokoudis G, Gerber N, Rathgeb C, et al. Robotic middle ear access for cochlear implantation: first in man. *PLoS ONE.* (2019) 14:e0220543. doi: 10.1371/journal.pone.0220543
34. Colombo G, Ferreli F, Di Bari M, Cugini G, Miceli S, De Virgilio A, et al. Introducing the high-definition 3D exoscope in ear surgery: preliminary analysis of advantages and limits compared with operative microscope. *Eur Arch Otorhinolaryngol.* (2020) 55:952–6. doi: 10.1007/s00405-020-06510-w

Conflict of Interest: The authors declare that the research was conducted in the absence of any commercial or financial relationships that could be construed as a potential conflict of interest.

frontiers in Surgery

ORIGINAL RESEARCH
published: 10 September 2021
doi: 10.3389/fsurg.2021.729736

Restoration of High Frequency Auditory Perception After Robot-Assisted or Manual Cochlear Implantation in Profoundly Deaf Adults Improves Speech Recognition

Renato Torres[1,2,3,4*], *Hannah Daoudi*[1,2,3], *Ghizlene Lahlou*[1,2,3], *Olivier Sterkers*[1,2,3], *Evelyne Ferrary*[1,2,3], *Isabelle Mosnier*[1,2,3] *and Yann Nguyen*[1,2,3]

[1] *Unité Fonctionnelle Implants Auditifs, Service Oto-Rhino-Laryngologie, AP-HP/Sorbonne Université, Paris, France,* [2] *Centre de Recherche en Audiologie Adulte, GHU Pitié-Salpêtrière/Fondation Pour l'Audition, AP-HP, Paris, France,* [3] *Technologies et Thérapie Génique Pour la Surdité, Institut de l'Audition, Institut Pasteur, INSERM, Paris, France,* [4] *Departamento de Ciencias Fisiológicas, Facultad de Medicina, Universidad Nacional de San Agustín de Arequipa, Arequipa, Peru*

OPEN ACCESS

Edited by:
Haralampos Gouveris, Johannes Gutenberg University Mainz, Germany

Reviewed by:
Philip Rajan, Raja Permaisuri Bainun Hospital, Malaysia
Hans Thomeer, University Medical Center Utrecht, Netherlands

****Correspondence:***
Renato Torres
victor.torres-lazo@pasteur.fr

Specialty section:
This article was submitted to Otorhinolaryngology - Head and Neck Surgery, a section of the journal Frontiers in Surgery

Received: *23 June 2021*
Accepted: *17 August 2021*
Published: *10 September 2021*

Citation:
Torres R, Daoudi H, Lahlou G, Sterkers O, Ferrary E, Mosnier I and Nguyen Y (2021) Restoration of High Frequency Auditory Perception After Robot-Assisted or Manual Cochlear Implantation in Profoundly Deaf Adults Improves Speech Recognition. Front. Surg. 8:729736. doi: 10.3389/fsurg.2021.729736

Background and Purpose: Robot-assisted cochlear implantation has recently been implemented in clinical practice; however, its effect on hearing outcomes is unknown. The aim of this preliminary study was to evaluate hearing performance 1 year post-implantation whether the electrode array was inserted manually or assisted by a robot.

Methods: Forty-two profoundly deaf adults were implanted either manually ($n = 21$) or assisted by a robot (RobOtol®, Collin, Bagneux, France) with three different electrode array types. Participants were paired by age, and electrode array type. The scalar position of the electrode array in the cochlea was assessed by 3D reconstruction from the pre- and post-implantation computed tomography. Pure-tone audiometry and speech perception in silence (percentage of disyllabic words at 60 dB) were tested on the implanted ear 1 year post-implantation in free-field conditions. The pure-tone average was calculated at 250–500–750 Hz, 500–1,000–2,000–3,000 Hz, and 3,000–4,000–8,000 Hz for low, mid, and high frequencies, respectively.

Results: One year after cochlear implantation, restoration of the high-frequency thresholds was associated with better speech perception in silence, but not with low or mid frequencies ($p < 0.0001$; Adjusted $R^2 = 0.64$, polynomial non-linear regression). Although array translocation was similar using either technique, the number of translocated electrodes was lower when the electrode arrays had been inserted with the assistance of the robot compared with manual insertion ($p = 0.018$; Fisher's exact test).

Conclusion: The restoration of high-frequency thresholds (3,000–4,000–8,000 Hz) by cochlear implantation was associated with good speech perception in silence. The numbers of translocated electrodes were reduced after a robot-assisted insertion.

Keywords: ear surgery, hearing loss, translocation, pure-tone audiometry, hearing performance, hearing outcomes

INTRODUCTION

Cochlear implants are medical devices aiming to electrically stimulate ganglion of the auditory nerve and to restore hearing in patients with severe to profound hearing loss. The hearing outcomes after cochlear implantation depend on improvable (e.g., electrode array insertion, technological advances of array/processor), and definite factors (e.g., age at implantation, duration of preoperative profound deafness, etiology of the hearing loss).

Electrode array insertion is performed surgically with micro-instruments under microscopic view. Optimization of this surgical step has been associated with hearing outcomes, and aims to insert the electrode array into the scala tympani (1–4), and to avoid, whenever possible, damage to the basilar membrane to preserve residual hearing when acoustic stimulation of the higher turns of the cochlea is possible (5). For this purpose, there is growing interest in using robots for cochlear implantation with different approaches such as direct external access to the cochlea (6, 7), using a teleoperated robot to insert the electrode array (8–10), and coupling robot and navigation to correctly align the electrode array with the insertion axis (11, 12). A robot overcomes the inaccuracy of manual insertion, and presumably allows cochlear trauma to be reduced during electrode array insertion (10). However, hearing outcomes after robot-assisted cochlear implantation remain to be analyzed and compared to those obtained after manual cochlear implantation.

With regard to speech perception in cochlear implanted patients, its relationship with restoration of post-implantation pure-tone thresholds is not clear. Some studies show that pure-tone performance is not related to speech perception (13). On the other hand, preservation of low-frequency auditory hearing is associated with better speech perception after cochlear implantation (14). However, in non-implanted patients, a deterioration of the speech perception is associated with an impairment of the mid and high-frequency thresholds (15).

The aim of the study was to assess speech perception in silence 1 year postoperatively in profoundly deaf adults who underwent robot-assisted or manual cochlear implantation, and its relationship with restoration of pure-tone audiometry.

MATERIALS AND METHODS

Patients

This is a retrospective study that included 42 patients who underwent cochlear implantation in a tertiary referral center. All patients give their consent to participate in the study, and the protocol was approved by the Institutional Review Board–CNIL N° 20191219182243. Two groups were established according to the electrode array insertion technique: robot-assisted ($n = 21$) or manual ($n = 21$). Each patient from the robot-assisted group was paired with one of the manually inserted group by age, and cochlear implant type. Robot-assisted cochlear implantations were performed between July 2019 and March 2020, and between July 2018 and November 2019 for manual implantation. Data on the electrode array position have been partially published (17 cases from the robot-assisted group and 21 cases from the manually inserted group) (10). All patients had no residual hearing before the surgery and underwent hearing tests 1 year after surgery.

Cochlear Implant

Three types of electrode arrays were inserted:

- Cochlear™ Nucleus® CI522 or CI622 (Cochlear, Lane Cove, Australia) ($n = 22$). This is a straight electrode array with an active length of 19.1 mm and 22 electrodes;
- Advanced Bionics HiFocus™ Slim J (Advanced Bionics, Valencia, CA, USA) ($n = 16$). This is a straight electrode array with an active length of 20 mm and 16 electrodes;
- Advanced Bionics HiFocus™ Mid-Scala electrode array ($n = 6$). This pre-curved electrode array has an active length of 15.5 mm and 16 electrodes.

Robot Assisted and Manual Electrode Array Insertion

All surgical procedures were performed by two senior surgeons (IM and YN). A classical surgical approach was used to reach the round window region: retroauricular incision, mastoidectomy, and posterior tympanotomy. The array was usually inserted through the round window except in two cases in whom a cochleostomy was performed due to a non-visible round window.

With regard to the robot-assisted insertions, the RobOtol® arm (Collin, Bagneux, France) was controlled by the surgeon using a SpaceMouse® (3DConnexion, Waltham, MA, USA). For straight arrays, insertion was completely performed at a speed of 0.25 mm/s with specifically designed insertion tools (Collin, Bagneux, France; Cochlear CI522/622: RBT-2302, and AB SlimJ: RBT-2301). The Mid-Scala array was positioned on the insertion tool and both were coupled to the robot arm (Collin, Bagneux, France; AB Mid-Scala: RBT-0406). The array was partially inserted up to the mark indicating the beginning of the coiling of the basal turn and then manually ejected from the insertion tool. With regard to the manual insertions, they were performed using surgical instruments specially designed by the manufacturer.

Radiological Analysis

Pre-implantation computed tomography (CT) was performed in all patients. Distance A (from the center of the round window and the lateral wall at 180° passing through the modiolus), and distance B (perpendicular to distance A from the lateral wall at 90° and 270° and passing through the modiolus) were determined using 3D multiplanar reconstruction of the images performed using Horos v.2.2.0 open source software (https://horosproject.org/). Post-implantation CT was performed 24 h after surgery. Using the same 3D multiplanar reconstruction, the number of extracochlear electrodes, and the depth of insertion (measured in degrees from the line between the center of the round window and the modiolus and the most apical electrode) were determined.

Three-dimensional reconstruction models were obtained using ITK-SNAP v.3.4.0 (http://www.itksnap.org). This method was used to determine the intrascalar position of each

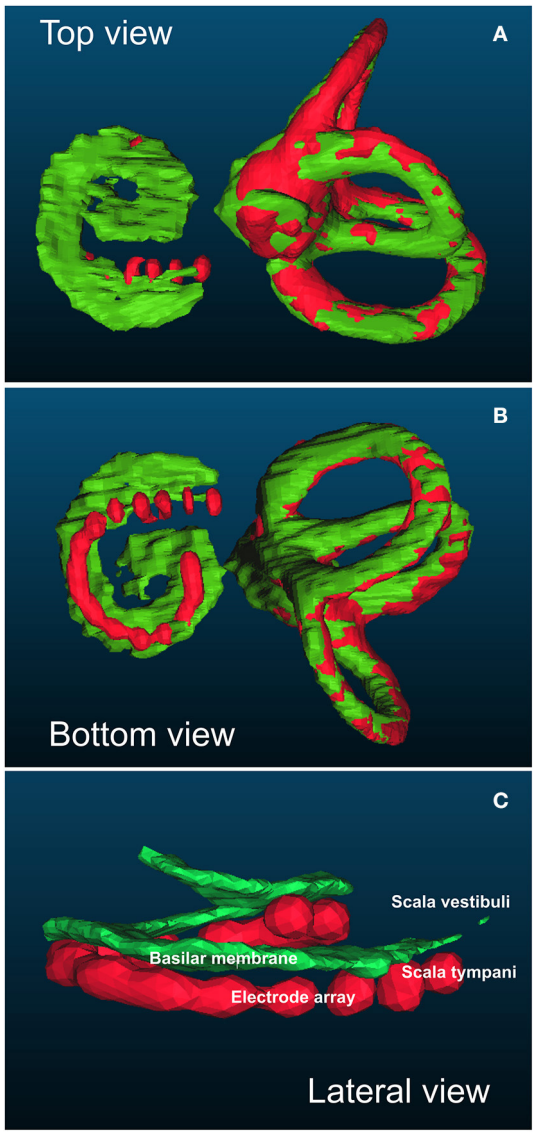

FIGURE 1 | Example of top **(A)**, bottom **(B),** and lateral **(C)** views of the basilar membrane to assess the position of each electrode in relation to the basilar membrane. The positions of the basilar membrane and semicircular canals were obtained from the pre-implantation computed tomography (CT) (in green). The positions of the electrode array and semicircular canals were obtained from the post-implantation CT (in red). Both models were automatically merged according to the position of the semicircular canals that were not modified by the artefact of the electrode array. In this example, the electrode array was below the basilar membrane and consequently fully inserted into the scala tympani (no array translocation).

electrode according to the basilar membrane as previously described (10) and validated with microscopy analysis (16). 3D reconstructions of the semicircular canals and the basilar membrane were obtained from the pre-implantation CT images. 3D reconstructions of the semicircular canals and the electrode array were obtained from the post-implantation CT. The fusion of both pre- and post-implantation 3D models was achieved automatically based on the orthogonal position of the semicircular canals using CloudCompare v.2.10.2 GPL software (http://www.cloudcompare.org/) (**Figure 1**).

The position of each electrode was determined according to its position relative to the basilar membrane as either a non-translocated electrode (under the basilar membrane) or a translocated electrode (above the basilar membrane). Array translocation was defined when at least one electrode was located in the scala vestibuli. The location of the translocation was determined according to the baseline (0° degrees) between the center of the round window and the modiolus and classified as proximal (start of array translocation before 180°), or distal (after 180°). The percentage of translocated electrodes was calculated as the number of translocated electrodes/total number of electrodes in the array × 100.

Evaluation of Hearing Performance

Hearing tests were performed 1 year after surgery. The implanted ear was independently assessed in an acoustically isolated room, without any hearing aid on the contralateral side and the ear plugged if necessary. The speaker was placed 1 meter in front of the patient. Free-field pure-tone audiometry was assessed to determine the hearing thresholds at the frequencies 250, 500, 750, 1,000, 2,000, 3,000, 4,000, and 8,000 Hz. Based on the Committee on Hearing and Equilibrium guidelines, the pure-tone average (PTA) was calculated as the mean of the thresholds at 500, 1,000, 2,000, and 3,000 Hz (17). From this interval, a low-frequency PTA (250–500–750 Hz) and a high-frequency PTA (3,000–4,000–8,000 Hz) were calculated.

Speech perception in silence was assessed using disyllabic words and the speech discrimination score (SDS) was determined at 60 dB SPL and expressed as the percentage of words correctly recognized at this acoustic pressure.

Statistical Analysis

All numeric variables were expressed as means and standard deviations. Non-parametric tests were performed to assess the association between hearing performance and robotic/manual insertion and the intrascalar position of the electrode array. Linear and non-linear regression were performed to analyze the association between speech perception in silence and pure-tone audiometry threshold. The models were compared using ANOVA analysis to choose the best fitted model. All statistical analysis was performed using R v3.3.3 statistical software (https://www.R-project.org/). A $p < 0.05$ was considered to be significant.

RESULTS

Hearing Performance and Electrode Array Insertion Technique

Pre-implantation clinical data from the patients are shown in **Table 1**. There was no difference in speech perception in silence between robot-assisted and manual electrode array insertion techniques (**Table 2**). Regarding the pure-tone thresholds, again similar results were observed between robot and manual insertion techniques for low-, mid-, and high-frequency PTA (**Table 2**).

TABLE 1 | Clinical characteristics of the implanted patients.

Patient characteristics	Robot-assisted insertion ($n = 21$)	Manual insertion ($n = 21$)
Age (years)	57 ± 20.8 [21–86]	54 ± 1.6 [22–82]
Sex: M/F	(8), 38%/(13), 62%	(10), 48%/(11), 52%
Duration of deafness (years)	23 ± 11.5 [4–45]	24 ± 17.3 [4–64]
Preoperative PTA–implanted ear (dB)	114 ± 11.9 [95–120]	111 ± 16.3 [89–120]
Preoperative SDS–implanted ear (%)	0 ± 0	0 ± 0
Preoperative PTA–non-implanted ear (dB)	93 ± 18.5 [64–120]	102 ± 18.2 [59–120]
Preoperative SDS–non-implanted ear (%)	1 ± 3.2 [0–10]	3 ± 8.0 [0–30]
Side (Left/Right)	(7), 33%/(14), 67%	(9), 43%/(12), 57%
Etiology		
Genetic	(8), 38%	(7), 33%
Unknown	(7), 33%	(11), 52%
Otosclerosis	(3), 14%	(1), 5%
Ménière's disease	(2), 10%	(1), 5%
Trauma	(1), 5%	(0)
Meningitis	(0)	(1), 5%

Data are expressed as mean ± standard deviation [min–max], and (n), %.

TABLE 2 | Hearing outcomes according to electrode array insertion technique, array translocation, and distal (>180°) and proximal (<180°) translocations.

	SDS	PTA		
	60 dB	Low-frequency	Mid-frequency	High-frequency
Insertion technique				
Robot-assisted (21)	66 ± 30.8 [0–100]	30 ± 8.6 [19–48]	33 ± 11.2 [16–50]	42 ± 22.6 [13–110]
Manual (21)	65 ± 25.8 [0–100]	31 ± 9.9 [20–66]	33 ± 15.1 [23–92]	35 ± 21.6 [23–110]
Position of the electrode array				
No translocation (30)	69 ± 27.2 [0–100]	31 ± 10.1 [19–66]	33 ± 14.5 [16–91]	42 ± 23.8 [13–110]
Translocation (12)	58 ± 29.5 [0–90]	31 ± 6.5 [20–40]	33 ± 9.1 [18–51]	42 ± 17.1 [22–75]
Localization of the translocation				
Distal (4)	71 ± 14.3 [60–90]	27 ± 3.1 [25–32]	27 ± 4.8 [23–34]	28 ± 5.6 [25–36]
Proximal (8)	51 ± 33.5 [0–90]	33 ± 6.8 [20–40]	37 ± 9.3 [19–51]	49 ± 16.9 [22–75]*

Data are expressed as mean ± SD [min–max].
SDS: speech discrimination score at 60 dB in silence (%).
PTA: pure-tone average (dB).
**Comparison between distal and proximal translocation, $p < 0.05$ (Mann–Whitney test).*

Hearing Performance and the Hearing Loss Etiology

The speech perception at 1 year was similar according to the etiology of the hearing loss ($p = 0.3$; Kruskal-Wallis and Bonferroni *post-hoc* test). The translocation rate was not associated with the etiology of the hearing loss ($p = 0.75$; Chi-square and *post-hoc* pairwise comparisons; **Table 3**).

Hearing Performance and Intrascalar Position of the Electrode Array

Twelve array translocations (28%) were observed, and the translocation rate was similar whatever the type of electrode array ($p = 0.09$; Fisher's exact test). Moreover, the ratio of array translocation was similar in robot-assisted ($n = 5$, 24%), and manual ($n = 7$, 33%) insertion. However, considering the number of translocated electrodes, this was lower in the case of robot-assisted insertion ($n = 34$, 8.6%) compared to manual insertion ($n = 56$, 14%) ($p = 0.018$; CI 95%: =0.35–0.91; Fisher's exact test; **Figure 2**).

Array translocation was not associated with an impaired speech perception in silence (translocation: 58 ± 29.5% $n = 12$; no translocation: 69 ± 27.2% $n = 30$; $p = 0.23$, Mann–Whitney test). With regard to pure tone audiometry, there were no differences between translocation and no translocation of the electrode and the low-frequency PTA ($p = 0.62$), mid-frequency PTA ($p = 0.51$), or high-frequency PTA ($p = 0.53$; Mann–Whitney test; **Table 2**). Considering the location of the translocation of the array, the high-frequency PTA was significantly better in distal than in proximal translocations (28 ± 5.6 dB, and 49

± 16.9 dB, respectively; $p = 0.04$, Mann–Whitney test; **Table 2**).

Regarding the number of translocated electrodes, there was still no correlation between the percentage of translocated electrodes and speech performance in silence ($p = 0.14$; rho = −0.23; Spearman's rank correlation). This trend did not vary for the low-frequency PTA ($p = 0.35$; rho 0.15; Spearman's rank correlation), mid-frequency PTA ($p = 0.34$; rho = 0.15; Spearman's rank correlation), and high-frequency PTA ($p = 0.40$; rho = 0.13; Spearman's rank correlation).

In two cases (4%), the electrode was inserted through a cochleostomy (**Figure 2**). In both cases, the electrode array was translocated and had a poor speech perception (robot insertion-MS: 30% and manual insertion-CI522/622: 0%). Regarding the pure-tone audiometry thresholds, both cases had an increased high-frequency PTA (45 and 75 dB, respectively).

TABLE 3 | Speech perception and array translocation according to the etiology of the hearing loss.

Etiology	N	SDS 60 dB	Array translocations
Unknown	18	57 ± 28.6	4 (22)
Genetic	15	74 ± 28.9	5 (33)
Otosclerosis	4	68 ± 28.7	2 (50)
Meniere's disease	3	81 ± 17.5	0 (0)
Meningitis	1	80	1 (100)
Traumatic	1	55	0 (0)

SDS 60 dB: speech discrimination score at 60 dB in silence (%).
The array translocation is expressed as the number of array translocation and the percentage by etiology: n (%).

Relationship Between Speech Perception in Silence and High-Frequency Thresholds in Pure-tone Audiometry

At 1 year post-implantation, the overall speech perception in silence with the implanted ear was improved: pre-implantation SDS: 0 ± 0%; post-implantation: manual: 65 ± 25.8% ($n = 21$), and post-implantation: robot-assisted: 66 ± 30.8% ($n = 21$). Neither low-frequency PTA nor mid-frequency PTA was associated with the speech perception scores (**Figure 3**). On the other hand, restoration of high-frequency thresholds was associated with better speech perception (fractional polynomial non-linear regression, $p < 0.0001$; Adjusted $R^2 = 0.64$). Patients with speech perception scores > 50% clearly had better high-frequency PTA (36 ± 16.0 dB; $n = 34$) than those with speech

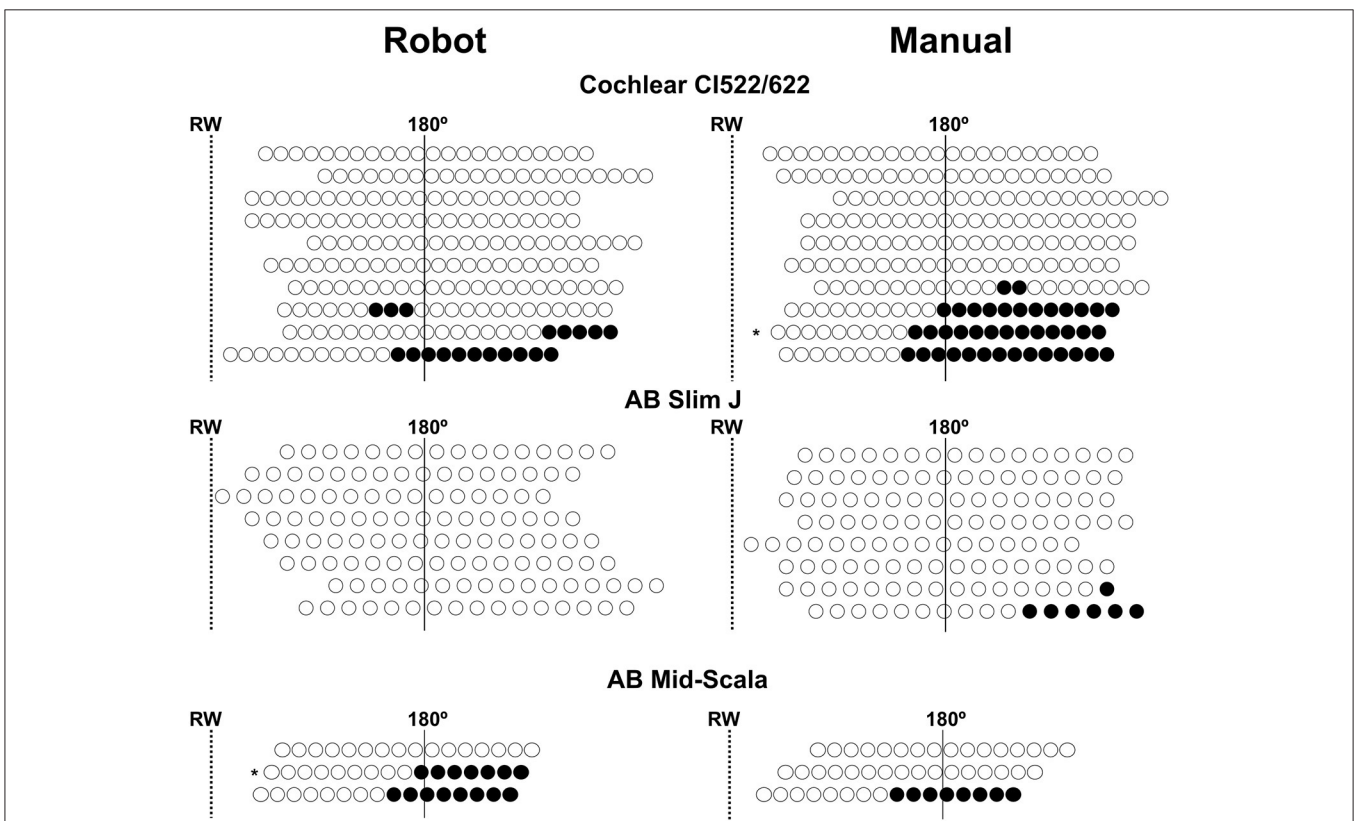

FIGURE 2 | Representation of the position of each electrode following robot-assisted and manual electrode array insertion. The position of the electrode array was adjusted according to the round window position (RW) (dotted line) and 180° position (continuous line). The translocation rate of the electrode array was similar in both insertion groups, however, the number of translocated electrodes after a robot-assisted insertion was lower than with manual insertion. Unfilled circles: non-translocated electrode, filled circles: translocated electrode. AB, Advanced Bionics; * electrodes inserted through a cochleostomy.

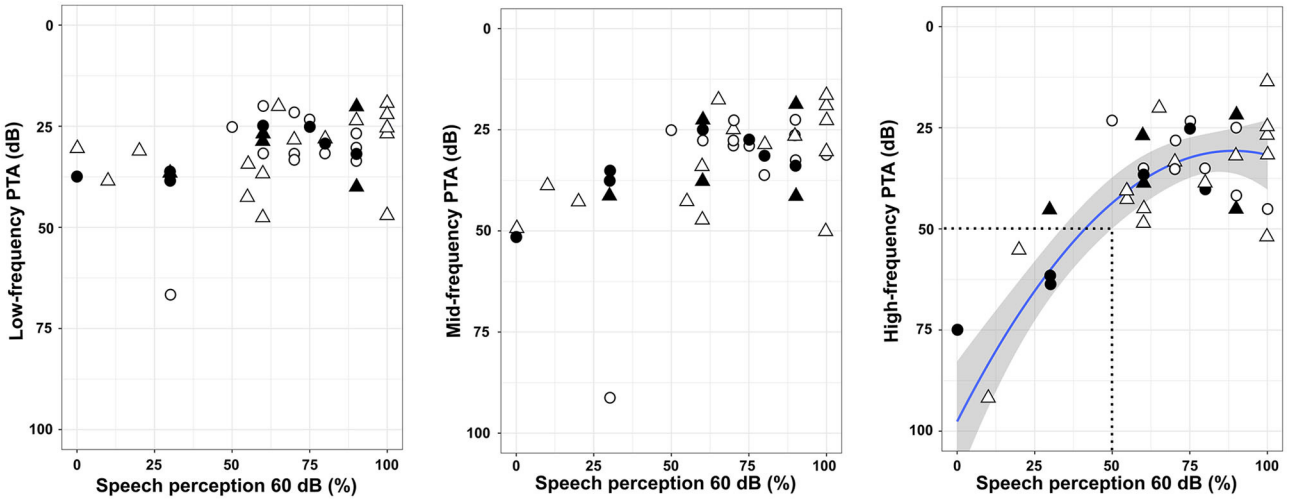

FIGURE 3 | Speech perception at 60 dB in silence and pure-tone audiometry thresholds. The line represents a non-linear regression [$f_{(x)} = 0.008x^2$-$0.38x + 35.1$, $p < 0.0001$; Adjusted $R^2 = 0.64$], and the gray zone represents the 95% confidence interval. The area within the dotted lines indicates a poor speech perception lower than 50% and a high-frequency PTA higher than 50 dB. Triangles: robot-assisted insertion; circles: manual insertion; filled symbols: translocation of the electrode array; unfilled symbols: non-translocation.

perception scores $\leq$ 50% (76 $\pm$ 24.8 dB; $n = 8$) ($p < 0.001$; Mann–Whitney test). With regard to the electrode array type, the speech performance in silence was similar whatever the electrode array used (AB Mid-Scala: 70 $\pm$ 25.2%, $n = 6$; AB Slim J: 72 $\pm$ 27.6%, $n = 16$; CI522/622: 70 $\pm$ 30.0% $n = 20$; $p = 0.92$, Kruskal–Wallis test). The depth of insertion was not correlated with speech perception in silence ($p = 0.52$; rho = 0.10, Spearman's Rank correlation).

DISCUSSION

In this preliminary study, hearing outcomes after robot-assisted or manual array insertion were evaluated 1 year after cochlear implantation. Regardless the electrode array insertion technique, speech perception in silence was improved when the pure tone thresholds at high frequencies were restored after cochlear implantation. In the case of translocation of the electrode array, robot-assisted insertion reduced the number of translocated electrodes compared with manual insertion, but this was not related to an improvement in speech perception in silence.

Although the association between speech perception in silence and high-frequency thresholds in pure-tone audiometry has not been reported in cochlear-implanted patients, previous reports showed the association of speech perception in non-implanted patients with hearing loss, especially at high frequencies (15, 18). Another study, in non-implanted patients, showed the importance of preservation of the extended high frequencies (>8,000 Hz) and the performance in noise (19). Our findings are in agreement with an earlier study showing no correlation between speech perception and PTA (125–8,000 Hz) in cochlear-implanted patients (13). Another study reported five patients successfully implanted with the RobOtol® and a restoration of frequencies from 250 to 4,000 Hz; however, its association with speech perception was not analyzed (9). Regarding the electroacoustic stimulation of cochlear implant candidates, the improvement in hearing performance was focused on preservation of the low-frequency range (5, 20). However, the spectral range of voice, which includes vowels and consonants, could involve a wider frequency range from 200 to 10,000 Hz for fricative consonants such as "s" or "f" (21). As the cochlear ramp is tonotopically arranged and due to the characteristics of the electrode array, merely medium and high frequencies could be stimulated and restored.

Our results showed similar hearing outcomes for speech perception in silence and pure-tone audiometry thresholds with robot and manual electrode array insertions. This could be explained by the fact that the robot was entirely handled by the surgeon according to its mental representation of the cochlear structures. Earlier studies reported the importance of inserting the electrode array along the optimal axis to reduce intracochlear trauma (11). In addition, for pre-curved arrays such as the Mid-Scala, alignment of the array tip with the coiling direction of the scala tympani could be a critical step to reduce intracochlear trauma (12). The alignment of the array with the insertion axis could be similar to manual insertion or using the RobOtol®, because in both insertion techniques, the surgeon had no visual information to correctly determine the optimal axis of insertion. However, the advantages of using the RobOtol® are to insert the electrode array in a smooth way, to decompose motion into pure rotation or translation and to eliminate the involuntary movements of the hand such as tremor, all these movements are very difficult to perform manually. The next step could be accomplished by coupling the robot and navigation to insert the electrode array in the most appropriate way. A personalization of the array insertion would aim to reduce the intracochlear trauma according to the anatomy of the patients and the surgical

circumstances such as inserting the electrode array in the optimal axis (11), align the array with the coiling direction of the ST specifically for the pre-curved electrodes (12), and adapting the insertion through the round window or a cochleostomy considering the hook region of the cochlea (22). Likewise, future investigation should be focused to have a haptic feedback, control the direction of the array with steering tools, and/or have an intracochlear visualization during the array insertion.

Our results are in contrast to earlier studies showing worse speech performance when translocation of the electrode array was observed (2, 3, 23, 24). We performed a detailed analysis of the position of the electrode array to determine the intrascalar position of each electrode, and our findings are in contrast to previous reports that showed an association between an array fully inserted into the scala tympani and better speech performance (1–3). Regarding the localization of the translocation, a proximal translocation was associated with a decrease in high-frequency PTA. This decrease could be due to the fact that high-frequencies are delivered to the spiral ganglion by the proximal electrodes. Although a decrease in the high-frequency thresholds would be more deleterious for speech perception, no difference was observed between proximal and distal translocation.

The electrode array position was reconstructed and evaluated from the postoperative CT imaging made in the first 24 h. Previous studies showed that a migration (25) or an extrusion of the electrode array is a complication that could be suspect when a gradual increase of the impedances is observed (26). In our study, there was no assessed a slight migration of the electrode array, however a postoperative CT scan was performed in case of an unexplained degradation or a persistence of poor hearing performance. Thus, no extrusion of the electrode array was detected in our series.

The study has some limitations. First: the groups (robot-assisted and manual insertion) were paired by age, duration of profound deafness and electrode array type. However, we cannot exclude variability due to the etiology of hearing loss. Second: the sampling method was taken in a non-probability way (hearing performance at 1 year of the first patients implanted by the robot). A randomized study would be required to compare the hearing performance of the robot-assisted array insertion to manual ones.

In summary, this is a preliminary study to provide hearing outcomes for robot-assisted electrode array insertion. Regardless the array insertion technique (robot-assisted or manual), our data suggest that restoration of high frequency thresholds (3,000–4,000–8,000 Hz) is associated with better speech perception in silence 1 year postoperatively. The intrascalar position of the array was not associated with hearing performance but proximal translocation was deleterious to high frequency thresholds. A prospective and randomized trial with comparable groups will be required to assess the relevance of robot-based insertion in hearing performance.

DATA AVAILABILITY STATEMENT

The raw data supporting the conclusions of this article will be made available by the authors, without undue reservation.

ETHICS STATEMENT

The studies involving human participants were reviewed and approved by CNIL N° 20191219182243. The patients/participants provided their written informed consent to participate in this study.

AUTHOR CONTRIBUTIONS

RT, HD, GL, OS, EF, IM, and YN contributed to conception and design of the study. RT and HD organized the database. RT performed the statistical analysis and wrote the first draft of the manuscript. All authors contributed to manuscript revision, read, and approved the submitted version.

FUNDING

The study was supported by research funding from Fondation pour l'Audition (Starting Grant IDA-2020), ANR Robocop ANR-19-CE19-0026-02.

ACKNOWLEDGMENTS

The authors appreciate the support of Institut de l'Audition and the Fondation pour l'Audition.

REFERENCES

1. Finley CC, Holden TA, Holden LK, Whiting BR, Chole RA, Neely GJ, et al. Role of electrode placement as a contributor to variability in cochlear implant outcomes. *Otol Neurotol.* (2008) 29:920–8. doi: 10.1097/MAO.0b013e318184f492
2. Holden LK, Finley CC, Firszt JB, Holden TA, Brenner C, Potts LG, et al. Factors affecting open-set word recognition in adults with cochlear implants. *Ear Hear.* (2013) 34:342–60. doi: 10.1097/AUD.0b013e3182741aa7
3. Wanna GB, Noble JH, Carlson ML, Gifford RH, Dietrich MS, Haynes DS, et al. Impact of electrode design and surgical approach on scalar location and cochlear implant outcomes. *Laryngoscope.* (2014) 124 Suppl 6:S1–7. doi: 10.1002/lary.24728
4. O'Connell BP, Hunter JB, Wanna GB. The importance of electrode location in cochlear implantation. *Laryngoscope Investig Otolaryngol.* (2016) 1:169–74. doi: 10.1002/lio2.42
5. Gifford RH, Dorman MF, Skarzynski H, Lorens A, Polak M, Driscoll CLW, et al. Cochlear implantation with hearing preservation yields significant benefit for speech recognition in complex listening environments. *Ear Hear.* (2013) 34:413–25. doi: 10.1097/AUD.0b013e31827e8163
6. Kratchman LB, Blachon GS, Withrow TJ, Balachandran R, Labadie RF, Webster RJ. Design of a bone-attached parallel robot for percutaneous cochlear implantation. *IEEE Trans Biomed Eng.* (2011) 58:2904–10. doi: 10.1109/TBME.2011.2162512

7. Caversaccio M, Wimmer W, Anso J, Mantokoudis G, Gerber N, Rathgeb C, et al. Robotic middle ear access for cochlear implantation: first in man. *PLoS ONE.* (2019) 14:e0220543. doi: 10.1371/journal.pone.0220543
8. Vittoria S, Lahlou G, Torres R, Daoudi H, Mosnier I, Mazalaigue S, et al. Robot-based assistance in middle ear surgery and cochlear implantation: first clinical report. *Eur Arch Otorhinolaryngol.* (2021) 278:77–85. doi: 10.1007/s00405-020-06070-z
9. Barriat S, Peigneux N, Duran U, Camby S, Lefebvre PP. The use of a robot to insert an electrode array of cochlear implants in the cochlea: a feasibility study and preliminary results. *Audiol Neurootol.* (2021) 26:1–7. doi: 10.1159/000513509
10. Daoudi H, Lahlou G, Torres R, Sterkers O, Lefeuvre V, Ferrary E, et al. Robot-assisted cochlear implant electrode array insertion in adults: a comparative study with manual insertion. *Otol Neurotol.* (2021) 42:438–44. doi: 10.1097/MAO.0000000000003002
11. Torres R, Jia H, Drouillard M, Bensimon J-L, Sterkers O, Ferrary E, et al. An optimized robot-based technique for cochlear implantation to reduce array insertion trauma. *Otolaryngol Head Neck Surg.* (2018) 159:900–7. doi: 10.1177/0194599818792232
12. Torres R, Hochet B, Daoudi H, Carré F, Mosnier I, Sterkers O, et al. Atraumatic insertion of a cochlear implant pre-curved electrode array by a robot-automated alignment with the coiling direction of the scala tympani. *Audiol Neurotol.* (2021). doi: 10.1159/000517398. [Epub ahead of print]
13. Rüegg U, Dalbert A, Veraguth D, Röösli C, Huber A, Pfiffner F. Correlation between speech perception outcomes after cochlear implantation and postoperative acoustic and electric hearing thresholds. *J Clin Med.* (2021) 10:324. doi: 10.3390/jcm10020324
14. Carlson ML, Driscoll CLW, Gifford RH, Service GJ, Tombers NM, Hughes-Borst BJ, et al. Implications of minimizing trauma during conventional cochlear implantation. *Otol Neurotol.* (2011) 32:962–8. doi: 10.1097/MAO.0b013e3182204526
15. Maeda Y, Takao S, Sugaya A, Kataoka Y, Kariya S, Tanaka S, et al. Relationship between pure-tone audiogram findings and speech perception among older Japanese persons. *Acta Otolaryngol.* (2018) 138:140–4. doi: 10.1080/00016489.2017.1378435
16. Torres R, Drouillard M, De Seta D, Bensimon J-L, Ferrary E, Sterkers O, et al. Cochlear implant insertion axis into the basal turn: a critical factor in electrode array translocation. *Otol Neurotol.* (2018) 39:168–76. doi: 10.1097/MAO.0000000000001648
17. Monsell EM. New and revised reporting guidelines from the committee on hearing and equilibrium. American Academy of Otolaryngology-Head and Neck Surgery Foundation, Inc. *Otolaryngol Head Neck Surg.* (1995) 113:176–8. doi: 10.1016/S0194-5998(95)70100-1
18. Mukari SZMS, Yusof Y, Ishak WS, Maamor N, Chellapan K, Dzulkifli MA. Relative contributions of auditory and cognitive functions on speech recognition in quiet and in noise among older adults. *Braz J Otorhinolaryngol.* (2020) 86:149–56. doi: 10.1016/j.bjorl.2018.10.010
19. Motlagh Zadeh L, Silbert NH, Sternasty K, Swanepoel DW, Hunter LL, Moore DR. Extended high-frequency hearing enhances speech perception in noise. *Proc Natl Acad Sci USA.* (2019) 116:23753–9. doi: 10.1073/pnas.1903315116
20. Mamelle E, Granger B, Sterkers O, Lahlou G, Ferrary E, Nguyen Y, et al. Long-term residual hearing in cochlear implanted adult patients who were candidates for electro-acoustic stimulation. *Eur Arch Otorhinolaryngol.* (2020) 277:705–13. doi: 10.1007/s00405-019-05745-6
21. Metzger L. *Intérêt d'un test d'audiométrie vocale adapté à chaque patient* (dissertation). Nancy: Université de Lorraine (2015). Available onlien at: http://docnum.univ-lorraine.fr/public/BUPHA_MAUDIO_2015_METZGER_LAURA.pdf
22. Atturo F, Barbara M, Rask-Andersen H. On the anatomy of the 'hook' region of the human cochlea and how it relates to cochlear implantation. *Audiol Neurootol.* (2014) 19:378–85. doi: 10.1159/000365585
23. Skinner MW, Holden TA, Whiting BR, Voie AH, Brunsden B, Neely JG, et al. In vivo estimates of the position of advanced bionics electrode arrays in the human cochlea. *Ann Otol Rhinol Laryngol Suppl.* (2007) 197:2–24. doi: 10.1177/00034894071160S401
24. Jwair S, Prins A, Wegner I, Stokroos RJ, Versnel H, Thomeer HGXM. Scalar translocation comparison between lateral wall and perimodiolar cochlear implant arrays - a meta-analysis. *Laryngoscope.* (2021) 131:1358–68. doi: 10.1002/lary.29224
25. Mitmann P, Rademacher G, Mutze S, Ernst A, Todt I. Electrode migration in patients with perimodiolar cochlear implant electrodes. *Audiol Neurootol.* (2015) 20:349–53. doi: 10.1159/000435873
26. Dietz A, Wennström M, Lehtimäki A, Löppönen H, Valtonen H. Electrode migration after cochlear implant surgery: more common than expected? *Eur Arch Otorhinolaryngol.* (2016) 273:1411–8. doi: 10.1007/s00405-015-3716-4

Conflict of Interest: The authors declare that the research was conducted in the absence of any commercial or financial relationships that could be construed as a potential conflict of interest.

Publisher's Note: All claims expressed in this article are solely those of the authors and do not necessarily represent those of their affiliated organizations, or those of the publisher, the editors and the reviewers. Any product that may be evaluated in this article, or claim that may be made by its manufacturer, is not guaranteed or endorsed by the publisher.

frontiers in Surgery

ORIGINAL RESEARCH
published: 29 September 2021
doi: 10.3389/fsurg.2021.736217

In Silico Assessment of Safety and Efficacy of Screw Placement for Pediatric Image-Guided Otologic Surgery

Jan Hermann[1], Fabian Mueller[1], Stefan Weber[1], Marco Caversaccio[2] and Gabriela O'Toole Bom Braga[1]*

[1] ARTORG Center for Biomedical Engineering Research, Faculty of Medicine, University of Bern, Bern, Switzerland,
[2] Department of Otorhinolaryngology, Head and Neck Surgery, Inselspital, University Hospital Bern, Bern, Switzerland

Introduction: Current high-accuracy image-guided systems for otologic surgery use fiducial screws for patient-to-image registration. Thus far, these systems have only been used in adults, and the safety and efficacy of the fiducial screw placement has not yet been investigated in the pediatric population.

Materials and Methods: In a retrospective study, CT image data of the temporal region from 11 subjects meeting inclusion criteria (8–48 months at the time of surgery) were selected, resulting in $n = 20$ sides. These datasets were investigated with respect to screw stability efficacy in terms of the cortical layer thickness, and safety in terms of the distance of potential fiducial screws to the dura mater or venous sinuses. All of these results are presented as distributions, thickness color maps, and with descriptive statistics. Seven regions within the temporal bone were analyzed individually. In addition, four fiducial screws per case with 4 mm thread-length were placed in an additively manufactured model according to the guidelines for robotic cochlear implantation surgery. For all these screws, the minimal distance to the dura mater or venous sinuses was measured, or if applicable how much they penetrated these structures.

Results: The cortical layer has been found to be mostly between 0.7–3.3 mm thick (from the 5th to the 95th percentile), while even thinner areas exist. The distance from the surface of the temporal bone to the dura mater or the venous sinuses varied considerably between the subjects and ranged mostly from 1.1–9.3 mm (from the 5th to the 95th percentile). From all 80 placed fiducial screws of 4 mm thread length in the pediatric subject younger than two years old, 22 touched or penetrated either the dura or the sigmoid sinus. The best regions for fiducial placement would be the mastoid area and along the petrous pyramid in terms of safety. In terms of efficacy, the parietal followed by the petrous pyramid, and retrosigmoid regions are most suited.

Conclusion: The current fiducial screws and the screw placement guidelines for adults are insufficiently safe or effective for pediatric patients.

Keywords: image-guided surgery, pediatric, cortical layer, screw placement, skull thickness, robotics

OPEN ACCESS

Edited by:
Olivier Sterkers, Sorbonne Universités, France

Reviewed by:
Vincent Van Rompaey, University of Antwerp, Belgium
Hans Thomeer, University Medical Center Utrecht, Netherlands

****Correspondence:***
Fabian Mueller
fabian.mueller@artorg.unibe.ch

Specialty section:
This article was submitted to Otorhinolaryngology - Head and Neck Surgery, a section of the journal Frontiers in Surgery

Received: *04 July 2021*
Accepted: *02 September 2021*
Published: *29 September 2021*

Citation:
Hermann J, Mueller F, Weber S, Caversaccio M and O'Toole Bom Braga G (2021) In Silico Assessment of Safety and Efficacy of Screw Placement for Pediatric Image-Guided Otologic Surgery. Front. Surg. 8:736217. doi: 10.3389/fsurg.2021.736217

INTRODUCTION

Image guidance provides a technological solution for accurate anatomy and instrument localization through anatomy-to-image registration (1). Registration is the process of finding the transformation that maps a point in the anatomy with a corresponding point on the image. Commonly used methods include paired-point-based registration (with fiducial points), surface-based registration and more rarely automatic registration (2). Additionally, image-guided surgery (IGS) uses tracking systems which allows real-time determination of instrument position. The tracking system is based on either electromagnetic or optical tracking and both require the placement of an intraoperative tracker (2, 3). Lastly, the image is transferred to the IGS software and the displayed information can be used to localize in real time anatomical structures.

Otorhinolaryngological applications to date are mainly focused on rhinology. In endoscopic sinus surgery (ESS), the use of image guidance has demonstrated a potential to improve surgical outcomes (1). Achieving total resection in tumor cases, confirming complete anatomical dissection, and assisting in intraoperative decision-making are some of the applications of IGS. Recently, this technology has been applied in cochlear implant (CI) surgery with the use of fiducial screws for registration (3, 4). This requires the surgeon to implant and manually localize on the temporal bone each fiducial screw with a registration probe. The screws must be rigidly fixed to the skull and remain immovable on the bone. Failure to do so can result in registration error, inaccurate targeting, or damage to the related structures at the implantation and surgical sites (2, 5). The length and the number of the screws used vary according to the technology applied (e.g. template based, mechatronic arm). The Hannover group (6) uses five micro titanium screws of 1.5 × 6 mm (Martin, Tuttlingen, Germany) for registration, and a bone-anchored cranial reference array (BrainLAB AG, Munich, Germany), to reference the object and a reference adapter clamped to the surgical drill (Aesculap, Tuttlingen, Germany). Meanwhile, the template-based technique from Vanderbilt University uses 3 titanium anchors of 4 mm wide and 8 mm long with 4 mm of this length screwed into the skull (7). Currently, the Bern group (mechatronic arm) uses five 4 mm thread length titanium screws implanted on the skull, either bone screws intended for orthognathics (3, 8) or task-specific screws for image-guided application on the lateral skull base (9, 10). All these technologies are presently only used for adult patients.

Recent guidelines for cochlear implant surgery recommend implantation in pre-lingual phase as early as 6 months old in order to obtain optimal hearing outcomes (11). The bone growth process of the mastoid in small children has been shown to create additional surgical obstacles, especially during the first 4 years of life. Dura exposure during well preparation and facial nerve vulnerability at the mastoid tip are common in early childhood. In general, the posteroinferior portion of the temporalis muscle and along the supra-mastoid crest bear a bone thickness between 3–6 mm depending on age (10, 12, 13). Additionally, the growth process of the mastoid bone during childhood is accompanied by the increase in mastoid pneumatization. This ceases around puberty, with the development of the last air cells in the petrous apex (14). These air cells can create further difficulty for screw placement for it decreases the thickness of the cortical layer of the bone, which is defined as the dense outer surface of bone that forms a protective layer around the internal cavity (15). If the screw is placed in an air-cell, then screw stability, accuracy and procedure safety can potentially be compromised.

Another obstacle posed by the most recently described IGS techniques that can be applied in pediatrics for CI surgery is the need of a dynamic reference screw placement to bear the tracker as described in previous studies (3, 8, 10). This screw is usually placed towards the occipital region of the calvarium, increasing the chances of dura and vascular trauma. Recent studies for the use of IGS in pediatric subjects in CI surgery have demonstrated not enough bone support in some areas of the temporal bone, raising the need for age-specific screw designs (10). However, in the future it might not be necessary anymore to place multiple fiducial screws. Studies are being conducted to design a patient tracker that is fixed to the skull with only one screw and multiple legs, containing the necessary fiducials for IGS.

Hence, the primary aim of this study is to investigate the efficacy and safety of screw placement in pediatric cases. The efficacy is measured in terms of the thickness of the cortical layer of the temporal bone (CLT – cortical layer thickness) derived from computed tomography data of pediatric cases. The safety is measured in terms of distance to dura mater or venous sinuses (DDVS – distance to dura or venous sinuses), i.e. sigmoid and transverse sinus. The secondary aim is to further evaluate the safety of screw placement by implanting screws in patient-specific 3D-printed models, and subsequently investigating their distance to the dura and the venous sinus (4 mm thread length screws).

MATERIALS AND METHODS

Image Data

With permission of the local institutional review board (KEK 2017-01722), CT image data from 11 subjects meeting inclusion criteria (8–48 months at the time of surgery, CI surgery at the Otolaryngology Department of Inselspital between 2014 and 2017) were selected, resulting in $n = 20$ sides included in the study protocol. The two remaining sides were discarded due to image quality issues. An algorithm was used to estimate the thickness of the cortical bone and the distance of the fiducial screws to anatomical structures (dura and venous sinuses).

Phantom Preparation

Using medical image analysis software (Amira, Thermo Fisher Scientific, Waltham, Massachusetts, USA) the temporal bone, dura and sigmoid sinus were segmented (**Figure 1**). Surface models of the temporal bone were used for stereolithographic 3D-printed phantom creation (Eden260VS, Stratasys, MN, USA) where the fiducial screws were implanted following manufacturer's guidelines.

Each of the phantoms were implanted with four titanium reference cone screws (3.2 mm thread diameter × 4 mm thread length, and 9.3 mm total length, CASCINATION AG, Bern, Switzerland) on the mastoid tip, posterior to MacEwen's triangle

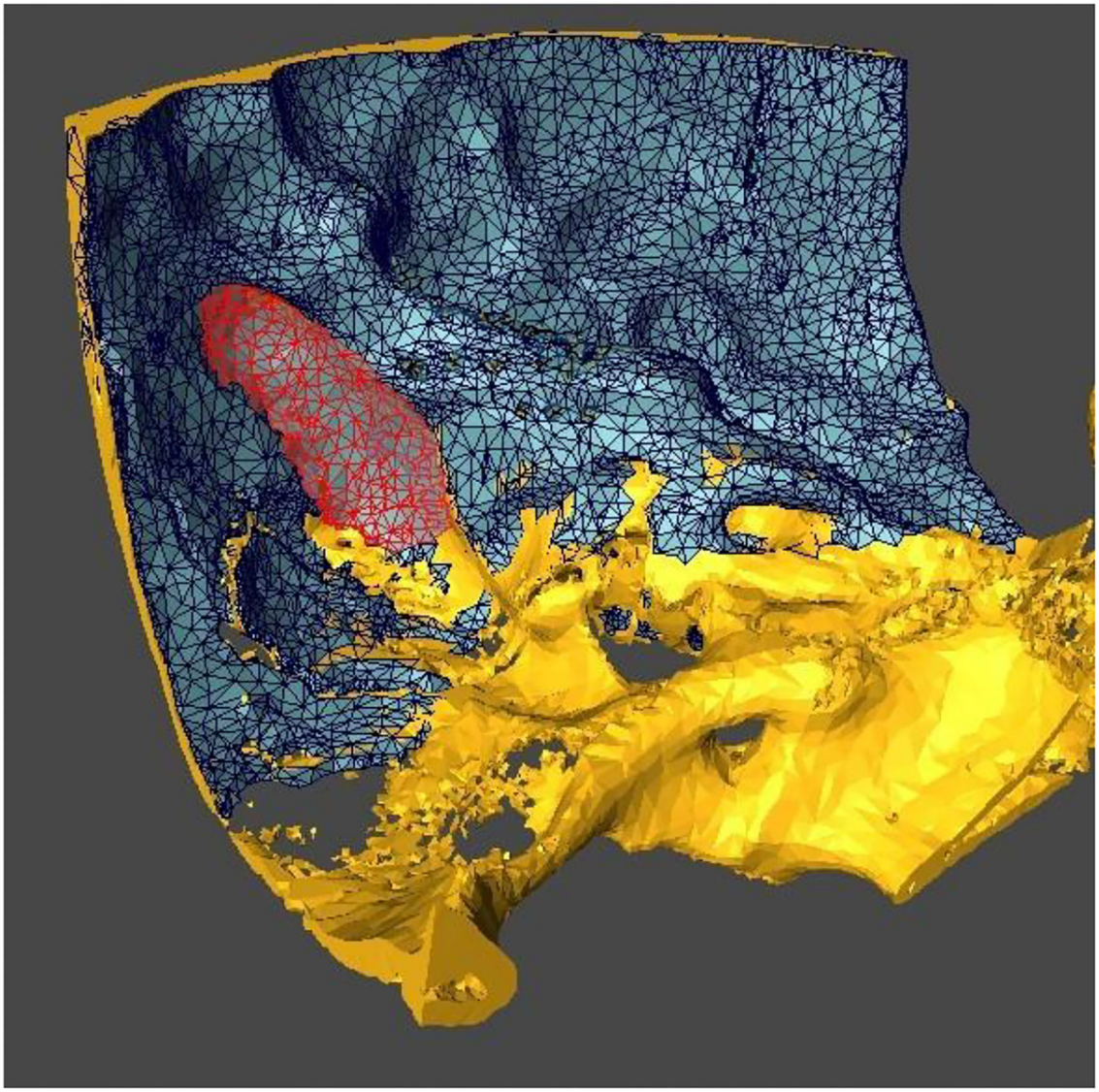

FIGURE 1 | Segmented temporal bone (yellow), dura (blue and black lines) and sigmoid sinus (red).

(temporal line superiorly tangent to external auditory canal and postero-inferior rim of the canal) and parallel to the temporal line and superior and posterior to the spine of Henle (**Figure 2**). The fifth screw, which is usually used to attach the patient tracker, was not placed in these phantoms. After insertion of the screws, high resolution computed tomography (CT) images (voxel size 0.15 $\times$ 0.15 $\times$ 0.2 mm^3, XCAT XL, Xoran, MI, USA) were acquired. By means of registration through a mutual information approach (Amira), the original CT was co-registered to the phantom cone-beam CT scan (CBCT) and the relative positions of the screws were added to the segmented temporal bone anatomy.

Thickness Analysis in Virtual Surface Meshes

A study was conducted to investigate the suitability of cortical bone thickness in the mastoid region at the potential sites for screw implantation. Available datasets were divided into four groups of different ages (group G1: 8–10 months old; group G2: 13–14 months old; group G3: 24 months old; group G4: 48 months old). Between all the aforementioned IGS techniques for CI surgery, we chose to use the most recent guidelines for screw placement provided by a commercially available otological surgical system (HEARO, CASCINATION AG, Bern, Switzerland). These techniques require the placement of five 4 mm thread length fiducial screws around the mastoid area.

To investigate bone thickness, measurements were conducted in digital reconstructed models of the temporal bone, and the results analyzed statistically, as well as presented as thickness maps over the region of interest. Similar measurement methodologies in digital reconstructed models have been used in the literature (13, 16, 17). Temporal bone segmentation was achieved using threshold adjustments such that the air cells

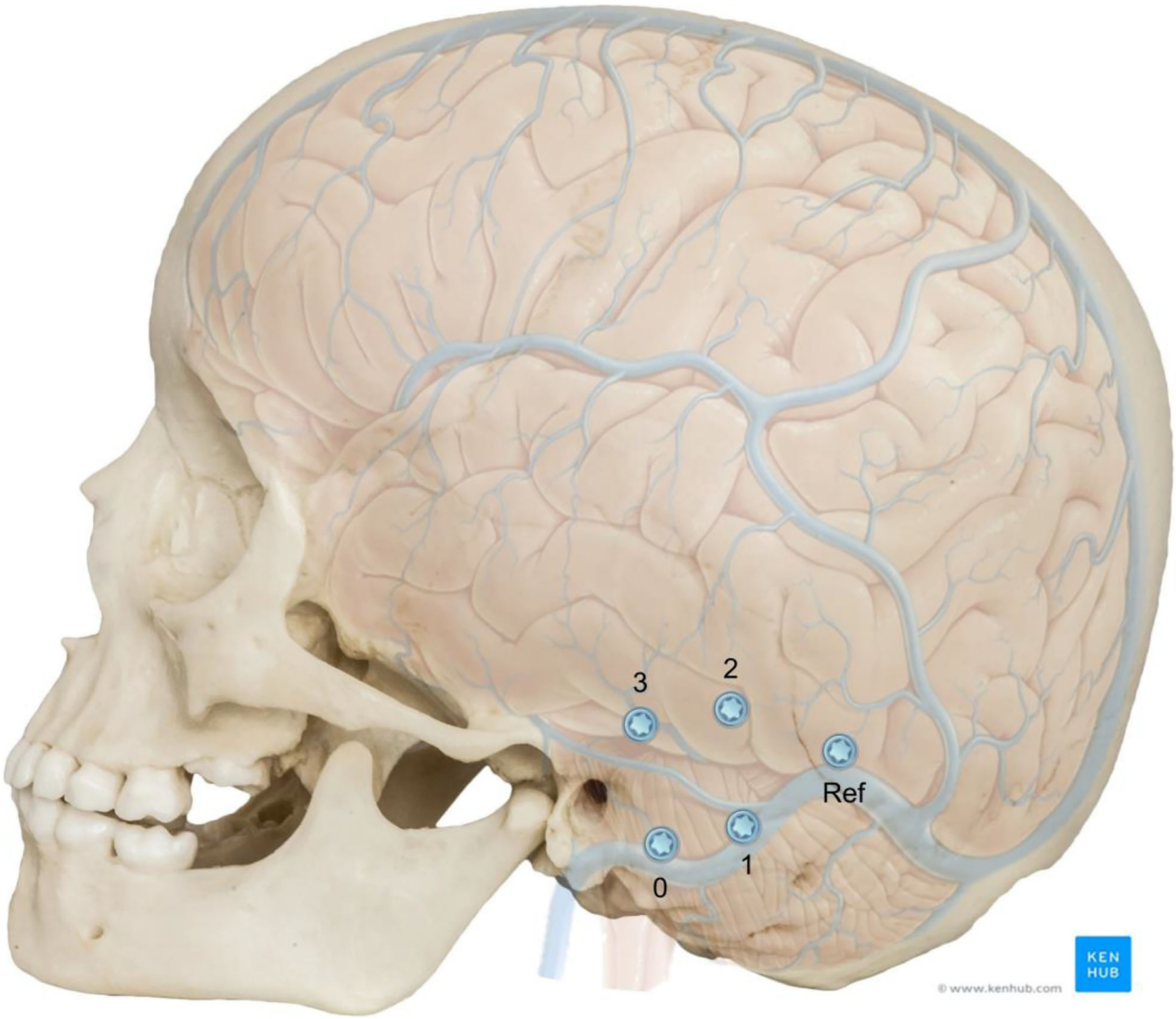

FIGURE 2 | Adjusted position of the fiducial screws relative to the neurovascular anatomy in a 5 year old skull. The screws positions were numbered for better identification and the reference screw position is shown. Image adapted from sources: © Bone Clones (www.boneclones.com); © Kenhub (https://www.kenhub.com/en/library/anatomy/veins-of-the-brain), Illustrator: P. Kim.

are included in the model, highlighting the cortical layer. All the temporal bones were aligned to a global axis to allow for calculation of descriptive statistics such as average measurements in the medical image analysis software Amira. The z-axis was chosen to be the auditory canal, pointing outwards. The x-axis is parallel to the temporal line pointing posteriorly. The region of interest for screw placement was described, as seen in **Figure 3**, first as a region between an angle of −60 and 30 degrees around the z-axis, with respect to the x-axis, and secondly between a radius of 15 and 50 mm from the origin in the external auditory canal with a linear angular relationship. The maximal distance of 50 mm lies along a line with an inclination of 30 degrees. The individual regions are separated as shown in **Figure 3**. The mastoid region is contained within a circle band of 15 to 30 mm in diameter, separated by a 45 degree line. The petrous pyramid is contained within a region at an angle of 45 degrees, with a band thickness of 15 mm, separated from the parietal region at a distance from origin at the center of the auditory canal of 30 mm. This region is shifted 4 mm in the negative y-axis direction. The mastoid tip region is defined as all space within the region of interest below 8 mm from the origin in the negative y-axis direction, and not further than 16 mm from the origin in the negative x-axis direction.

The dura mater and sigmoid sinus segmentation used the already segmented temporal bone, in a way that only the medial (interior) surface was segmented. The interior surface of the bone also contains channels from nerves and vessels, which were removed manually from the three-dimensional mesh. The

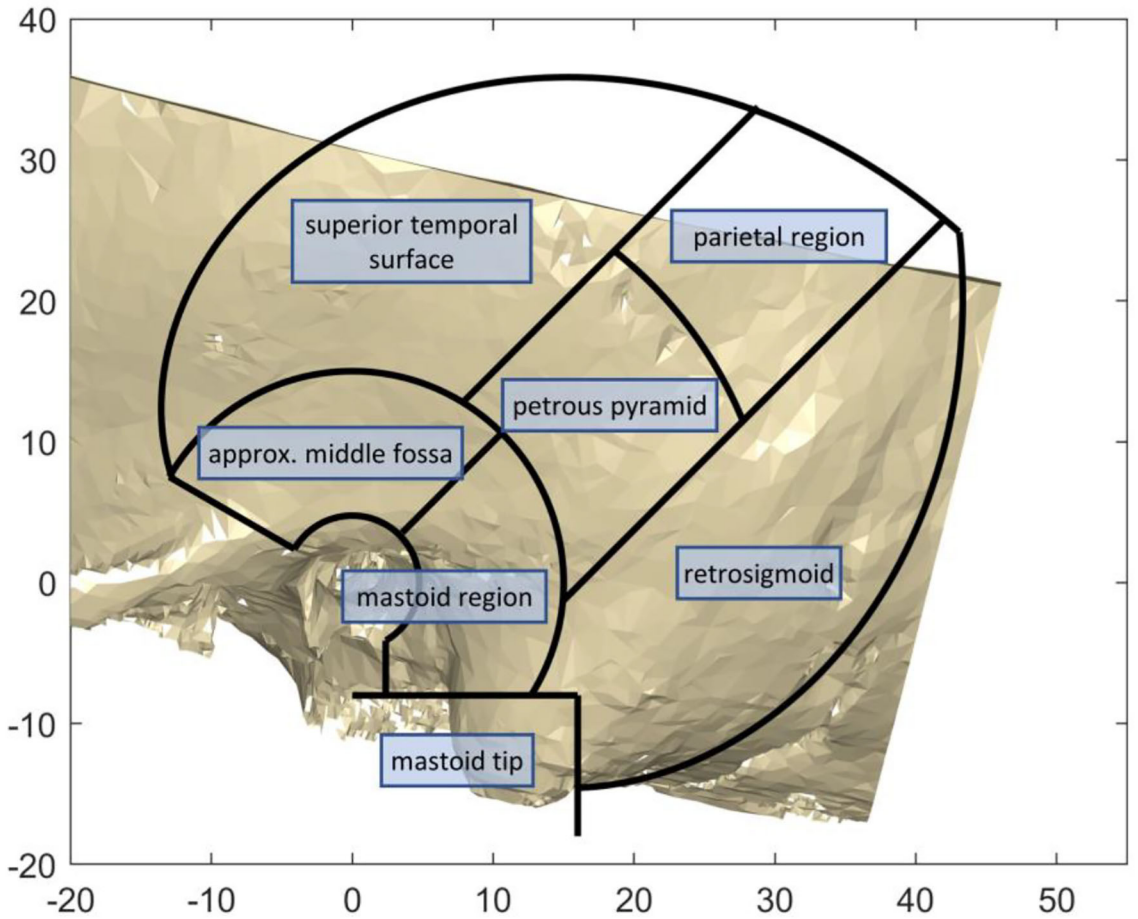

FIGURE 3 | The anatomical regions of the temporal bone used for the analysis.

fiducial screws were also segmented, and the axes were manually determined using the tip and screw head. All the data was exported as STL files providing a 3D representation.

The available cortical bone thickness in the temporal bone region, the CLT, was measured in the surface mesh data from the segmented temporal bones with a custom-developed script in MATLAB (MathWorks, Natick MA, USA). Thickness was calculated as the minimal distances from grid points projected onto the surface of the temporal bone to the nearest opposite surface. These opposite surfaces can be either an air cell or the interior surface of the temporal bone.

The distance from the surface of the temporal bone to either dura mater or the venous sinuses, the DDVS, was calculated as the minimal distances from projected grid points onto the surface of the temporal bone to a manually segmented dura and sigmoid sinus surface mesh.

The measurements of the distance of the fiducial tip to the dura or sigmoid sinus were carried out by first determining the screws head and tip points. Then, either the minimal distance was measured from the screw tips to the dura mesh, or how much the tip lies beyond the dura mesh along the axis of the screw.

RESULTS

Without prior knowledge the screws can easily be placed in areas where the distance to the dura or the venous sinuses is short (**Figure 4**). In fact, the distance between the screws and the anatomical structures underneath expose a separation of less than 0 mm demonstrating potential trauma to the dura mater or the venous sinuses in all four age groups. From all 80 placed fiducial screws in the 3d-printed temporal bones, 22 would likely have touched or penetrated either the dura mater or the venous sinuses if it had been a patient.

The results show a great anatomical variance between the 11 subjects, even unrelated to age. A result overview is displayed in **Figure 4**, showing the histogram of the CLT and the DDVS. Additionally, both of these measurements are presented as color maps overlying the 3D reconstructed model from the CT scan. On these maps, the color corresponds to the measurement value, as indicated by the color bar on the right of the figure. The DDVS varied considerably between the subjects and ranged mostly from 1.1 to 9.3 mm on average (from the 5^{th} to the 95^{th} percentile), depending on the location.

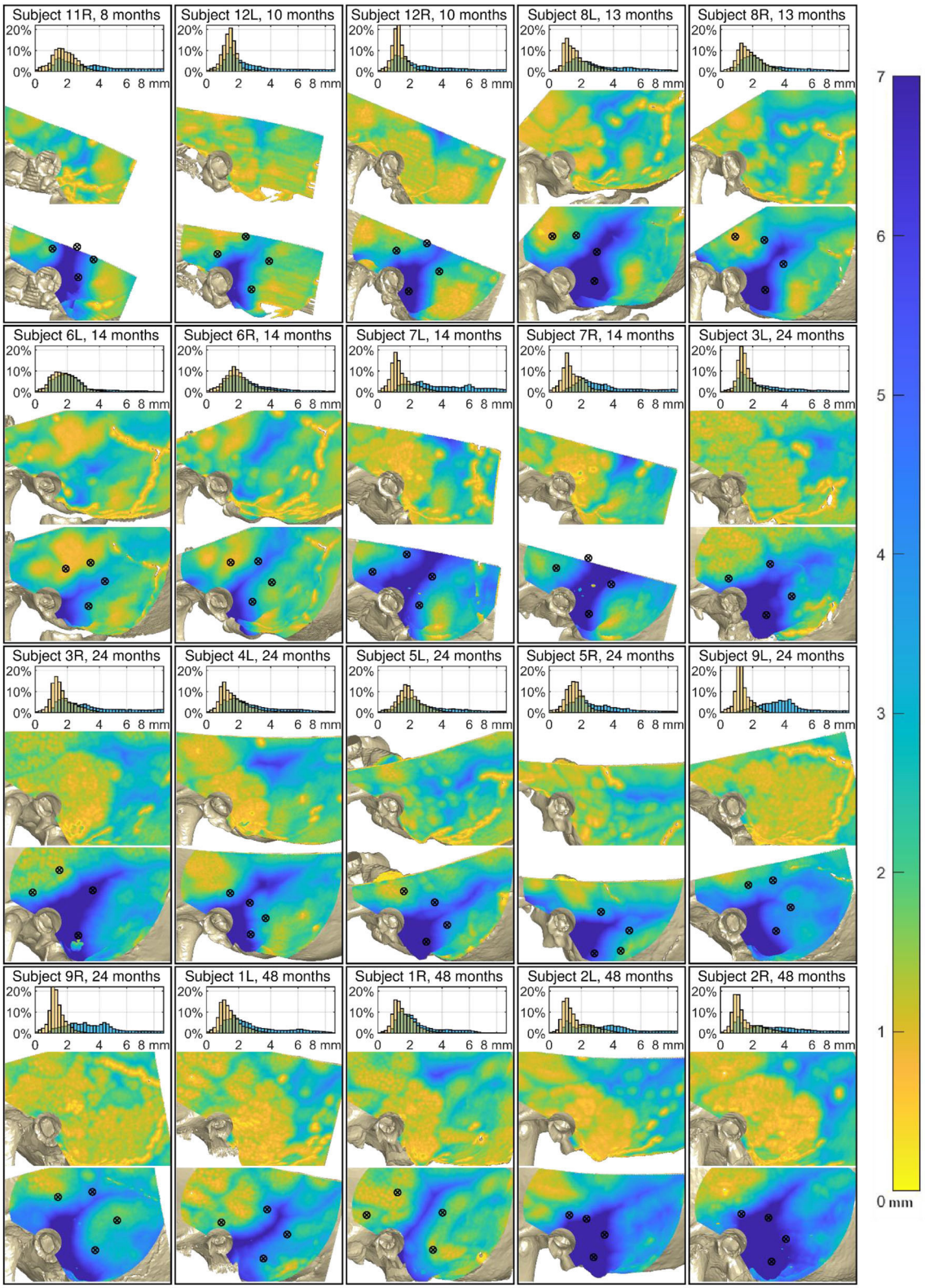

FIGURE 4 | Analysis of the 20 cases. Top of each case: Relative distribution of the cortical layer thickness (CLT, orange) and the distance to the dura or venous sinuses (DDVS, light blue). Middle: The thickness of the cortical layer. Bottom: The distance to the dura or the venous sinuses. The black markers designate the locations where the fiducial screws were placed. The maps of all subjects are aligned relative to the external auditory canal and temporal line.

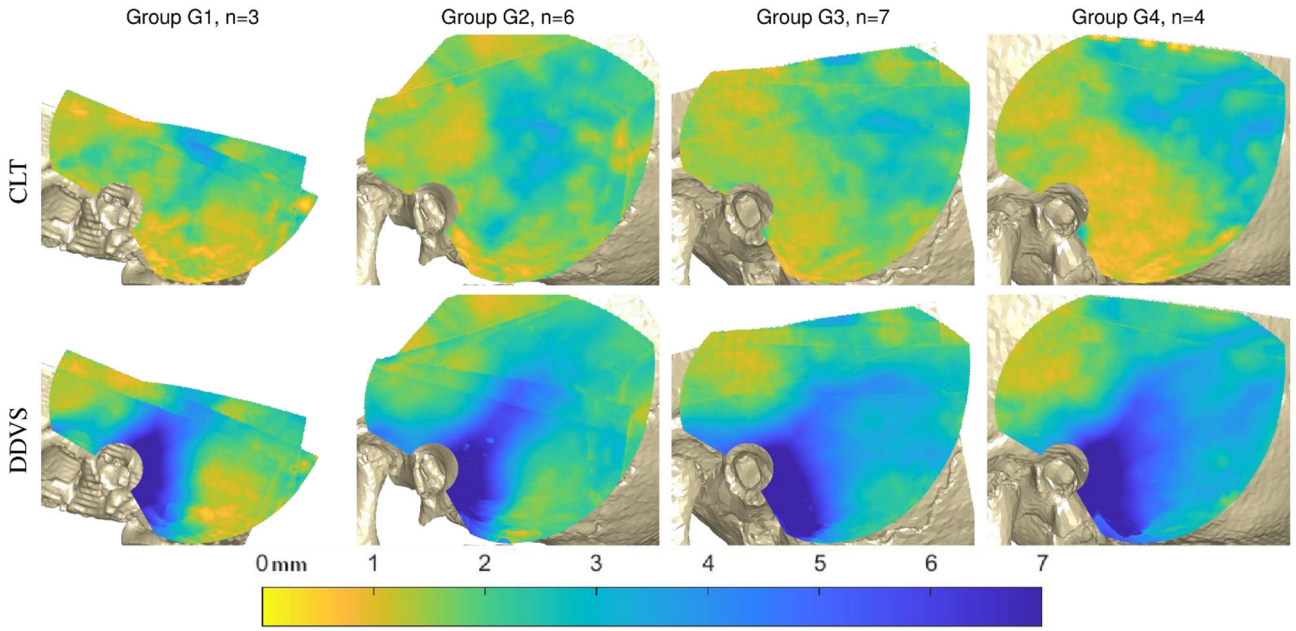

FIGURE 5 | Analysis of the 20 cases in age groups. Top: the average cortical layer thickness (CLT). Bottom: the average distance to dura mater or venous sinuses (DDVS) in all subjects according to the age groups G1 (8–10 months old), G2 (12–14 months old), G3 (24 months old), and G4 (48 months old).

Figure 5 shows the average measurements taken on the reconstructed CT scan per subject groups based on age. While the mastoid pneumatization with air cells is not yet visible in the younger age groups G1, and G2, it can clearly be distinguished in groups G3, and G4.

The mastoid region and petrous pyramid can be clearly seen due to the long distance to the dura and venous sinuses (**Figure 6**, bottom left), while the superior temporal surface shows short distances (**Figure 6**, top left). The minimal cortical layer map show the minimal cortical thickness values encountered across all subjects. This map demonstrates how almost everywhere in the region of interest for screw placement, an air cell or thin cortical layer could be encountered, especially in the mastoid area. The fine yellow lines in that figure stem from either the borders of the reconstructed temporal bone models, or from the cranial suture lines (**Figure 6**, top right). The minimal distance map of the DDVS on the bottom right shows that in the mastoid region, along the petrous pyramid, and at small areas within the parietal and retrosigmoid regions, there are places where the minimal distance to the delicate anatomical structures dura mater and venous sinuses is greater or equal than 2 mm. However, this area is small and non-uniform (**Figure 6**, bottom right).

The cortical layer has been found to be mostly 0.7–3.3 mm thick (from the 5th to the 95th percentile) in the region of interest for screw placement in all four age groups. In all age groups there are areas that are thinner than 0.7 mm, and areas that are thicker than 3.3 mm (**Figure 7**). For screw placement efficacy in terms of the cortical layer thickness, the parietal region followed by the petrous pyramid regions and retrosigmoid regions seem best, with cortical layer thicknesses of mostly 1.0–3.9 mm and a median of 2.3 mm, mostly 0.9–4.3 mm with a median of 1.9 mm, and 0.7–3.3 mm and a median of 1.7 mm, respectively. For screw placement safety in terms of the distance to dura or venous sinuses, the mastoid region is best with distances mostly between 2.0 and 11.1 mm and a median of 7.3 mm, followed by the petrous pyramid region with distances of 1.7–7.1 mm with a median of 3.9 mm (see **Table 1**, **Figure 7**).

The results of the cortical layer thickness and the distance to dura mater or venous sinuses are summarized in **Table 1**, containing the 1st, 5th, and 95th percentile values, as well as the median over all 20 temporal bones.

DISCUSSION

Bone is a living tissue that is always under remodeling through a balanced process of resorption and formation that keeps bone integrity and homeostasis. Usually during the growth process the mastoid thickness increases from a minimum of 17 to 34 mm from 6 months to 20 years (19). These numbers are under the influence of factors such Eustachian tube permeability (that allows for middle ear ventilation through positive pressure), infection history, genetics and mechanical influences (20). Creating more or less aerated mastoids impacts on the thickness of the cortical layer and screw fixation. For example, case 5 (group G3, 24 months old) where the patient had bilateral ventilation tubes presenting a more aerated mastoid on the left side than the right side. Leading to a thicker cortical layer on the right side than on the left. Meanwhile, case 9 from the same age group but without evident history of middle ear disease, the patient presents less aeration than expected on both mastoids

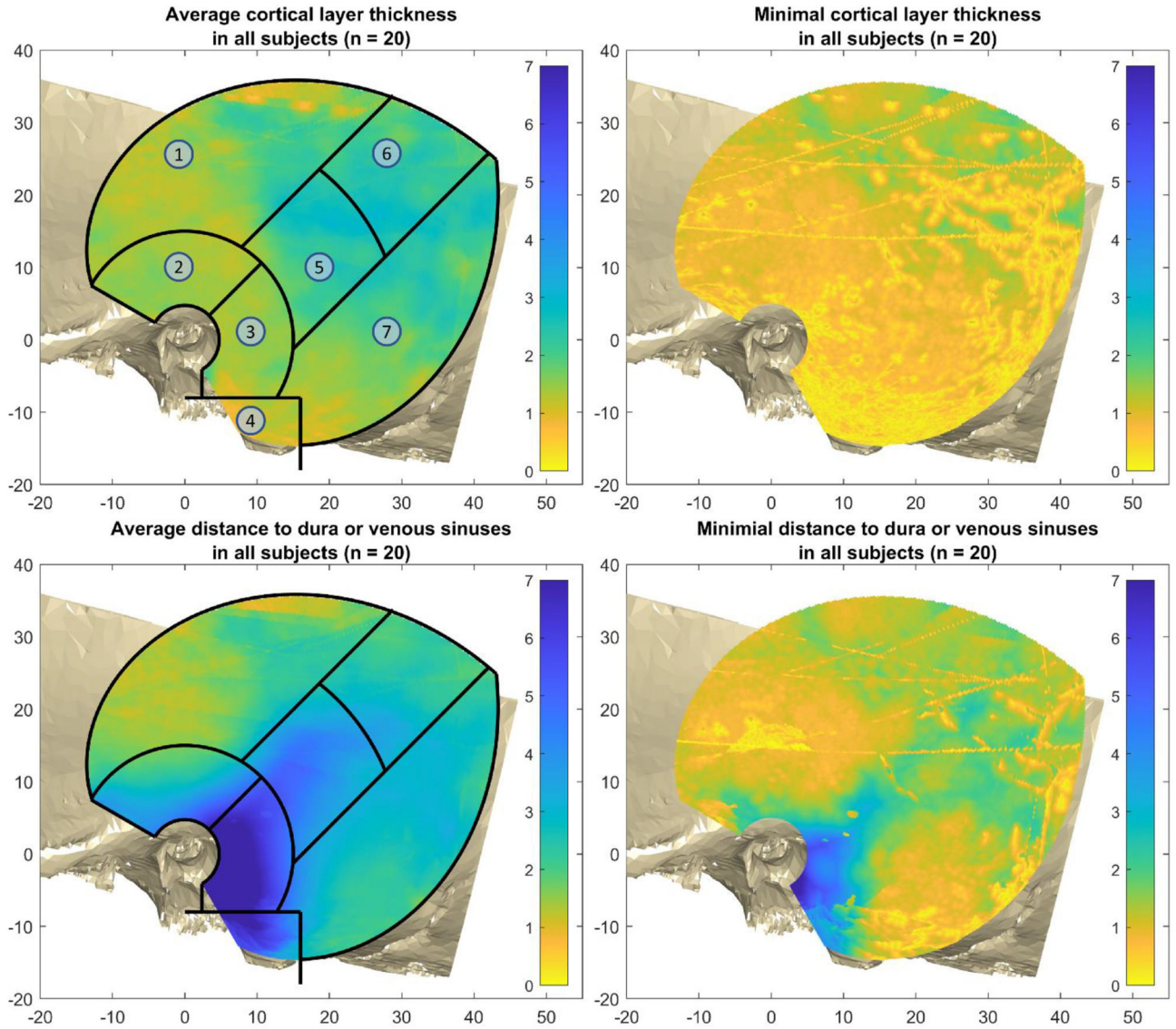

FIGURE 6 | Average and minimal thicknesses over all 20 subjects. Top left: the average cortical layer thickness (CLT). Top right: the minimal cortical layer thickness over all subjects. Bottom right: The average distance to dura or venous sinuses (DDVS). Bottom right: the minimal distance to dura or venous sinuses over all subjects. The regions are as follows: 1) superior temporal surface, 2) approximately the middle fossa, 3) mastoid region, 4) mastoid tip, 5) petrous pyramid, 6) parietal region, and 7) retrosigmoid region.

and thinner cortical layer. Other example are cases 3 and 4 (also in G3), where the mastoids have the expected aeration, a thin cortical layer with a thickness of no more than 2 mm is found. Similar situation is observed on cases 6 and 7 (in G2, 14 months old). Patient 6 presented soft density material taking over the mastoid and middle ear regions and a thicker cortical layer, typical of a diseased mastoid. While patient 7 had both cavities filled with air and a thinner cortical layer and, therefore, a higher chance of screw implantation in an air cell. Therefore, these cases demonstrate that not only the patient age should be taken under consideration but also their pathological history pose as a challenge for the use of IGS technology.

Due to the anatomical situation on the pediatric calvarium, the manufacturer's guidelines for screw positioning in adults had to be adapted to children. The mastoid tip actually has the lowest median cortical layer thickness, and a high median safety distance. However, in children the mastoid tip cannot be used as a screw placement due to the anatomical position of the facial nerve that is exposed until 2 years of age. This way, the screw placement had to be shifted to a more superior position, where the skull density (cartilaginous parts and not fully-ossified bones) create an additional obstacle. Causing the more superior screw to be often localized in the middle fossa region. Furthermore, to keep accuracy, a certain distance between

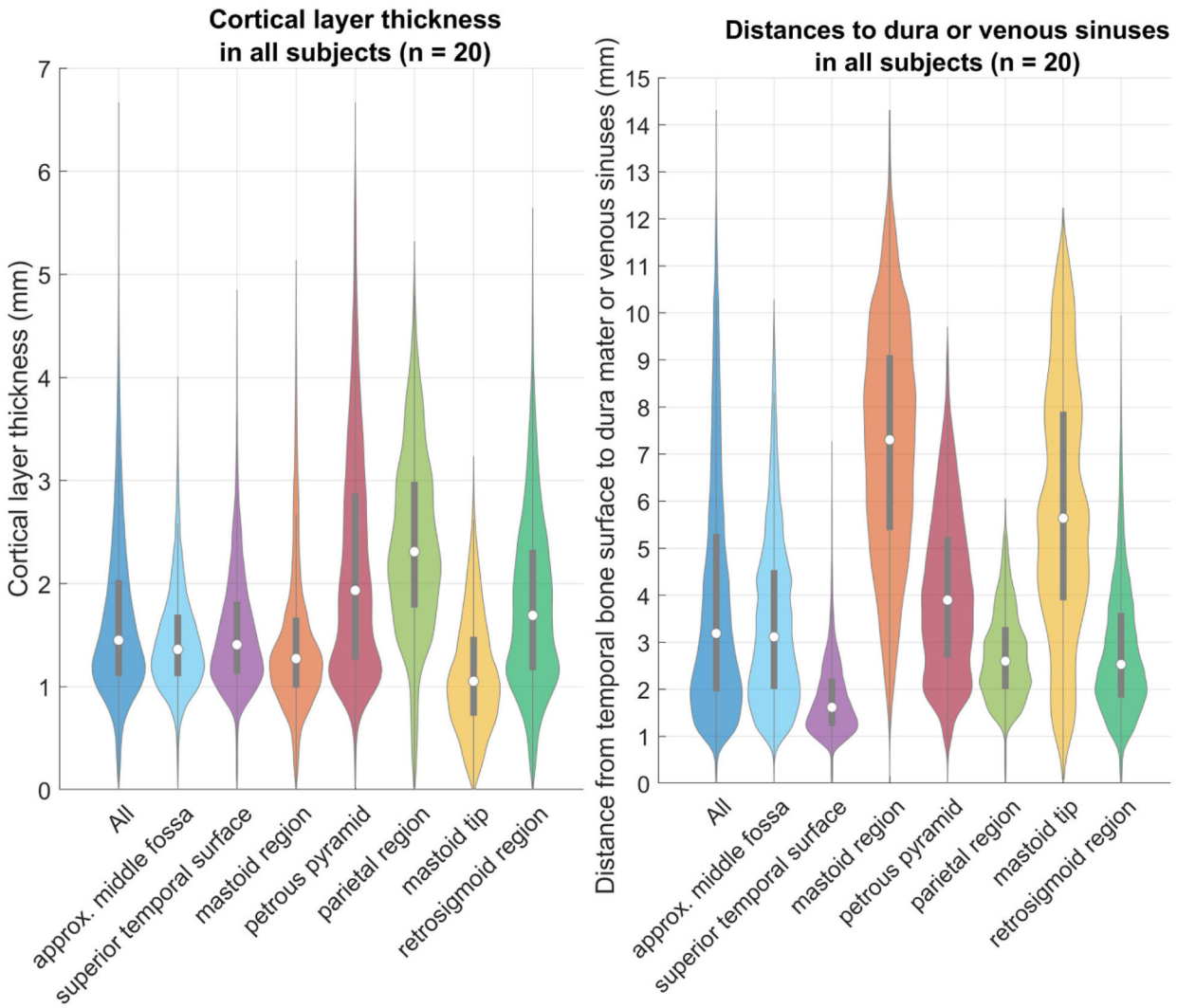

FIGURE 7 | Left: relative distributions of the cortical layer thickness (CLT) in the individual regions as defined above. Right: relative distributions of the distance to the dura or venous sinuses (DDVS). These violin plots are a variation of boxplots, that also show the distribution similar to a histogram (18). The gray bars within the violin plots are the lower and upper quartiles, and the white circle is the median value.

TABLE 1 | Select percentiles of both cortical layer thickness, and distance to dura mater or venous sinuses.

Percentile	**1st**	**5th**	**50th**	**95th**	**1st**	**5th**	**50th**	**95th**
Region	**CLT - cortical layer thickness (mm)**				**DDVS - distance to dura mater or venous sinuses (mm)**			
All	0.3	0.7	1.5	3.3	0.8	1.1	3.2	9.3
Approx. middle fossa	0.5	0.8	1.4	2.4	0.9	1.2	3.1	7.0
Superior temporal surface	0.5	0.8	1.4	2.6	0.5	0.9	1.6	3.3
Mastoid region	0.2	0.6	1.3	2.9	2.0	3.1	7.3	11.1
Petrous pyramid	0.6	0.9	1.9	4.3	1.0	1.7	3.9	7.1
Parietal region	0.4	1.0	2.3	3.9	1.0	1.4	2.6	4.5
Mastoid tip	0.1	0.3	1.2	2.2	0.9	1.5	5.6	10.3
Retrosigmoid region	0.3	0.7	1.7	3.3	0.7	1.1	2.5	5.5

the screws must be respected. Creating a smaller area for middle ear access trajectory placement in IGS surgery, while obeying the limits posed by the facial recess and cochlear angles on this age group. Although the mastoid bone itself present adequate thickness for the screws (10), the surrounding temporal bone is still not fully formed, so care must be taken to preserve enclosing anatomy. Especially the dura, sigmoid and transverse sinuses are at risk. Measurements of the positions of these structures are usually done with the aid of computed tomography, but excessive exposure to children to ionizing radiation should be avoided. The use of point-of-care ultrasound (POCUS) have also been mentioned in literature (21, 22) for fracture determination and bone-anchored hearing aid placement with promising results. The use of this technology can assist in screw placement for pediatric subjects before screw implantation.

The results show thin cortical layers in this pediatric population, which are mostly 0.6–3.2 mm thick (from the 5^{th} to the 95^{th} percentile) in the region of interest for screw placement across all subjects. Even if only the thickest regions (i.e. parietal, petrous pyramid, retrosigmoid) are considered, the thickness values are still in a similar range. Hence, it is likely that a thin cortical layer is encountered during screw placement, and the screws could become loose during surgery, leading to navigational errors and potentially dangerous situations. The results of the distance to dura mater or the venous sinuses are mostly 1.1–9.3 mm with a median of 3.3 mm. Thus, the screw placement with the thread lengths of the current IGS systems (i.e. around 4 mm) run into the risk of penetrating the dura mater or venous sinuses.

If a new screw thread length for this pediatric population had to be chosen, it would need to be only 0.8 mm long to be able to place the screw in 99% of the area of interest for screw placement across (see **Table 1**), and 1.1 mm long for 95% of the area of interest. If only the mastoid region, and petrous pyramid region was chosen, then the maximal screw thread length to place the screws in 99% of the area in the studied population (i.e. younger than 48 months old) would be 1.0, and 1.7 mm for 95%. Screws that are this small are bound to be less stable than the current screws, and thus could be dislocated easier. It would seem logical to adapt the registration probe to be as lightweight as possible, since in some systems currently the registration probe is a fairly heavy drilling end-effector with a registration tool inserted. The same logic applies to the patient tracker attached with the reference screw.

Limitations of this study are the manual rigid alignment of the anatomies for the statistics, and the small sample size. Calculating the average over multiple thickness maps includes the assumption that all data shares the same coordinate system. While the temporal bones have been rigidly aligned manually, no non-linear morphing of the anatomy was executed, which would make landmarks match locations (e.g. all ear canals, all mastoid tips, all temporal lines would be at the same coordinates). Especially in the data for the cortical layer, there are zero thickness values. These values stem mainly from the cranial suture lines, where the cortical layer thickness can be understood to be zero on the map. Although our sample size is small, some clinical considerations can be drawn regarding expected complications. Meningitis, fistula, thrombophlebitis, subdural empyema, otogenic suppurative thrombophlebitis, brain abscess and CSF (cerebral spinal fluid) leakage can be expected from damage to the dura. Venous air embolism, thrombosis, infarction, thrombophlebitis and death can happen if the sigmoid or the transverse sinuses (at risk with the reference screw positioning) are damaged. Although these complications are rare in daily CI surgical procedures, but with the introduction of new technology and its new requirements, care must be taken to avoid them.

This study demonstrated potential damage to the dura and venous sinuses in all screw positions for the pediatric population with the currently used fiducial screws and screw placement guidelines. The measurements taken show thin cortical layers, and short distances from the temporal bone surface to the delicate anatomy underneath.

CONCLUSION

Due to the thin cortical layer and distance to vital anatomical structures (e.g. dura mater, sigmoid and transverse sinuses), the current fiducial screws and the screw placement guidelines might pose a challenge for safety and efficacy in image-guided surgery for patients younger than 48 months old. Therefore, an adaptation of current fiducial screws and/or their placement is necessary. Additionally, the use of image-guided technology (e.g. with navigated surface matching), or technologies such as ultrasound for screw placement could potentially assist in increasing safety and efficacy of the procedure.

DATA AVAILABILITY STATEMENT

The raw data supporting the conclusions of this article will be made available by the authors, without undue reservation.

AUTHOR CONTRIBUTIONS

GO'T and JH created the study design. SW and MC reviewed the study design. MC provided the data used in the study. JH and FM developed the software for the analysis of the virtual surface meshes of the anatomy. GO'T, FM, and JH conducted the phantom study on the additively manufactured models. GO'T and JH analyzed the collected data and wrote the manuscript. All authors reviewed the manuscript and approved the submitted version.

FUNDING

This work was supported by the Swiss National Science Foundation SNF (Project 176007).

ACKNOWLEDGMENTS

We would like to thank Marco Matulic (CASCINATION AG, Bern, Switzerland) and Dr. Masoud Zoka Assadi (MED-EL GmbH, Innsbruck, Austria) for their support and assistance in study design aspects.

REFERENCES

1. Schmale IL, Vandelaar LJ, Luong AU, Citardi MJ, Yao WC. Image-guided surgery and intraoperative imaging in rhinology: clinical update and current state of the art. *Ear Nose Throat J*. (2020). doi: 10.1177/0145561320928202. [Epub ahead of print].
2. Balachandran R, Fritz MA, Dietrich MS, Danilchenko A, Mitchell JE, Oldfield VL, et al. Clinical testing of an alternate method of inserting bone-implanted fiducial markers. *Int J Comput Assist Radiol Surg.* (2014) 9:913–20. doi: 10.1007/s11548-014-0980-5
3. Weber S, Gavaghan K, Wimmer W, Williamson T, Gerber N, Anso J, et al. Instrument flight to the inner ear. *Sci Robot*. (2017) 2:eaal4916. doi: 10.1126/scirobotics.aal4916
4. Labadie RF, Balachandran R, Noble JH, Blachon GS, Mitchell JE, Reda FA, et al. Minimally invasive image-guided cochlear implantation surgery: first report of clinical implementation. *Laryngoscope.* (2014) 124:1915–22. doi: 10.1002/lary.24520
5. Schneider D, Hermann J, Mueller F, Braga GOB, Anschuetz L, Caversaccio M, et al. Evolution and stagnation of image guidance for surgery in the lateral skull: a systematic review 1989–2020. *Front Surg.* (2021) 7:604362. doi: 10.3389/fsurg.2020.604362
6. Majdani O, Bartling SH, Leinung M, Stöver T, Lenarz M, Dullin C, et al. True minimally invasive approach for cochlear implantation. *Otol Neurotol.* (2008) 29:120–3. doi: 10.1097/mao.0b013e318157f7d8
7. Labadie RF, Noble JH, Dawant BM, Balachandran R, Majdani O, Fitzpatrick JM. Clinical validation of percutaneous cochlear implant surgery: initial report. *Laryngoscope.* (2008) 118:1031–9. doi: 10.1097/MLG.0b013e31816b309e
8. Caversaccio M, Wimmer W, Anso J, Mantokoudis G, Gerber N, Rathgeb C, et al. Robotic middle ear access for cochlear implantation: first in man. *PLoS ONE.* (2019) 14:e0220543. doi: 10.1371/journal.pone.0220543
9. Schneider D, Stenin I, Ansó J, Hermann J, Mueller F, Pereira Bom Braga G, et al. Robotic cochlear implantation: feasibility of a multiport approach in an *ex vivo* model. *Eur Arch Oto-Rhino-Laryngology.* (2019) 276:1283–9. doi: 10.1007/s00405-019-05318-7
10. Bom Braga GOT, Schneider D, Muller F, Hermann J, Weber S, Caversaccio M. Feasibility of pediatric robotic cochlear implantation in phantoms. *Otol Neurotol.* (2020) 41:e192–200. doi: 10.1097/MAO.0000000000002434
11. Holman MA, Carlson ML, Driscoll CLW, Grim KJ, Petersson RS, Sladen DP, et al. Cochlear implantation in children 12 months of age and younger. *Otol Neurotol.* (2013) 34:251–8. doi: 10.1097/MAO.0b013e31827d0922
12. Simms DL, Neely JG. Thickness of the lateral surface of the temporal bone in children. *Ann Otol Rhinol Laryngol.* (1989) 98:726–31. doi: 10.1177/000348948909800913
13. Wimmer W, Gerber N, Guignard J, Dubach P, Kompis M, Weber S, et al. Topographic bone thickness maps for Bonebridge implantations. *Eur Arch Oto-Rhino-Laryngology.* (2015) 272:1651–8. doi: 10.1007/s00405-014-2976-8
14. Cinamon U. The growth rate and size of the mastoid air cell system and mastoid bone: a review and reference. *Eur Arch Oto-Rhino-Laryngology.* (2009) 266:781–6. doi: 10.1007/s00405-009-0941-8
15. Lillie EM, Urban JE, Lynch SK, Weaver AA, Stitzel JD. Evaluation of skull cortical thickness changes with age and sex from computed tomography scans. *J Bone Miner Res.* (2016) 31:299–307. doi: 10.1002/jbmr.2613
16. Rahne T, Svensson S, Lagerkvist H, Holmberg M, Plontke SK, Wenzel C. Assessment of temporal bone thickness for implantation of a new active bone-conduction transducer. *Otol Neurotol.* (2021) 42:278–84. doi: 10.1097/MAO.0000000000002919
17. Guignard J, Arnold A, Weisstanner C, Caversaccio M, Stieger C, A. Bone-thickness map as a guide for bone-anchored port implantation surgery in the temporal bone. *Mater (Basel, Switzerland).* (2013) 6:5291–301. doi: 10.3390/ma6115291
18. Bechtold B. *Violin Plots for Matlab, Github Project*. (2016)
19. Almuhawas FA, Dhanasingh AE, Mitrovic D, Abdelsamad Y, Alzhrani F, Hagr A, et al. Age as a factor of growth in mastoid thickness and skull width. *Otol Neurotol.* (2020) 41:709–14. doi: 10.1097/MAO.0000000000002585
20. Hindi K, Alazzawi S, Raman R, Prepageran N, Rahmat K. Pneumatization of mastoid air cells, temporal bone, ethmoid and sphenoid sinuses. Any correlation? *Indian J Otolaryngol Head Neck Surg.* (2014) 66:429–36. doi: 10.1007/s12070-014-0745-z
21. Parri N, Crosby BJ, Mills L, Soucy Z, Musolino AM, Da Dalt L, et al. Point-of-care ultrasound for the diagnosis of skull fractures in children younger than two years of age. *J Pediatr*. (2018) 196:230–6.e2. doi: 10.1016/j.jpeds.2017.12.057
22. Stölzel K, Bauknecht C, Wernecke K, Schrom T. Sonographische bestimmung der kalottendicke. *Laryngo-Rhino-Otologie.* (2006) 86:107–11. doi: 10.1055/s-2006-944755
23. Inc. SUI. Replica 5-year-old Human Child Skull Dentition Exposed For Sale – Skulls Unlimited International, Inc. Available online at: https://www.skullsunlimited.com/products/replica-5-year-old-human-child-skull-dentition-exposed-bc-189?variant=32142315225160. (accessed July 30, 2021)
24. Kenhub. Veins of the brain: Anatomy and clinical notes | Kenhub. Available online at: https://web.archive.org/web/20210730084322if_/https://www.kenhub.com/en/library/anatomy/veins-of-the-brain-the-brain. (accessed July 30, 2021)

Conflict of Interest: SW is cofounder, shareholder, and chief executive officer of CASCINATION AG, Bern, Switzerland, that commercializes the robotic cochlear implantation technology.

The remaining authors declare that the research was conducted in the absence of any commercial or financial relationships that could be construed as a potential conflict of interest.

Publisher's Note: All claims expressed in this article are solely those of the authors and do not necessarily represent those of their affiliated organizations, or those of the publisher, the editors and the reviewers. Any product that may be evaluated in this article, or claim that may be made by its manufacturer, is not guaranteed or endorsed by the publisher.

frontiers in Surgery

ORIGINAL RESEARCH
published: 29 September 2021
doi: 10.3389/fsurg.2021.742219

Robotic Cochlear Implant Surgery: Imaging-Based Evaluation of Feasibility in Clinical Routine

*Alice Barbara Auinger, Valerie Dahm, Rudolfs Liepins, Dominik Riss, Wolf-Dieter Baumgartner and Christoph Arnoldner**

Department of Otorhinolaryngology, Head and Neck Surgery, Medical University of Vienna, Vienna, Austria

Background: Robotic surgery has been proposed in various surgical fields to reduce recovery time, scarring, and to improve patients' outcomes. Such innovations are ever-growing and have now reached the field of cochlear implantation. To implement robotic ear surgery in routine, it is of interest if preoperative planning of a safe trajectory to the middle ear is possible with clinically available image data.

Methods: We evaluated the feasibility of robotic cochlear implant surgery in 50 patients (100 ears) scheduled for routine cochlear implant procedures based on clinically available imaging. The primary objective was to assess if available high-resolution computed tomography or cone beam tomography imaging is sufficient for planning a trajectory by an otological software. Secondary objectives were to assess the feasibility of cochlear implant surgery with a drill bit diameter of 1.8 mm, which is the currently used as a standard drill bit. Furthermore, it was evaluated if feasibility of robotic surgery could be increased when using smaller drill bit sizes. Cochlear and trajectory parameters of successfully planned ears were collected. Measurements were carried out by two observers and the interrater reliability was assessed using Cohen's Kappa.

Results: Under the prerequisite of the available image data being sufficient for the planning of the procedure, up to two thirds of ears were eligible for robotic cochlear implant surgery with the standard drill bit size of 1.8 mm. The main reason for inability to plan the keyhole access was insufficient image resolution causing anatomical landmarks not being accurately identified. Although currently not applicable in robotic cochlear implantation, narrower drill bit sizes ranging from 1.0 to 1.7 mm in diameter could increase feasibility up to 100%. The interrater agreement between the two observers was good for this data set.

Discussion: For robotic cochlear implant surgery, imaging with sufficient resolution is essential for preoperative assessment. A slice thickness of <0.3 mm is necessary for trajectory planning. This can be achieved by using digital volume tomography while radiation exposure can be kept to a minimum. Furthermore, surgeons who use the software tool, should be trained on a regular basis in order to achieve planning consistency.

Keywords: cochlear implantation, robotic surgery, robotic cochlear implantation, minimal invasive surgery, keyhole access

OPEN ACCESS

Edited by:
Olivier Sterkers, Sorbonne Universités, France

Reviewed by:
Ing Ping Tang, Universiti Malaysia Sarawak, Malaysia
Ghizlene Lahlou, Hôpitaux Universitaires Pitié Salpêtrière, France
Juan Anso, University of California, San Francisco, United States

****Correspondence:***
Christoph Arnoldner christoph.arnoldner@meduniwien.ac.at

Specialty section:
This article was submitted to Otorhinolaryngology - Head and Neck Surgery, a section of the journal Frontiers in Surgery

Received: *15 July 2021*
Accepted: *30 August 2021*
Published: *29 September 2021*

Citation:
Auinger AB, Dahm V, Liepins R, Riss D, Baumgartner W-D and Arnoldner C (2021) Robotic Cochlear Implant Surgery: Imaging-Based Evaluation of Feasibility in Clinical Routine. Front. Surg. 8:742219. doi: 10.3389/fsurg.2021.742219

INTRODUCTION

According to the World Health Organization, 430 million people require hearing rehabilitation due to hearing loss (WHO, 2021).[1] For people with no functional hearing, cochlear implantation (CI) has become the standard treatment for hearing rehabilitation (1). The standard procedure is a cortical mastoidectomy followed by a posterior tympanotomy. Both steps require extensive drilling of the mastoid bone. Additionally, during posterior tympanotomy, the facial nerve is at risk of injury. Within the last 30 years, the use of robotics for minimal invasive surgeries has been growing in various surgical fields such as orthopedic hip replacements, laparoscopic cholecystectomies, or urological, cardiological and transoral procedures (2–5). Recently, minimal invasive surgical techniques have been proposed for middle and inner ear access in order to reduce the extent of the surgical approach such as a direct access to the round window region originating from the surface of the mastoid and without performing a mastoidectomy (6, 7). Several studies using cadaveric specimens have proven feasibility of a robot to perform neurotological surgeries (8–11).

For robotic CI surgery, high expectations are raised for preserving residual hearing. The patients' outcome and hearing performance might be improved due to a reduced trauma to the inner ear. By eliminating the surgeon's tremor, more consistent insertion techniques can be achieved with a robot compared to manual insertion (12, 13). Labadie et al. reported on a stereotactic frame-based robotic CI surgery (14). Based on the robot developed by Bell et al. (11), CI surgery was later performed in a patient with a task-specific robotic system including computer-assisted surgery planning, intraoperative stereotactic image guidance, and multipolar facial neuromonitoring (15, 16). Since then, a few adult patients have been successfully implanted with this technique in Europe (17). CE mark for the so-called HEARO robot (CAScination AG, Bern, Switzerland and MED-EL GmbH, Innsbruck, Austria) was obtained in March 2020 for the use in patients above the age of 18 years (17). Using the HEARO system, a tunnel bordered by the facial nerve and chorda tympani is directly drilled through the mastoid to the round window (11, 15, 17). While the facial nerve is often skeletonized in conventional CI surgery, there is no direct visualization during robotic CI surgery. For the HEARO procedure, several safety steps are currently implemented (15, 17) and with current facial nerve monitoring using multipolar stimulation probes, sufficient safety distance margins $\geq$0.4 mm can be correctly identified (18). Safety margins $<$ 0.4 mm can be achieved without structural nerve damage, but whether the nerve's functional integrity can be preserved, remains unclear in clinical application (19).

The first step in robotic CI surgery is to assess a safe path for the drill through the facial recess. A surgical planning software is used to segment the middle and inner ear anatomy with manual, semiautomated and fully automated tools (20). Semiautomated instruments calculate anatomic models based on selected points on image data by the examiner, which can be completed within a few minutes. It can be also used to measure the cochlear duct length (CDL) and electrode visualization aids the surgeon to choose the most suitable electrode array. Consequently, complications such as incomplete insertion, tip fold-over or kinking can be reduced. In contrast, planning via manual segmentation is time consuming and has to be done by an experienced examiner.

So far, the robotic procedure has been done in only a few patients and its applicability in clinical routine needs yet to be assessed. The first step in preparing for robotic CI surgery is checking the feasibility based on the individual anatomy. Trajectory planning has to be performed on an otological software with uploaded image data (computed tomography or cone-beam tomography) in order to assess the ideal path to the round window, starting from the surface of the mastoid through the facial recess and to the middle ear. Consequently, it has to be evaluated if clinically available image data is sufficient for planning or if adaptations to the preoperative assessment are necessary. In this study, we evaluated the possibility of robotic CI surgery based on clinically available imaging. Results of the current study should improve preoperative management of CI candidates in order to fulfill all criteria for robotic CI surgery.

MATERIALS AND METHODS

Patients

Fifty patients (100 ears) with existing preoperative computed tomography (CT) scans who were planned for CI surgery at our department were consecutively screened for the study. Based on the clinically available preoperative CT scan, a trajectory path to the round window was assessed with OTOPLAN (CAScination AG, Bern, Switzerland in collaboration with MED-EL GmbH, Innsbruck, Austria), an otological planning software used on a computer tablet or a computer desktop. Preoperative imaging was usually performed in external and different radiological institutes and therefore, quality of image data differs. As the study was primarily performed to assess feasibility of planning a trajectory path to the round window, we did not exclude any patients in advance. All consecutive patients planned for CI surgery were included, whether they were adults, children, had chronic middle ear disease, were previously implanted with any type of hearing prosthesis or showed malformations. The study was approved by the local institutional review board (1620/2019) and the study was conducted according to the ethical standards of the Helsinki Declaration (21).

Procedures

Imaging files of preoperative CT scans were transferred to OTOPLAN in Digital Imaging and Communications in Medicine (DICOM) file format. For robotic CI surgery, a trajectory tunnel to the round window can be preoperatively planned with the software. Furthermore, the CDL can be assessed to enable individualized CI surgery in terms of choosing the correct electrode array length. Therefore, OTOPLAN guides segmentation of anatomic landmarks and enables 3D reconstruction of middle and inner ear structures based on selected points on CT images by an examiner. The software

[1]https://www.who.int/news-room/fact-sheets/detail/deafness-and-hearing-loss, accessed on May, 21st, 2021.

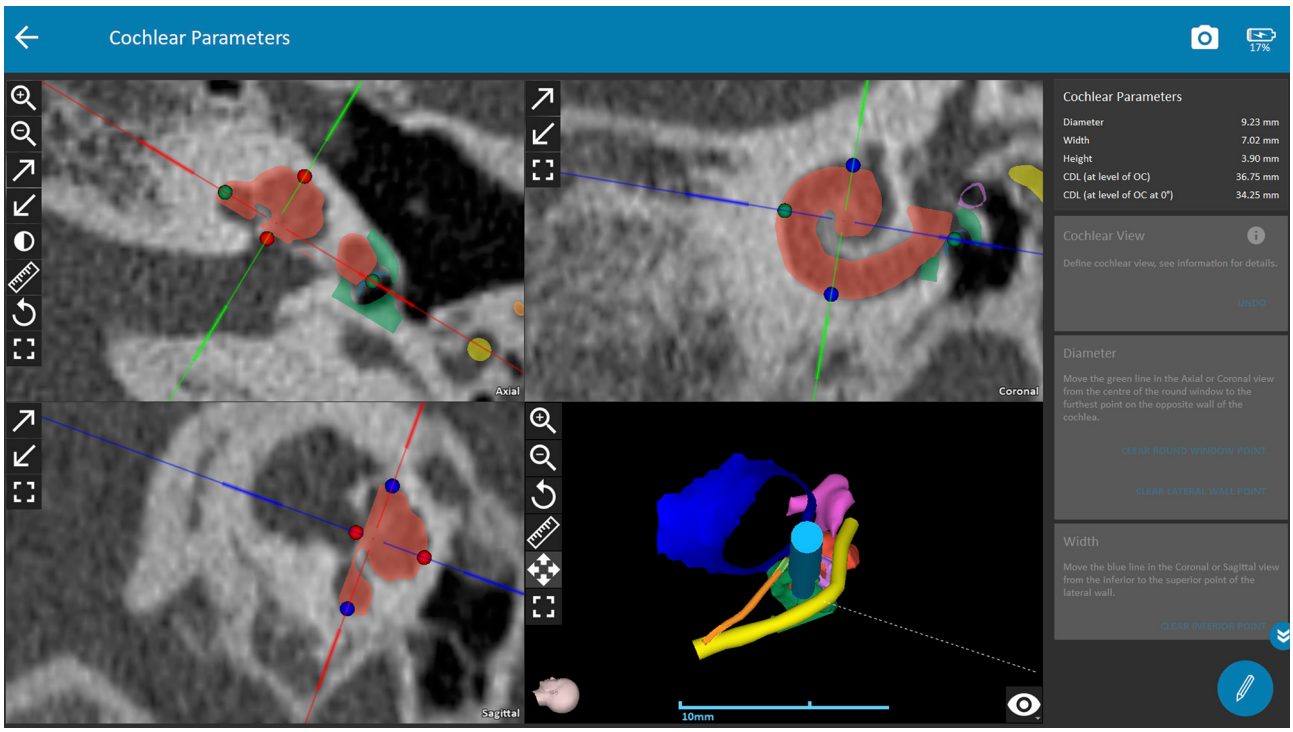

FIGURE 1A | Planning procedures with OTOPLAN. Cochlear view for assessing the software-guided cochlear parameters. The observer defines the cochlear view which corresponds to the center of the modiolus, the basal turn of the cochlear, and the round window in the axial, coronal and sagittal view. The diameter, height, width and length of the cochlear are then defined by the observer based on instructions of the software. Consequently, the software automatically calculates the cochlear parameters. The right lower picture displays a 3D model of the planned trajectory. Green dots (selection of round window and lateral wall), blue dots (selection of superior and inferior wall in coronal view), red dots (inferior and superior walls of cochlear in axial view), red shading (cochlear segmentation automatically calculated by the software), green shading (bony overhang automatically calculated by the software), yellow shading (facial nerve), dark blue shading (external ear canal), pink shading (ossicles), orange shading (chorda tympani), light blue shading (drill in position of the automated trajectory).

is fully compatible with the HEARO cochlear implant surgical robot. Postoperatively, the software allows for an anatomy-based fitting if the actual location of each electrode within the cochlear is displayed on cone beam CT.

Two examiners (observer 1 and observer 2) first checked if they could perform software-guided segmentation of anatomical landmarks based on image properties. In cases in which relevant anatomical structures could be sufficiently defined, planning of a 3D ear and a trajectory to the round window was performed. Both examiners were well trained in the use of the software and had experience for at least two years. Observer 1 was the first author of the study, observer 2 was an engineer of MED-EL (MED-EL GmbH, Innsbruck, Austria) who also instructs surgeons with the use of the software.

The trajectory for CI surgery was planned based on the instructions by the software. Both observers were blinded to the results of the other one and measured both ears of each patient independently. The software calculates 3D models of anatomic structures after manual selection of the following anatomical structures: the ear canal, incus, malleus, stapes, facial nerve, chorda tympani, sigmoid sinus, temporal bone and the cochlea. For assessing cochlear parameters, the examiner had to define the cochlear view (center of the modiolus, the basal turn of the cochlear, the round window in the axial, coronal and sagittal view, see **Figure 1A**). Cochlear parameters such as the diameter, width, height and the cochlear duct length were calculated by the software based on points selected by the examiner (round window, lateral, inferior and superior walls of the cochlear). Finally, a virtual trajectory to the round window was automatically calculated for a drill bit size of 1.8 mm which is the currently used as the standard size of the HEARO robotic system (see **Figure 1B**). A successful access to the cochlea was possible if sufficient safety margins of critical structures were maintained, which is a minimum of 0.4 mm to the facial nerve and 0.3 mm to the chorda tympani. Consequently, a facial recess of at least 2.5 mm is necessary to access the middle ear with a standard drill bit of 1.8 mm. If the output of an automated trajectory was not possible, adjustments were made. If there was still no safe access possible with the standard drill bit, the data was set as "not possible with standard drill bit." The next steps included evaluation of a safe access to the middle and inner ear with narrower drill bit sizes in 0.1 mm steps ranging from 1.7 to 1.0 mm as determined by the software. However, these calculations using smaller drill bits are more of a theoretic interest for future applications, as the HEARO procedure is based on the use of 1.8 mm drill bits as of today. If a safe trajectory could

be automatically computed by the software, the data was set as "possible with < 1.8 mm drill bit." For all successfully planned trajectories, the distance to relevant anatomical structures such as the facial neve, the chorda tympani, the ossicles, and the external auditory canal was noted. All distances were automatically calculated by the software. Furthermore, the in- and out-plane angles, also automatically calculated, were assessed. The software displays the in-plane angle as offset between an ideal trajectory and the planned trajectory with respect to the plane of the basal turn with a given target (round window) (22). The out-plane angle is computed as the offset between the planned trajectory and an ideal trajectory in the plane orthogonal to the basal turn. For cases in which a sufficient software-guided planning procedure was not possible, no such parameters were collected.

Statistics

Data of 50 patients (100 ears) were included in the study. Each ear was planned by two observers revealing 200 measured ears. The primary goal of the study was to assess how many of the available datasets were suitable for robotic CI surgery using the standard drill bit size. Secondary objective was to expand the possibility of robotic CI surgery based on the available imaging data if narrower drilling bits were used. Descriptive statistics, i.e., mean and standard deviation (SD) were computed for ear parameters. The interrater reliability between the two observers was assessed based on Cohen's Kappa. A Cohen's Kappa (K) of $\leq$0.1 corresponds to no agreement, $0.1 < K \leq 0.4$ weak agreement, $0.4 < K \leq 0.6$ good agreement, $0.6 < K \leq 0.8$ strong agreement and $0.8 < K \leq 1$ complete agreement.[2] Statistical analysis was performed using MATLAB (The Mathworks, Inc., Natick, USA).

RESULTS

Image data of 100 ears from 50 patients (26 males, 24 females) with a mean age of 51 +/−23 years were independently analyzed by the two observers. Image resolution ranged from 0.1 x 0.1 x 0.1 mm^3 to 0.6 x 0.6 x 1.5 mm^3. For observer 1, 39 out of 100 ears (39%) were rated as sufficient in order to perform the software-guided planning procedure, whereas observer 2 rated data of 46 ears (46%) as sufficient. Consequently, computation of cochlear and trajectory parameters was not possible in the remaining ears and reasons for planning failures are depicted in **Table 1**. Image slice thickness was categorized in three groups (slice thickness $\leq$ 0.3 mm, > 0.3 and $\leq$ 0.5 mm, > 0.5 mm). Percentages of useful imaging quality according to slice thickness group are depicted in **Figure 2**. None of the scans with a slice thickness of > 0.5 mm enabled assessment of a safe virtual trajectory to the round window. A minimum distance to critical anatomic landmarks has to be maintained for successful planning. Mean distances to certain important structures are shown in **Table 2**.

Observer 1 could plan a safe trajectory in 19 ears (48.7%,) out of 39 sufficiently measurable images. Observer 2 successfully planned 35 out of 46 sufficiently measurable (76.1%) ears. Both these measurements were carried out using the 1.8 mm standard drill bit size. Measurements were then repeated with smaller drill bit sizes with 0.1 mm steps (1.0–1.7 mm). Consequently, the feasibility of the HEARO procedure could be increased to 100% of patients rated as sufficient for the planning procedure. **Table 3** depicts successfully planned cases based on the used drill bit size as suggested by the planning software. The calculations for the interrater reliability (trajectory planning) revealed 0.52 corresponding to a good agreement.

The mean safety distances achieved in successfully planned trajectories (including all drill bit sizes) as well as the diameter of the facial recess, the in- and out-plane angles are depicted in **Table 2**. Cochlear parameters such as the cochlear diameter, height, width, and length are also reported as mean and standard deviation in **Table 2**.

TABLE 1 | Reasons for trajectory planning failures.

	Examiner 1	Examiner 2
Bad image resolution	37 (60.7%)	36 (66.7%)
Software failure	9 (14.8%)	5 (9.3%)
Incomplete 3D ear	9 (14.8%)	9 (16.7%)
Corrupted image	6 (9.8%)	4 (7.4%)
	61	54

The number and percentage (%) of planning failures based on depicted reasons. An incomplete 3D ear was existent in cases in which anatomical landmarks could not be sufficiently annotated (i.e. malformations of the middle ear or a preexisting CI on the contralateral ear in one case).

DISCUSSION

With an increasing application of robotics in ear surgery, it is of interest how patients should be properly prepared for surgery. One essential step is preoperative planning of the trajectory path to the region of interest, which is the round window in case of CI surgery. The primary goal of the study was to assess feasibility of robotic CI surgery based on clinically available data of CT scans, which are mostly performed in external radiologic institutes and have therefore different image quality.

The standard drill bit size used by the HEARO robot is currently 1.80 mm in diameter. In this study and depending on the examiner, up to two thirds of measured ears were eligible for the HEARO procedure with the standard drill bit if image data was rated as sufficient. Williamson et al. created a statistical model in which approximately 46.7% of the population could accommodate necessary safety regions with a standard drill bit of 1.8 mm and a CT slice thickness of 0.2 mm (23), which is similar to our results. The smallest drill bit size the software offers is 1 mm. In the current study population, feasibility of robotic CI surgery could be increased if narrower drill bit sizes were used. This was of theoretic interest for future applications as the HEARO procedure is currently based on the use of 1.8 mm drill bits, but providing the HEARO robot with narrower drill bit sizes in the future, extension of candidacy seems achievable.

[2]https://www.medistat.de/glossar/uebereinstimmung/cohens-kappa-koeffizient

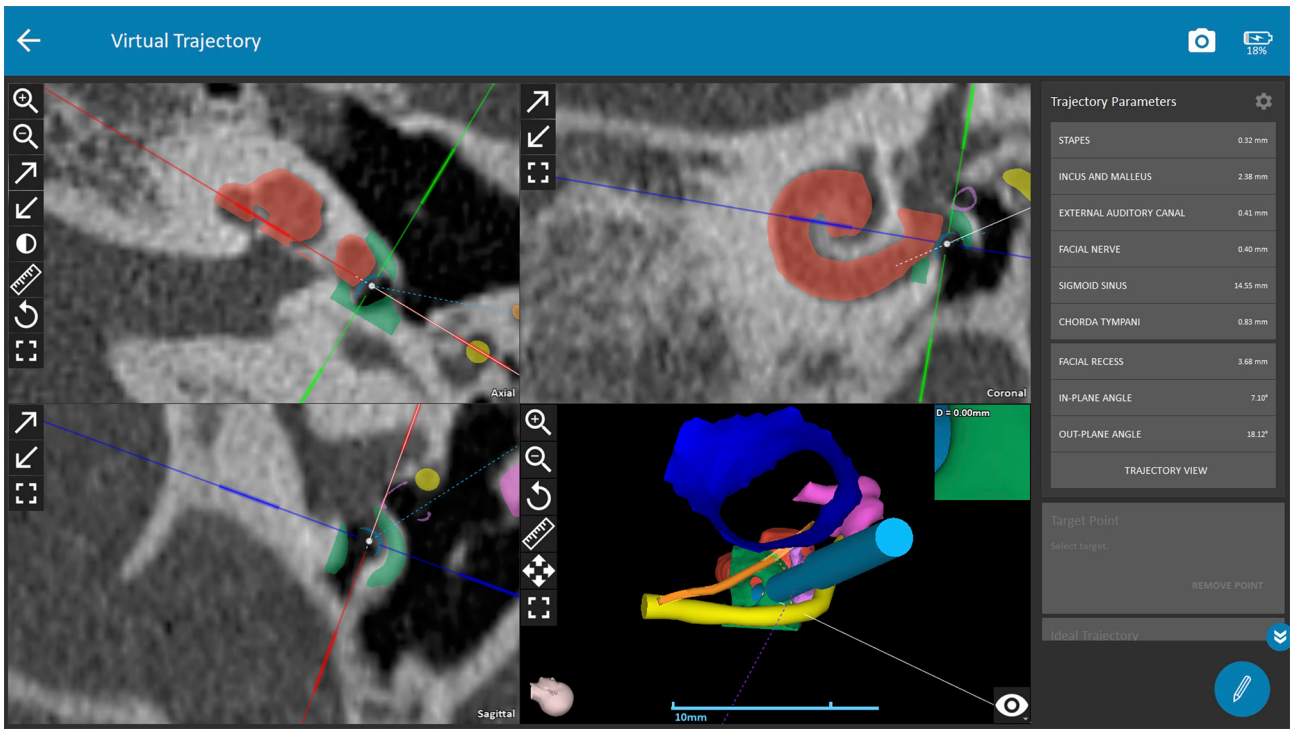

FIGURE 1B | Planning procedures with OTOPLAN. The trajectory path to the middle ear/round window is calculated automatically and safety distances to critical anatomic structures are displayed by the software. Red shading (cochlear segmentation automatically calculated by the software), green shading (bony overhang automatically calculated by the software), yellow shading (facial nerve), dark blue shading (external ear canal), pink shading (ossicles), orange shading (chorda tympani), light blue shading (drill in position of the automated trajectory).

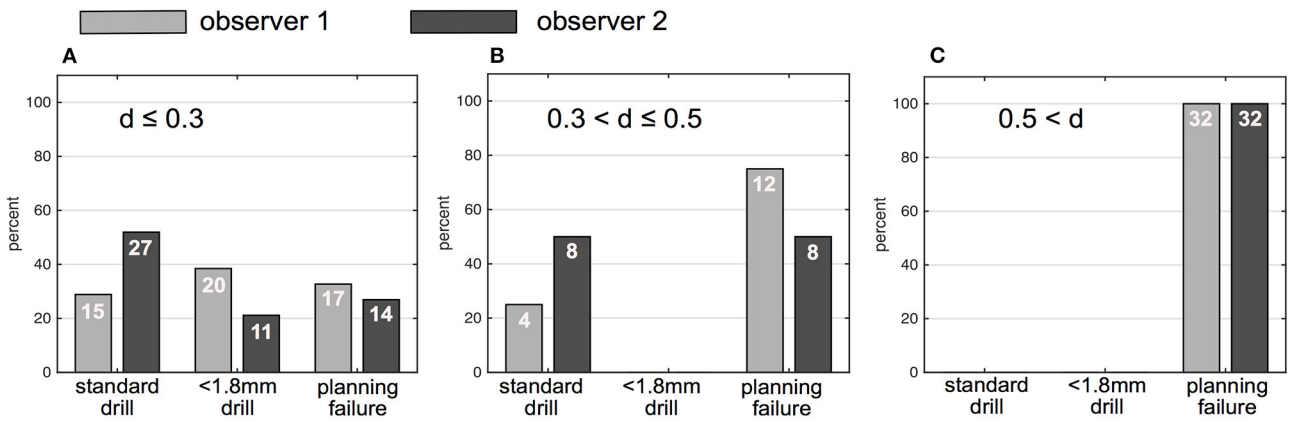

FIGURE 2 | Percentage and numbers (in white) of successfully planed ears based on drill bit size (1.8 and < 1.8 mm) and percentage of unsuccessfully planned ears. **(A)** Ears planned on CT with ≤ 0.3 mm slice thickness. **(B)** Ears planned based on CT with a slice thickness between 0.3 and ≤ 0.5 mm. **(C)** Ears planned based on CT with a slice thickness > 0.5 mm; gray bars indicate results of observer 1, black bars indicate results of observer 2; d (slice thickness).

Although some image data with a slice thickness of up to 0.5 mm were sufficient enough to plan a trajectory, bad imaging resolution was the most frequent reason for a failure in planning, followed by software problems, failure in 3D ear reconstruction, and corrupted image data. A slice thickness of up to 1.3 mm might be enough for CDL planning in some cases (24, 25), but based on the current data and our experience, sufficient visualization of the facial nerve or the chorda tympani is almost impossible. Even in imaging with a slice thickness of 0.3–0.5 mm, the chorda tympani can be only visualized if the angle of the X-ray is in favor of the nerve's location and reconstruction allows for sufficient presentation on the image. None of the scans thicker than 0.5 mm could be used for planning a safe trajectory in the current study.

TABLE 2 | Cochlear parameters and distance of planned trajectory to critical anatomic structures.

	Observer 1		Observer 2		
	mean (mm)	SD	mean (mm)	SD	absolute difference
Distance of trajectory to:					
Stapes	0.55	0.5	0.64	0.48	0.09
Incus/Malleus	2.46	0.98	2.63	0.76	0.17
External ear canal	1.33	0.92	1.44	0.61	0.11
Facial nerve	0.41	0.02	0.41	0.02	0.00
Chorda tympani	0.65	0.54	0.70	0.38	0.05
Facial recess	3.04	0.58	3.13	0.46	0.09
In-plan angle	9.21	8.43	5.37	6.38	3.84
Out-plane angle	17.48	6.76	19.41	5.15	1.93
Cochlear parameters:					
Cochlear diameter	9.44	0.47	9.16	0.46	0,28
Cochlear width	6.86	0.32	6.76	0.32	0.10
Cochlear height	3.79	0.30	3.88	0.25	0,09
CDL	36.48	1.57	35.16	1.56	1.32

Means are depicted in millimeters. SD, standard deviation; CDL, cochlear duct length.

TABLE 3 | Success rate of planning a safe trajectory for the HEARO procedure.

Drill bit size	Cases feasible for HEARO	
	Observer 1	Observer 2
1.8 mm (standard size)	19 (48.7%)	35 (76.1%)
1.7 mm	+3 (56.4%)	+1 (78.3%)
1.6 mm	+4 (66.7%)	+3 (84.8%)
1.5 mm	+5 (79.5%)	+1 (87.0%)
1.4 mm	+2 (84.6%)	+2 (91.3%)
1.3 mm	+2 (89.7%)	+2 (95.6%)
1.2 mm	+2 (94.8%)	+1 (97.8%)
1.1 mm	+1 (97.4%)	+1 (100%)
1.0 mm	+1 (100%)	0
	39	46

Successfully planned ears are depicted as number and total (percentage) for different drill bit sizes. Feasibility could be increased to 100% with including narrower drill bit sizes as small as 1.00 mm.

As a consequence, preoperative assessment should include good image resolution with a slice thickness of maximum 0.3 mm, preferably 0.1–0.2 mm. Otherwise, a high risk of planning failure remains. Considering the exposure to radiation, repetition of scans should be strictly avoided. A standard CT examination protocol for the temporal bone applies an effective dose of ∼0.6 millisievert (mSv). By reducing the tube current (milliampere, mA), an effective dose of 0.3–0.5 mSv can be achieved without the loss of diagnostic information (26, 27), which is the case for one scan in the robotic CI set-up. Up until now, two to three scans are necessary during robotic CI surgery; one for assessment of the head with fiducials drilled to the bone before the drilling of the HEARO procedure starts and another scan is performed for safety reasons before the facial recess is entered by the drill bit. With increased experience in robotics in the future, fewer scans might be necessary and could reduce exposure to radiation.

Software crashes counted for some planning failures but with regularly offered software updates, this should not pose a problem in the future. A few patients had malformations of the middle ear such as missing ossicles, resulting in failure of 3D ear reconstruction because segmentation of software-requested landmarks was not possible. One patient was already implanted with a CI contralateral to the measured ear and therefore some steps of the planning course could not be carried out.

One of the advantages expected from robotic ear surgery is planning a safe approach to middle and inner ear structures in case of malformations, which could be a great challenge if the surgery is performed manually. At present, trajectory planning is based on selection of specific landmarks (e.g., selection of the incudostapedial joint). In cases of a malformed middle ear, delineation of those landmarks is currently not possible. Therefore, more flexible measurement procedures should be implemented in order to find a reliable path to the round window.

Although the interrater reliability was good in assessing the trajectory, feasibility of the HEARO procedure with the standard drill bit was less often assessed with observer 1 than with observer two (19 vs. 35 ears). It seems that the measurement procedure differed systematically between both examiners. This further points out that people using this software should be well trained. Case discussions and training lessons on a regular basis should therefore aid consistency of planning results. However, both observers agreed very well on which data was not sufficient enough to plan with the software.

The current results show that the mean CDL of analyzed ears was in the range with previously published data (24, 25). Between well trained examiners, the CDL differed by 1.5 mm on average, which was reported by Canfarotta et al. (28). Here, the absolute difference of the mean CDL between observers was 1.34 mm suggesting strong inter- and intrarater reliability. The ideal insertion angle for different surgical techniques has been demonstrated earlier and would not deviate much from 0° but with given anatomic landmarks, the facial nerve could be harmed (22). Therefore, an optimal trajectory respects vulnerable anatomical structures with the lowest deviation from 0°. In this study, the assessed in-plane angles ranged from 0.1 to 39.5° and calculated out-plane angles ranged between 5.2 and 29°. This is in line with reported optimal out-plane angles varying between −3° and 21° for a posterior tympanotomy approach to the round window and for a given facial recess (22).

A shortcoming of this study is that only four children were included. We primarily collected data of adult patients because at this time, robotic surgery is only accredited in patients older than 18 years due to safety reasons. Concern is raised by the use of radiation before and during the procedure. Children will hopefully benefit from this new technique in the future if acquisition of imaging can be avoided by improving the accuracy of intraoperative facial nerve monitoring. Another limitation is that the time investment for training lessons and study

measurements was not assessed and therefore no specific learning curve can be reported.

CONCLUSION

Sufficient image resolution, preferably 0.1–0.2 mm slice thickness achieved in low-dose radiation cone beam CT scanners or high-resolution CT, should be performed in the preoperative patient assessment. Otherwise, a high rate of planning failures has to be expected and repetition of scans should not be an option due to unnecessary exposure to radiation. Surgeons should be well and systematically trained in the software planning procedure. With increasing experience in robotic ear surgery, some of the downsides with this new technique - such as exclusion of children - will hopefully be diminished.

DATA AVAILABILITY STATEMENT

The raw data supporting the conclusions of this article will be made available by the authors, without undue reservation.

AUTHOR CONTRIBUTIONS

AA, CA, and DR planned the study. AA and VD performed measurements. DR and W-DB provided help in interpretation of the results. RL performed statistics. AA wrote the main paper. All authors contributed to this work, discussed the results, and commented on the manuscript at all stages.

FUNDING

The study was funded by MED-EL GmbH (Innsbruck, Austria). The funding source had no influence on the presented data of this study.

ACKNOWLEDGMENTS

The authors thank Michael Kalcher (Med-El GmbH) for all measurements and his constant support with OTOPLAN and image data preparation.

REFERENCES

1. House WF. Cochlear implants. *Ann Otol Rhinol Laryngol.* (1976) 85:1–93. doi: 10.1177/00034894760850S302
2. Davies B. A review of robotics in surgery. *Proc Inst Mech Eng H.* (2000) 214:129–40. doi: 10.1243/0954411001535309
3. Marescaux J, Leroy J, Rubino F, Smith M, Vix M, Simone M, et al. Transcontinental robot-assisted remote telesurgery: feasibility and potential applications. *Ann Surg.* (2002) 235:487–92. doi: 10.1097/00000658-200204000-00005
4. George EI, Brand TC, LaPorta A, Marescaux J, Satava RM. Origins of robotic surgery: from skepticism to standard of care. *JSLS.* (2018) 22:e2018.00039. doi: 10.4293/JSLS.2018.00039
5. McLeod IK, Melder PC, Da. Vinci robot-assisted excision of a vallecular cyst: a case report. *Ear Nose Throat J Ear Nose Throat J.* (2005) 84:170–2. doi: 10.1177/014556130508400315
6. Panara K, Shahal D, Mittal R, Eshraghi AA. Robotics for Cochlear Implantation Surgery: Challenges and Opportunities. *Otol Neurotol.* (2021) 42:e825–35. doi: 10.1097/MAO.0000000000003165
7. Warren FM, Balachandran R, Fitzpatrick JM, Labadie RF. Percutaneous cochlear access using bone-mounted, customized drill guides: demonstration of concept in vitro. *Otol Neurotol.* (2007) 28:325–9. doi: 10.1097/01.mao.0000253287.86737.2e
8. Federspil PA, Geisthoff UW, Henrich D, Plinkert PK. Development of the first force-controlled robot for otoneurosurgery. *Laryngoscope.* (2003) 113:465–71. doi: 10.1097/00005537-200303000-00014
9. Danilchenko A, Balachandran R, Toennies JL, Baron S, Munske B, Fitzpatrick JM, et al. Robotic mastoidectomy. *Otol Neurotol.* (2011) 32:11–6. doi: 10.1097/MAO.0b013e3181fcee9e
10. Yoo MH, Lee HS, Yang CJ, Lee SH, Lim H, Lee S, et al. A cadaver study of mastoidectomy using an image-guided human-robot collaborative control system. *Laryngoscope Investig Otolaryngol.* (2017) 2:208–14. doi: 10.1002/lio2.111
11. Bell B, Stieger C, Gerber N, Arnold A, Nauer C, Hamacher V, et al. A self-developed and constructed robot for minimally invasive cochlear implantation. *Acta Otolaryngol Taylor & Francis.* (2012) 132:355–60. doi: 10.3109/00016489.2011.642813
12. Torres R, Jia H, Drouillard M, Bensimon J-L, Sterkers O, Ferrary E, et al. An Optimized Robot-Based Technique for Cochlear Implantation to Reduce Array Insertion Trauma. *Otolaryngol Head Neck Surg.* (2018) 159:900–7. doi: 10.1177/0194599818792232
13. Kontorinis G, Lenarz T, Stöver T, Paasche G. Impact of the insertion speed of cochlear implant electrodes on the insertion forces. *Otol Neurotol.* (2011) 32:565–70. doi: 10.1097/MAO.0b013e318219f6ac
14. Labadie RF, Balachandran R, Noble JH, Blachon GS, Mitchell JE, Reda FA, et al. Minimally invasive image-guided cochlear implantation surgery: first report of clinical implementation. *Laryngoscope.* (2014) 124:1915–22. doi: 10.1002/lary.24520
15. Caversaccio M, Wimmer W, Anso J, Mantokoudis G, Gerber N, Rathgeb C, et al. Robotic middle ear access for cochlear implantation: First in man. *PLoS ONE Public Library of Science.* (2019) 14:e0220543. doi: 10.1371/journal.pone.0220543
16. Weber S, Gavaghan K, Wimmer W, Williamson T, Gerber N, Anso J, et al. Instrument flight to the inner ear. *Sci Robot.* (2017) 2:eaal4916. doi: 10.1126/scirobotics.aal4916
17. Caversaccio M, Gavaghan K, Wimmer W, Williamson T, Anso J, Mantokoudis G, et al. Robotic cochlear implantation: surgical procedure and first clinical experience. *Acta Otolaryngol.* (2017) 137:447–54. doi: 10.1080/00016489.2017.1278573
18. Anso J, Scheidegger O, Wimmer W, Gavaghan K, Gerber N, Schneider D, et al. Neuromonitoring during robotic cochlear implantation: initial clinical experience. *Ann Biomed Eng.* (2018) 46:1568–81. doi: 10.1007/s10439-018-2094-7
19. Anso J, Dür C, Apelt M, Venail F, Scheidegger O, Seidel K, et al. Prospective validation of facial nerve monitoring to prevent nerve damage during robotic drilling. *Front Surg.* (2019) 6:58. doi: 10.3389/fsurg.2019.00058
20. Gerber N, Bell B, Gavaghan K, Weisstanner C, Caversaccio M, Weber S. Surgical planning tool for robotically assisted hearing aid implantation. *Int J Comput Assist Radiol Surg.* (2014) 9:11–20. doi: 10.1007/s11548-013-0908-5
21. World Medical Association. World Medical Association Declaration of Helsinki: ethical principles for medical research involving human subjects. *JAMA.* (2013) 310:2191–4. doi: 10.1001/jama.2013.281053
22. Topsakal V, Matulic M, Assadi MZ, Mertens G, Rompaey VV, Van de Heyning P. Comparison of the surgical techniques and robotic techniques for cochlear implantation in terms of the trajectories toward the inner ear. *J Int Adv Otol.* (2020) 16:3–7. doi: 10.5152/iao.2020.8113
23. Williamson T, Gavaghan K, Gerber N, Weder S, Anschuetz L, Wagner F, et al. Population statistics approach for safety assessment in robotic cochlear implantation. *Otol Neurotol.* (2017) 38:759–64. doi: 10.1097/MAO.0000000000001357

24. Spiegel JL, Polterauer D, Hempel JM, Canis M, Spiro JE, Müller J. Variation of the cochlear anatomy and cochlea duct length: analysis with a new tablet-based software. *Eur Arch Otorhinolaryngol.* (2021) 1–11. doi: 10.1007/s00405-021-06889-0
25. Cooperman SP, Aaron KA, Fouad A, Tran E, Blevins NH, Fitzgerald MB. Assessment of inter- and intra-rater reliability of tablet-based software to measure cochlear duct length. *Otol Neurotol.* (2021) 42:558–65. doi: 10.1097/MAO.0000000000003015
26. Lutz J, Jäger V, Hempel MJ, Srivastav S, Reiser M, Jäger L. Delineation of temporal bone anatomy: feasibility of low-dose 64-row CT in regard to image quality. *Eur Radiol.* (2007) 17:2638–45. doi: 10.1007/s00330-007-0578-1
27. Husstedt HW, Prokop M, Dietrich B, Becker H. Low-dose high-resolution CT of the petrous bone. *J Neuroradiol.* (2000) 27:87–92.
28. Canfarotta MW, Dillon MT, Buss E, Pillsbury HC, Brown KD, O'Connell BP. Validating a New Tablet-based Tool in the Determination of Cochlear Implant Angular Insertion Depth. *Otol Neurotol.* (2019) 40:1006–10. doi: 10.1097/MAO.0000000000002296

Conflict of Interest: The authors declare that the research was conducted in the absence of any commercial or financial relationships that could be construed as a potential conflict of interest.

frontiers in Surgery

ORIGINAL RESEARCH
published: 30 September 2021
doi: 10.3389/fsurg.2021.740008

Quantitative Analysis of Temporal Bone Density and Thickness for Robotic Ear Surgery

Emile Talon[1,2], *Miranda Visini*[2], *Franca Wagner*[3], *Marco Caversaccio*[1,2] *and Wilhelm Wimmer*[1,2*]

[1] *Hearing Research Laboratory, ARTORG Center for Biomedical Engineering Research, University of Bern, Bern, Switzerland,*
[2] *Department for Otolaryngology, Head and Neck Surgery, Inselspital University Hospital Bern, Bern, Switzerland,*
[3] *Department of Diagnostic and Interventional Neuroradiology, Inselspital, Bern University Hospital, Bern, Switzerland*

Background and Objective: Quantitative assessment of bone density and thickness in computed-tomography images offers great potential for preoperative planning procedures in robotic ear surgery.

Methods: We retrospectively analyzed computed-tomography scans of subjects undergoing cochlear implantation (*N* = 39). In addition, scans of Thiel-fixated *ex-vivo* specimens were analyzed (*N* = 15). To estimate bone mineral density, quantitative computed-tomography data were obtained using a calibration phantom. The temporal bone thickness and cortical bone density were systematically assessed at retroauricular positions using an automated algorithm referenced by an anatomy-based coordinate system. Two indices are proposed to include information of bone density and thickness for the preoperative assessment of safe screw positions (Screw Implantation Safety Index, SISI) and mass distribution (Column Density Index, CODI). Linear mixed-effects models were used to assess the effects of age, gender, ear side and position on bone thickness, cortical bone density and the distribution of the indices.

Results: Age, gender, and ear side only had negligible effects on temporal bone thickness and cortical bone density. The average radiodensity of cortical bone was 1,511 Hounsfield units, corresponding to a bone mineral density of 1,145 mg HA/cm^3. Temporal bone thickness and cortical bone density depend on the distance from Henle's spine in posterior direction. Moreover, safe screw placement locations can be identified by computation of the SISI distribution. A local maximum in mass distribution was observed posteriorly to the supramastoid crest.

Conclusions: We provide quantitative information about temporal bone density and thickness for applications in robotic and computer-assisted ear surgery. The proposed preoperative indices (SISI and CODI) can be applied to patient-specific cases to identify optimal regions with respect to bone density and thickness for safe screw placement and effective implant positioning.

Keywords: BAHA, bone conduction implants, screw safety, bone thickness, bone mineral density, calibrated Hounsfield units, quantitative computed-tomography

OPEN ACCESS

Edited by:
Paul van de Heyning,
University of Antwerp, Belgium

Reviewed by:
Mario Zernotti,
Catholic University of Córdoba, Argentina
Cindy Nabuurs,
Radboud University Nijmegen Medical Centre, Netherlands

***Correspondence:**
Wilhelm Wimmer
wilhelm.wimmer@artorg.unibe.ch

Specialty section:
This article was submitted to Otorhinolaryngology – Head and Neck Surgery, a section of the journal Frontiers in Surgery

Received: *12 July 2021*
Accepted: *06 September 2021*
Published: *30 September 2021*

Citation:
Talon E, Visini M, Wagner F, Caversaccio M and Wimmer W (2021) Quantitative Analysis of Temporal Bone Density and Thickness for Robotic Ear Surgery. Front. Surg. 8:740008. doi: 10.3389/fsurg.2021.740008

1. INTRODUCTION

In robotic ear surgery, high-resolution computed-tomography (CT) imaging has proven invaluable to evaluate the complex anatomy of the temporal bone and to ensure safe and effective surgical procedures. To avoid damage to at-risk anatomical structures, geometric information has been the focus of preoperative planning in computer-assisted otological microsurgery (1–6). Importantly, CT images can additionally provide information about bone density that could be utilized to infer on local bone strength for preoperative planning procedures related to robotic ear surgery. The temporal bone contains a variety of bone tissue ranging from pneumatized regions of low density (mastoid air cells) to regions with the highest density present in the human body (petrous bone). Uncalibrated CT radiodensity values expressed as Hounsfield units (HU) enable to study the maturation of temporal bone tissue (7). However, a verified correspondence between the indicated radiodensity and the actual bone mineral density requires the acquisition of calibrated CT images (8, 9). So-called quantitative CT imaging is commonly applied to diagnose and monitor osteoporosis (10), but so far only received limited attention in otology (11).

In robotic cochlear implantation, fiducial screws are implanted retroauricularly as artificial landmarks to achieve the required patient-to-image registration accuracy and to fix the dynamic reference base for tracking patient motion (12, 13). As a firm placement of the fiducial screws is crucial to guarantee safe procedures, the locations for screw insertion have to provide sufficient cortical layer thickness and surrounding bone density. To the best of our knowledge, the direct link between screw osseointegration and bone mineral density has not been specifically analyzed for the temporal bone. However, studies were performed for other regions: the direct relation between screw pullout strength and bone mineral density was verified in the lumbar spine (14) and orthopedic screw fixation was analyzed with respect to bone mineral density in a computational study (15). Fiducial screws placed inferiorly on the temporal bone often coincide with mastoid air cells causing reduced mechanical stability. Moreover, bone density is an important factor considered to minimize heat (16) and acoustic noise exposure during bone removal and drilling (17, 18). Firm screw placement is also desired for the immobilization of bone conduction, middle ear, or cochlear implant bodies, in particular in pediatric cases (19). For bone conduction implants, which exert vibrations to the bone to stimulate the inner ear, screws serve additionally as a means of sound transmission, making a firm placement particularly important, along with the implant location and coupling type (20–22). In the case of bone-anchored hearing aids long-term osseointegration is required for efficient sound transmission (23, 24). Furthermore, primary instability is one of the main causes for hearing implant failure, together with surgical errors (25). All these applications require finding optimal positions in terms of available bone thickness and density.

Therefore, the aim of this work was to quantitatively assess the temporal bone density and thickness in adult subjects for applications in robotic ear surgery. In addition, we propose radiograph-based indices for the preoperative assessment of implant body and screw locations for optimized screw stability and mass distribution in the temporal bone.

2. MATERIALS AND METHODS

2.1. Study Design and Data Collection

We performed a retrospective analysis on clinical high-resolution CT scans (Somatom Definition Edge, Siemens, Germany; 94 mA, 120 kV, voxel size: $0.156 \times 0.156 \times 0.2$ mm^3) taken at the Department of Neuroradiology at the University Hospital in Bern between 2015 and 2017. In total, temporal bone scans of 39 subjects (17 female, 21 male; mean age 55 years, range 21 to 79 years) undergoing cochlear implantation were evaluated. No subjects with temporal bone malformations or osteoporosis were included in the analysis. In addition, to assess the influence of specimen preparation on bone densities, we included high-resolution temporal bone CT scans of Thiel-fixed whole head specimens ($N = 19$) (26) in the analysis.

2.2. Temporal Bone Segmentation and Surface Mesh

For each subject, the temporal bone was segmented using the open-source platform 3D Slicer (27). Bone structures were labeled for voxel intensities above a threshold of 620 HU [according to the compact bone threshold reported by (28)] in a region bounded anteriorly by the posterior wall of the external auditory canal, inferiorly by the tip of the mastoid process, posteriorly by the occipitomastoid suture, and superiorly by the temporal line. To obtain a uniform label structure and to account for the pneumatization of the temporal bone, the labels were post-processed by removing single islands containing less than 300 voxels. Using the labels, a three-dimensional surface mesh was generated using a marching cubes algorithm and smoothed with a kernel size of 4 mm. For the consecutive analysis, the DICOM data together with the surface meshes were imported into Matlab (The MathWorks Inc., Natick, MA, USA).

2.3. Retroauricular Coordinate System

We defined a retroauricular coordinate system using anatomical landmarks that are easily and reliably identifiable during otological procedures (5, 29). With this approach, the surgeon can transfer preoperatively planned positions on the temporal bone using a ruler. The origin of the Cartesian coordinate system is defined by the most superior point on Henle's spine, while two manually selected points along the center of the zygomatic process specify the orientation of the x-axis. Using the coordinate system, a region of interest (ROI) with a grid of 64 probe positions was specified (**Figure 1**).

2.4. Bone Mineral Density Calibration

To enable a quantitative analysis of bone mineral density expressed as the concentration of hydroxyapatite (mg HA/cm^3), we calibrated the radiodensity of the applied CT imaging protocol on the same scanner using a dedicated phantom (QRM-BDC-6, QRM GmbH, Moehrendorf, Germany). The phantom contains 6 cylindrical inserts providing references for 0 HU (water), as well as 100, 200, 400, 600, and 800 mg HA/cm^3. The obtained

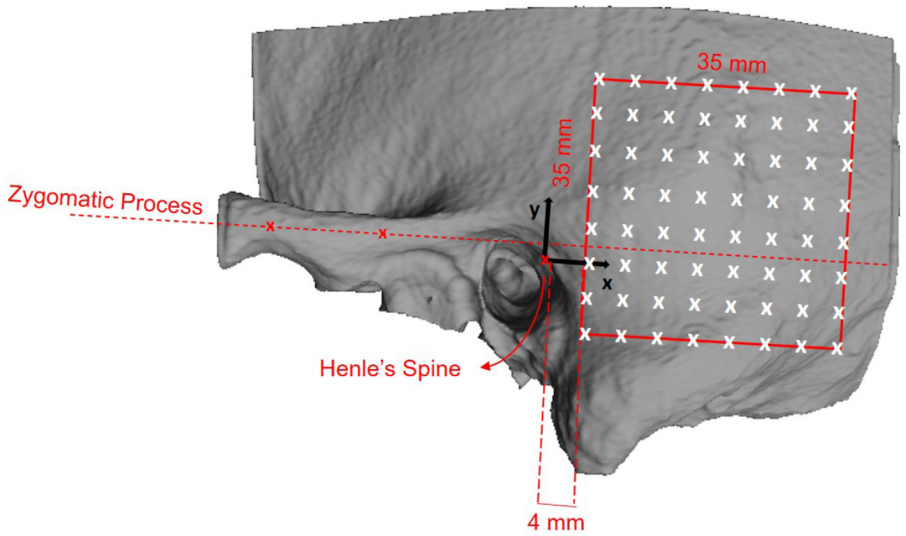

FIGURE 1 | Definition of the retroauricular coordinate system and grid specification for the analyzed region of interest (ROI). The origin of the coordinate system lies at Henle's spine. The x-axis is oriented along the zygomatic process, as specified by two landmarks. The x/y-plane is perpendicular to the transversal image plane as defined by the clinical protocol. The red square indicates the ROI containing the 8 × 8 probe grid. The probe positions are equally spaced by a distance of 5 mm, resulting in a covered area of 35 × 35 mm^2. The lower anterior corner of the ROI is positioned at x = 4 mm and y = −10 mm.

calibration graph shows a linear relation between radiodensity (HU) and bone mineral density (9) (**Figure 2**). Negative values of HU were set to 0 in order to obtain only positive values of the calibrated bone mineral density.

2.5. Evaluation of Bone Thickness and Cortical Density

The probe positions of the grid were projected onto the surface mesh along the surface normal of the x/y-plane (**Figure 3**, left). Every probe (blue line in **Figure 3**, right) intersects the temporal bone mesh in a specific point (highlighted in green) that lays inside one of the triangles of the mesh. This point is then the origin of a trajectory normal to the triangle surface. Consecutively, the intensity values (in HU) of voxels intersecting each trajectory were extracted (**Figure 3**, right). An example of the extracted intensity profile along a trajectory is shown in **Figure 4**. Using the surface mesh, the temporal bone thickness (d_{TB}) was defined as the distance from the start position to the last intersected triangle on the opposite surface. The maximum bone thickness was limited to 18 mm. For the computation of the external cortical bone density, the intensity values were averaged over a thickness of 1.5 mm, starting from the first point along the trajectory with a radiodensity of at least 1,000 HU (see **Figure 4**), as suggested by (7).

2.6. Preoperative Planning Indices

2.6.1. Screw Implantation Safety Index (SISI)

To assess the level of safety for the implantation of screws in the temporal bone, e.g., surgical fiducial screws in robotic ear surgery or for implant fixation, we propose the Screw Implantation Safety Index (SISI). The SISI considers both, the available bone thickness and the bone density along the probe trajectory. First, to avoid interference of the screw with soft tissue, a bone thickness threshold (d_{min}) is specified. In our analysis, d_{min} was chosen with 4 mm and 5 mm according to screw lengths commonly used in ear surgery. Probe locations that have a smaller bone thickness than the required threshold have a SISI of 0. Locations with sufficient bone thickness (at least d_{min} mm) are considered for the next computation step. To compute the SISI (in %), the number of sampled voxels with a radiodensity of at least 1,000 HU (30) are counted (N_S) and divided by the total number of sampled voxels (N) present within the thickness threshold (d_{min}) along the probing trajectory:

$$\mathrm{SISI} = \begin{cases} \frac{N_S}{N} \cdot 100 & d_{TB} > d_{min} \\ 0 & d_{TB} \leq d_{min}. \end{cases}$$

2.6.2. Column Density Index (CODI)

To provide quantitative information about bone mass distribution in the temporal bone, we propose a second index, the Column Density Index (CODI). It is defined as the sum of the bone mineral density values measured along the probing trajectory for the full temporal bone thickness (d_{TB}). The CODI represents a mass per unit surface area, also called column density (expressed in mg HA/mm^2):

$$\mathrm{CODI} = \sum_{i=0}^{N} \rho_{TB}(i) \cdot \Delta d,$$

where N denotes the total number of sampled voxels along the probing trajectory (and within d_{min}), $\rho_{TB}(i)$ is the bone mineral density for each sampled voxel (in mg HA/mm^3), and Δd is the sampling interval along the trajectory (in our case 0.15 mm).

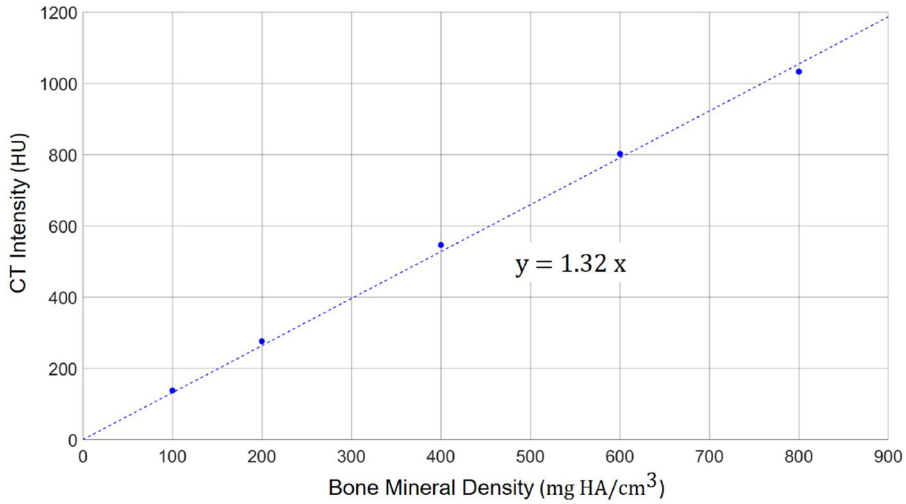

FIGURE 2 | Calibration scale between the radiodensity in the applied high-resolution CT imaging protocol (in HU) and the actual bone mineral density. A linear relation can be observed with a scaling factor of 1.32 between HU and mg HA/cm^3.

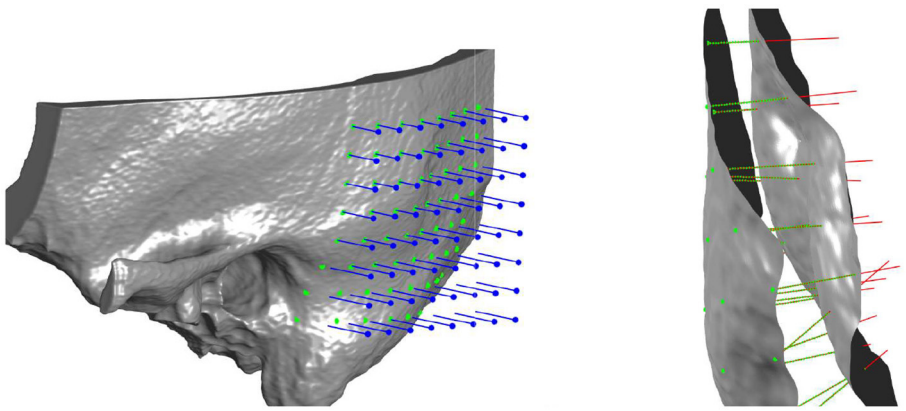

FIGURE 3 | Left: Three-dimensional visualization of the projection of grid points onto the outer surface of the temporal bone mesh. **Right**: Probe evaluation in a section of the temporal bone. Blue lines represent the probes that from the mask intercept the outer bone surface. Red lines represent the normal direction to the external surface, along which thickness and densities are computed. In green are highlighted the points where density is measured for every probe, spaced between each other by 0.15 mm.

2.7. Statistical Analysis

Differences in bone thickness, cortical bone density, as well as the SISI and CODI indices were estimated using separate linear mixed-effects models, with fixed effects for the retroauricular coordinates in the x and y directions (in mm), age (in years) gender (female vs. male), and ear side (left vs. right). A subject-level random effect was included to account for paired measurements. A significance level of 0.05 was used for all comparisons. The statistical analysis was performed using R Studio and the "lme4" package (31).

3. RESULTS

3.1. Temporal Bone Thickness

Figure 5 illustrates the temporal bone thickness averaged across all subjects, excluding *ex-vivo* samples. The corresponding numerical values for the retroauricular grid can be found in **Supplementary Table 1**. The temporal bone is known to be thicker in the sinodural angle, becoming thinner superior to the lateral skull base and posterior to the occipitomastoid suture (5, 29). On average, the bone thickness decreases by 0.16 mm ($p < 0.001$) and 0.19 mm ($p < 0.001$) per millimeter distance from the origin (Henle's spine) in the x and y directions, respectively. Neither age ($p = 0.25$), gender ($p = 0.54$), nor ear side ($p = 0.46$) had a statistical significant effect on the bone thickness in our data (see **Supplementary Table 2**).

3.2. Cortical Bone Density

Figure 6 shows the spatial distribution of cortical bone density across the temporal bone. The average radiodensity was 1511 HU (standard deviation: 241 HU), corresponding to a bone mineral density of 1145 mg HA/cm^3. Age ($p = 0.52$) and

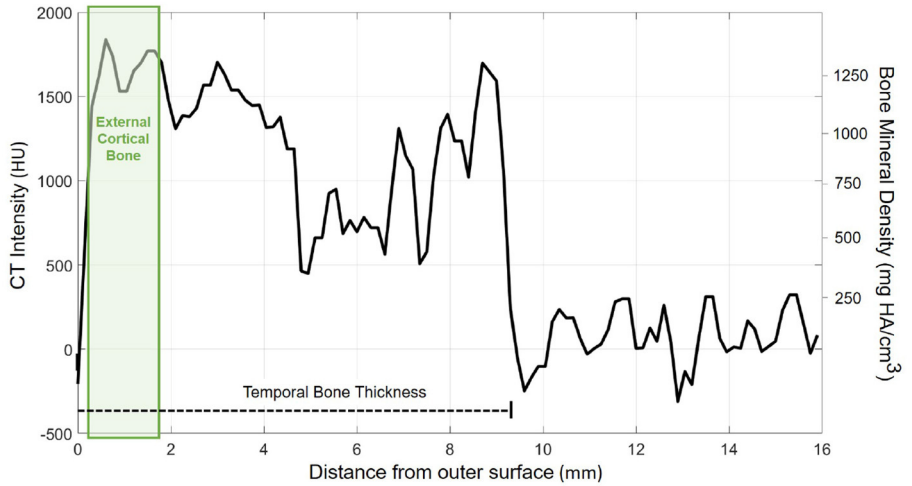

FIGURE 4 | Exemplary course of radiodensity (in HU) and bone mineral density (in mg HA/cm^3) along a probe trajectory. The temporal bone thickness (d_{TB}) along the trajectory is indicated by a dashed line. The green shaded area indicates the region considered for external cortical bone density computation.

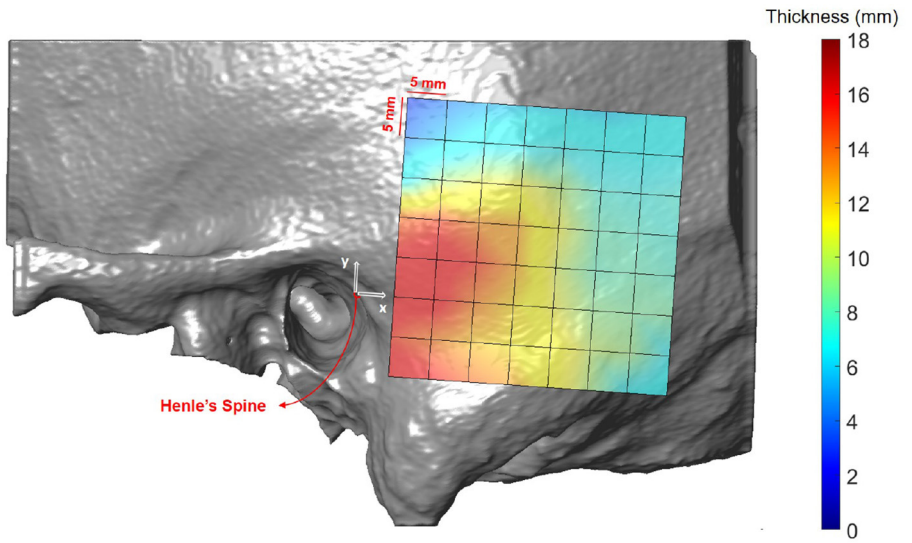

FIGURE 5 | Heat map visualization of temporal bone thickness in the retroauricular region of interest averaged across all subjects.

gender (p = 0.72) did not have an effect on bone density (see **Supplementary Table 4**), while right ear sides tended to have slightly smaller densities (difference 47 HU; p = 0.03) The cortical bone density did not change significantly along the y-axis (p = 0.30), however, it reduced by 1.8 HU ($p < 0.001$) per millimeter distance along the x-axis. The relation between the average cortical bone density of individual subjects and age is provided in **Figure 7**. For comparison, the bone density development curve of (7) is also plotted.

3.3. Screw Implantation Safety Index (SISI)

Figures 8, **9** illustrate the spatial distribution of the SISI calculated for 4 and 5 mm screw lengths, respectively. The distributions are similar, with generally higher values for the SISI for the 4 mm screw lengths, as these require less bone thickness. Neither ear side, age nor gender had an effect on SISI 4 and 5 values. For both indices, higher values were observed on average for increasing distances along the x direction, where variations along the y direction had less influence on the SISI (see **Supplementary Tables 6**, **8**). In regions closer to Henle's spine, the higher occurrence of mastoid air cells is reflected in generally lower SISI values, although the temporal bone has a greater thickness (see **Figure 5**).

3.4. Column Density Index (CODI)

Results averaged across all the subjects (excluding *ex-vivo* samples) are shown in **Figure 10** and summarized in **Supplementary Table 9**. In the region posterior to the

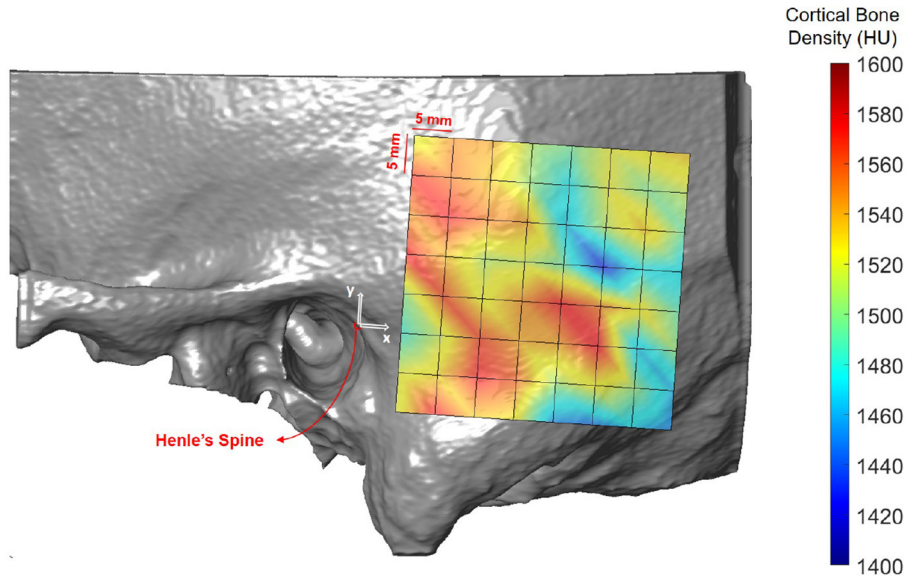

FIGURE 6 | Heat map visualization of cortical bone density (in HU) in the retroauricular region of interest averaged across all subjects.

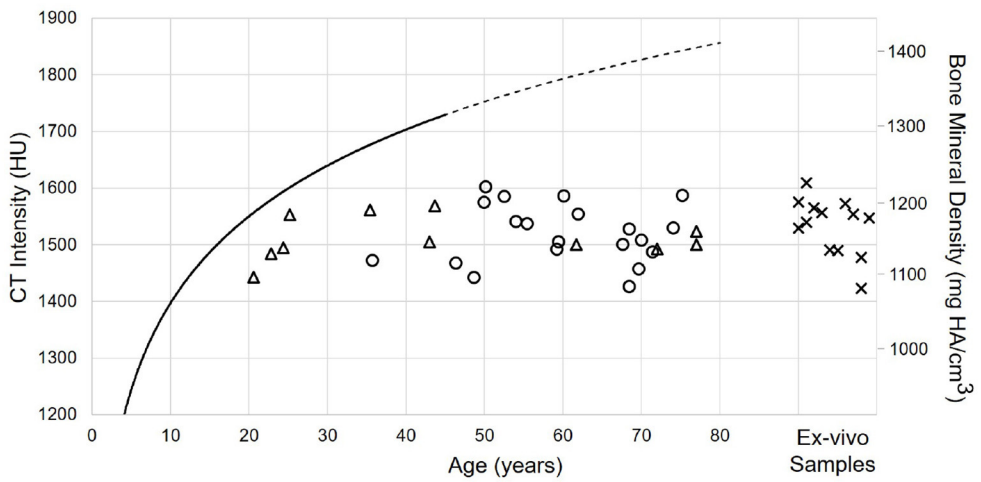

FIGURE 7 | Relation between age and cortical bone density for male (circles) and female subjects (triangles), as well as Thiel fixed *ex-vivo* specimens (crosses). The solid black line indicates the model described by (7). The line is dashed for the prediction of the model.

supramastoid crest (i.e., at positions 19 mm along the x-axis and 10 mm along the y-axis) the highest column densities were observed, indicating a local concentration of bone mass.

4. DISCUSSION

Minimally invasive robot-assisted ear surgery relies on preoperative planning procedures to identify landmarks for patient image registration and to plan access routes at safe distances from structures at risk. Obviously, assessment of geometric properties, particularly available bone thickness, is central to screw and implant placement. The presented study highlights novel aspects that include bone density in the preoperative planning phase. We show how information about radiodensity (or calibrated bone mineral density) can be used to provide a refined assessment of the local bone situation and associated mechanical strength properties. We introduced quantitative CT imaging, i.e., the assessment of calibrated bone mineral density, to the domain of computer-assisted otological planning procedures. Quantitative CT imaging offers several interesting applications for preoperative assessment, e.g., for the classification of otosclerotic cases (32). We applied a clinically motivated reference frame in the retroauricular region to allow

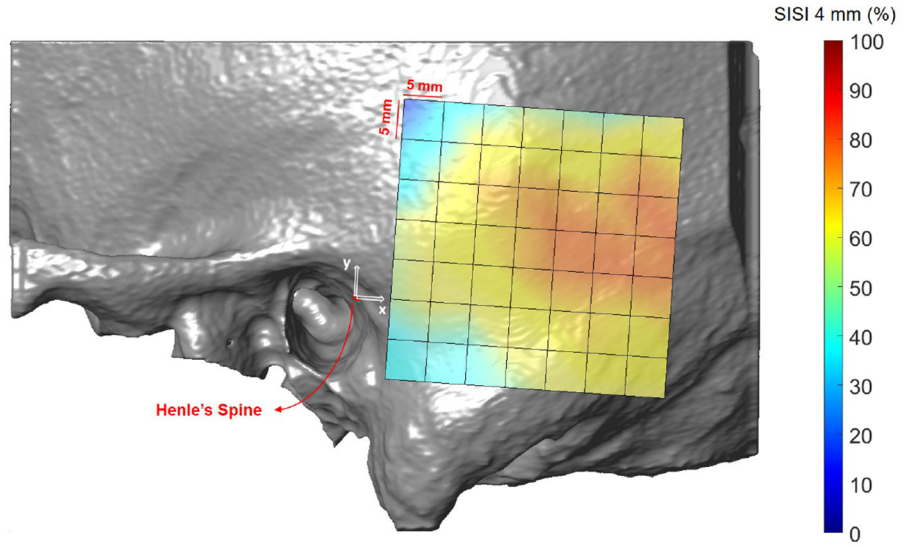

FIGURE 8 | Visualization of the screw implantation safety index (SISI) for a screw length of 4 mm in the region of interest, averaged across all subjects.

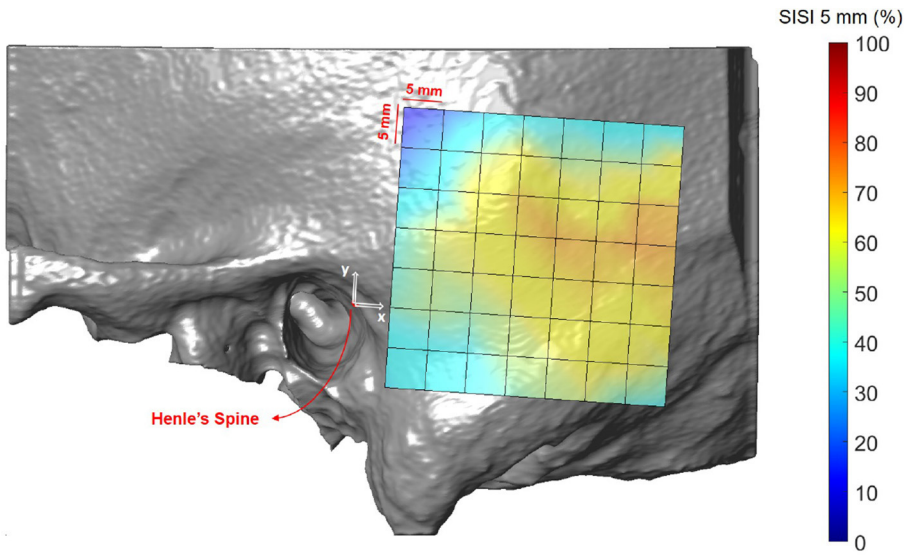

FIGURE 9 | Visualization of the screw implantation safety index (SISI) for a screw length of 5 mm in the region of interest, averaged across all subjects.

coordinate transfer by identifying anatomic landmarks *in situ* and using rulers, in case of preparatory steps are required (e.g., fiducial screw placement) or no navigation system is available. Other transfer methods, such as template-guided approaches (33), could also be used. For patient-specific planning, the proposed methods and indices could be computed using automated segmentation tools (34, 35).

4.1. Temporal Bone Thickness

Temporal bone thickness has been extensively studied in the context of otological surgery (5, 34, 36–38). Our study reproduces the known variability, showing the largest available bone thickness within a radius of 19 mm from *Henle's* Spine. As expected, temporal bone thickness is not age dependent in adult subjects. For bone-anchored hearing aids, the suggested screw implantation position is limited in proximity to the auditory ear canal to avoid contact with the pinna. The implantation site commonly used in bone-anchored hearing aids is located at a distance of 45–50 mm to Henle's spine and 30° inclination with respect to the zygomatic process (39). In our reference frame, this corresponds to positions at x = 39 mm and y = 20–25 mm. In these locations, the observed thickness varied from 5.9 to 7.0

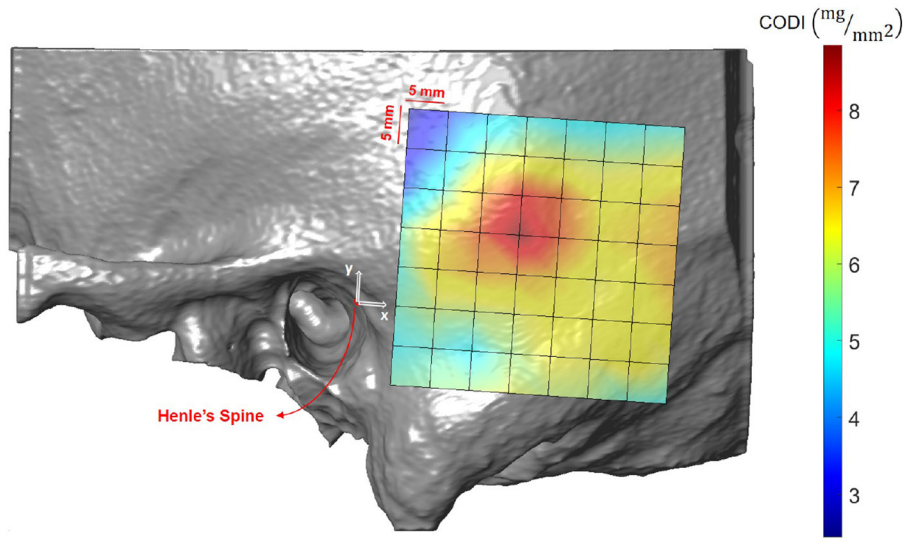

FIGURE 10 | Visualization of the column density index (CODI) in the region of interest, averaged across all subjects.

mm, which is sufficient to host a 4 mm implant without damaging underlying soft tissue (39). One limitation of our study is the limited sample size. Studies including additional data need to be performed to test if our findings can also be reproduced in larger cohorts. As our data set does not include pediatric cases, no conclusions about children (exhibiting significantly lower bone thickness) can be drawn (40). Children exhibit smaller temporal bones (41), and screw lengths of 4 mm are usually only applicable at age 6 or older, while screw lengths of 3 mm often are only possible at age 2 or older. This highlights also the limitation of application of fiducial screws for robotic ear surgery in very young subjects or subjects with temporal bone malformations.

4.2. Cortical Bone Density

The distribution of cortical bone density can be considered rather uniform within and in-between subjects, regardless of age, gender, ear side or preservation of specimens. This is in accordance to (7), who analyzed the maturation of bone density in different regions in the temporal bone, such as the lateral surface or the otic capsule. The overall higher densities in the model of (7) can be explained by the differences in the applied assessment methods. (7) used a two-dimensional approach in single CT slices with small probing areas (0.3 mm^2) to avoid partial volume effects. In addition, their study included subjects aged 3 months to 42 years. In contrast, in this study, the cortical bone density was computed as the average along a 1.8 mm thick probing trajectory, including also less dense regions. Future studies could include data from subjects younger than 20 years to provide a comparable measure in the maturation of the cortical bone density. Moreover, larger, age-matched data sets are required to validate our findings.

4.3. Screw Implantation Safety Index

The first preoperative planning index that we propose is the Screw Implantation Safety Index (SISI). It could provide guidelines to surgeons for patient-specific screw placement in otological surgery. Herein, we analyzed the SISI for 4 and 5 mm screw lengths, which are dimensions typically used for implants (e.g., bone-anchored hearing aids) or fiducial screws used in robotic ear surgery. However, the index can be adapted to other screw dimensions. As shown in **Figures 8**, **9**, the visualization of the SISI using a heat map provides an intuitive representation of bone density and thickness to identify optimal regions for screw placement. Our results indicate that ideal locations for screw placement on the temporal lie within 24–39 mm posteriorly and 5–15 mm superiorly to Henle's spine. Optimal implantation locations for 5 mm screws are located approximately 25 mm posterior to Henle's spine.

4.4. Column Density Index (CODI)

As a second preoperative indicator, we propose the column density index (CODI) quantifying the amount of bone mass in the temporal bone. The main motivation behind the CODI is to identify suitable regions for efficient coupling of bone conduction implants (20). For example, the local concentration of mass posterior to the supramastoid crest could be preferred for fixation, as more mass should result in more efficient coupling and sound transmission. The local maximum results from the contribution of two parameters: temporal bone thickness and the presence of mastoid air cells.

5. CONCLUSIONS

This study applied a combined assessment of temporal bone density and thickness to provide novel

perspectives for the preoperative planning in robotic ear surgery. Quantitative verification of the proposed indices related to mechanical properties requires further evaluation with larger sample size, including biomechanical testing.

DATA AVAILABILITY STATEMENT

The original contributions presented in the study are included in the article/**Supplementary Material**, further inquiries can be directed to the corresponding author/s.

ETHICS STATEMENT

Data collection and analysis for this study was approved by the local institutional review board (reference numbers 2017-01462 and 2016-00887).

AUTHOR CONTRIBUTIONS

ET and WW: conceptualization. ET, FW, and WW: methodology. ET, MV, and WW: formal analysis. FW and MC: resources. ET: writing/original draft preparation. MV, FW, MC, and WW: writing/review and editing. MC and WW: funding acquisition. All authors contributed to the article and approved the submitted version.

FUNDING

This work was funded by the Bern University Hospital (Inselspital).

SUPPLEMENTARY MATERIAL

The Supplementary Material for this article can be found online at: https://www.frontiersin.org/articles/10.3389/fsurg.2021.740008/full#supplementary-material

REFERENCES

1. Vittoria S, Lahlou G, Torres R, Daoudi H, Mosnier I, Mazalaigue S, et al. Robot-based assistance in middle ear surgery and cochlear implantation: first clinical report. *Eur Arch Otorhino Laryngol*. (2021) 278:77–85. doi: 10.1007/s00405-020-06070-z
2. Caversaccio M, Wimmer W, Anso J, Mantokoudis G, Gerber N, Rathgeb C, et al. Robotic middle ear access for cochlear implantation: first in man. *PLoS ONE*. (2019) 14:e0220543. doi: 10.1371/journal.pone.0220543
3. Majdani O, Rau TS, Baron S, Eilers H, Baier C, Heimann B, et al. A robot-guided minimally invasive approach for cochlear implant surgery: preliminary results of a temporal bone study. *Int J Comput Assist Radiol Surg*. (2009) 4:475–486. doi: 10.1007/s11548-009-0360-8
4. Gerber N, Bell B, Gavaghan K, Weisstanner C, Caversaccio M, Weber S. Surgical planning tool for robotically assisted hearing aid implantation. *Int J Comput Assist Radiol Surg*. (2014) 9:11–20. doi: 10.1007/s11548-013-0908-5
5. Wimmer W, Gerber N, Guignard J, Dubach P, Kompis M, Weber S, et al. Topographic bone thickness maps for Bonebridge implantations. *Eur Arch Otorhino Laryngol*. (2015) 272:1651–8. doi: 10.1007/s00405-014-2976-8
6. Wimmer W, Bell B, Huth ME, Weisstanner C, Gerber N, Kompis M, et al. Cone beam and micro-computed tomography validation of manual array insertion for minimally invasive cochlear implantation. *Audiol Neurotol*. (2014) 19:22–30. doi: 10.1159/000356165
7. Takahashi K, Morita Y, Ohshima S, Izumi S, Kubota Y, Horii A. Bone density development of the temporal bone assessed by computed tomography. *Otol Neurotol*. (2017) 38:1445–9. doi: 10.1097/MAO.0000000000001566
8. Schileo E, Dall'Ara E, Taddei F, Malandrino A, Schotkamp T, Baleani M, et al. An accurate estimation of bone density improves the accuracy of subject-specific finite element models. *J Biomech*. (2008) 41:2483–91. doi: 10.1016/j.jbiomech.2008.05.017
9. Vickers DS, Flynn MJ. A technique for measuring regional bone mineral density in human lumbar vertebral bodies. *Med Phys*. (1989) 16:766–72. doi: 10.1118/1.596430
10. Engelke K. Quantitative computed tomography-current status and new developments. *J Clin Densitometry*. (2017) 20:309–21. doi: 10.1016/j.jocd.2017.06.017
11. Monsell E, Cody D, Bone H. *Measurement of Regional Bone Mineral Density*. Vol. 14. Palm Desert, CA: The American Journal of Otology (1993). doi: 10.1097/00129492-199309000-00007
12. Caversaccio M, Gavaghan K, Wimmer W, Williamson T, Ansó J, Mantokoudis G, et al. Robotic cochlear implantation: surgical procedure and first clinical experience. *Acta Otolaryngol*. (2017) 137:447–54. doi: 10.1080/00016489.2017.1278573
13. Weber S, Gavaghan K, Wimmer W, Williamson T, Gerber N, Anso J, et al. Instrument flight to the inner ear. *Sci Robot*. (2017) 2:eaal4916. doi: 10.1126/scirobotics.aal4916
14. Halvorson T. Effects of bone mineral density on pedicle screw fixation. *Spine*. (1994) 19:2415–20. doi: 10.1097/00007632-199411000-00008
15. Zanetti EM, Salaorno M, Grasso G, Audenino AL. Parametric analysis of orthopedic screws in relation to bone density. *Open Med Inform J*. (2009) 3:19. doi: 10.2174/1874431100903010019
16. Feldmann A, Wandel J, Zysset P. Reducing temperature elevation of robotic bone drilling. *Med Eng Phys*. (2016) 38:1495–504. doi: 10.1016/j.medengphy.2016.10.001
17. Du X, Zhang Y, Boulgouris N, Brett PN, Mitchell-Innes A, Coulson C, et al. Noise exposure on human cochlea during cochleostomy formation using conventional and a hand guided robotic drill. *Otol Neurotol*. (2020) 41:e829–35. doi: 10.1097/MAO.0000000000002699
18. Kylen P, Arlinger S. Drill-generated noise levels in ear surgery. *Acta Otolaryngol*. (1976) 82:402–9. doi: 10.3109/00016487609120925
19. Roland Jr JT, Fishman AJ, Waltzman SB, Alexiades G, Hoffman RA, Cohen NL. Stability of the cochlear implant array in children. *Laryngoscope*. (1998) 108:1119–23. doi: 10.1097/00005537-199808000-00003
20. Rohani SA, Bartling ML, Ladak HM, Agrawal SK. The BONEBRIDGE active transcutaneous bone conduction implant: effects of location, lifts and screws on sound transmission. *J Otolaryngol Head Neck Surg*. (2020) 49:1–6. doi: 10.1186/s40463-020-00454-1
21. Wimmer W, Von Werdt M, Mantokoudis G, Anschuetz L, Kompis M, Caversaccio M. Outcome prediction for Bonebridge candidates based on audiological indication criteria. *Auris Nasus Larynx*. (2019) 46:681–6. doi: 10.1016/j.anl.2018.12.012
22. Dobrev I, Sim JH, Pfiffner F, Huber AM, Röösli C. Experimental investigation of promontory motion and intracranial pressure following bone conduction: stimulation site and coupling type dependence. *Hear Res*. (2019) 378:108–25. doi: 10.1016/j.heares.2019.03.005
23. Wazen JJ, Gupta R, Ghossaini S, Spitzer J, Farrugia M, Tjellstrom A. Osseointegration timing for Baha system loading. *Laryngoscope*. (2007) 117:794–6. doi: 10.1097/01.mlg.0000231281.76358.cc
24. Kompis M, Wimmer W, Caversaccio M. Long term benefit of bone anchored hearing systems in single sided deafness. *Acta Otolaryngol*. (2017) 137:398–402. doi: 10.1080/00016489.2016.1261410
25. Drinias V, Granström G, Tjellström A. High age at the time of implant installation is correlated with increased loss of osseointegrated implants

in the temporal bone. *Clin Implant Dentist Relat Res*. (2007) 9:94–9. doi: 10.1111/j.1708-8208.2007.00047.x
26. Thiel W. The preservation of the whole corpse with natural color. *Ann Anat*. (1992) 174:185–95. doi: 10.1016/S0940-9602(11)80346-8
27. Kikinis R, Pieper SD, Vosburgh KG. 3D Slicer: a platform for subject-specific image analysis, visualization, and clinical support. In: Jolesz FA, editor. *Intraoperative Imaging and Image-Guided Therapy*. New York, NY: Springer (2014). p. 277–89. doi: 10.1007/978-1-4614-7657-3_19
28. Chougule VN, Mulay AV, Ahuja BB. Clinical case study: spine modeling for minimum invasive spine surgeries (MISS) using rapid prototyping. *Proc Eng*. (2018) 97:212–9. doi: 10.1016/j.proeng.2014.12.244
29. Guignard J, Arnold A, Weisstanner C, Caversaccio M, Stieger C. A bone-thickness map as a guide for bone-anchored port implantation surgery in the temporal bone. *Materials*. (2013) 6:5291–301. doi: 10.3390/ma6115291
30. Koistinen A, Santavirta SS, Kröger H, Lappalainen R. Effect of bone mineral density and amorphous diamond coatings on insertion torque of bone screws. *Biomaterials*. (2005) 26:5687–94. doi: 10.1016/j.biomaterials.2005.02.003
31. Bates D, Maechler M, Bolker B, Walker S, Christensen RHB, Singmann H, et al. *Package "lme4*." Vienna: CRAN R Foundation for Statistical Computing (2012).
32. Bozorg Grayeli A, Saint Yrieix C, Imauchi Y, Cyna-Gorse F, Ferrary E, Sterkers O. Temporal bone density measurements using CT in otosclerosis. *Acta Otolaryngol*. (2004) 124:1136–40. doi: 10.1080/00016480410018188
33. Takumi Y, Matsumoto N, Cho B, Ono H, Mori K, Tsukada K, et al. A clinical experience of "STAMP" plate-guided Bonebridge implantation. *Acta Otolaryngol*. (2014) 134:1042–6. doi: 10.3109/00016489.2014.900703
34. Neves C, Tran E, Kessler I, Blevins N. Fully automated preoperative segmentation of temporal bone structures from clinical CT scans. *Sci Rep*. (2021) 11:1–11. doi: 10.1038/s41598-020-80619-0
35. Barakchieva MM, Wimmer W, Dubach P, Arnold AM, Caversaccio M, Gerber N. Surgical planning tool for BONEBRIDGE implantation using topographic bone thickness maps. *Int J Comput Assist Radiol Surg*. (2015) 10:S97–8. doi: 10.7892/boris.70185
36. Federspil PA, Tretbar SH, Böhlen FH, Rohde S, Glaser S, Plinkert PK. Measurement of skull bone thickness for bone-anchored hearing aids: an experimental study comparing both a novel ultrasound system (SonoPointer) and computed tomographic scanning to mechanical measurements. *Otol Neurotol*. (2010)31:440–6. doi: 10.1097/MAO.0b013e3181d2775f
37. Rahne T, Svensson S, Lagerkvist H, Holmberg M, Plontke SK, Wenzel C. Assessment of temporal bone thickness for implantation of a new active bone-conduction transducer. *Otol Neurotol*. (2021) 42:278–84. doi: 10.1097/MAO.0000000000002919
38. Simms DL, Neely JG. Thickness of the lateral surface of the temporal bone in children. *Ann Otol Rhinol Laryngol*. (1989) 98:726–31. doi: 10.1177/000348948909800913
39. De Wolf MJF, Hol MKS, Huygen PLM, Mylanus EAM, Cremers CWRJ. Clinical outcome of the simplified surgical technique for BAHA implantation. *Otol Neurotol*. (2008) 29:1100–8. doi: 10.1097/MAO.0b013e31818599b8
40. Almuhawas FA, Dhanasingh AE, Mitrovic D, Abdelsamad Y, Alzhrani F, Hagr A, et al. Age as a factor of growth in mastoid thickness and skull width. *Otol Neurotol*. (2020) 41:709–14. doi: 10.1097/MAO.0000000000002585
41. Baker A, Fanelli D, Kanekar S, Isildak H. A review of temporal bone CT imaging with respect to pediatric bone-anchored hearing aid placement. *Otol Neurotol*. (2016) 37:1366–9. doi: 10.1097/MAO.0000000000001172

Conflict of Interest: The authors declare that the research was conducted in the absence of any commercial or financial relationships that could be construed as a potential conflict of interest.

The handling editor PH declared a past co-authorship with the authors MC and WW.

Publisher's Note: All claims expressed in this article are solely those of the authors and do not necessarily represent those of their affiliated organizations, or those of the publisher, the editors and the reviewers. Any product that may be evaluated in this article, or claim that may be made by its manufacturer, is not guaranteed or endorsed by the publisher.

frontiers in Surgery

ORIGINAL RESEARCH
published: 30 September 2021
doi: 10.3389/fsurg.2021.723897

Cochlear Size Assessment Predicts Scala Tympani Volume and Electrode Insertion Force- Implications in Robotic Assisted Cochlear Implant Surgery

Anandhan Dhanasingh[1,2*†], *Chloe Swords*[3*†], *Manohar Bance*[4], *Vincent Van Rompaey*[2,5] *and Paul Van de Heyning*[2,5]

[1] Research and Development Department, MED-EL, Innsbruck, Austria, [2] Department of Translational Neurosciences, Faculty of Medicine and Health Sciences, University of Antwerp, Antwerp, Belgium, [3] Department of Physiology, Development and Neurosciences, University of Cambridge, Cambridge, United Kingdom, [4] Department of Clinical Neurosciences, University of Cambridge, Cambridge, United Kingdom, [5] Department of Otorhinolaryngology and Head & Neck Surgery, Antwerp University Hospital, Antwerp, Belgium

OPEN ACCESS

Edited by:
Ingo Todt,
Bielefeld University, Germany

Reviewed by:
Silke Helbig,
University Hospital Frankfurt, Germany
Omid Majdani,
Wolfsburg Hospital, Germany
Yann Nguyen,
Sorbonne Universités, France

***Correspondence:**
Anandhan Dhanasingh
anandhan.dhanasingh@medel.com
Chloe Swords
cs521@cam.ac.uk

[†]These authors have contributed equally to this work

Specialty section:
This article was submitted to Otorhinolaryngology - Head and Neck Surgery, a section of the journal Frontiers in Surgery

Received: 11 June 2021
Accepted: 06 September 2021
Published: 30 September 2021

Citation:
Dhanasingh A, Swords C, Bance M, Van Rompaey V and Van de Heyning P (2021) Cochlear Size Assessment Predicts Scala Tympani Volume and Electrode Insertion Force- Implications in Robotic Assisted Cochlear Implant Surgery. Front. Surg. 8:723897. doi: 10.3389/fsurg.2021.723897

Objectives: The primary aim was to measure the volume of the scala tympani (ST) and the length of the straight portion of the cochlear basal turn from micro-computed tomography (μCT) images. The secondary aim was to estimate the electrode insertion force based on cochlear size and insertion speed. Both of these objectives have a direct clinical relevance in robotic assisted cochlear implant (CI) surgery.

Methods: The ST was segmented in thirty μCT datasets to create a three-dimensional (3D) model and calculate the ST volume. The diameter (A-value), the width (B-value), and the straight portion of the cochlear basal turn (S-value) were measured from the oblique coronal plane. Electrode insertion force was measured in ST models of two different sizes, by inserting FLEX24 (24 mm) and FLEX28 (28 mm) electrode arrays at five different speeds (0.1, 0.5, 1, 2, and 4 mm/s).

Results: The mean A-, B-, and S-values measured from the 30 μCT datasets were 9.0 ± 0.5, 6.7 ± 0.4, and 6.9 mm ± 0.5, respectively. The mean ST volume was 34.2 μl ± 7 (range 23–50 μl). The ST volume increased linearly with an increase in A- and B-values (Pearson's coefficient $r = 0.55$ and 0.56, respectively). The A-value exhibited linear positive correlation with the B-value and S-value (Pearson's coefficient $r = 0.64$ and $r = 0.66$, respectively). In the smaller of the two ST models, insertion forces were higher across the range of insertion speeds during both array insertions, when compared to the upscaled model. Before the maximum electrode insertion depths, a trend toward lower insertion force for lower insertion speed and vice-versa was observed.

Conclusion: It is important to determine pre-operative cochlear size as this seems to have an effect upon electrode insertion forces. Higher insertion forces were seen in a smaller sized ST model across two electrode array lengths, as compared to an upscaled larger model. The ST volume, which cannot be visualized on clinical CT, correlates with clinical cochlear parameters. This enabled the creation of an equation capable of

predicting ST volume utilizing A- and B-values, thus enabling pre-operative prediction of ST volume.

Keywords: scala tympani volume, cochlear size, electrode insertion speed, electrode insertion force, robot assisted surgery

INTRODUCTION

Cochlear implant (CI) technology has evolved over the last 40 years reaching its maturity in terms of basic technological advancements (1). Throughout the years, surgical importance has been placed on the optimal placement of the CI electrode array in order to preserve the intra-cochlear structures (2). The steps in CI surgery, including cortical mastoidectomy, posterior tympanotomy, round window (RW) opening and the electrode array insertion, are performed manually. As a result, the hearing outcomes of CI recipients may be influenced by the surgical learning curve of every CI surgeon (3).

Intra-cochlear structures are delicate. Ishii et al. reported that electrode array insertion force above 35 milli-newtons (mN) would result in disturbance of the basilar membrane (4). The ability of humans to manually respond to minute changes in insertion forces in the range of 35 mN may be less reliable when compared to the haptic feedback systems available with automated insertion systems. In addition, it has been reported that electrode insertion speed has an influence on structure and hearing preservation (5). Thus, as research interests turn toward automated and robotic-assisted electrode insertion, the quantification of the optimal insertion speed that offers the minimum insertion force along with the ability to insert the electrode fully inside the cochlea would be beneficial. During the insertion process, the tip of an electrode array is angulated toward the lateral wall at the end of the straight portion of cochlear basal turn and is likely to collide with this. Appreciating how this straight portion length varies with the overall variation in other cochlear parameters, such as scala tympani (ST) volume, would enable automated adjustment of insertion speeds when approaching the end of the cochlear basal turn.

Personalized treatment in cochlear implantation is being developed at multiple timepoints throughout the patient's journey, for instance during audio processor fitting (6) and otological pre-planning software (e.g., OTOPLAN®) in assessing cochlear size and choosing electrode array length matching the cochlear size (7). Robotic assisted CI surgery and controlled speed electrode array insertion, such as the HEARO® system and ROBOTOL®, respectively (8–10) are in the early stages of clinical practice. To complement these technological advancements and to take the concept of personalized CI treatment to the next level where the electrode insertion speed can be personalized to the individual's ST size and volume, a study on the following objectives is essential. Estimating the ST volume and length of the straight portion of cochlear basal turn based on pre-operative assessment of cochlear parameters. Studying the changes in electrode array insertion force from *in-vitro* insertion experiments in different sized ST models with varying volumes, employing different electrode array lengths inserted with different insertion speeds.

Therefore, the primary aim of this study was to measure the volume of the ST from micro-computed tomography (μCT) images and establish whether there is a relationship with basic cochlear parameters [length of straight portion of the basal turn (S-value), basal turn diameter (A-value) and cochlear width (B-value)]. This would help in the estimation of ST volume from the pre-operative clinical images. The secondary aim was to study the electrode array insertion forces of two variants of FLEX electrodes (FLEX28 and FLEX24), inserted at various insertion speeds in two different sized ST plastic models. This would allow us to understand how the electrode insertion forces changes with the changes in the ST volume indirectly estimated from the cochlear parameters. ST fluid itself would act as an impedance to electrode insertion and therefore the knowing the ST volume is of clinical interest. All this pre-operative information will add to the wealth of information available to the operating surgeon to potentially influence intra-operative behavior.

MATERIALS AND METHODS

Image Analysis

Image analysis was performed on thirty μCT image datasets of cadaveric temporal bones. There were no inner ear malformations present. Fifteen raw datasets were sourced from the HEAR-EU project (https://cordis.europa.eu/project/id/304857), and the other fifteen raw datasets were from Cambridge (CS and MB). The μCT images [24–30 micron (μ) isotropic voxel-sizes] were analyzed using Slicer Version 4.10.2 (https://www.slicer.org/) in the HEAR-EU data, and Stradview (Version 6.1) for the Cambridge data. The reason for using two different image analysis software was due to the availability of the specific software at MED-EL Innsbruck and University of Cambridge, Cambridge, respectively. Three-dimensional (3D) segmentation of the ST from these combined raw datasets was performed in this study following the steps described by Dhanasingh et al. (11). In brief, the image datasets were loaded into two different 3D segmentation software. Segmentation of the ST was performed as precisely as possible in the axial plane in every slice of the cochlea by setting tight grayscale threshold to avoid capturing undesired structures (**Figure 1A**). Grayscale thresholding to capture the desired structures was done individually for every individual image data set. **Figure 1B** shows an example of grayscale thresholding; the grayscale of the otic capsule is 6,089 (bright = bone) and the grayscale of membranous labyrinth (dark = labyrinth) is −1,014, thus setting the thresholding −1,014 and 6,089 for this temporal bone. The volume of ST was measured using the command "segment statistics."

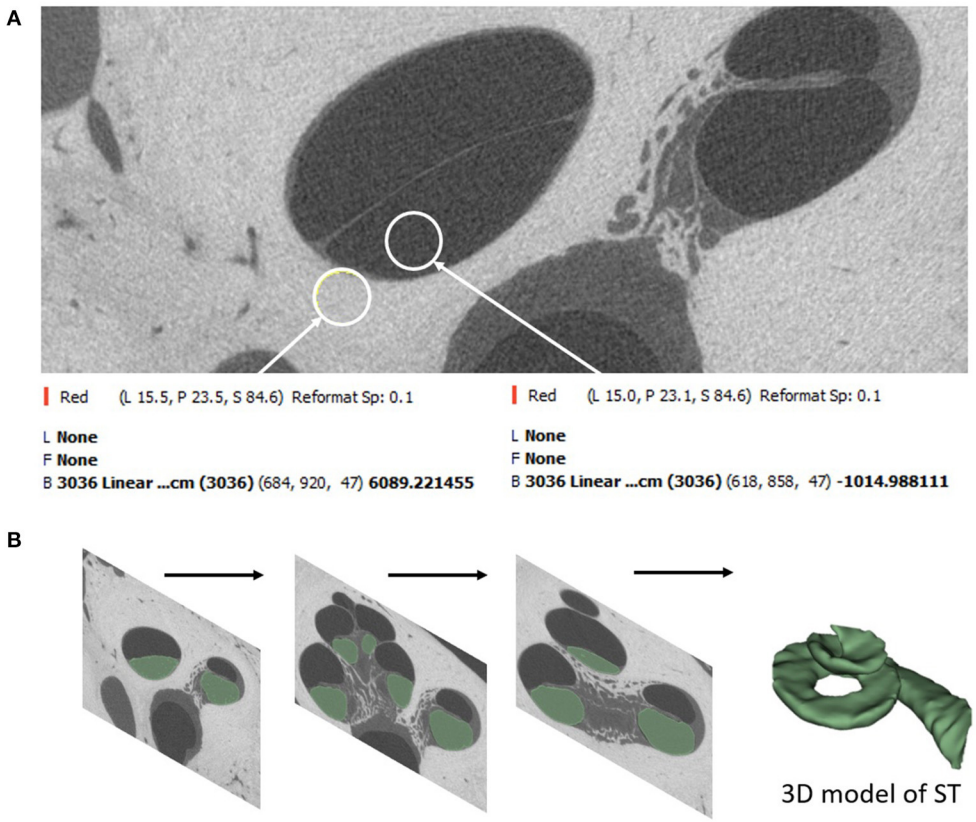

FIGURE 1 | Segmentation of ST starts by setting a tight grayscale threshold that distinguishes between the fluid filled ST and the surrounding bony region **(A)**. Segmentation is done by shading the areas of interest from all image slices **(B)**.

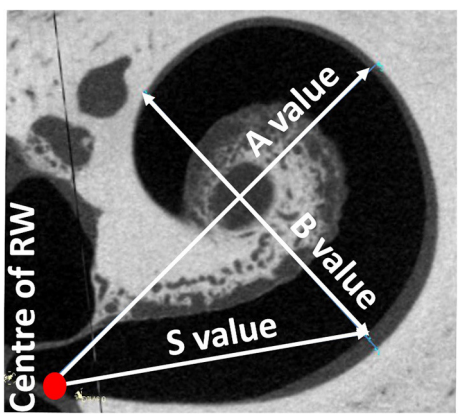

FIGURE 2 | Oblique coronal plane through the basal turn with the cochlear parameters defined.

The A-value was measured in the oblique coronal plane starting from the center of the round window membrane (RWM) and passing through the centre of the cochlea to the opposite lateral wall, as originally described by Escude et al. (12) (**Figure 2**). The B-value refers to the width of the basal turn which is measured by drawing a line perpendicular to the A-value. The S-value refers to the length of the straight portion of the cochlear basal turn starting from the RWM to the inferior end of the B-value line. Measurements were cross-checked and validated by two authors.

Electrode Insertion Force Measurement

All electrode insertion experiments were performed in an acrylic 3D model of the ST in two different sizes (**Figures 3A,B**). The fabrication process is described by Leon et al. (13). The volume of the smaller model was 35 μl; whereas the larger model had the same morphology but was upscaled by 1.5 × to 52.5 μl. This enabled direct comparison of the impact of size, irrespective of confounding anatomical variations. Insertion forces were measured using a commercially available S-shaped, single axis (compression and tension) load cell with a measuring range up to 5 newtons (N) (Zwick Roell, Xforce HP https://www.zwickroell.com/accessories/xforce-load-cells/). The ST model was placed atop the load cell and filled with 0.1% soap solution to act as a lubricant. The sensor was mounted on a positioning device to enable the precise adjustment of the cochlear model's position and orientation with respect to insertion of the electrode array (**Figure 3C**). The experiment was performed across five insertion speeds (0.1, 0.5, 1, 2, and 4 mm/s) using two different electrode

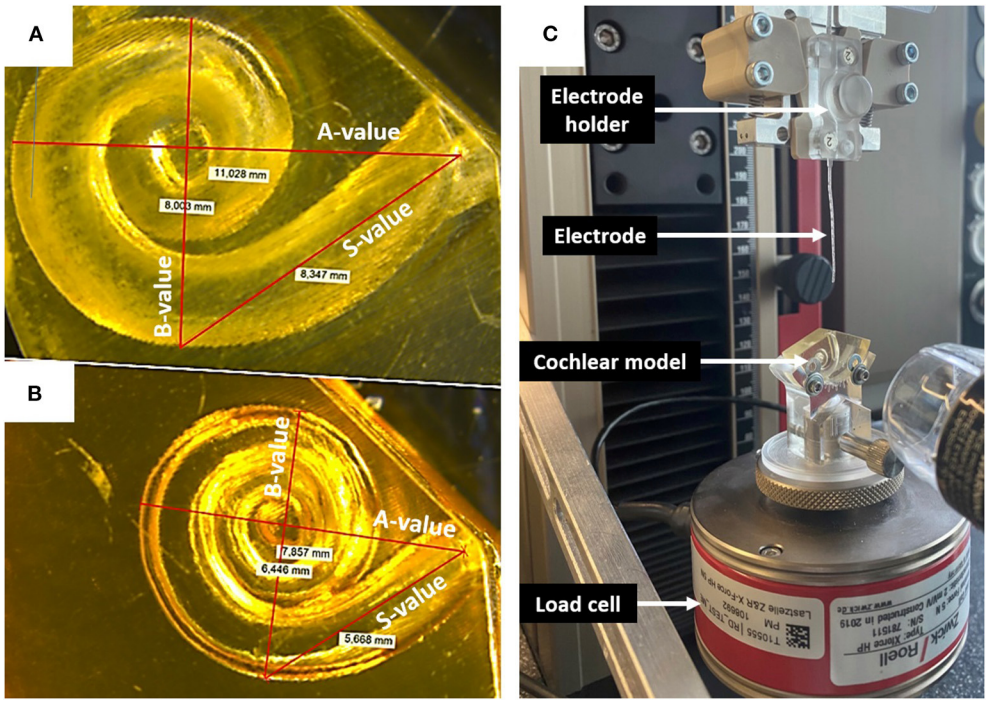

FIGURE 3 | (A) Upscaled ST model: A-value 11 mm; B-value 8 mm; S-value 8.3 mm. **(B)** Small ST model: A-value 7.9 mm; B-value 6.4; S-value 5.6 mm. **(C)** Electrode insertion force measurement test set-up.

array lengths of 24 mm (FLEX24) and 28 mm (FLEX28) at full insertion. The volume of FLEX24 and FLEX28 electrode arrays were calculated as 6.9 and 8.8 µl, respectively. For each length of the electrode array, the measurements were repeated three times, plus repeated with three different arrays. Thus, nine measurements were performed in total per implant length for each insertion speed.

Statistical Analysis

Regression estimates between the A- and B-values and A- and S-values (confidence level 0.95) were determined using the data analysis tool in STATISTICA software (version 14.0, https://www.tibco.com/products/data-science). Pearson's coefficient (r) was used to assess the strength of correlation between measurements. A multiple linear regression model was designed to formulate an equation that predicted the ST volume, using the A- and B-values. Two-way ANOVA test with replication was used to check the significance in electrode insertion forces comparing between the electrode length, ST models and the insertion speeds.

RESULTS

Data Analysis

Table 1 summarizes the cochlear parameters as measured by A-, B-, and S- values, and ST volume from both HEAR-EU and Cambridge datasets. The mean A-, B-, and S-values of combined datasets were 9.0 ± 0.5, 6.7± 0.4, and 6.9 ± 0.5 mm, respectively. The mean ST volume was 34.2 ± 7 µl although this value varied significantly between different samples (range 23–50 µl). The predicted ST volume was calculated applying Equation 1, applying the A-and the B-values, as described below.

The ST volume increased linearly with an increase in A- and B-values (Pearson's coefficient r 0.55 and 0.56, respectively) (**Figures 4A,B**). The A-value correlated with the B- and S-values (Pearson's coefficient *r* 0.64 and 0.66, respectively) (**Figures 4C,D**).

Prediction of ST Volume From Basic Cochlear Parameters

The multiple linear regression model to predict the ST volume from the A-, and the B-values resulted in the following equation (Equation 1). The A- and B-values were measured in mm.

$$Equation\ 1: Predicted\ ST\ volume\ (\mu l) = (A\ value^{*}5) + (B\ value^{*}5.8) - 49.7$$

The gray shaded columns in **Table 1** corresponded to the predicted ST volume when applying Equation 1 and the error percentage between the estimated and measured ST volume. The mean measured and predicted ST volume was 34.2 µl in both cases, although the range varied from 23–50 to 26.2–40.0 µl, respectively.

Electrode Insertion Force Measurement

As the electrode enters the cochlea, the tip touches the inner wall of the ST model at the S-value point (**Figure 5**).

TABLE 1 | A-, B-, S-values measured from the μCT images in the oblique coronal view of cochlear basal turn and ST volume measured from 3D segmented model of ST.

Source of μCT datasets	A-value (mm)	B-value (mm)	S-value (mm)	Measured ST volume (μl)	Predicted ST volume (μl)	Absolute error (%)
HEAR-EU ($n = 15$)	9.4	6.8	7.7	36	36.8	2.2
	8.7	6.2	6.8	33	29.7	11
	8.9	7.1	7.0	45	36.1	24.7
	8.4	6.7	6.6	33	31.2	5.6
	9.7	6.9	7.9	49	38.9	26
	8.7	6.6	6.9	34	32.2	5.7
	9.6	6.9	7.5	50	38.4	30.3
	8.6	7.0	7.1	46	34	35.4
	8.7	6.1	6.9	28	29.2	4.2
	8.6	6.0	7.1	28	28.2	0.55
	8.8	6.5	7.5	28	32.1	12.7
	9.2	6.8	7.2	35	35.81	2.3
	8.8	6.2	6.7	29	30.3	4.3
	8.7	6.5	7.0	34	32	7.7
	9.3	6.0	7.0	43	37	17.6
Cambridge ($n = 15$)	9.7	7.2	6.9	36	41	11.4
	8.0	6.2	5.8	23	26.3	12.5
	8.8	6.4	6.0	29	31.3	7.4
	9.0	7.0	6.6	31	35.5	12.8
	8.5	6.6	6.3	27	31	12.8
	8.7	6.0	6.3	23	28.4	19
	9.5	7.0	7.1	36	38.4	6.3
	9.1	7.4	6.3	34	38.7	12.2
	9.1	7.3	6.8	32	38	15.7
	9.4	7.1	7.0	41	38.8	5.7
	9.2	7.0	6.9	36	36.9	2.4
	9.1	6.4	6.7	30	32.4	7.4
	9.5	7.4	7.4	31	41	24.3
	8.1	6.5	6.3	32	28.6	11.9
	9.5	7.1	6.9	34	39.4	13.6
Range	8.0–9.7	6.0–7.4	5.8–7.9	23–50	26.2–40.9	0.55–35.4
Mean +/- standard deviation	9.0 ± 0.5	6.7 ± 0.4	6.9 ± 0.5	34.2 ± 7	34.2 ± 4.2	12.2 ± 8.7

The S-value was 5.6 mm for the smaller sized ST model and 8.3 mm for the upscaled model. The insertion force was almost negligible when measured up to these points for both array lengths and all insertion speeds (**Table 2**).

Observation of insertion force in the first portion of the basal turn (at 15 mm of the insertion depth from the ST opening), indicated a trend for lower insertion forces at lower insertion speeds, whereby forces increased with higher insertion speeds (magnified view in **Figure 6**).

Overall, the insertion forces were lower in the upscaled model in comparison to the smaller sized ST model for both FLEX28 and FLEX24 electrodes at its full insertion depth, irrespective of the insertion speed, as shown in **Figure 6**. Two-way ANOVA test with replication showed a statistical significance of $p < 0.0001$ in insertion forces measured in smaller and upscaled ST models. Mean insertion forces for the insertion speeds are provided in **Table 3**.

DISCUSSION

As we move toward personalized cochlear implantation, there is a clinical need to characterize patient specific anatomical variations. Specific areas of interest include, but are not limited to, (i) ST volume relative to basic cochlear parameters, (ii) electrode insertion force relative to insertion speeds dependent upon cochlear size, and (iii) the impact of insertion speeds on the insertion force at the S-value point. This pre-operative information will add to the wealth of information available to the surgeon to potentially influence intra-operative behavior. Furthermore, this information will be crucial to influence the development of robotic-assisted CI surgery (HEARO® system), controlled speed electrode insertion (ROBOTOL® system), and patient-specific pre-operative planning tools (OTOPLAN®).

This study has demonstrated that there are significant differences in the size of anatomically normal cochlea, in terms of ST volume and basic cochlear parameters. The range in

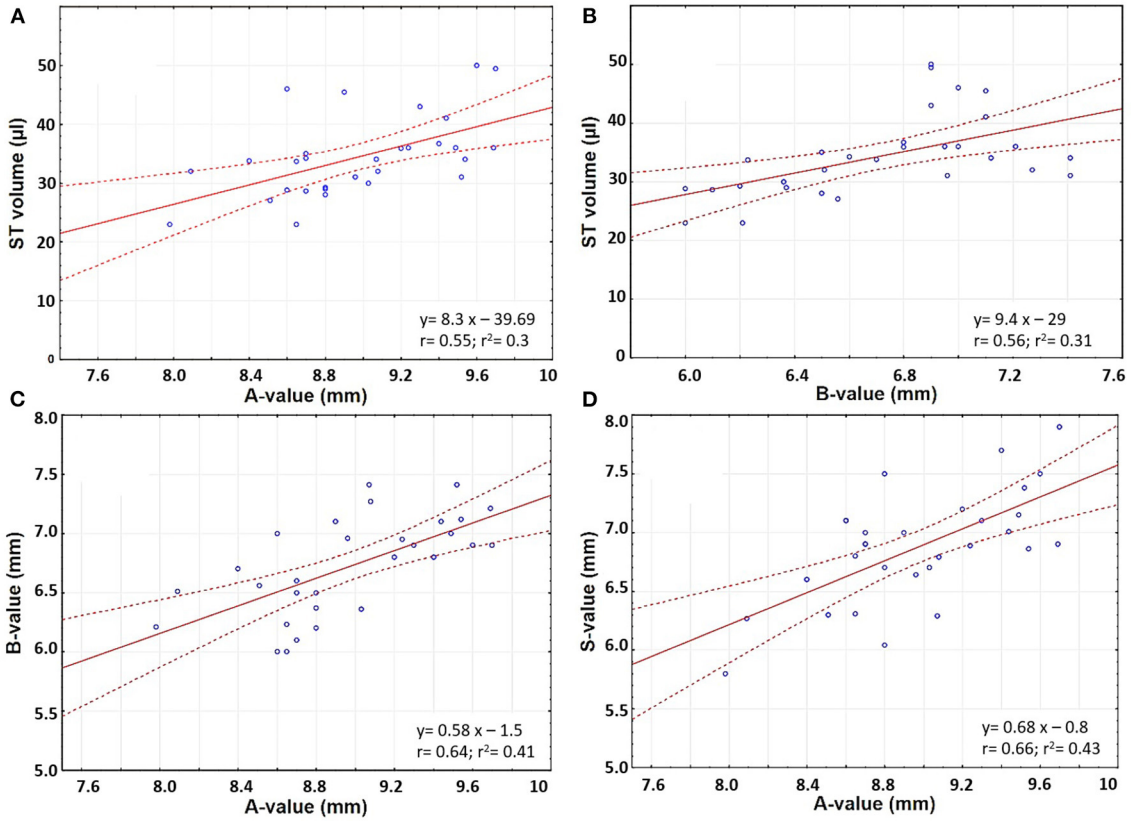

FIGURE 4 | Scatter plots comparing **(A)** A-value and ST volume; **(B)** B-value and ST volume; **(C)** A- and B- values; and **(D)** A- and S-values.

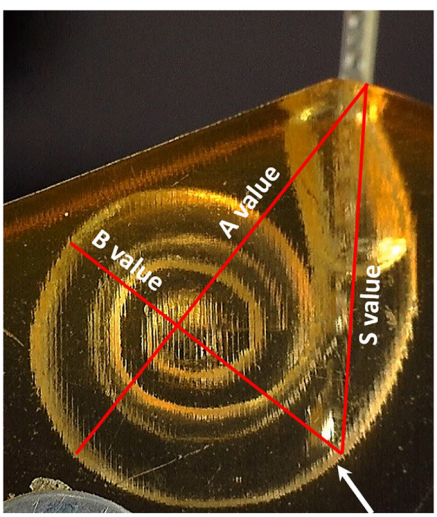

FIGURE 5 | The point where the electrode tip touches the inner wall of the cochlear model corresponds to the end of the S-value as pointed by the white arrow.

ST volume in this study is similar to earlier reports measured from three *u*CT datasets (14). For the clinician, knowledge of the ST volume has specific clinical relevance. Firstly, choice of electrode array relative to cochlear duct length (CDL) and ST volume may be predictive of hearing preservation after CI, as demonstrated by Takahashi et al. (15). The authors elegantly demonstrated that bony cochlear volume [combined ST and scala vestibuli (SV)] was a predictive factor for hearing preservation following CI surgery. Furthermore, pre-operative appreciation of ST volume might assist in injection of pharmaceutical agents into the ST at the time of implantation. When an array is inserted, the equivalent volume of perilymph is displaced from the ST. Thus, appreciation of pre-operative ST volume and volume of the electrode array, will enable prediction of the necessary concentration of pharmaceutical agent to be injected.

However, ST volume cannot be measured in clinical pre-operative CT scans owing to their low resolution (∼400 mm). Thus, a system which can predict ST volume is particularly valuable. In this study, the quasi-linear positive correlation between ST volume and A- and B-values enabled creation of a predictive algorithm to facilitate pre-operative prediction of ST

TABLE 2 | Electrode insertion force (N) measured at the S-value point in the two different sized cochlear model.

	Small sized model (S = 5.6 mm)					Upscaled model (S = 8.3 mm)				
Insertion speed (mm/sec)	0.1	0.5	1	2	4	0.1	0.5	1	2	4
FLEX^{28}	0	0.0004	0.0008	0.0001	0.0007	0	0.0003	0	0.0003	0.003
FLEX^{24}	0	0.0003	0.0002	0.0004	0.001	0	0.0002	0.0001	0.0002	0.0005

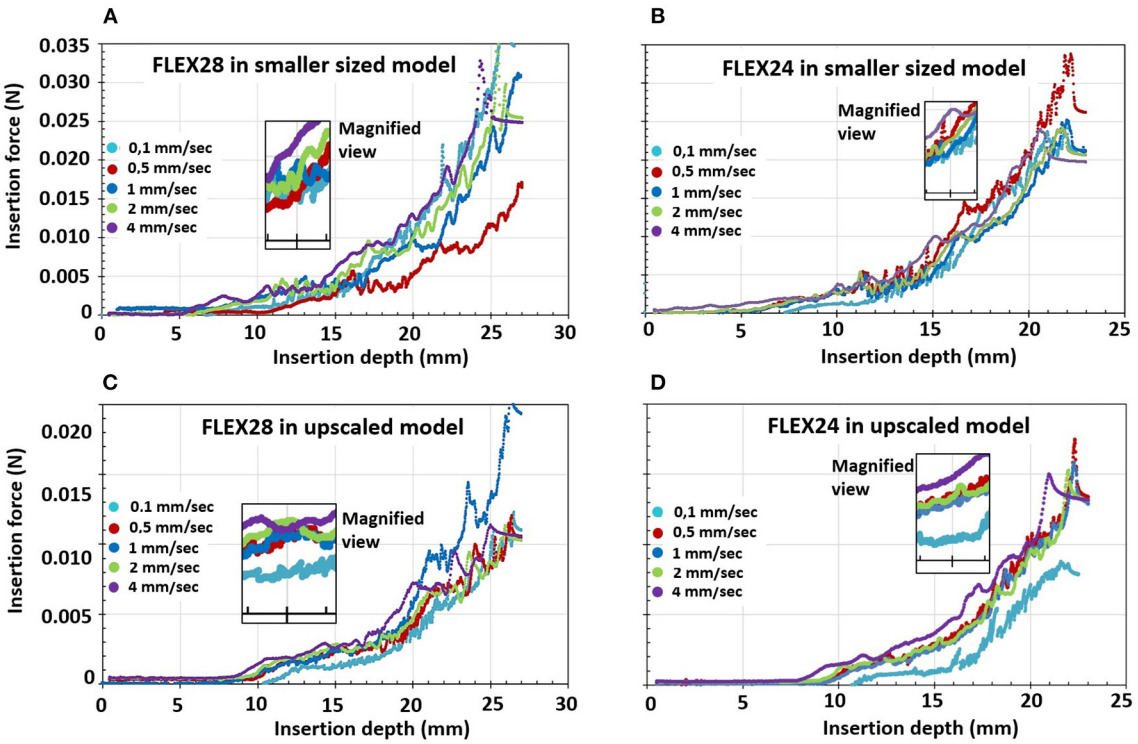

FIGURE 6 | Electrode insertion force measurement of FLEX28 and FLEX24 electrodes in two different sized cochlear model applying five different insertion speeds of 0.1, 0.5, 1, 2, and 4 mm/s. **(A)** FLEX28 and **(B)** FLEX24 in the average sized cochlea model. **(C)** FLEX28 and **(D)** FLEX24 in the upscaled model. The inner magnified view shows the insertion force curves for various insertion speeds at 15 mm of insertion depth. The purple curve corresponds to the highest insertion speed of 4 mm/s showing higher insertion forces and the turquoise curve corresponds to the lowest insertion speed of 0.1 mm/s showing lower insertion forces.

volume on the basis of purely the A- and B-values as a novel finding. These two values are routinely measured pre-operatively as part of the radiological work-up prior to implantation. This approach is consistent with findings by Schurzig et al. who demonstrated that estimation of CDL is more accurate when considering both A- and B-values, rather than solely the A-value (16).

The second part of this study assessed the importance of individual cochlea size by focusing upon electrode insertion force in ST models of two different sizes/volumes. Results indicated that cochlear size, electrode array length and insertion speed are of varying importance to the force that the cochlea experiences during insertion. Insertion forces increased during insertion. The lower insertion forces in the upscaled model are likely owing to the greater cross-sectional dimensions of the ST model around the electrode array, thus offering less resistance. In clinical setup, larger ST volume would minimize the physical contact between the electrode array surface and the intra-cochlear structures including the basilar membrane. The other assumption is that with larger ST volume, the helicotrema would also be larger allowing the cochlear fluid to escape from the ST to the scala vestibuli. Earlier reports by Kontorinis et al. and Landry et al. indicated that higher insertion speed was associated with higher insertion forces (17, 18). Our findings were reflected in a study recently published by Aebischer et al. (19). The authors reported higher insertion forces with higher insertion speed across six different ST models (19). This was reflected in our study as well. The highest insertion speed of 4 mm/s recorded the highest insertion forces in both ST models and for both electrode arrays tested.

The first potential contact that the array may make with the cochlear lateral wall is at the S-value. When measured, the insertion force at the S-value was negligible. This may be related to the highly flexible nature of the FLEX electrodes utilized during this study. However, the forces start to increase after an insertion depth of approximately 10 mm and that's

TABLE 3 | Mean insertion forces for FLEX28 and FLEX24 electrodes inserted at various insertion speeds in two different sized ST models.

Electrode type	ST model	Mean insertion forces at insertion speeds (Newtons)	Significance
FLEX28	Smaller model	0.025 (4 mm/s) 0.025 (2 mm/s) 0.03 (1 mm/s) 0.016 (0.5 mm/s) 0.034 (0.1 mm/s)	$p < 0.0001$
	Upscaled	0.01(4 mm/s) (2 mm/s) 0.02 (1 mm/s) (0.5 mm/s) 0.011 (0.1 mm/s)	
FLEX24	Smaller model	0.019 (4 mm/s) 0.02 (2 mm/s) 0.02 (1 mm/s) 0.026 (0.5 mm/s) 0.02 (0.1 mm/s)	$p < 0.0001$
	Upscaled	0.013 (4 mm/s) 0.013 (2 mm/s) 0.013 (1 mm/s) 0.013 (0.5 mm/s) 0.007 (0.1 mm/s)	

when the electrode start to bend inside the ST models. It is certainly of clinical interest to compare the insertion force at the S-value between arrays made of different materials from different CI brands. This could allow for adjustment of insertion speed at the S-value point depending on array material. Recently, Hendricks et al. studied the possibility of preventing the electrode tip touching the cochlear lateral wall, by magnetic guidance, by utilizing a modified electrode array with a magnet at the tip (20). All these research efforts work toward the aim of structure preservation during implantation to ensure hearing preservation and minimize the subsequent inflammatory process. Theoretically, it can be thought that the volume of the electrode array chosen for implantation in relation to the ST volume could as well be a deciding factor in the preservation of residual hearing as the electrode volume could restrict the vibrational properties of basilar membrane. This could be a study for the future on the evaluation of hearing preservation based on the electrode array length and volume chosen matching the ST volume estimated from the pre-operative cochlear parameters.

The ability to measure insertion forces during cochlear implantation is not feasible with manual clinician insertion; however, it may be incorporated into automated insertion devices. For instance, robotic insertion has the advantage of quantifiable haptic feedback, enabling direct feedback if insertion forces rise above a certain threshold. Our finding is in line with previous clinical reports on higher insertion forces and lower hearing preservation rates associated with higher insertion speed (21).

A wide variation in cochlear anatomy has been captured in this study of thirty μCT datasets. However, the variation in ST volume, A- and B-values resulted in a weaker correlation, which could be better defined by adding more datapoints. It would be more clinically relevant to compare insertion forces in cochleae of different sizes and shapes, with accurate RW reconstruction, rather than an upscaled model.

CONCLUSIONS

ST volume was positively correlated with the A- and B-value, allowing the potential for pre-operative ST volume prediction from clinical CT scans. The S-value also increased linearly with the A-value. The ST size influenced electrode insertion force, in that in general higher insertion forces were observed with the smaller sized ST model compared to the upscaled model irrespective of the length of the implant. A trend toward lower insertion force for lower insertion speed and vice-versa was observed from the insertion force curves before the electrode reached its maximum insertion depth. Taken together these findings indicate that there are significant patient variations in cochlear size, and this may impact upon insertion forces. Whilst insertion forces increase during advancement of the CI, the absolute value may be difficult to sense manually (measured in milli-newtons). Such small changes in force would be best measured by automated insertion systems, which employ more accurate haptic feedback than is possible by the human hand.

DATA AVAILABILITY STATEMENT

Half of the data were the result of HearEU project, https://cordis.europa.eu/project/id/304857. The data can be obtained by asking the project co-ordinator. The remaining raw data supporting the conclusions of this article will be made available by the authors, without undue reservation.

AUTHOR CONTRIBUTIONS

AD: study design, data collection, data analysis, figure preparation, manuscript writing, and literature search. CS: study design, data collection, data analysis, and manuscript writing. MB and PV: critical review, data analysis, and manuscript review. VV: critical review, literature search, and manuscript review. All authors contributed to the article and approved the submitted version.

ACKNOWLEDGMENTS

The authors kindly acknowledge Thomas Öfner from MED-EL for his support in the electrode insertion force measurements. Edwin Wappl-Kornherr from MED-EL is acknowledged for his support in statistical analyses. Philipp Schindler, former MED-EL employee is kindly remembered for his work in the preparation of the scala tympani models. We would like to acknowledge funding and support from the Anatomical Society.

REFERENCES

1. Dhanasingh A, Hochmair I. Thirty years of translational research behind MED-EL. *Acta Otolaryngol.* (2021) 141(suppl. 1): i-cxcvi. doi: 10.1080/00016489.2021.1918399
2. Friedland DR, Runge-Samuelson C. Soft cochlear implantation: rationale for the surgical approach. *Trends Amplif.* (2009) 13:124–38. doi: 10.1177/1084713809336422
3. Cubillana-Herrero JD, Fernandez JA, Cubillana MJ, Navarro A, Pelegrín JP. How the learning curve affects the cochlear implant program in the region of murcia. *J Otolaryngol Stud.* (2018) 1:103.
4. Ishii T, Takayama M, Takahashi Y. Mechanical properties of human round window, basilar and reissner's membranes. *Acta Otolaryngol Supp.* (1995) 519:78–82. doi: 10.3109/00016489509121875
5. Kaufmann CR, Henslee AM, Claussen A, Hansen MR. Evaluation of insertion forces and cochlea trauma following robotics-assisted cochlear implant electrode array insertion. *Otol Neurotol.* (2020) 41:631–8. doi: 10.1097/MAO.0000000000002608
6. Park LR, Teagle HFB, Gagnon E, Woodard J, Brown KD. Electric-acoustic stimulation outcomes in children. *Ear Hear.* (2019) 40:849–57. doi: 10.1097/AUD.0000000000000658
7. Niu XM, Ping L, Gao RZ, Xia X, Fan XM, Chen Y, et al. [Selection of cochlear electrode array implantation lengths and outcomes in patients with bilateral sensorineural hearing loss]. *Zhonghua Yi Xue Za Zhi.* (2021) 101:108–14. doi: 10.3760/cma.j.cn112137-20201005-02770
8. Caversaccio M, Gavaghan K, Wimmer W, Williamson T, Ansò J, Mantokoudis G, et al. Robotic cochlear implantation: surgical procedure and first clinical experience. *Acta Otolaryngol.* (2017) 137:447–54. doi: 10.1080/00016489.2017.1278573
9. Tekin AM, Matulic M, Wuyts W, Assadi MZ, Mertens G, Rompaey VV, et al. A new pathogenic variant in *POU3F4* causing deafness due to an incomplete partition of the cochlea paved the way for innovative surgery. *Genes.* (2021) 12:613. doi: 10.3390/genes12050613
10. Barriat S, Peigneux N, Duran U, Camby S, Lefebvre PP. The use of a robot to insert an electrode array of cochlear implants in the cochlea: a feasibility study and preliminary results. *Audiol Neurootol.* (2021) 15:77–82. doi: 10.1159/000513509
11. Dhanasingh A, Dietz A, Jolly C, Roland P. Human Inner-ear Malformation Types Captured in 3D. *J Int Adv Otol.* (2019) 15(1):77–82. doi: 10.5152/iao.2019.6246
12. Escude B, James C, Deguine O, Cochard N, Eter E, Fraysse B. the size of the cochlea and predictions of insertion depth angles for cochlear implant electrodes. *Audiol Neurotol.* (2006) 11(Suppl. 1):27–33. doi: 10.1159/000095611
13. Leon L, Cavilla MS, Doran MB, Warren FM, Abbott JJ. Scala-Tympani phantom with cochleostomy and round-window openings for cochlear-implant insertion experiments. *J Med Dev*. (2014) 8:10. doi: 10.1115/1.4027617
14. Available online at: https://or20.univ-rennes1.fr/sites/or20.univ-rennes1.fr/files/asset/document/aldhamarietal2018_0.pdf (accessed September 14, 2021).
15. Takahashi M, Arai Y, Sakuma N, Yabuki K, Sano D, Nishimura G, et al. Cochlear volume as a predictive factor for residual-hearing preservation after conventional cochlear implantation. *Acta Otolaryngol.* (2018) 138:345–50. doi: 10.1080/00016489.2017.1393840
16. Schurzig D, Timm ME, Batsoulis C, Salcher R, Sieber D, Jolly C, et al. A novel method for clinical cochlear duct length estimation toward patient-specific cochlear implant selection. *OTO Open.* (2018) 2:345–350. doi: 10.1177/2473974X18800238
17. Kontorinis G, Lenarz T, Stöver T, Paasche G. Impact of the insertion speed of cochlear implant electrodes on the insertion forces. *Otol Neurotol.* (2011) 32:565–70. doi: 10.1097/MAO.0b013e318219f6ac
18. Landry TG, Earle G, Brown JA, Bance ML. Real-time intracochlear imaging of automated cochlear implant insertions in whole decalcified cadaver cochleas using ultrasound. *Cochlear Implants Int.* (2018) 19:255–67. doi: 10.1080/14670100.2018.1460024
19. Aebischer P, Mantokoudis G, Weder S, Anschutz L, Caversaccio M, Wimmer W. *In-Vitro* study of speed and alignment angle in cochlear implant electrode array insertions. *IEEE Trans Biomed Eng.* (2021). 255–267. doi: 10.1109/TBME.2021.3088232
20. Hendricks CM, Cavilla MS, Usevitch DE, Bruns TL, Riojas KE, Leon L, et al. Magnetic steering of robotically inserted lateral-wall cochlear-implant electrode arrays reduces forces on the basilar membrane *In Vitro*. *Otol Neurotol.* (2021) 18:17–22. doi: 10.1097/MAO.0000000000003129
21. Rajan GP, Kontorinis G, Kuthubutheen J. The effects of insertion speed on inner ear function during cochlear implantation: a comparison study. *Audiol Neurootol*. (2013) 18(1):17–22. doi: 10.1159/000342821

Conflict of Interest: AD is employed at MED-EL in scientific roles with no marketing activities.

The remaining authors declare that the research was conducted in the absence of any commercial or financial relationships that could be construed as a potential conflict of interest.

Publisher's Note: All claims expressed in this article are solely those of the authors and do not necessarily represent those of their affiliated organizations, or those of the publisher, the editors and the reviewers. Any product that may be evaluated in this article, or claim that may be made by its manufacturer, is not guaranteed or endorsed by the publisher.

frontiers in Surgery

ORIGINAL RESEARCH
published: 06 October 2021
doi: 10.3389/fsurg.2021.740935

Robot-Assisted Middle Ear Endoscopic Surgery: Preliminary Results on 37 Patients

Marine Veleur[1], *Ghizlene Lahlou*[1,2], *Renato Torres*[2], *Hannah Daoudi*[1], *Isabelle Mosnier*[1,2], *Evelyne Ferrary*[1,2], *Olivier Sterkers*[1,2] *and Yann Nguyen*[1,2]*

[1] *ENT Department, Sorbonne University, AP-HP, GHU Pitié-Salpêtrière, GRC Robot and Surgery's Innovation, Paris, France,* [2] *Inserm/Pasteur UMR 1120 "Innovative Technologies and Translational Therapeutics for Deafness", Hearing Institute Paris, Paris, France*

OPEN ACCESS

Edited by:
Pavel Dulguerov, Geneva University Hospitals (HUG), Switzerland

Reviewed by:
Michael Cohen, Massachusetts Eye and Ear Infirmary and Harvard Medical School, United States
Jiang Yan, The Affiliated Hospital of Qingdao University, China

***Correspondence:**
Yann Nguyen
yann.nguyen@inserm.fr
orcid.org/0000-0003-4635-0658

Specialty section:
This article was submitted to Otorhinolaryngology–Head and Neck Surgery, a section of the journal Frontiers in Surgery

Received: *13 July 2021*
Accepted: *10 September 2021*
Published: *06 October 2021*

Citation:
Veleur M, Lahlou G, Torres R, Daoudi H, Mosnier I, Ferrary E, Sterkers O and Nguyen Y (2021) Robot-Assisted Middle Ear Endoscopic Surgery: Preliminary Results on 37 Patients. Front. Surg. 8:740935. doi: 10.3389/fsurg.2021.740935

Background: Endoscopy during middle ear surgery is advantageous for better exploration of middle ear structures. However, using an endoscope has some weaknesses as surgical gestures are performed with one hand. This may trouble surgeons accustomed to using two-handed surgery, and may affect accuracy. A robot-based holder may combine the benefits from endoscopic exposure with a two-handed technique. The purpose of this study was to assess the safety and value of an endoscope held by a teleoperated system.

Patients and Methods: A case series of 37 consecutive patients operated using endoscopic exposure with robot-based assistance was analyzed retrospectively. The RobOtol® system (Collin, France) was teleoperated as an endoscope holder in combination with a microscope. The following data were collected: patient characteristics, etiology, procedure type, complications, mean air and bone conduction thresholds, and speech performance at 3 months postoperatively. Patients had type I (myringoplasty), II (partial ossiculoplasty), and III (total ossiculoplasty) tympanoplasties in 15, 14, and 4 cases, respectively. Three patients had partial petrosectomies for cholesteatomas extending to the petrous apex. Finally, one case underwent resection of a tympanic paraganglioma. Ambulatory procedures were performed in 25 of the 37 patients (68%).

Results: Complete healing with no perforation of the tympanic membrane was noted postoperatively in all patients. No complications relating to robotic manipulation occurred during surgery or postoperatively. The mean air conduction gain was 3.8 ± 12.6 dB for type I (n = 15), 7.9 ± 11.4 dB for type II (n = 14), and −0.9 ± 10.8 for type III tympanoplasties (n = 4), and the postoperative air-bone conduction gap was 13.8 ± 13.3 dB for type I, 19.7 ± 11.7 dB for type II and 31.6 ± 13.0 dB for type III tympanoplasty. They was no relapse of cholesteatoma or paraganglioma during the short follow-up period (<1 year).

Conclusion: This study indicates that robot-assisted endoscopy is a safe and trustworthy tool for several categories of middle ear procedures. It combines the benefits of endoscopic exposure with a two-handed technique in middle ear surgery. It can be used as a standalone tool for pathology limited to the middle ear cleft or in combination with a microscope in lesions extending to the mastoid or petrous apex.

Keywords: PORP, TORP, cholesteatoma, tympanoplasty, safety, robotics, robot, surgery

BACKGROUND

Endoscopy during middle ear surgery offers several benefits over microscopic exposure as it can provide an angled view of middle ear cavities and a closer view of structures (1, 2). Surgeons may have different uses for an endoscope ranging from a simple check after cholesteatoma removal at the end of surgery to exclusive use for exposure during the entire surgical procedure (3–5). An endoscopic technique allows a trans canal, minimally invasive approach in cholesteatoma surgery with long-term results similar to techniques using a posterior approach (6). Endoscopy is particularly useful in preventing residual cholesteatoma (7). Nevertheless, this technique is not widely used despite longstanding publications by early adopters (7–9).

Classifications to better describe the exclusive use of an endoscope or in combination with a microscope have been reported to aid comparisons with traditional techniques (10). However, endoscopic surgery has some limitations as surgical gestures are performed using one hand. This may trouble surgeons accustomed to two-handed surgery. It can affect accuracy and gestures, especially in complex surgical steps requiring delicate interactions with middle ear structures (11). Middle ear surgery is performed in a reduced anatomic space using a keyhole approach and often requires constant blood suction. Even moderate bleeding can easily fill the operating field obscuring vision of critical and fragile structures such as the ossicular chain or facial nerve. Holding the endoscope means that surgeons have to choose between suction or a surgical tool in their dominant hand. This is the main reason why conventional one-handed endoscopic surgery has a lengthy learning curve (11).

To overcome this obstacle, several modified endoscope holders have been described (12–14). These devices allow double-handed surgery to be performed as in the conventional microscopic technique. Another method of holding the endoscope to assist the surgeon is to use a motorized micro-manipulator. The RobOtol® system (Collin Medical, Bagneux, France) was specifically designed for middle ear microsurgery and cochlear implantation, and has been adapted to include a teleoperated endoscope holder. Its safety has been reported in a limited number of patients (15, 16). Motion of the arm bearing the endoscope is achieved by a serial kinematic chain of three perpendicular linear links at the base and three rotatory links on the distal arm. This gives six degrees of freedom, three translational and three rotational axes.

The aim of this study was to assess the safety and value of an endoscope held by a teleoperated system such as the RobOtol® during middle ear surgery.

PATIENTS AND METHODS

This retrospective study included a consecutive series of patients who were treated surgically for the following pathologies: cholesteatoma, chronic otitis, tympanic perforation, retraction pocket, tympanic paraganglioma or ossicular lysis. It included cases operated on between September 2018 and February 2021. This period followed on from our previous report on our early experience (16). The surgical procedures performed were tympanoplasty type I (myringoplasty), II (partial ossiculoplasty) or III (total ossiculoplasty), revision surgical procedures for middle ear cholesteatoma or ossicular pathology, resection of tympanic paraganglioma or resection of cholesteatoma of the petrous apex. We used the RobOtol® system teleoperated as an endoscope holder alone or in combination with a microscope. The system could carry 0° or 30°, 3.3 mm endoscopes (REF RBT-END-0 and REF RBT-END-30, Karl Storz, Tuttlingen, Germany). These were connected to an IMAGE1 STORZ Professional Image Enhancement System with CLARA image post-processing mode. The RobOtol system included a cart, a controller, a human–machine interface and a robot-based arm (**Figure 1**). We used the arm as an endoscope holder. The system is driven by the surgeon with a SpaceMouse (3Dconnexion, Waltham, MA, USA) allowing it to move the endoscope with six degrees of freedom. The robot arm is covered with a dedicated sterile drape, and a sterile adaptor provides the link between the arm and the endoscope (**Figure 2**). It allows to use a suction and an effector tool combined with an endoscopic exposure (**Figure 3**).

Our earlier study showed that the duration of set-up of the robot was 3.2–5 min and required robot cart and endoscopy column placement in the operating room, robotic arm dressing, and connection of the camera head and light source cable (16). The robot was always used in combination with a microscope as back-up, classifying all operations as two according to the EES classification (10). The duration of the operation was noted. The incision was either transcanal or retroauricular depending on the location of the cholesteatoma. The following data were collected: demographic data (age, sex), pathology, procedure type, side, previous history of otological surgery on the same side, complications during surgery, incision type, duration of surgery, and type of hospitalization (ambulatory,

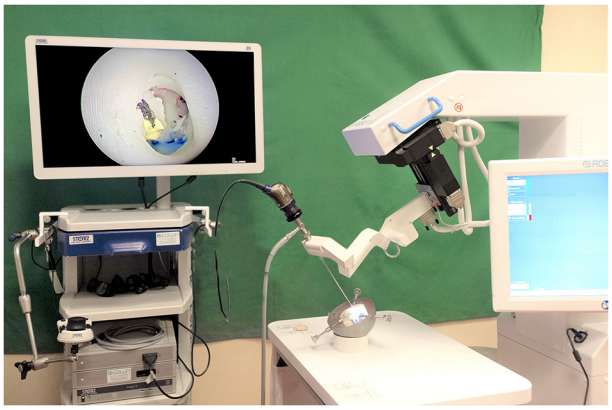

FIGURE 1 | RobOtol System in endoscope holder configuration with an artificial temporal bone. The RobOtol System (Collin, Bagneux, France) is a tele-operated arm that can bear instruments or an endoscope. It can be connected to any HD camera system (Here a Image1 Storz HD endoscopy column, Karl Storz, Tuttlingen, Germany). The robot is composed of a cart bearing the arm, a display screen used to change speed and control settings. The device is driven by a space mouse (3D Connection, Waltham, MA, USA, not shown here).

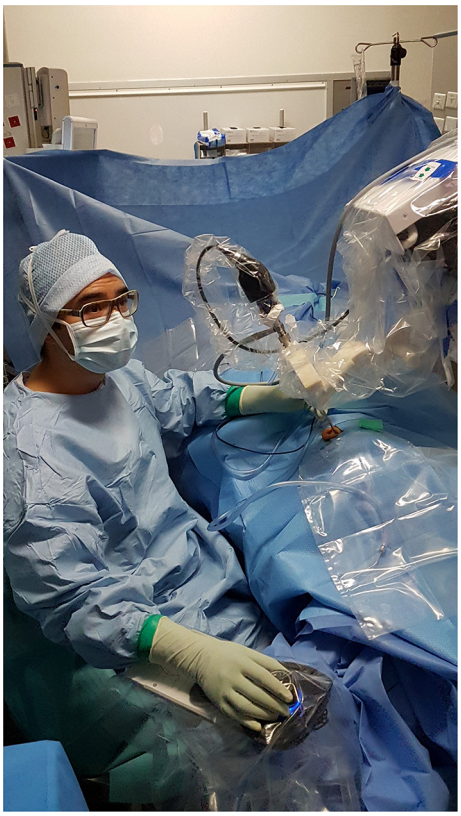

FIGURE 2 | RobOtol System installed in an operating room environment. In clinical use, the robot and the endoscopy column are placed in front of the patient. The arm of the robot and the camera head are covered with a sterile drape. The device is teleoperated by a space mouse (3D Connection, Waltham, MA, USA) covered by a sterile drape.

or conventional). Preoperative assessment included otoscopy, and pure-tone audiometry with headphones. Postoperative assessment included anatomic results with otoscopy, audiometry and complications. All patients had a preoperative audiometric test and a postoperative test 3 months after surgery. Air conduction (AC) (125–8,000 Hz) and bone conduction (BC) (250–4,000 Hz) thresholds were recorded. Thresholds at 500, 1,000, 2,000, and 4,000 Hz were used to calculate the pure-tone average (PTA) for both PTA AC and PTA BC, and the air-bone gap (ABG) as BC PTA minus AC PTA (ABG before surgery as PRE-OP ABG, ABG after surgery as POST-OP ABG). We also collected signal intensity for maximum speech intelligibility (mean "maximum speech intensity level" in dB) and mean speech recognition threshold ("SRT" in dB) before surgery and 3 months postoperatively.

Safety was defined by completion of surgery, operative time, no adverse events, and no insurmountable hindrance of visibility. All procedures performed in studies involving human participants were in accordance with the ethics standards of the institutional and/or national research committee and with the 1964 Helsinki Declaration and its later amendments or comparable ethics standards. All participants included accepted and signed a consent form to authorize data collection for this retrospective study. Data analysis was performed using the Student's *t*-test. Results are presented as mean ± standard deviation [minimum — maximum]. A $p < 0.05$ was considered to indicate a statistically significant difference between groups.

RESULTS

This retrospective study included 37 patients (21 women, 16 men) operated on between September 2018 and February 2021. Their mean age was 41 ± 14 years old [16–71]. Pathologies were 11 cholesteatomas, eight tympanic perforations, even chronic suppurative otitis media w/o cholesteatoma, sic retraction pockets, three cholesteatomas extending to the petrous apex, one tympanic paraganglioma, and one ossicular traumatism For these pathologies, the surgical procedures were 15 type I tympanoplasties (myringoplasty), 14 type II tympanoplasties (partial ossiculoplasty), and four type III tympanoplasties (total ossiculoplasty) (**Table 1**). We also performed three partial petrosectomies for cholesteatomas extending to the petrous apex and one resection of a tympanic paraganglioma. Ambulatory procedures were carried out in 25 of 37 patients (68%). Twenty-two procedures used a transcanal approach (59%). There were 22 primary surgical procedures (59%). Mean duration of surgery was 155 ± 49 min [121–363 min]. Complete healing with no perforation of the tympanic membrane was noted postoperatively in all patients. No complications related to the robotic manipulation occurred during surgery or in the postoperative period. No recurrent cholesteatoma or paraganglioma was observed postoperatively but one should take into account that the follow-up period was short (<1 year on average).

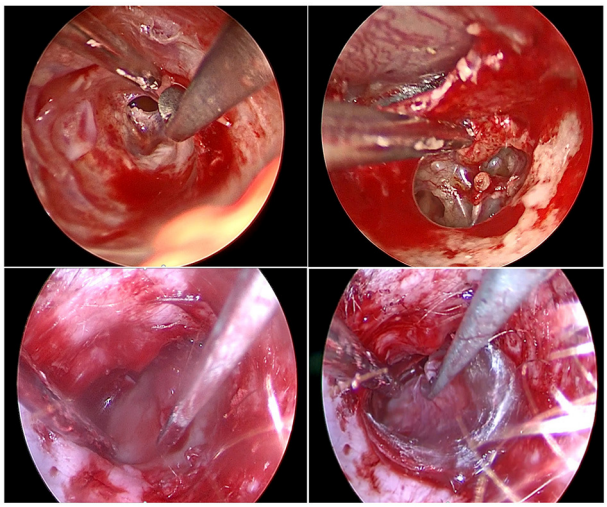

FIGURE 3 | Endoscopic view of various surgical steps during middle ear surgery. Top left, Skin incision and tympano-meatal flap raising; top right, Malleus handle dissection from tympanic membrane; bottom left, cartilage grafting placement; bottom right, temporal fascia grafting placement. Note that on all picture a suction and a tool are used for a two-handed technique in combination with an endoscopic exposure.

TABLE 1 | Demographic and pathological characteristics of the 37 cases in this study.

		N (%)
Sex	Women	21 (57%)
	Men	16 (43%)
Side	Right	14 (38%)
	Left	23 (68%)
Pathology	Cholesteatoma	11 (30%)
	Chronic suppurative otitis media w/o cholesteatoma	7 (19%)
	Retraction pocket	6 (16%)
	Tympanic perforation	8 (22%)
	Ossicular traumatism	1 (3%)
	Cholesteatoma of petrous apex	3 (7%)
	Tympanic paraganglioma	1 (3%)
Surgery	Primary surgery	22 (59%)
	Revision surgery	15 (41%)
	Tympanoplasty I	15 (41%)
	Tympanoplasty II	14 (38%)
	Tympanoplasty III	4 (11%)
	Petrosectomy	3 (7%)
	Resection of tympanic paraganglioma	1 (3%)

Tympanoplasties (Type I;II and III Results)

For all tympanoplasties, the pathologies were 11 cholesteatomas (33%), eight perforations (24%), seven chronic suppurative otitis media w/o cholesteatoma (21%), six retraction pockets (18%), and one ossiculoplasty (3%) (one malleus fracture with incus luxation), and **Table 1**. It was the first surgical procedure for 20 patients (61%). We used 22 transcanal incisions (67%) and nine posterior incisions (27%). Mean bone conduction (BC) gain was 0.5 ± 9.2 dB [−15.0–22.5], mean speech recognition threshold (SRT) gain was 4.6 ± 13.6 dB [−24.0–35.0] and mean "Max speech intensity level" gain was 2.9 ± 18.2 dB [−25.0–45.0]. All differences were not statistically significant ($p = 0.76$, $p = 0.13$, $p = 0.67$, respectively). Mean air conduction (AC) gain was 5.0 ± 11.9 dB [−21.3–38.8], with a significant improvement from preoperative to postoperative ($p = 0.022$). PRE-OP ABG was 23.0 ± 13.2 [1.3–48.8], POST-OP ABG was 18.5 ± 13.5 [1.3–51.3], again with a significant improvement from preoperative to postoperative values ($p = 0.042$). Results are reported on **Figure 4**.

Group: Tympanoplasty Type I

Fifteen type 1 tympanoplasties were performed [10 women (67%)]. There were 13 ambulatory procedures (87%), 11 transcanal incisions (73%) and four posterior incisions (27%). It was the first surgery for 12 patients (80%), and revision surgery for three patients (and among these, one had multiple revisions). Mean operating time was 113 ± 32 min [51–170]. Surgery included two cholesteatomas (13%), two retraction pockets (13%), six tympanic perforations (40%), and five chronic suppurative otitis media w/o cholesteatoma (33%). Mean bone conduction gain was 0.4 ± 8.0 dB [−8.8–22.5]. Mean air conduction gain was 3.8 ± 12.6 dB [−21.3–38.8]. Mean SRT gain was 4.4 ± 7.8 dB [−8.0–18.0] and mean maximum speech intensity level was 1.4 ± 13.4 dB [−20.0–35.0]. All of these gains were not statistically significant ($p = 0.84$, $p = 0.26$, $p = 0.06$, $p = 0.70$, respectively). PRE-OP ABG was 17.3 ± 11.7 [1.3–38.8], POST-OP ABG was 13.8 ± 13.3 [1.3–51.3], and the difference was not statistically significant ($p = 0.13$).

Group: Tympanoplasty Type II

Fourteen type II tympanoplasties were performed on six women (43%). There were 10 ambulatory procedures (71%), and eight transcanal incisions (57%). It was the first surgery for six patients (43%), and revision surgery for eight patients (and among these, four had multiple revisions). Mean operating time was 148 ± 38 min [97–225]. Surgery included eight cholesteatomas (57%), one traumatism (incus luxation) (7%), three retraction pockets (21%), and two perforations (14%). In seven cases (50%), we used a titanium partial ossicular prosthesis (Heinz Kurz GmbH Medizintechnik, Dusslingen, Germany). The size of the prosthesis was 2.8 ± 0.2 mm [2.5–3.0]. In five cases (36%), we used Otomimix bone cement (Olympus, Hamburg, Germany). In one case (7%), we removed fibrosis around a partial prosthesis. In one case (7%), we used cartilage to perform the ossiculoplasty. Mean air conduction gain was 7.9 ± 11.4 dB [−6.3–36.3] and the difference between preoperative and postoperative values was significant ($p < 0.05$). Mean bone conduction variation was 1.7 ± 11.3 dB [−15.0–21.3], mean SRT gain was 4.6 ± 19.0 dB [−24.0–35.0] and mean maximum speech intensity level gain was 5.0 ± 23.2 dB [−25.0–45.0]. All of these gains were not statistically significant ($p = 0.58$, $p = 0.69$, $p = 0.79$, respectively). PRE-OP ABG was 26.0 ± 13.9 [6.3–48.8], POST-OP ABG was 19.7 ± 11.7 [6.3–40.0], and the difference was statistically significant ($p = 0.003$).

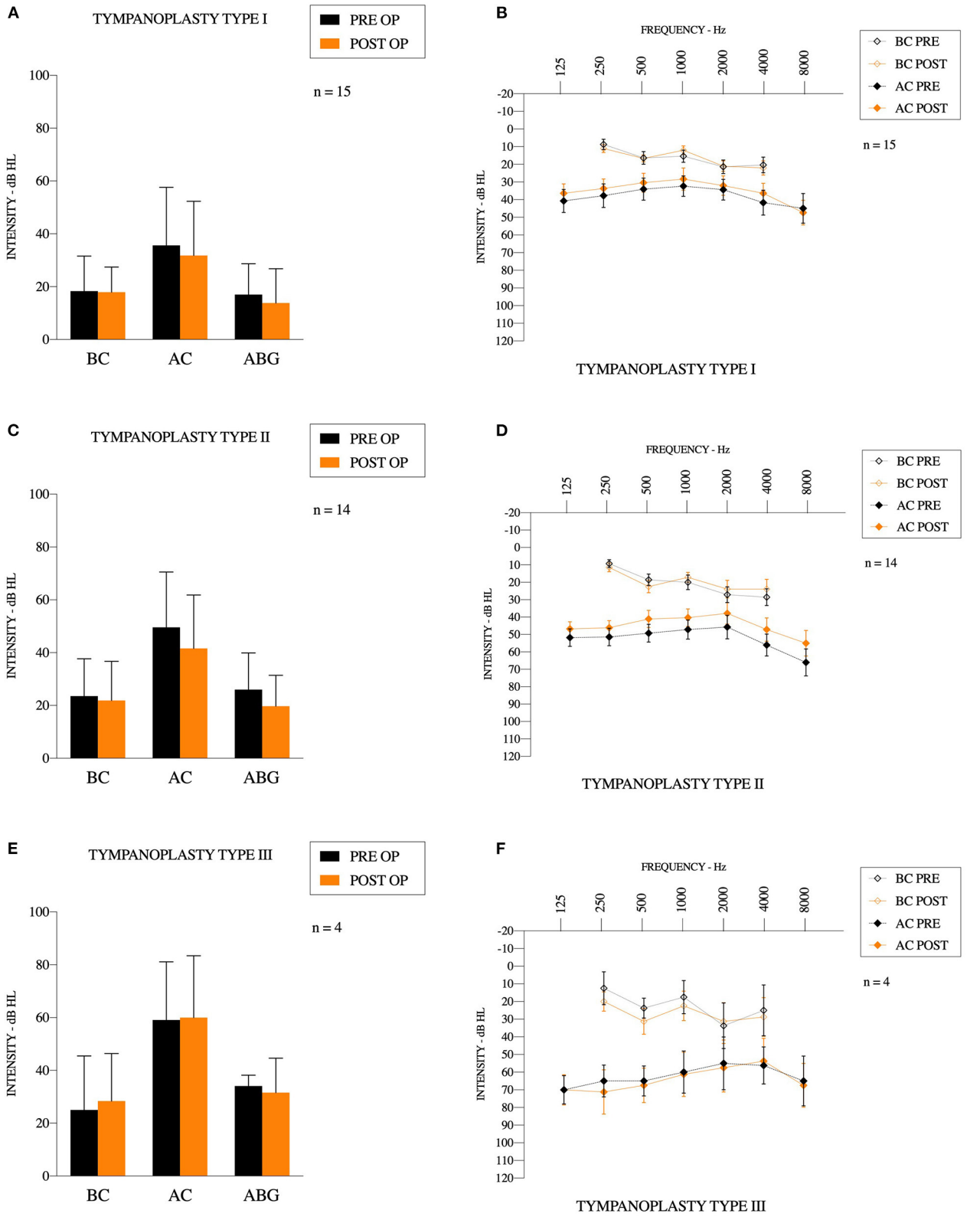

FIGURE 4 | Audiometric results **(A,C,E)** results for bone conduction, air conduction and air-bone gap for Type 1,2, and 3 tympanoplasties, respectively. **(B,D,F)** Mean preoperative and postoperative audiogram for Type 1,2, and 3 tympanoplasties, respectively.

Group: Tympanoplasty Type III

Four type III tympanoplasties were performed on three women (75%) and a man (25%). There were two ambulatory procedures (50%), and three transcanal incisions (75%). It was the first surgery for two patients (50%), and revision surgery for two patients (multiple revisions). Mean operating time was 153 ± 52 min [77–195]. Surgery included one cholesteatoma (25%), one retraction pocket (25%), and one chronic otitis (50%). In all cases, we used a titanium total ossicular prosthesis (Heinz Kurz GmbH Medizintechnik, Dusslingen, Germany). The size of the prosthesis was 4.4 ± 0.7 mm [4.0–5.5]. Mean bone conduction gain was −3.4 ± 5.6 dB [−11.3–1.3]. Mean air conduction gain was −0.9 ± 10.8 dB [−13.3–12.5]. Mean SRT gain was 5.5 ± 11.9 dB [−2.0–23.0] and mean max speech intensity level gain was 1.3 ± 19.3 dB [−10.0–30.0]. PRE-OP ABG was 34.1 ± 4.1 [30.0–38.8], and POST-OP ABG was 31.6 ± 13.0 [15.0–43.8]. All of these gains were not statistically significant ($p = 0.84$, $p = 0.26$, $p = 0.06$, $p = 0.70$, $p = 0.74$, respectively).

Group: Cholesteatoma of the Petrous Apex

We performed three surgical procedures on the petrous apex of one woman (33%) and two men (66%) and none were ambulatory procedures. We only used posterior incisions. It was the first surgery for one patient and the others already had multiple surgical procedures. Mean operating time for the three procedures was 181 ± 100 min [100–293].

Group Resection of Tympanic Paraganglioma

One resection of tympanic paraganglioma was performed on one woman, with conventional hospitalization and with a retroauricular incision. The operating time was 84 min and it was a primary procedure.

DISCUSSION

Middle ear surgery has always been a highly specialized surgical procedure. It requires lengthy training due to the confined surgical space, the risk of injury to sensorineural structures requiring excellent anatomic knowledge, and the intense practice that is required. Endoscopes have shown some benefits over the microscope in different aspect of this surgery (9), with decreased morbidity for second-look procedures, enhanced visualization including a wider angle of view and reduced operating time (17, 18). Difficult exposure of middle ear recesses demanding extensive drilling is one of the major reasons for residual disease, particularly for hidden structures such as the sinus tympani, anterior epitympanic recess, and eustachian tube as these areas are considered to be at risk of cholesteatoma recurrence (7). Indications and popularity have been steadily increasing and endoscope holders have been described, confirming the efficacy of two-handed endoscopic surgery (12–14).

In this study, the first aim was to demonstrate the safety and feasibility of endoscopic robot-assisted surgery in various middle ear operations such as type I, II or III tympanoplasties,

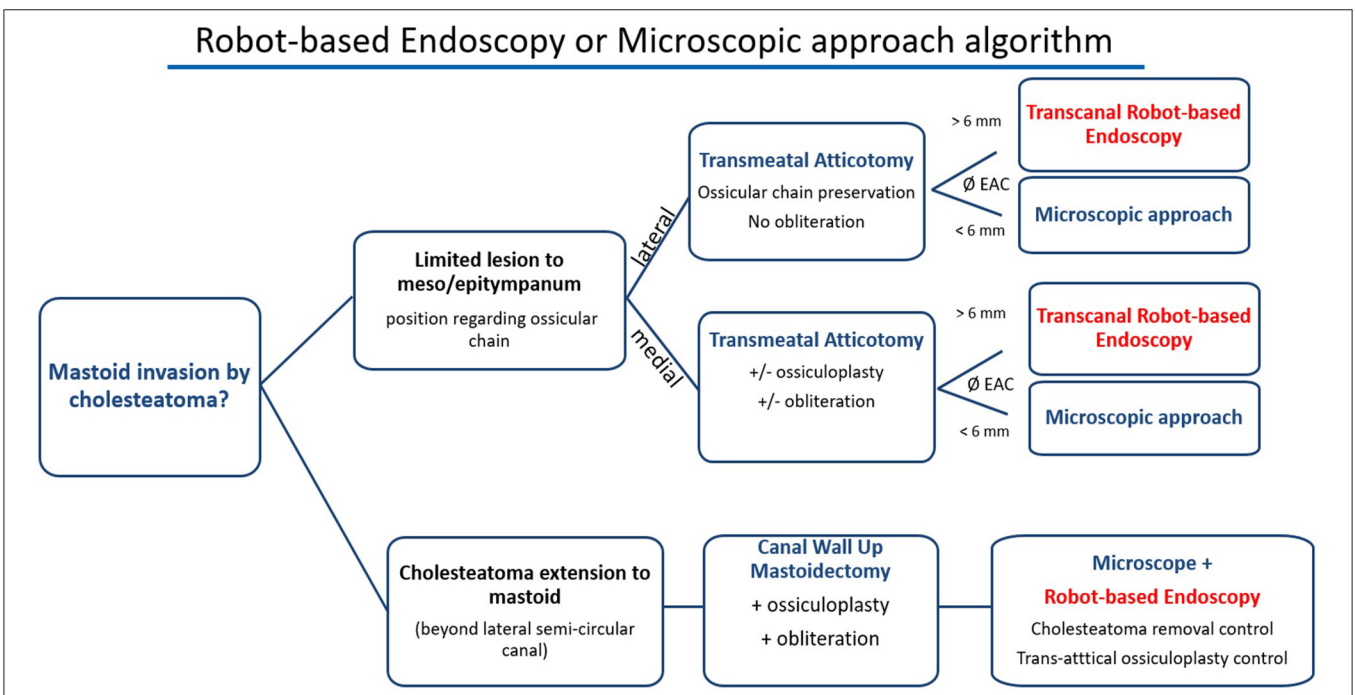

FIGURE 5 | Proposed algorithm for robot-based endoscopy indication. Robot-based endoscopy should be used as an additional tool to the microscope and not as a competing device. Its main limitation is the external auditory canal (EAC) diameter that may limit the use of two tools and the endoscope. We propose the following decision tree to choose the use of the robot-based endoscopy, the microscope and both to perform the approach and surgery.

cholesteatoma of the petrous apex, and tympanic paraganglioma. In this study, all patients benefited from complete healing with no perforation of the tympanic membrane and no complications related to the robotic manipulation either during surgery or in the postoperative period. All procedures were completed, and the robotic arm did not interfere with exposure of the surgical field, and was able to expose every middle ear location. For type I, II, and III tympanoplasties, the first aim was to close the tympanic membrane, and improve the air conduction (or obtain stable air conduction) without changes in bone conduction.

We have previously reported our surgical results for partial ossicular replacement prosthesis (PORP) and total ossicular replacement prosthesis (TORP) ossiculoplasties performed with a microscopic technique and using titanium prostheses (19); success was defined as a postoperative ABG $\leq$ 20 dB. At 2 months postoperatively, surgical success was achieved in 66% of the PORP group and 49% of the TORP group in that earlier series (19). The results in the present series were 57% success in the PORP group and 25% success in the TORP group. This can be explained by the fact that the main operator had no previous experience of endoscopic surgery and proceeded straight to robot-based endoscopic surgery. Previous reports comparing one-handed endoscopic surgery with microscopic surgery showed that audiometric results were similar in both techniques and we expect the audiometric results to be similar once the learning curve is overcome (1, 20). Future prospective studies will have to be conducted to compare our results with microscopic or robot-based technique. Comparison of robot-based technique will also have to be performed by groups who have more experience than we for one-handed ear endoscopic surgery.

For cholesteatoma of the petrous apex and tympanic paraganglioma, the aim was to achieve no relapse of the pathology, and, so far, this is the case for every patient in this study (at least on 1-year postoperative MRI, but this result needs to be confirmed in a longer follow-up period). In cholesteatoma cases, we were able to see every hidden structure in the middle ear, even behind the jugular bulb in extended lesions. In tympanic paraganglioma, it was easier to control the retraction of the paraganglioma during laser treatment and localize its vascular pedicles. The mean operating time was acceptable in all procedures, and preparation of the robot was performed during patient anesthesia induction to reduce the duration of installation. Clearly, robot-assisted endoscopy does not erase every disadvantage of endoscopes such as loss of depth of perception and binocular vision. But using a robot removes the disadvantage of a one-handed surgical technique, allows suction to control bleeding, and reduces vapor through constant replacement of the air in the external auditory canal (this could be further improved by humidifying the tip of the endoscope with diluted soap). If condensation or blood hinders endoscopic vision, instead of removing the endoscope from the external auditory canal, the surgical field could be washed out with saline serum. Endoscope cleaning was not time-consuming.

Compared to the other endoscope holders, the robot-based holder offers a more accurate control with tremor suppression. In the future, upgrades such as contact or collision detection or coupling with navigation system and augmented reality can also be envisioned. In the future, we could also implement a video based instruments automated tracking and the robot could drive the endoscope to follow the instrument all along. This can be done a surgical assistant today. On the other hand, the robot-based technique is less dynamic than a conventional endoscopic technique. Placing in and removing the endoscope is faster with a manual technique and dynamic constant changes of endoscope position may help the operator to obtain a depth perception of the anatomical structure that is impaired with an endoscope.

In this series, the duration of surgery was not reduced compared to a microscopic technique. Learning curve analysis with cumulative summation test for learning curve (LC/CUSUM) needs to be performed to check if the surgeons had reached the necessary skill plateau. Pan et al. have shown that neuro-endoscopes (such as those used with the RobOtol system) cause higher thermal release in the surgical cavity so it is important to apply submaximal light intensity. For the whole procedure, LEDs should be used at submaximal intensity and the operating field should be regularly rinsed (21).

The main limitation of the technique that we encountered was the external auditory canal diameter. We did not systematically measure its size but it was difficult to perform an exclusive endoscopic approach when a 6-mm diameter speculum could not fit into the external auditory canal. In the case of a narrow canal, we experienced collisions between the two tools and the endoscope limited access with the tool in some anatomic regions. This could be resolved by maintaining the endoscope further from the middle ear cleft in the canal but this reduced the quality of exposure. This may limit the use of robot-based endoscopy in children. Therefore, we would not recommend the use of a two-handed technique and a 3.3-mm diameter robot-based endoscope if the external auditory canal is $<$6 mm wide (**Figure 5**). This limitation will be eliminated in the near future as narrower endoscopes are currently being developed for the RobOtol system.

CONCLUSION

This study indicates that robot-assisted endoscopy is a safe and trustworthy tool for several categories of middle ear procedures. It combines the benefits of endoscopic exposure with a two-handed technique in surgery of the middle ear. It can be used as a standalone tool for pathology limited to the middle ear cleft or in combination with a microscope in lesions extending to the mastoid or petrous apex. The RobOtol system can be used safely and with accurate control as an endoscope holder. The next step will be to compare robot-assisted endoscopy with conventional microscope surgery.

DATA AVAILABILITY STATEMENT

The raw data supporting the conclusions of this article will be made available by the authors, without undue reservation.

ETHICS STATEMENT

The studies involving human participants were reviewed and approved by institutional review board (CNIL National Committee for data protection number 20191219182243). The patients/participants provided their written informed consent to participate in this study.

AUTHOR CONTRIBUTIONS

MV and YN collected the data and wrote the article. EF and OS contributed to the design and implementation of the research. GL, HD, and RT revised the manuscript and contributed to data analysis. All authors contributed to the article and approved the submitted version.

FUNDING

The study was supported by research funding from Fondation pour l'Audition (Starting Grant IDA-2020) and ANR- 18-CE19-0005 (Murocs).

REFERENCES

1. Manna S, Kaul VF, Gray ML, Wanna GB. Endoscopic versus microscopic middle ear surgery: a meta-analysis of outcomes following tympanoplasty and stapes surgery. *Otol Neurotol.* (2019) 40:983–93. doi: 10.1097/MAO.0000000000002353
2. Kozin ED, Gulati S, Kaplan AB, Lehmann AE, Remenschneider AK, Landegger LD, et al. Systematic review of outcomes following observational and operative endoscopic middle ear surgery: observational and operative EES outcomes. *Laryngoscope.* (2015) 125:1205–14. doi: 10.1002/lary.25048
3. Migirov L, Shapira Y, Horowitz Z, Wolf M. Exclusive endoscopic ear surgery for acquired cholesteatoma: preliminary results. *Otol Neurotol.* (2011) 32:433–6. doi: 10.1097/MAO.0b013e3182096b39
4. Presutti L, Gioacchini FM, Alicandri-Ciufelli M, Villari D, Marchioni D. Results of endoscopic middle ear surgery for cholesteatoma treatment: a systematic review. *Acta Otorhinolaryngol Ital.* (2014) 34:153–7.
5. Presutti L, Marchioni D, Mattioli F, Villari D, Alicandri-Ciufelli M. Endoscopic management of acquired cholesteatoma: our experience. *J Otolaryngol Head Neck Surg.* (2008) 37:481—7.
6. Tarabichi M. Endoscopic management of cholesteatoma: long-term results. *Otolaryngol Head Neck Surg.* (2000) 122:874–81. doi: 10.1016/S0194-5998(00)70017-9
7. Thomassin JM, Korchia D, Doris JMD. Endoscopic-guided otosurgery in the prevention of residual cholesteatomas. *Laryngoscope.* (1993) 103:939. doi: 10.1288/00005537-199308000-00021
8. Tarabichi M. Endoscopic middle ear surgery. *Ann Otol Rhinol Laryngol.* (1999) 108:39–46. doi: 10.1177/000348949910800106
9. Tarabichi M. Endoscopic management of acquired cholesteatoma. *Am J Otol.* (1997) 18:544—9.
10. Cohen MS, Basonbul RA, Barber SR, Kozin ED, Rivas AC, Lee DJ. Development and validation of an endoscopic ear surgery classification system: endoscopic ear surgery classification system. *Laryngoscope.* (2018) 128:967–70. doi: 10.1002/lary.26802
11. Dogan S, Bayraktar C. Endoscopic tympanoplasty: learning curve for a surgeon already trained in microscopic tympanoplasty. *Eur Arch Otorhinolaryngol.* (2017) 274:1853–8. doi: 10.1007/s00405-016-4428-0
12. de Zinis LOR, Berlucchi M, Nassif N. Double-handed endoscopic myringoplasty with a holding system in children: preliminary observations. *Int J Pediatr Otorhinolaryngol.* (2017) 96:127–30. doi: 10.1016/j.ijporl.2017.03.017
13. Khan MM, Parab SR. Novel concept of attaching endoscope holder to microscope for two handed endoscopic tympanoplasty. *Indian J Otolaryngol Head Neck Surg.* (2016) 68:230–40. doi: 10.1007/s12070-015-0916-6
14. Ozturan O, Yenigun A, Aksoy F, Ertas B. Proposal of a budget-friendly camera holder for endoscopic ear surgery. *J Craniofac Surg.* (2018) 29:e47–9. doi: 10.1097/SCS.0000000000004022
15. Daoudi H, Lahlou G, Torres R, Sterkers O, Lefeuvre V, Ferrary E, et al. Robot-assisted cochlear implant electrode array insertion in adults: a comparative study with manual insertion. *Otol Neurotol.* (2021) 42:e438–44. doi: 10.1097/MAO.0000000000003002
16. Vittoria S, Lahlou G, Torres R, Daoudi H, Mosnier I, Mazalaigue S, et al. Robot-based assistance in middle ear surgery and cochlear implantation: first clinical report. *Eur Arch Otorhinolaryngol.* (2021) 278:77–85. doi: 10.1007/s00405-020-06070-z
17. McKennan KX. Endoscopic second look mastoidoscopy to rule out residual epitympanic/mastoid cholesteatoma. *Laryngoscope.* (1993) 103:810–14. doi: 10.1288/00005537-199307000-00016
18. Youssef TF, Poe DS. Endoscope-assisted second-stage tympanomastoidectomy. *Laryngoscope.* (1997) 107:1341–4. doi: 10.1097/00005537-199710000-00009
19. Lahlou G, Sonji G, de Seta D, Mosnier I, Russo FY, Sterkers O, et al. Anatomical and functional results of ossiculoplasty using titanium prosthesis. *Acta Otorhinolaryngol Ital.* (2018) 38:377–83. doi: 10.14639/0392-100X-1700
20. Tseng C-C, Lai M-T, Wu C-C, Yuan S-P, Ding Y-F. Comparison of the efficacy of endoscopic tympanoplasty and microscopic tympanoplasty: a systematic review and meta-analysis: endoscopic and microscopic tympanoplasty. *Laryngoscope.* (2017) 127:1890–6. doi: 10.1002/lary.26379
21. Pan J, Tan H, Shi J, Wang Z, Sterkers O, Jia H, et al. Thermal safety of endoscopic usage in robot-assisted middle ear surgery: an experimental study. *Front Surg.* (2021) 8:659688. doi: 10.3389/fsurg.2021.659688

Conflict of Interest: YN and OS are consultants for Collin Medical.

The remaining authors declare that the research was conducted in the absence of any commercial or financial relationships that could be construed as a potential conflict of interest.

Publisher's Note: All claims expressed in this article are solely those of the authors and do not necessarily represent those of their affiliated organizations, or those of the publisher, the editors and the reviewers. Any product that may be evaluated in this article, or claim that may be made by its manufacturer, is not guaranteed or endorsed by the publisher.

frontiers in Surgery

ORIGINAL RESEARCH
published: 08 November 2021
doi: 10.3389/fsurg.2021.741401

Fusion of Technology in Cochlear Implantation Surgery: Investigation of Fluoroscopically Assisted Robotic Electrode Insertion

Greg Eigner Jablonski[1,2]*, *Benedicte Falkenberg-Jensen*[3], *Marie Bunne*[2], *Muneera Iftikhar*[2], *Ralf Greisiger*[2], *Leif Runar Opheim*[2], *Hilde Korslund*[4], *Marte Myhrum*[1,2] *and Torquil Mcdonald Sørensen*[2]

[1] Institute of Clinical Medicine, University of Oslo, Oslo, Norway, [2] Department of Otorhinolaryngology & Head and Neck Surgery, Oslo University Hospital, Rikshospitalet, Oslo, Norway, [3] Department of Radiology, Oslo University Hospital, Rikshospitalet, Oslo, Norway, [4] Interventional Centre, Oslo University Hospital, Rikshospitalet, Oslo, Norway

OPEN ACCESS

Edited by:
Paul Van de Heyning, University of Antwerp, Belgium

Reviewed by:
Hans Thomeer, University Medical Center Utrecht, Netherlands
Jiang Yan, The Affiliated Hospital of Qingdao University, China

***Correspondence:**
Greg Eigner Jablonski
greg.jablonski@medisin.uio.no; gjablons@ous-hf.no

Specialty section:
This article was submitted to Otorhinolaryngology - Head and Neck Surgery, a section of the journal Frontiers in Surgery

Received: *14 July 2021*
Accepted: *29 September 2021*
Published: *08 November 2021*

Citation:
Jablonski GE, Falkenberg-Jensen B, Bunne M, Iftikhar M, Greisiger R, Opheim LR, Korslund H, Myhrum M and Sørensen TM (2021) Fusion of Technology in Cochlear Implantation Surgery: Investigation of Fluoroscopically Assisted Robotic Electrode Insertion. Front. Surg. 8:741401. doi: 10.3389/fsurg.2021.741401

The HEARO cochlear implantation surgery aims to replace the conventional wide mastoidectomy approach with a minimally invasive direct cochlear access. The main advantage of the HEARO access would be that the trajectory accommodates the optimal and individualized insertion parameters such as type of cochlear access and trajectory angles into the cochlea. To investigate the quality of electrode insertion with the HEARO procedure, the insertion process was inspected under fluoroscopy in 16 human cadaver temporal bones. Prior to the insertion, the robotic middle and inner ear access were performed through the HEARO procedures. The status of the insertion was analyzed on the post-operative image with Siemens Artis Pheno (Siemens AG, Munich, Germany). The completion of the full HEARO procedure, including the robotic inner ear access and fluoroscopy electrode insertion, was possible in all 16 cases. It was possible to insert the electrode in all 16 cases through the drilled tunnel. However, one case in which the full cochlea was not visible on the post-operative image for analysis was excluded. The post-operative analysis of the electrode insertion showed an average insertion angle of 507°, which is equivalent to 1.4 turns of the cochlea, and minimal and maximal insertion angles were recorded as 373° (1 cochlear turn) and 645° (1.8 cochlear turn), respectively. The fluoroscopy inspection indicated no sign of complications during the insertion.

Keywords: cochlear implant, robot-assisted cochlear implantation, RCI, HEARO®, robot-assisted surgery, OTOPLAN®, fluoroscopy at implantation, CBCT (cone beam computed tomography)

INTRODUCTION

Cochlear implantation has been the gold standard treatment for severe to profound sensorineural hearing loss over several decades (1). This conventional surgical method is well established and practiced in many countries; however, its success relies not only on the surgical skills but also on the anatomical variations in the patient. To overcome these variables, the development of robotic cochlear implantation took place.

The idea behind robotic cochlear implantation is to obtain a system that is minimally invasive, reproducible, reliable, safe, and effective. Robotic cochlear implantation is an image-guided system,

which drills a trajectory from the mastoid surface to the middle ear bypassing the critical anatomical structures such as the facial nerve, chorda tympani, ossicles, and the posterior ear canal wall. Caversaccio (2), Labadie (3), and Bell (4) have previously described the safety and success of this procedure; however, their experience with robotic assisted surgery was limited to the middle ear access and not to the inner ear.

Our aim is to describe further development of this method by using the robotic cochlear implantation to access the round window (RW), without damaging the critical structures and achieve an optimized angle for manual electrode insertion through the drilled trajectory.

This is achieved by using OTOPLAN, which is an image-based system that allows accurate patient-to-image registration using bone anchored fiducial screws implanted into the mastoid surface. The system calculates a distance to the facial nerve, chorda tympani, the ossicles, the posterior ear canal wall, and plans out a trajectory from the mastoid surface to the RW, as described by Weber et al. (5).

Such a procedure does not only demand thorough radiological planning but also visual inspection and assessment of repetitive achievement of RW access to the cochlea. We have utilized transtympanal endoscopy (0-degree endoscope, Karl Storz) together with fluoroscopy and Cone Beam CT (CBCT) acquired by Siemens Artis Pheno with robotic C-arm (Siemens AG, Germany). This was possible due to the advanced fusion of technology at our Intervention Centre, Oslo University Hospital, Norway.

There has been a major development in robotically assisted cochlear implantation surgery over the last decade. The image-guided robot system has been shown to be highly precise and safe as previously described by Bell (4), Caversaccio (2), and Weber (5). Robotically assisted cochlear implantation has been performed by drilling a direct tunnel from the mastoid surface to the middle ear and gaining manual access to the inner ear, keyhole access (2, 6). Considering microanatomy with the closely adjacent facial nerve and chorda tympani, the procedure requires high levels of navigation accuracy and additional independent tool position and orientation methodologies (7). The image-guided robotic system described by Caversaccio (2) and Weber (5) has demonstrated a high level of tool positioning accuracy and precision (0.15 ± 0.08 mm at the level of cochlea).

In a procedure like robotic cochlear implantation, which is performed at a microsurgical scale with submillimetric distance to the facial nerve, the necessity for several safety mechanisms is paramount–in case of navigation error and to avoid thermal and mechanical damage to the relevant anatomical structures.

It utilizes (a) Visual surveying scheme by an optical position measurement system that tracks the end effector of the robot and the head of the patient by means of rigidly fixed optical reference, (b) estimates of the drill position and orientation by correlating the drill force and bone density, (c) neuro-stimulation feedback mechanism of the facial nerve and interval drilling with saline flushing during the interval to minimize heat accumulation, and (d) intra-operative CBCT imaging (Siemens Artis Pheno). Previous studies have demonstrated the reliability of robotic cochlear implantation where the trajectory has been drilled from the mastoid surface to the middle ear and thereby gaining manual access to the cochlea for electrode placement (2, 5–7).

The aim of our study was to gain access to the RW solely by the image-guided robotic system rather than manually drilling into the RW.

The surgeon controls the robotic drilling by continuously pressing a pedal. Hence, the drilling can be stopped immediately at any time by releasing the pedal.

MATERIALS AND METHODS

The Regional Committee for Medical and Health Research Ethics of Northern Norway evaluated the *ex vivo* study (REC North, reference: 2018/378/REK nord). Eight formalin-flushed (C7-Th1) *ex vivo* human head specimens (16 temporal bones) were included in this study. The HEARO procedure workflow included the following steps:

1. Incision and fiducial screw placement
2. Imaging and planning
3. Robotic middle ear access
4. Robotic inner ear access
5. Electrode insertion
6. Post-operative analysis.

Incision and Screw Placement

The Robotic arm was attached to the operating room (OR) table and covered in sterile draping. The human cadaver head specimen was placed relative to the robot system and immobilized in the radio-translucent HEARO headrest, using inflatable pressure pads. A C-shaped retroauricular incision was performed on all cases, and a retractor was used to keep the skin flaps away from the surgical field. After incision, five fiducial screws (four for patient-to-image registration and one for assembling of the patient marker attachment) were inserted into the surface of the mastoid (8).

Imaging and Planning

After the fiducial screws were positioned, a high-resolution CBCT image was acquired by Siemens Artis Pheno with Robotic C-arm (Siemens AG, Germany). A 0.1 mm reconstruction protocol was used for the surgical planning. The image quality was validated by excluding artifacts and confirming the inclusion of all four registration screws, facial canal, middle ear, and labyrinth (9). The raw data were then transferred to OTOPLAN software (CASCINATION AG, Switzerland). A senior radiologist identified, and 3D reconstructed the following structures using a semi-automatic segmentation algorithm:

- External ear canal
- The ossicles including the stapes
- The RW of the cochlea
- The tympanic and mastoid segment of the facial nerve
- The mastoid segment of the chorda tympani.

The target point of the drilling was placed on the RW. The OTOPLAN software automatically calculates distances from the drilling tunnel to the surrounding anatomy. This trajectory was

adjusted to a minimum safe distance of 0.4 mm to the facial nerve, and 0.3 mm to the external auditory canal, ossicles, and the chorda tympani. Before exporting the planned trajectory to HEARO, a qualified senior ear surgeon approved the trajectory.

Robotic Middle Ear Access

After the patient-to-image registration, the first stage of drilling was carried out from the mastoid surface to 3 mm from the level of the facial nerve. The keyhole was created using a drill bit with a diameter of 1.8 mm. Interval drilling and irrigation were carried out with a drilling speed of 1,000 rpm. On completion of the first stage of drilling, the patient marker was removed, and a trajectory reference rod was fitted into the tunnel. An intra-operative CBCT image (Siemens Artis Pheno) was performed to assess the safety and accuracy of the drilling trajectory. On confirmation, the patient marker was assembled and the registration was repeated. The second stage of the drilling was commenced with a reduced drilling interval depth of 0.5 mm, in contrast to the 2 mm of the first stage (8). The second stage of drilling stopped at the drill stopping point prior to the RW according to the plan from OTOPLAN.

An additional tympanomeatal flap was created for direct endoscopic visualization of the tympanic cavity, and manual assistance of electrode array insertion procedure. The alignment of the drilled tunnel with the target (RW) was visually confirmed with a microscope and/or 0-degree endoscope (Karl Storz, diameter of 2.7 mm, Germany) through the external auditory canal into the middle ear while inserting a titanium rod through the drilled tunnel.

Robotic Inner Ear Access

The milling of the inner ear access was carried out with a 1 mm diamond burr at a feed rate of 0.01 mm/s, 2,000 rpm. The milling was performed under direct visualization using a 0-degree endoscope (Karl Storz, Germany) and/or microscope. Water irrigation was not used for milling. The surgeon actively terminated milling by releasing the pedal, when the force sensitive measurement (10) on the screen showed a sudden drop, indicating a sufficient opening through the bony overhang of the RW. Finally, the surgeon performed a visual evaluation of the RW membrane integrity.

Electrode Insertion

Prior to electrode insertion, the drilled tunnel was cleansed of bone dust. A protective barrier guide tube was used to prevent any kinking or displacement of the electrode into the air cells during insertion. We used a radio-translucent biodegradable-type tube, which could be left inside the channel after insertion in nine cases, and a two-part longitudinally divided metallic version in seven cases, which had to be removed after electrode insertion. Prior to the insertion, the RW membrane was removed manually using a micro-needle. The electrode array was coated with hyaluronic acid [12 mg/ml, stabilized, Restylane Skinboosters (Vital &Vital Light)] to minimize friction, and then inserted manually under visual (with endoscope/microscope) and fluoroscopic guidance. Fluoroscopic monitoring was performed using a CBCT (Siemens Artis Pheno). The cadaver head was placed in a carbon fiber HEARO headrest to avoid any artifact. The X-ray source was placed under the operating table and the detector above the cadaver head specimen, ∼90-degree angle of the X-ray direction to the plane of the basal turn of the cochlea. During fluoroscopy, an X-ray tube acceleration voltage of ∼70 kV and a tube current of ∼250 mA were used. The fluoroscopy frame rate was set to four or five frames per second. A FLEX28 electrode (MED-EL, Innsbruck, Austria) was used in all cases for the insertion. The electrode array contacts and internal wiring were visible on the fluoroscopy, despite the presence of the guide tube. We did not perform sealing around the electrode, as there was not much space left around the electrode after insertion.

Post-operative Analysis

Upon completion of the electrode insertion, a post-operative CBCT scan was performed (also using the Siemens Artis Pheno, and a cubic voxel size of side length 0.1 mm was used in the volume reconstruction) in order to analyze the insertion status of the electrode using the post-operative analysis feature of OTOPLAN.

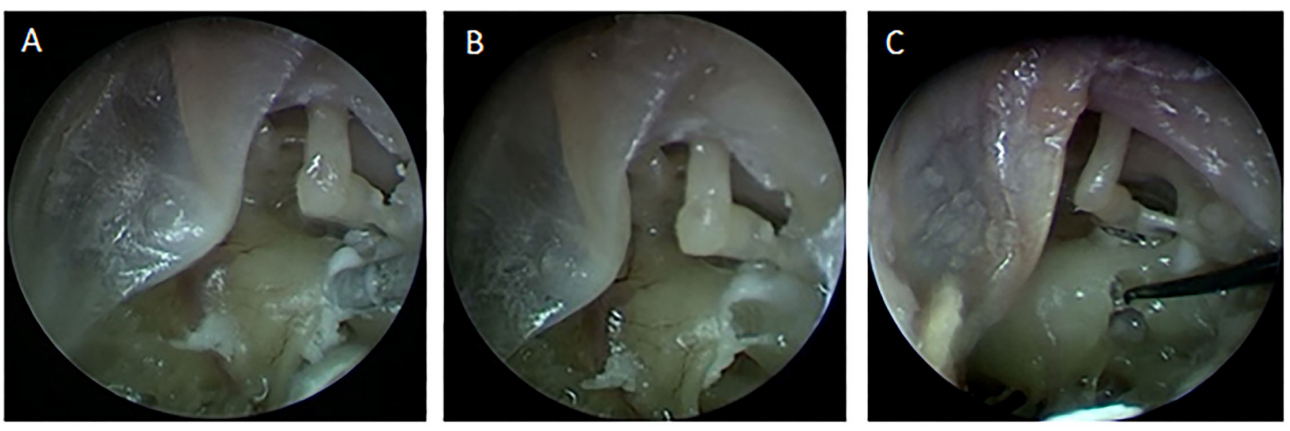

FIGURE 1 | (A) The milling of the inner ear access with visual endoscopic inspection through the tympanomeatal flap. **(B)** The 1 mm inner ear access created for the electrode insertion. **(C)** Opening of the Round Window membrane using a micro-needle.

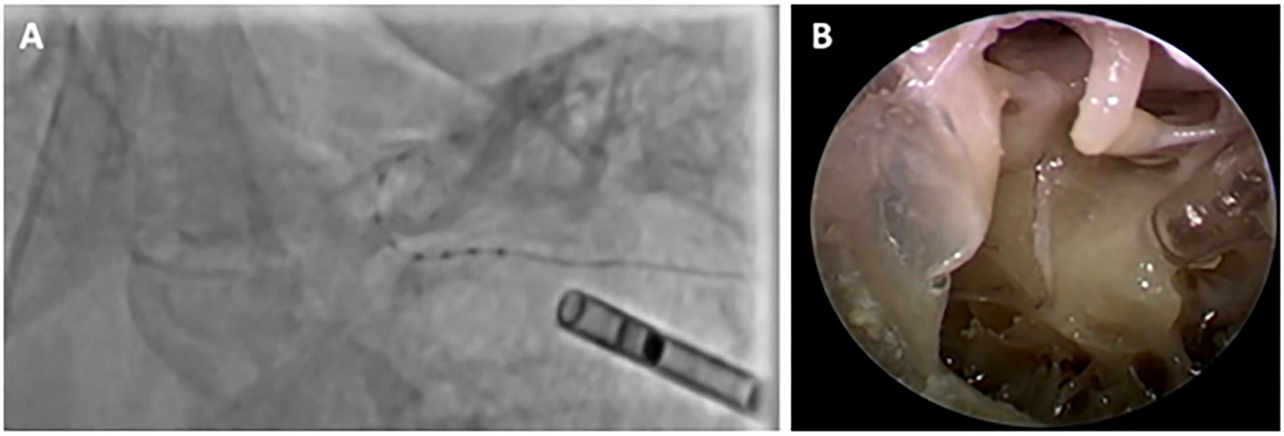

FIGURE 2 | (A) The electrode insertion through fluoroscopic view, **(B)** Electrode insertion through the transparent tube, endoscopically supervised.

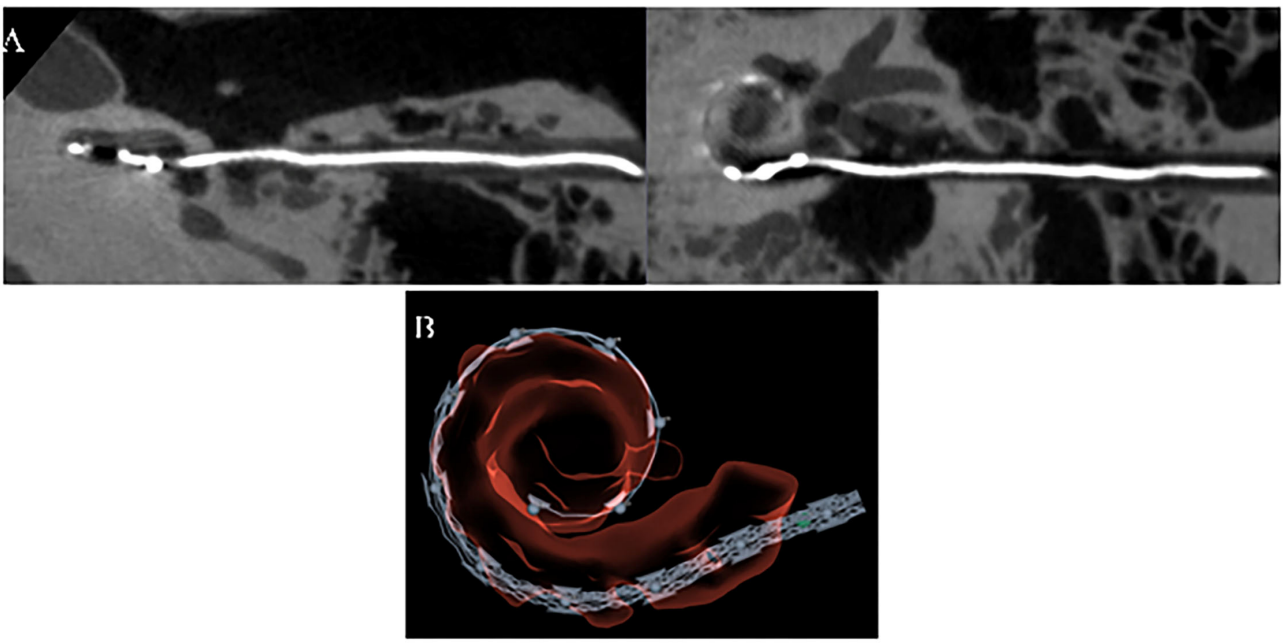

FIGURE 3 | Post-op analysis of electrode insertion using **(A)**. CBCT Siemens Artis Pheno and **(B)**. OTOPLAN®.

RESULTS

The completion of the full HEARO procedure, including the robotic inner ear access and the intra-operative analysis, has shown no damage to the facial nerve during the middle ear access. Intra-operative and post-operative CBCT showed and maintained visible bone borders between the drilled canal and the facial nerve, the chorda tympani, and the external ear canal in all cases. In addition, there was no damage to the ossicles. The visual endoscopic supervision of creating a 1 mm window on the bony overhang of the cochlea and subsequent opening of the RW membrane is shown in **Figure 1**.

It was possible to insert the electrode in all 16 cases through the drilled tunnel after the robotic inner ear access under the fluoroscopy guidance. A protective barrier tube was placed inside the tunnel prior to the insertion. An example of fluoroscopy and endoscopic supervision of the electrode insertion process is shown in **Figure 2**.

Post-operatively the insertion status of all cases was verified with CBCT (Siemens Artis Pheno) and analyzed using the OTOPLAN software to determine the insertion depth, electrode location, and possibility of tip fold-over or scala deviation. An example of such analysis is shown in **Figure 3**.

One case (03_Left), in which the full cochlea was not visible on the post-operative image for analysis, was excluded. The post-operative analysis of the electrode insertion showed a full insertion in 12 cases. A minimum of one turn of the cochlea was covered in all cases. The average insertion angle in 15 cases

TABLE 1 | Insertion status analysis from post-operative images.

Description	Number of cases ($n = 15$)
Full insertion	12/15
Average insertion angle	507° (1.4 Turns)
Min insertion angle	373° (1 Turn)
Max insertion angle	645° (1.8 Turns)
Tip fold-over	0/15
Scala deviation	0/15

was 507°, which is equivalent to 1.4 turns of the cochlea, and minimum and maximum insertion angles were recorded as 373° (1 cochlear turn) and 645° (1.8 cochlear turns), respectively. The partial insertion cases left a maximum of two contacts out, possibly due to the formalin fixation of the specimen. No tip fold-over or scala deviation was observed in the 15 cases. The summary and details of the insertion status of the post-operative images are shown in **Tables 1**, **2**, respectively.

DISCUSSION

In this study, the quality of the electrode insertion through a robotically drilled direct tunnel was validated using endoscopic and fluoroscopic supervision. To our knowledge, this is the first report of an electrode insertion study conducted using a robotic approach under fluoroscopic supervision. In 12 out of 15 analyzed cases, it was possible to fully insert the electrode and in all the cases, a steady electrode insertion was observed with no sign of scala deviation or tip-fold-over. This lack of complications may be due to feedback from fluoroscopic supervision, a high level of surgical CI experience among the participating surgeons, and the fact that this was an experimental setting. The three partial insertion cases could be due to formalin fixation of the specimens and hence increased endolymph viscosity in scala tympani. Without the mastoidectomy, the otomicroscopic visual feedback to the surgeon is lost and therefore endoscopic supervision was obtained through the tympanomeatal flap. However, creating the tympanomeatal flap implies an additional surgical procedure performed on the patient. Furthermore, manual insertion of the electrode array while simultaneously holding an endoscope can be a demanding task for the surgeon, hence influencing the placement of an electrode in the cochlea. However, due to the fixation of the head, an endoscope stand could help in this regard. A recent study (11) has shown the feasibility of a multiport approach through the HEARO procedure. This would imply the creation of a tunnel through the facial recess for electrode insertion and a second tunnel for placement of endoscope for visual inspection. By doing so, the endomeatal procedure could be avoided, enabling the surgeon to fit the endoscope in the holder within the tunnel. The future advancement toward robotic insertion of the electrode array would also facilitate a slower and more consistent electrode insertion.

The main purpose of our study was to gain access to the RW solely by the image-guided robotic system and to test

TABLE 2 | Detailed insertion status analysis from post-operative images.

Cases	Cochlea parameters	Insertion status
00_Left	Diameter (A) = 8.9 mm Width (B) = 7.1 mm Height (H) =3.6 mm CDL (from RW) = 34.1 mm	Insertion depth: 543° Full insertion Location: Scala tympani Scala deviation: No Tip fold-over: No
00_Right	Diameter (A) = 9.1 mm Width (B) = 6.7 mm Height (H) =3.3 mm CDL (from RW) = 32.8 mm	Insertion depth: 508° Full insertion Location: Scala tympani Scala deviation: No Tip fold-over: No
01_Left	Diameter (A) = 9.2 mm Width (B) =6.7 mm Height (H) =3.4 CDL (from RW) = 33.2mm	Insertion depth: 476° Full insertion Location: Scala tympani Scala deviation: No Tip fold-over: No
01_Right	Diameter (A)= 9.1 mm Width (B) = 6.5 mm Height (H) =4.0 mm CDL (from RW) = 32.0 mm	Insertion depth: 426° Full insertion Location: Scala tympani Scala deviation: No Tip fold-over: No
02_Left	Diameter (A) = 9.1 mm Width (B) =6.5 mm Height (H) =3.7 mm CDL (from RW) = 32.2 mm	Insertion depth: 586° Full insertion Location: Scala tympani Scala deviation: No Tip fold-over: No
02_Right	Diameter (A) = 9.2 mm Width (B) =6.5 mm Height (H) =3.5 mm CDL (from RW) = 32.1 mm	Insertion depth: 521° Full insertion Location: Scala tympani Scala deviation: No
03_Left	Skipped (image is cut)	/
03_Right	Diameter (A) = 8.7 mm Width (B) = 6.3 mm Height (H) = 3.8 mm CDL (from RW) = 31.0 mm	Insertion depth: 517° Full insertion Location: Scala tympani Scala deviation: No Tip fold-over: No
04_Left	Diameter (A) = 9.4 mm Width (B) =6.3 mm Height (H) =3.7 mm CDL (from RW) = 31.9 mm	Insertion depth: 557° Full insertion Location: Scala tympani Scala deviation: No Tip fold-over: No
04_Right	Diameter (A) = 9.3 mm Width (B) = 6.6 mm Height (H) = 3.4 mm CDL (from RW) = 32.7 mm	Insertion depth: 373° Partial insertion, two contacts outside Location: Scala tympani Scala deviation: No Tip fold-over: No
05_Left	Diameter (A) = 9.3 mm Width (B) = 6.9 mm Height (H) = 3.5 mm CDL (from RW) = 33.8 mm	Insertion depth: 475° Full insertion Location: Scala tympani Scala deviation: No Tip fold-over: No
05_Right	Diameter (A) = 9.3 mm Width (B) = 7.1 mm Height (H) = 3.7 mm CDL (from RW) = 34.7 mm	Insertion depth: 542° Full insertion Location: Scala tympani Scala deviation: No Tip fold-over: No
06_Left	Diameter (A) = 9.0 mm Width (B) = 6.4 mm Height (H) = 4.0 mm CDL (from RW) = 31.6 mm	Insertion depth: 483° Partial insertion, two contacts outside Location: Scala tympani Scala deviation: No Tip fold-over: No

(Continued)

TABLE 2 | Continued

Cases	Cochlea parameters	Insertion status
06_Right	Diameter (A) = 8.8 mm Width (B) = 6.5 mm Height (H) = 3.5 mm CDL (from RW) = 31.5 mm	Insertion depth: 645° Full insertion Location: Scala tympani Scala deviation: No Tip fold-over: No
07_Left	Diameter (A) = 8.4 mm Width (B) = 6.3 mm Height (H) = 3.5 mm CDL (from RW) = 30.4 mm	Insertion depth: 570° Full insertion Location: Scala tympani Scala deviation: No Tip fold-over: No
07_Right	Diameter (A) = 9.3 mm Width (B) = 6.8 mm Height (H) = 3.7 mm CDL (from RW) = 33.5 mm	Insertion depth: 377° Partial insertion, one contact outside Location: Scala tympani Scala deviation: No Tip fold-over: No

the feasibility of the Robot HEARO surgery technique. The image-guided robot system with dedicated OTOPLAN software has shown to be highly precise and safe, considering the microanatomy with the closely adjacent facial nerve and chorda tympani as previously described by Bell (4), Caversaccio (2), and Weber (5). In live patients, there is the same concern regarding the safety of facial nerve and chorda tympani in the surgical approach for CI. In this respect, Postelmans et al. (12) compared mastoidectomy with posterior tympanotomi (MPTA) with suprameatal approach (SMA) and proposed the latter as a safe and effective technique. No reduction in post-operative complications was demonstrated and in addition, this approach showed to be more hazardous to ossicles, which is an additional obstacle in maintaining the level of residual hearing. The SMA technique includes an increased risk of electrode kinking as a consequence of the difficult 30° more superior insertion of the electrode. In a recent publication, Topsakal et al. (13) compared the surgical techniques including MPTA, SMA, and robotic techniques for cochlear implantation in terms of the trajectories toward the inner ear. They concluded that posterior tympanotomi (PT) approaches allow much smaller angles of the cochlear approach (ACA) than those for SMA. They have also found that within different PT modalities, robotically assisted surgery provides the most optimal ACA, which is the prerequisite for easy access to an array and the best possible placement of the electrode in the cochlea. The most optimal ACA is vital for optimal positioning of the electrode array and residual hearing preservation in CI surgery. We believe that the Robot HEARO surgery technique together with the future robotic insertion of the electrode will increase the precision and standardize the CI surgery.

Finally, in this study, fluoroscopic supervision of the electrode insertion was also performed to visualize the trajectory and advancement of the array inside the cochlea. The fluoroscopic supervision has previously been found very useful on patients when combined with electrophysiological measurements study (14). Fluoroscopic monitoring is mainly used in research and not in mainstream CI surgery in our Clinic. Radiation exposure during this procedure is very low and was never a limiting factor in human studies. The use of human cadavers allowed us to monitor the different stages with CBCT, without considering accumulated radiation to the patient. In future clinical studies, we will have to consider the radiation exposure to the patient and reduce the use of intra-operative CBCT scans, based on the data of our cadaver study. Furthermore, if the technique becomes an established surgical procedure in daily clinical practice, the results from the radiology taken at different stages of the surgery during both the cadaver and the clinical studies will provide important information on which stages radiology is in excess of and can be avoided.

CONCLUSIONS

Electrode insertion with the robotic middle and inner ear access with the HEARO procedure is validated and found to be feasible and safe. It is a further step toward clinical application. The next stage of this study would be to perform the same methodology in clinical practice.

DATA AVAILABILITY STATEMENT

The raw data supporting the conclusions of this article will be made available by the authors, without undue reservation.

ETHICS STATEMENT

The Regional Committee for Medical and Health Research Ethics of Northern Norway (REC North, reference: 2018/378/REK nord) evaluated the study. Since the study was conducted on tissue from deceased persons and therefore not considered as research on humans in accordance with the Norwegian Research Health Act, the Ethics Committee concluded that the study was outside of their mandate. Thus, the study has been planned and conducted in accordance with the research policy and routines of Oslo University Hospital.

AUTHOR CONTRIBUTIONS

GJ: concept, design, and writing. GJ and TS: supervision, resource, and literature search. GJ, BF-J, and TS: materials, data collection, and processing. GJ, BF-J, TS, MB, MI, RG, LO, HK, and MM: analysis, interpretation, and critical reviews. All authors contributed to the article and approved the submitted version.

FUNDING

The study was funded by Oslo University Hospital.

ACKNOWLEDGMENTS

We thank Dr. Masoud Zoka Assadi (MED-EL), Nikola Ivanovic (MED-EL), and Marco Matulic (CASCINATION) for their extended help and technical assistance. Additionally, we would like to thank The Interventional Centre, Oslo University Hospital, with a special gratitude to Professor Erik Fosse for the possibility of performing the study and for the extended cooperation.

SUPPLEMENTARY MATERIAL

The Supplementary Material for this article can be found online at: https://www.frontiersin.org/articles/10.3389/fsurg.2021.741401/full#supplementary-material

Video 1 | RW electrode insertion.

Video 2 | Fluoroscopy of electrode insertion.

Video 3 | The milling of the inner ear access.

REFERENCES

1. House WF. Cochlear implants: it's time to rethink. *Am J Otol.* (1994) 15:573–87.
2. Caversaccio M, Gavaghan K, Wimmer W, Williamson T, Ansò J, Mantokoudis G, et al. Robotic cochlear implantation: surgical procedure and first clinical experience. *Acta Otolaryngol.* (2017) 137:447–54. doi: 10.1080/00016489.2017.1278573
3. Labadie RF, Balachandran R, Noble JH, Blachon GS, Mitchell JE, Reda FA, et al. Minimally invasive image-guided cochlear implantation surgery: first report of clinical implementation. *Laryngoscope.* (2014) 124:1915–22. doi: 10.1002/lary.24520
4. Bell B, Gerber N, Williamson T, Gavaghan K, Wimmer W, Caversaccio M, et al. *In vitro* accuracy evaluation of image-guided robot system for direct cochlear access. *Otol Neurotol.* (2013) 34:1284–90. doi: 10.1097/MAO.0b013e31829561b6
5. Weber S, Gavaghan K, Wimmer W, Williamson T, Gerber N, Anso J, et al. Instrument flight to the inner ear. *Sci Robot.* (2017) 2:eaal4916. doi: 10.1126/scirobotics.aal4916
6. Caversaccio M, Wimmer W, Anso J, Mantokoudis G, Gerber N, Rathgeb C, et al. Robotic middle ear access for cochlear implantation: first in man. *PLoS ONE.* (2019) 14:e0220543. doi: 10.1371/journal.pone.0220543
7. Rathgeb C, Wagner F, Wimmer W, Gerber N, Williamson T, Anschütz L, et al. The accuracy of image-based safety analysis for robotic cochlear implantation. *Int J Comput Assist Radiol Surg.* (2019) 14:83–92. doi: 10.1007/s11548-018-1834-3
8. Gerber N, Gavaghan KA, Bell BJ, Williamson TM, Weisstanner C, Caversaccio M, et al. High-accuracy patient-to-image registration for the facilitation of image-guided robotic microsurgery on the head. *IEEE Trans Biomed Eng.* (2013) 60:960–8. doi: 10.1109/TBME.2013.2241063
9. Gerber N, Bell B, Gavaghan K, Weisstanner C, Caversaccio M, Weber S. Surgical planning tool for robotically assisted hearing aid implantation. *Int J Comput Assist Radiol Surg.* (2014) 9:11–20. doi: 10.1007/s11548-013-0908-5
10. Williamson T, Du X, Bell B, Coulson C, Caversaccio M, Proops D, et al. Mechatronic feasibility of minimally invasive, atraumatic cochleostomy. *Biomed Res Int.* (2014) 2014:181624. doi: 10.1155/2014/181624
11. Schneider D, Stenin I, Ansó J, Hermann J, Mueller F, Pereira Bom Braga G, et al. Robotic cochlear implantation: feasibility of a multiport approach in an ex vivo model. *Eur Arch Otorhinolaryngol.* (2019) 276:1283–9. doi: 10.1007/s00405-019-05318-7
12. Postelmans JTF, Grolman W, Tange RA, Stokroos RJ. Comparison of two approaches to the surgical management of cochlear implantation. *Laryngoscope.* (2009) 119:1571–8. doi: 10.1002/lary.20487
13. Topsakal V, Matulic M, Assadi MZ, Mertens G, Rompaey VV, de Heyning PV. Comparison of the surgical techniques and robotic techniques for cochlear implantation in terms of the trajectories toward the inner ear. *J Int Adv Otol.* (2020) 16:3–7 doi: 10.5152/iao.2020.8113
14. Greisiger R. *Objective measurements and cochlear implants imaging.* Dissertation. University of Oslo, Norway (2016).

Conflict of Interest: The authors declare that the research was conducted in the absence of any commercial or financial relationships that could be construed as a potential conflict of interest.

The study was conducted with service and collaboration from MED-EL, Innsbruck, Austria, and CASCINATION, Bern, Switzerland.

frontiers in Surgery

ORIGINAL RESEARCH
published: 11 November 2021
doi: 10.3389/fsurg.2021.742147

Robotic Milling of Electrode Lead Channels During Cochlear Implantation in an *ex-vivo* Model

Jan Hermann, Fabian Mueller, Daniel Schneider, Gabriela O'Toole Bom Braga and Stefan Weber*

ARTORG Center for Biomedical Engineering Research, Faculty of Medicine, University of Bern, Bern, Switzerland

Objective: Robotic cochlear implantation is an emerging surgical technique for patients with sensorineural hearing loss. Access to the middle and inner ear is provided through a small-diameter hole created by a robotic drilling process without a mastoidectomy. Using the same image-guided robotic system, we propose an electrode lead management technique using robotic milling that replaces the standard process of stowing excess electrode lead in the mastoidectomy cavity. Before accessing the middle ear, an electrode channel is milled robotically based on intraoperative planning. The goal is to further standardize cochlear implantation, minimize the risk of iatrogenic intracochlear damage, and to create optimal conditions for a long implant life through protection from external trauma and immobilization in a slight press fit to prevent mechanical fatigue and electrode migrations.

Methods: The proposed workflow was executed on 12 *ex-vivo* temporal bones and evaluated for safety and efficacy. For safety, the difference between planned and resulting channels were measured postoperatively in micro-computed tomography, and the length outside the planned safety margin of 1.0 mm was determined. For efficacy, the channel width and depth were measured to assess the press fit immobilization and the protection from external trauma, respectively.

Results: All 12 cases were completed with successful electrode fixations after cochlear insertions. The milled channels stayed within the planned safety margins and the probability of their violation was lower than one in 10,000 patients. Maximal deviations in lateral and depth directions of 0.35 and 0.29 mm were measured, respectively. The channels could be milled with a width that immobilized the electrode leads. The average channel depth was 2.20 mm, while the planned channel depth was 2.30 mm. The shallowest channel depth was 1.82 mm, still deep enough to contain the full 1.30 mm diameter of the electrode used for the experiments.

Conclusion: This study proposes a robotic electrode lead management and fixation technique and verified its safety and efficacy in an *ex-vivo* study. The method of image-guided robotic bone removal presented here with average errors of 0.2 mm and maximal errors below 0.5 mm could be used for a variety of other otologic surgical procedures.

Keywords: robotic cochlear implantation, electrode lead channel, electrode fixation, robotic surgery, image-guidance, patient-specific planning, *ex-vivo* human cephalic study, robotic milling

OPEN ACCESS

Edited by:
Vincent Van Rompaey, University of Antwerp, Belgium

Reviewed by:
Jiang Yan, The Affiliated Hospital of Qingdao University, China
Shuji Izumi, Niigata University, Japan

****Correspondence:***
Jan Hermann
jan.hermann@artorg.unibe.ch

Specialty section:
This article was submitted to Otorhinolaryngology - Head and Neck Surgery, a section of the journal Frontiers in Surgery

Received: *15 July 2021*
Accepted: *14 October 2021*
Published: *11 November 2021*

Citation:
Hermann J, Mueller F, Schneider D, O'Toole Bom Braga G and Weber S (2021) Robotic Milling of Electrode Lead Channels During Cochlear Implantation in an ex-vivo Model. Front. Surg. 8:742147. doi: 10.3389/fsurg.2021.742147

INTRODUCTION

Cochlear implantation is a neuro-otologic technique used to restore hearing to profoundly deaf patients with sensorineural hearing loss. A microphone and audio processor are worn around the auricle, and a transmission coil is magnetically connected to the implanted receiver-stimulator. This receiver-stimulator is placed in the temporal region underneath the skin in a subperiosteal pocket, while an attached electrode array is inserted into one of the ducts of the cochlea, specifically into the scala tympani. In the manual surgery, the excessive electrode lead is stored and stabilized with various techniques in the mastoidectomy cavity, an access cavity posterior to the auditory canal, to prevent electrode migration and fatigue breaks through micro-movements. On the temporal bone surface, a groove or split-bridge is created from the mastoidectomy cavity to the recessed implant bed or the subperiosteal pocket.

In the emerging robotic technique of cochlear implantation (1, 2), a small-diameter access tunnel is drilled from the surface of the temporal bone directly to the round window of the cochlea following an optimized trajectory. Because no mastoidectomy cavity exists when performing the robotic procedure, the standard process of stowing the excess electrode lead in the mastoidectomy cavity is not possible. Therefore, a purposeful electrode lead management specific to robotic cochlear implantation is needed. In the first clinical studies of robotic cochlear implantation, a channel was manually milled after cochlear insertion. However, milling near the electrode lead poses a risk for damage to the electrode lead directly and indirectly to the delicate intracochlear structures due to the movements caused by the manipulation. Furthermore, milling after insertion risks bone dust and blood contaminating the cochlea, which increases the risk of damage to the organ (3, 4). Hence, it is advisable to mill before electrode insertion. However, prior to insertion, the exact electrode lead length needed and the potential electrode surplus cannot be ascertained by the surgeon, since the electrode lead is not yet inside the cochlea. This can be resolved with an accurate surgical planning on the medical images taken for the robotic procedure.

A dedicated electrode management and fixation system for robotic cochlear implantation can use the patient-specific intervention planning and the high-precision functionality of the robotic platform and extend from the robotic middle and inner ear access. Using the image-guided approach, the robotic electrode management technique can ensure that the electrode can be immobilized against micromovements and resulting mechanical fatigue. Furthermore, the electrode lead can be protected from external trauma by embedding it within the bone over the whole length. We assess that adequately sized margins to vital structures in the surgical site mean that the procedure can be conducted safely. We hypothesize that this fixation technique reduces the frequency of micro-fractures of the wires in the electrode due to the micromovements, and that it minimizes iatrogenic intracochlear damage due to electrode manipulation after insertion, which could result in better hearing outcomes from robotic cochlear implantation.

BACKGROUND OF COCHLEAR IMPLANTATION

Surgical Techniques

During manual cochlear implantation surgery, the receiver-stimulator is usually fixated either with the standard bone recess and bony tie-down suture technique, or the tight subperiosteal pocket technique with or without a bone recess (5–9). In addition to that, there are fixation techniques using screws, meshes, bridges, and pins or pedestals (10, 11).

To prevent electrode migration, the electrode itself is often stabilized with various techniques. Electrode migration refers to any movement of the electrode array relative to its initial position within the cochlea at some point in time after surgery. Placing the electrode in channels within the mastoidectomy cavity in an S-form is recommended, completely below the bone surface, while bony overhangs should be kept to prevent extrusion. Furthermore, small hooks, open bony bridges, and bone paté or bone wax over a channel are used (7, 8, 12).

At the site of cochlear insertion the electrode is kept in place with a tight packing of tissues such as fascia, muscle, fat or with fibrin glue (13). Others create stabilizing grooves in a corner of the facial recess or split-bridges in the incus buttress (14–17), which has been shown to decrease electrode migration rates significantly (16). For this, Leinung and Loth et al. proposed an about 3 mm long groove with a diameter of 1.1 ± 0.05 mm with an opening of 0.9 ± 0.05 mm to secure a 1.3 mm electrode lead, creating holding forces equivalent to another fixation technique using a titanium clip on the posterior buttress (18, 19). Further techniques described suturing the electrode to the incus buttress or the posterior canal wall (20, 21).

Cochlear Implantation Complications

Cochlear implantation has an average revision surgery rate of about 7.6% (22) and the device failure rate as recorded in clinics is about 5.1% (22). In the patient's timeframe, revision surgery rate has been measured as 1.0–1.9% per year (22–24). However, revision and device failure rates vary greatly between clinics with reported rates between 1.2 and 15.1%, and 0.5 and 14.7%, respectively (22), suggesting a great influence of other factors such as surgeon experience, the used surgical technique, or improved device reliability of new generations of implants (25).

Failed electrodes, most likely due to breakages of the thin wires, were found in 5.6–9.0% of devices (26–29). Furthermore, 54% of all devices had deliberately deactivated electrodes through reprogramming (27). As such, these failures did not appear to cause a decline in performance, however devices with more than three electrode failures were at high risk for future device performance deterioration leading to explantation (26, 30). The causes for these failures included loss of hermetic seal, fatigue fractures due to micro-movements in the electrode lead exit or the electrode lead itself (31–34), or external trauma, where the latter was reportedly more common in children (32, 35). In a recent revision case of robotic cochlear implantation, Morrel et al. observed wire fractures at the acute turn from the mastoid surface into the drilled tunnel (36), and have suggested smoothing the edges of the tunnel at the surface of the mastoid.

Electrode migrations can result in outcome decrement, due to insufficient stimulation of the low-frequency regions in the cochlear apex, and can also cause pain, vertigo, tinnitus or nonauditory stimulation (37, 38). A displacement of 3 mm results in a tonotopic change of about one octave (39), but the change in audiologic characteristics can usually be corrected through signal remapping (40). Studies have suggested a lower incidence of electrode migrations in perimodiolar electrode arrays than in straight lateral wall arrays (37, 41–43). However, perimodiolar have been found to have a higher incidence of primary scala vestibuli insertion or scala tympani to vestibuli translocations, and probably slightly higher incidence of tip fold-over (43). Both of these findings might be more related to surgical technique than the distinction between straight and perimodiolar array (43). Revision surgery caused by electrode migration is rare at around 0.2–2.5% (23, 42–48) per cochlear implant surgery in clinics, but electrode migration itself could have a much higher incidence. With various imaging modalities, electrode migration rates (at least one electrode out of the cochlea, or displacements >1 mm) have been reported anywhere from 0.4% in a direct postoperative scan (49), 7.4% 1 month after activation only in cases with an impedance increase (41), 13.4% at least 1 month after surgery (50), 29% after a mean follow-up time of 24 months (39), to 61% after a mean follow-up time of 34 months (51).

Background of Robotic Bone Removal

Robotic surgical systems for bone removal in neurosurgery and otology have been studied in the past.

Federspil et al. created recesses for cochlear implants with a six degrees-of-freedom industrial robot arm in human *ex-vivo* specimens. Patient registration was performed by recording three points on the bone surface with a tracked tool, while the patient was fixated rigidly. Their optimal milling parameters were 30,000 revolutions per minute (RPM) spindle speed, a feed forward rate of 5 mm/s for calvarium, and 1 mm/s for mastoid bone. Furthermore, to maintain physiologically sparing temperatures of the bone during milling, the spiral path was preferable (52, 53). In a later work with the same robot and the same application, Stolka et al. presented an intraoperative method to generate bone surface meshes for planning through tracked ultrasound measurements with a reconstruction precision of about 0.7 mm, and a final implant bed precision of about 1 mm (54).

Korb et al. eliminated a lesion in the petrous bone in a clinical study on one patient with an image-guided serial robot arm. Patient-to-image registration was performed through four fiducial screws. Their cranial fixation system consisted of a vacuum mouthpiece-based fixation coupled with vacuum cushions, thus allowing for a non-invasive fixation. The measurement attempt of the end-to-end accuracy was 0.66 ± 0.2 mm, and a maximum deviation of 1.06 mm. The researchers noted that the use of an adapted industrial robot would hardly be possible in routine surgical interventions, mainly due to the necessary technical, logistic and regulatory constraints to be overcome. Furthermore, preoperative planning times of half an hour to an hour would be incompatible with clinical reality, so any new concepts must rely on fast and semi-automatic intraoperative planning (55).

Danilchenko et al. performed autonomous robotic mastoidectomies using an image-guided industrial six-axis robot arm in human *ex-vivo* temporal bones. Patient-to-image registration was performed through four fiducial screws. They used a feed rate of 1 mm/s and reported maximum errors of 0.6 mm. They also state that while the fundamental engineering concepts were well developed, the translation into clinics was less well studied, in particular issues around maintenance of sterility, transportation and setup of the system in the operating room and safety considerations (56).

Dillon et al. demonstrated robotic mastoidectomies and access cavities to the vestibular system with a four degrees-of-freedom compact skull-mounted robot in human *ex-vivo* specimens. Patient-to-image registration was performed through a positioning frame on fiducial screws. They reported an average surface border error of 0.38 mm, and standard deviations ranging from 0.13 to 0.39 mm for the mastoidectomy, and a root mean squared surface accuracy between 0.23 and 0.65 mm for the access to the vestibular system. While they could show that a compact bone-attached robot can efficiently perform bone-removal, they stated that translation of this approach to clinical use would face additional challenges (57, 58). Dillon et al. showed that to avoid relatively large transient forces, the burr should be kept as perpendicular to the bone surface as possible. Further, shallow cuts with larger velocities were better in terms of forces than deeper cuts with slower velocities (59).

MATERIALS AND METHODS

Concept

The proposed technique for the electrode lead management during robotic cochlear implantation foresees the creation of a channel without self-crossings on the surface of the temporal bone, starting in the middle ear access tunnel, and leading to a ramped bone recess for the electrode lead exit of the receiver-stimulator (**Figure 1A**). Insertion depth of the electrode array into the cochlea can deviate slightly from planning, changing the amount of surplus electrode lead to be stowed below the temporal bone surface. Thus, one or more widenings of the channel are introduced (**Figure 1A**). Widenings provide space to accommodate a range of different paths within, resulting in different lengths of the electrode lead stowed.

Standardization and Reproducibility

The image-guided planning and robotic execution coupled with a software-guided clinical workflow creates a standardized and reproducible method for electrode management during robotic cochlear implantation.

Prevention of Iatrogenic Intracochlear Damage

Using the image-guided robotic approach, the electrode lead channel is milled before insertion. Thus, after insertion the electrode lead is first fixated in the press fit channel at the tunnel-to-surface transition. From then on, further movements of the electrode lead on the surface will not transfer to the electrode array in the cochlea, thus prohibiting further iatrogenic intracochlear damage.

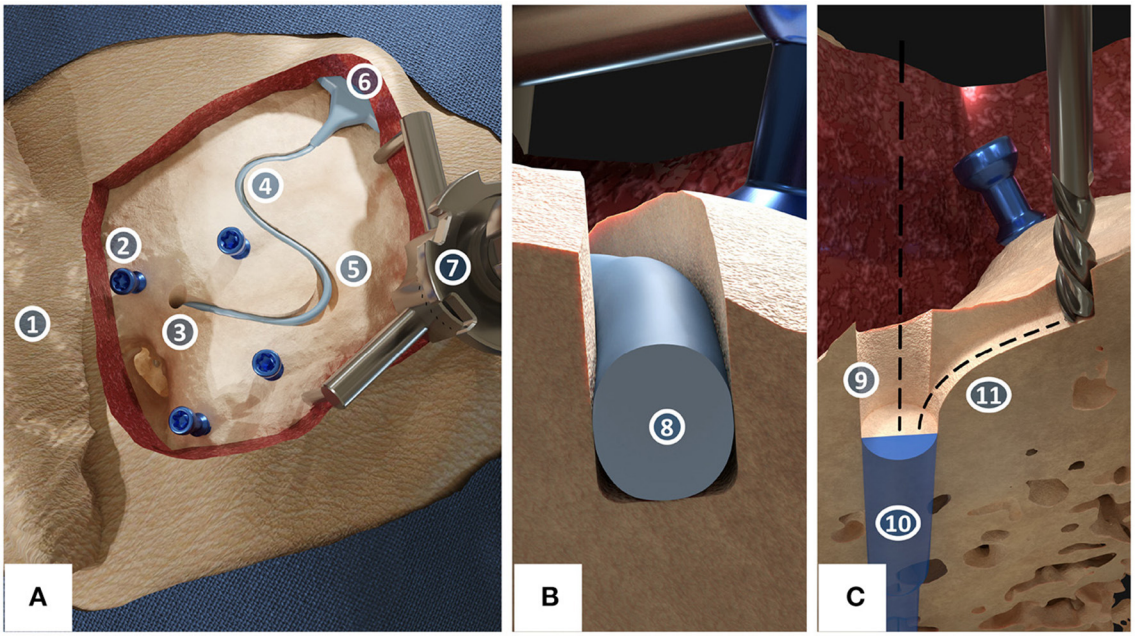

FIGURE 1 | The proposed concept for robotic milling of electrode lead channels during robotic cochlear implantation. **(A)** Surgical site of a left ear with its pinna (1) after the incision and placement of four fiducial screws (2) in which center the middle ear access hole (3) has been drilled. The electrode lead lies within the milled channel (4) and channel widenings (5) while the receiver-stimulator (6) is placed in a subperiosteal pocket. The patient marker attachment tripod (7) is fixed to the skull using a fifth screw. **(B)** Cross-sectional view of the immobilization of the electrode (8) in the channel with a slight press fit. **(C)** Cross-sectional view of the access point preparation (9) for the planned middle ear access drill hole (10). The sharp edge between the drill hole and the channel has been rounded off to create a smooth tunnel-to-surface transition (11).

Consistent Protection of the Electrode Lead From Mechanical Fatigue Due to Micro-Movements

To prevent fatigue fractures due to micro-movements, the channel is milled with a cylindrical milling cutter that is slightly smaller than the electrode diameter, creating a press fit that keeps the electrode lead immobilized in a stable fixation (**Figure 1B**). To further avoid the sharp angle between the middle ear access tunnel and the mastoid surface, a rounded path is milled to create a smooth tunnel-to-surface transition (**Figure 1C**), as suggested by Morrel et al. (36). The rest of the channel is also curvature-optimized to achieve a fixation for the electrode lead requiring minimal bending. Milling the electrode lead channel before the middle ear access tunnel presents the opportunity to shape the potentially inclined cortical bone surface at the access point to the tunnel into a flat surface to provide for optimal conditions for the high-accuracy requirements of drilling through the facial recess (**Figure 1C**).

Consistent Protection of the Electrode Lead From External Trauma

Using an image-guided approach, protection of the electrode lead from trauma can be ensured through the creation of a channel at a uniform and sufficient depth below the bone surface. The press fit design of the channel will hold the electrode lead below the bone surface.

Consistent Protection of the Electrode Lead From Electrode Migrations

Similar to other fixation techniques, the electrode lead will be fixated on the temporal bone surface with a press fit channel and constrained in the drill tunnel toward the entrance to the cochlea, thus prohibiting electrode migration.

Workflow in the Clinic

A clinical workflow for robotic lead channel milling during robotic cochlear implantation was developed (**Figure 2**).

First, patient anesthesia is performed and the surgical site is prepared. A retroauricular incision is created, in our experiments with a lazy-S incision. A tight subperiosteal pocket and flat surface, or a ramped bone recess for the receiver-stimulator is created, and a receiver-stimulator mock-up is inserted and tested for good fixation. Same as during the manual surgery, the surgeon chooses the location based on the local anatomy (e.g., flat and smooth bone surface), and considers the necessary distance from the pinna, such that the external audio processor will not interfere with the internal receiver-stimulator. Surgeons consider glasses, aesthetics like the visible bump from the internal device, and the hairline. Another possibility is the virtual mirroring of the contralateral implant in bilateral cases.

After the preparation of the receiver-stimulator fixation, five fiducial screws for robotic cochlear implantation are placed. High-resolution medical images (e.g., CBCT scan) are acquired and used for the planning of the robotic procedure. Once

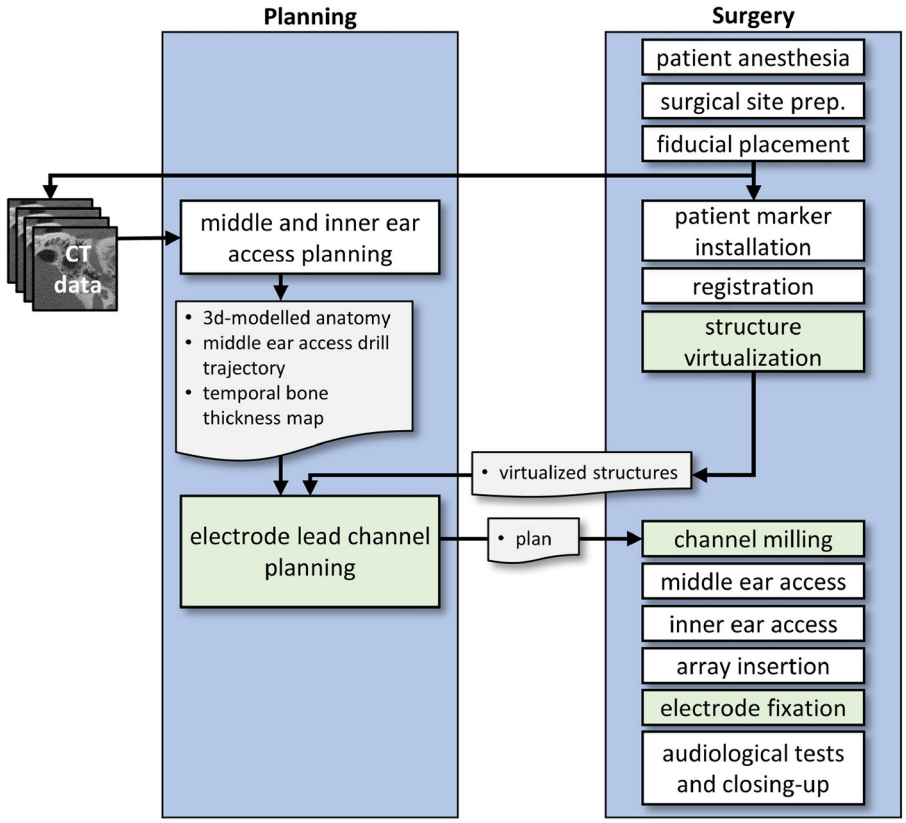

FIGURE 2 | Conceptual workflow of the proposed electrode lead management technique. During middle ear and inner ear access planning, there is a possible concurrency when the structure virtualization can be completed. The results of both processes are required for electrode lead channel planning. Workflow elements that are developed and investigated in this work are marked in green color.

the relevant anatomy has been segmented (i.e., temporal bone, the incus and malleus, the stapes, the facial nerve, the chorda tympani, the cochlea and its bony overhang, and the sigmoid sinus), and the cochlear parameters as well as the cochlear duct length measured, the middle and inner ear access can be planned.

In the meantime, the patient marker is attached to the skull using one of the screws. Patient-to-image registration is performed by digitizing the four other fiducial screws using a screw-specific tracked registration tool. For the planning of where to create the electrode lead channel, the accessible temporal bone surface must be known. Thus, the user is guided through the steps of virtualizing structures of the surgical site. The skin incision borders are mapped with a tracked tool, as well as the attachment of the patient marker. The position of the receiver-stimulator is recorded with the tracked tool at this point, or, if a contrast-enhanced version of the receiver-stimulator had been used, it is automatically detected by the navigation software.

The electrode lead management is planned. Now that all relevant structures have been mapped and visualized in the virtual patient anatomy, the channel path can be defined on the surface of the temporal bone model. The length of the channel is calculated from the position of the receiver-stimulator relative to the entrance of the middle ear access drill hole, the length of the drill hole until the round window, and the length of the electrode lead of the chosen cochlear implant. For the insertion depth, full insertion is assumed when no reasons for a partial insertion are detected (e.g., cochlear ossification). Curvatures are required to be below a threshold where the electrode might be damaged. The robotic execution shall not collide with other structures present in the surgical site. With the planned middle ear access trajectory, the insertion depth, and the position of the receiver-stimulator determined, the excessive lead length on the surface can be calculated up to intraoperative uncertainties. A safety margin of 1.0 mm is respected from the planned channel to surrounding structures such as dura mater, sigmoid sinus, external auditory canal, the skin incision, as well as to the structures necessary for the image-guided surgery, namely the fiducial screws and the patient marker attachment.

The lead channel milling is then executed under constant irrigation. The image-guided robot mills the channel along the planned path while controlling the feed-forward speed based on force measurements and navigation errors.

In the next steps, the rest of the robotic cochlear implantation workflow is executed, as described by Weber et al. (1, 60–62). This incorporates the middle ear access, the inner ear access, and the insertion of the cochlear implant electrode array through guiding

FIGURE 3 | Left: The custom-developed surgery planning software, implemented in Blender. The visualized objects are the HEARO Patient Marker Attachment tripod (1), the silicone template of the receiver-stimulator (2), the four HEARO Fiducial Screws (3), the end-effector with the milling cutter (4) in the planned electrode lead channel widening (5), and the planned drill access hole to the middle ear (6). All these structures reside on the patient's reconstructed temporal bone, onto which a red-green map is overlayed showing where the bone thickness is sufficient to place a channel plus safety margin (7). Right: A possible user interface implementation for the planning workflow (8).

metal half-tubes, which are removed as soon as the insertion is complete.

Lastly, the electrode is embedded in the milled channel beginning in the tunnel-to-surface transition, then from the receiver-stimulator toward the widening where the rest of the excess lead is stored. The surgeon closes the wound as soon as the audiologist has successfully tested the functionality of the implant.

Software Pipeline for Planning of Electrode Lead Channels

A prototype of a surgery planning software was developed as an add-on to the computer graphics software Blender (Blender Foundation, Amsterdam, Netherlands). This planning add-on (**Figure 3**) allows the loading of the patient case from the otologic planning software OTOPLAN (CASCINATION AG, Bern, Switzerland), containing the information about the middle and inner ear accesses, and all the reconstructed anatomical structures (i.e., temporal bone, the incus and malleus, the stapes, the facial nerve, the chorda tympani, the cochlea and its bony overhang, and the sigmoid sinus). It displays the previously virtualized structures, that is, the receiver-stimulator, tripod attachment of the patient marker, the patient marker itself, and the skin incision borders.

Virtualization of the Surgical Site

The position and orientation of the receiver-stimulator was obtained by recording first the end of the electrode lead exit, the fantail, then the two other points on the triangle shape of the fantail in a counter-clockwise fashion. On the tripod, equidistant recording of the three legs was sufficient to define its pose. The skin incision was virtualized by recording individual points along its border. With this plus the overlayed thickness map onto the temporal bone, the available areas for safe electrode channel milling were known.

Access Point Preparation

This part of the milling path was calculated automatically with the information about the middle ear access trajectory. It was milled in levels of 1.0 mm to a depth of 5.0 mm by first plunging down in the middle in the orientation of the trajectory, then creating the cylindrical shape by following a circle around the trajectory axis.

Electrode Channel

The channel path was expressed as three connected Bézier splines, creating an overall path with two curves. The ends were fixed at the position of the receiver-stimulator electrode lead exit, and the middle ear access trajectory entrance. First, the shape of the two curves was chosen, where the choice is between an S-shape that first starts in the posterior direction, or the mirrored S-shape that starts in the anterior direction. The position of the two curves was determined with two control points. Three input sliders determine the channel shape, two controlling the distance of the two control points from the entrance in the direction of the receiver-stimulator, and one the offset of the two control points in the perpendicular direction (**Figure 3**).

The remaining degrees-of-freedom were used to optimize the channel shape for low curvatures in all turns, and to achieve the required length. The navigation software warned the user if the calculated channel path had curvatures exceeding a critical threshold (i.e., a curvature radius of 5.0 mm). Another slider controlled the angle of the milling cutter relative to the middle ear access trajectory orientation around the axis in-between the receiver-stimulator and the drill hole entrance. This enabled the tilting of the milling cutter away from structures such as the patient marker attachment. The display of the channel's safety margin allowed the visual confirmation that the channel will not collide with any structures in the surgical site. Additionally, a map showing areas of sufficient thickness for the placement of a channel could be overlaid onto the temporal bone (**Figure 3**). The channel depth was automatically calculated to be at a uniform distance below the bone surface along the whole length, to protect the electrode lead from external impacts.

Tunnel-to-Surface Transition

This transition from drill tunnel to electrode channel was calculated automatically with a curvature-optimized Bézier spline in-between the already defined access point preparation path and the electrode channel path.

Widening

The location of the widening could be chosen in either the first curve, the second curve, or in both (**Figure 3**). The other choice was the size of the widening (e.g., small size was 1.0 mm shorter, 2.0 mm longer than the planned length). The boundaries of the widening were achieved by finding two tangent Bézier splines to the curve that satisfy the length requirements. Then, the milling path for the widening cavity was calculated through iterative contour-offsetting of the widening shape with a path overlap of 70%, then connecting the resulting paths in an outwards-spiral fashion. This spiral pattern had been previously suggested by Federspil et al. (52). Additionally, climb milling (also called down-cutting) was planned where the cut of the bone chips is started at the maximal width, as different from conventional milling (i.e., up-cutting) since this generates less heat (63).

Implant Bed

With this implementation of a planning software, only a ramped bone recess for the fantail was milled. Same as with the widening, the milling path was calculated by taking the outer contour of the fantail, offsetting this contour and then connecting the resulting paths in a spiral fashion. There was a possibility to add pin holes for receiver-stimulator versions with pins.

Adaptation of a Surgical Robotic System

For the execution of the experiments, the commercially available robotic surgical system HEARO (CASCINATION AG, Bern, Switzerland) for minimally invasive cochlear implantation was modified to enable electrode lead channel milling, instead of the middle and inner ear access drilling purpose for which it is intended (**Figure 4**). The HEARO Step Drill 1.8 mm was used to create the middle ear access drill hole. The technology and function of the system has been described by Weber et al. (1).

The modifications to the system include a HEARO Drill end-effector capable of reaching high spindle-speed of up to 80,000 RPM with an external motor controller and power supply, a custom-developed H10F tungsten carbide 1.2 mm diameter cylindrical three-fluted milling cutter with a center tap, and the necessary software modifications to adapt the system to milling purposes.

Workflow of the Experiments

An experimental study on formalin-flushed full-head human *ex-vivo* specimens with the approval from the local ethics committee (KEK Bern, Switzerland, Project-ID 2018-00770) was conducted to determine the safety and efficacy of the proposed approach.

The experimental study was conducted as follows: first, the robotic system was set up, and the end-effector calibrated. Then, the robotic channel milling, middle ear access and inner ear access were executed as described above.

The milling parameters were chosen as follows: an approximately perpendicular inclination to the surface normal, with spindle speeds of 30,000 RPM at a depth of 2.3 mm with a forward velocity setpoint of 2.0 mm/s, and force-based linear feed-forward velocity control above 4 N up to a threshold of 10 N, where the system interrupts the procedure and asks for user interaction. These milling parameters were previously determined in a pilot study based on milling forces, channel accuracy, navigational errors, and the drawn current by the end-effector (64). Each specimen was milled with a separate milling cutter. The introduced channel widening was designed to allow deeper insertions into the cochlea than planned by 1 mm, and shallower insertions by 2 mm. The location of the widening was chosen either in the first curve or in the second curve, based on the anatomy.

The cone-beam computed-tomography (CBCT) images for surgery planning were taken with an xCAT XL mobile head scanner (Xoran Technologies LLC, Ann Arbor, MI, USA) with an X-ray tube voltage of 120 kV, a tube current of 7 mA, and an isotropic reconstruction resolution of 0.1 mm.

For the planning of the robotic surgery on these images the otologic planning software OTOPLAN Version 1.5 (CASCINATION AG, Bern, Switzerland) was used. This software supports the generation of patient-specific 3D reconstructions of the anatomy, and then allows planning of the middle and inner ear access for robotic cochlear implantation.

The robotic execution was followed by the excision of the temporal bone from the whole-head specimen, and the acquisition of a micro-CT scan at an external certified testing laboratory (units MITTELLAND AG, Zuchwil, Switzerland), using a calibrated (sphere distance difference smaller than 4 µm) industrial computer tomograph (Metrotom 800, Carl Zeiss IMT GmbH) with an isotropic reconstruction voxel size between 40 and 50 µm. Once returned, the insertion of the electrode array was performed on the temporal bone by G.B., an otorhinolaryngology surgeon with cochlear implantation experience. For this, a silicone mock-up of the MED-EL Synchrony 2 Mi1250 FLEX28 cochlear implant was used. Subsequently, photos of the embedded electrode were taken, and the following endpoints measured in the gathered data.

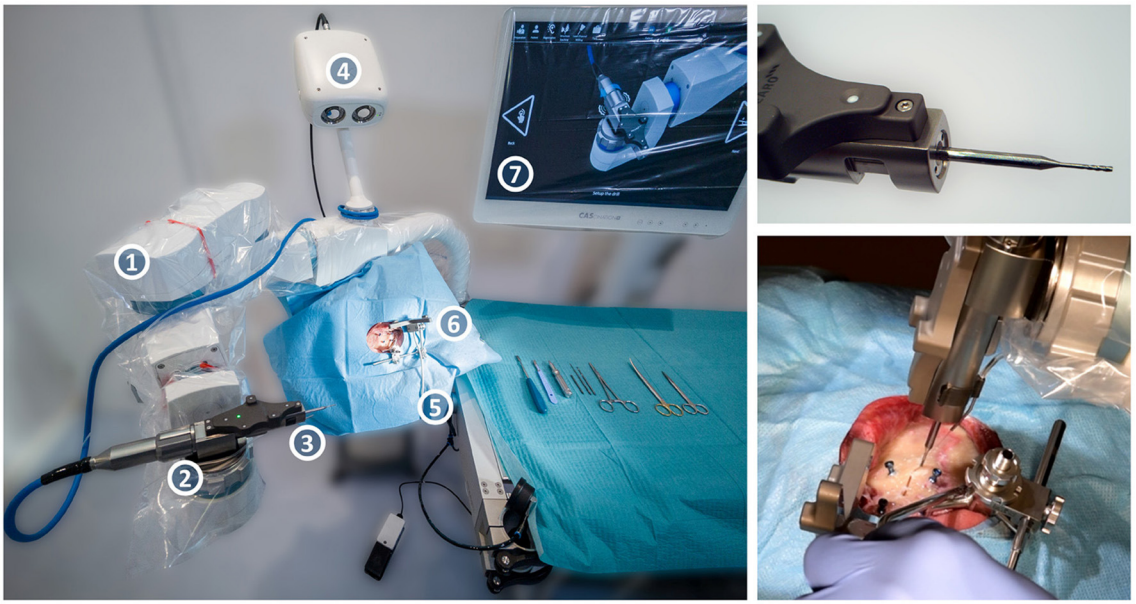

FIGURE 4 | The HEARO robotic surgical system, consisting of the five-axis HEARO Robot (1) with a tracked HEARO Drill end-effector on the quick-release wrist mount (2), the cylindrical milling cutter (3), a high-precision tracking camera (4), and a carbon-fiber headrest with air-pressure cushions (5) under a draped specimen with a patient marker attached (6). The navigation software displayed on the draped screen guides the surgeon through the procedure (7). On the top right, a close-up of the end-effector with the milling cutter, and on the bottom right the robotic system in the process of milling a channel during the *ex-vivo* study.

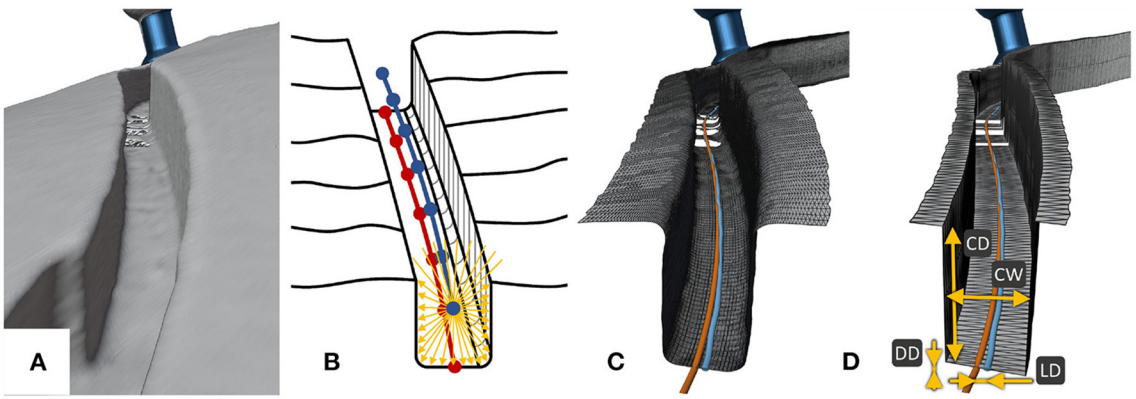

FIGURE 5 | The process for the analysis of the milled channels. **(A)** The reconstructed surface of the resulting electrode channel from the micro-CT. **(B)** This reconstructed surface was sampled radially to the approximate channel center line, resulting in **(C)** a resampled surface containing only the channel, which was then classified into top left, top right, left wall, right wall and bottom. **(D)** The measurements through these classifications were displayed as a simplified version of the channel, where CD stands for channel depth, CW for channel width, DD for depth displacement, and LD for lateral displacement.

Evaluation of Safety and Efficacy

We hypothesize that robotic electrode lead channel milling (planning and execution) can provide for an electrode lead channel that immobilizes the electrode lead and protects it from trauma. This can be further split into the following hypotheses: a channel for a cochlear implant electrode can (a) be robotically milled such that it remains within a planned safety margin, (b) be planned and executed such that postoperatively, the whole length of the electrode lead can be embedded within the channel, (c) be robotically milled such that it will create a slight press fit, designed to prohibit micro-movements, and (d) be planned and executed such that the depth is always greater than the electrode diameter.

The primary endpoint was the rate of completely milled lead channels, where the surgeon was able to immobilize the electrode lead without further manual milling, excluding the potential milling of an implant bed for the receiver before robotic execution. The secondary endpoints were split into subcategories safety and efficacy.

In terms of safety, the following measurements were carried out.

The Lateral Displacement and the Depth Displacement

The measurements were taken in the micro-CT scan on the reconstructed temporal bone surface (**Figure 5A**). For this, the temporal bone was segmented using a medical image analysis software (Amira, Thermo Fisher Scientific, Waltham, Massachusetts, USA), then postprocessed manually using the computer graphics software Blender. First, the co-registration of the postoperative micro-CT with the preoperative CBCT was carried out through paired-point matching of the positions of the four fiducial screws. Secondly, the approximate resulting center line of the channel was estimated, which ideally should correspond to the planned center line, that is, the milling path (**Figure 5B**, red line). Then, from each point along this approximate resulting center line (**Figure 5B**, blue line), the surrounding channel walls were mapped perpendicular to the path using ray intersections with the 3D reconstruction models. This resulted in a mapped version of the bone surface of connected cross sections (**Figure 5C)**. From the acquired points, the corresponding normal vectors, and their order, the channel walls can be classified into top left, left, bottom, right, and right top. Finally, the measured dimensions of the resulting channel were calculated by averaging the positions of the classified groups. The resulting center line is the line in the middle between left and right wall on the bottom (**Figure 5D**, blue line). The measurement results of the channel walls could then be displayed as a simplified channel model (**Figure 5D**). Measurements were split into lateral and depth directions based on the planned milling cutter orientation. In the widening, the right and left walls were treated separately. Air cells were removed from the reconstructed bone surface manually from the three-dimensional mesh, using the information of both the CBCT from planning and the micro-CT images. The resulting gaps in the channel were treated as missing data, and hence did not influence the measurements.

The Length of the Resulting Channel Outside the Safety Margin

This was measured manually by visual inspection in the postoperative micro-CT with the co-registered plan. The safety margin around the channel was overlayed transparently, and visually checked for an intersection with the resulting channel.

In terms of efficacy, the following measurements were carried out.

The Channel Width and the Channel Depth

The analysis from lateral and depth displacement was used. The channel width was measured as the distance between the left and right wall of the resulting lead channel, whereas the channel depth was measured as the height difference from the mean of the surface on the top left of the channel and the top right of the channel, to the bottom surface of the resulting electrode lead channel.

The Length of the Electrode Lead Outside the Resulting Channel

The insertion depth was checked visually by the surgeon (full insertion, partial insertion), and the length outside the channel was measured manually with a ruler during the experiments and was visualized in the photos taken.

Sample Size

The sample size was calculated based on a power analysis on a one sample variance and based on two experiments of a pilot study (64). One experiment had been conducted in bovine cortical bone, where 30 straight channels of various depths had been milled with three separate registrations, for a total of 717 mm milled channel length. The second experiment had been conducted in two preliminary cases with human *ex-vivo* temporal bones, resulting in a milled channel length of 44 mm. The root mean square errors for lateral displacement, depth displacement, channel width, and channel depth were 0.13, 0.17, 0.05, and 0.21 mm, respectively. Electrode lead channels for the implant used in the experiments (MED-EL Synchrony 2 Mi1250 FLEX28 Electrode Array) are about 60 mm long. The measurements were assumed to be independent from each other after the length of the tool diameter, so every 1.2 mm. Experience with drilling shows no systematic errors, but the patient-to-image registration does theoretically add a bias per case. However, over all cases the average bias was centered around zero.

For the endpoints of efficacy (i.e., channel width and channel depth), the risk threshold, that is the probability of violating the safety margin, was set to 1% per patient. For the endpoints of safety (i.e., lateral and depth displacement), the probability was set to 0.01% per patient, meaning that only in about one in 10,000 patients a safety violation would occur. Since the safety margin for the endpoints of safety are 3D reconstructions from a CBCT scan, their reconstruction error also had to be considered. According to Rathgeb et al. that segmentation error was $50 \pm 50\,\mu m$ in mean and standard deviation using the same technology (65). Using the binomial distribution, the probability for the hypothesis test can be calculated for one measurement point. Thus, to assume that the system can perform the tasks safely, the probability of going beyond the safety margins in one measurement point would need to be smaller than 0.0002% for safety endpoints, and 0.0201% for efficacy endpoints. For a safety margin of 1.0 mm, the corresponding root mean square error is 0.22 mm for the safety endpoints, and 0.28 mm for efficacy endpoints. For the power analysis, we use an alpha (Type I error) of 0.1%, and a power (Type II error) of 95%. Using this information, the required sample size returned six specimens. For redundancy, to account for unavailable measurements when mastoid air cells are present, and to account for anatomical variety, we conducted this study on seven anatomically distinct calvaria, resulting in a total of 12 temporal bones. Two sides were excluded, one had already been used for other experiments, the other presented a fractured temporal bone at arrival in the laboratory.

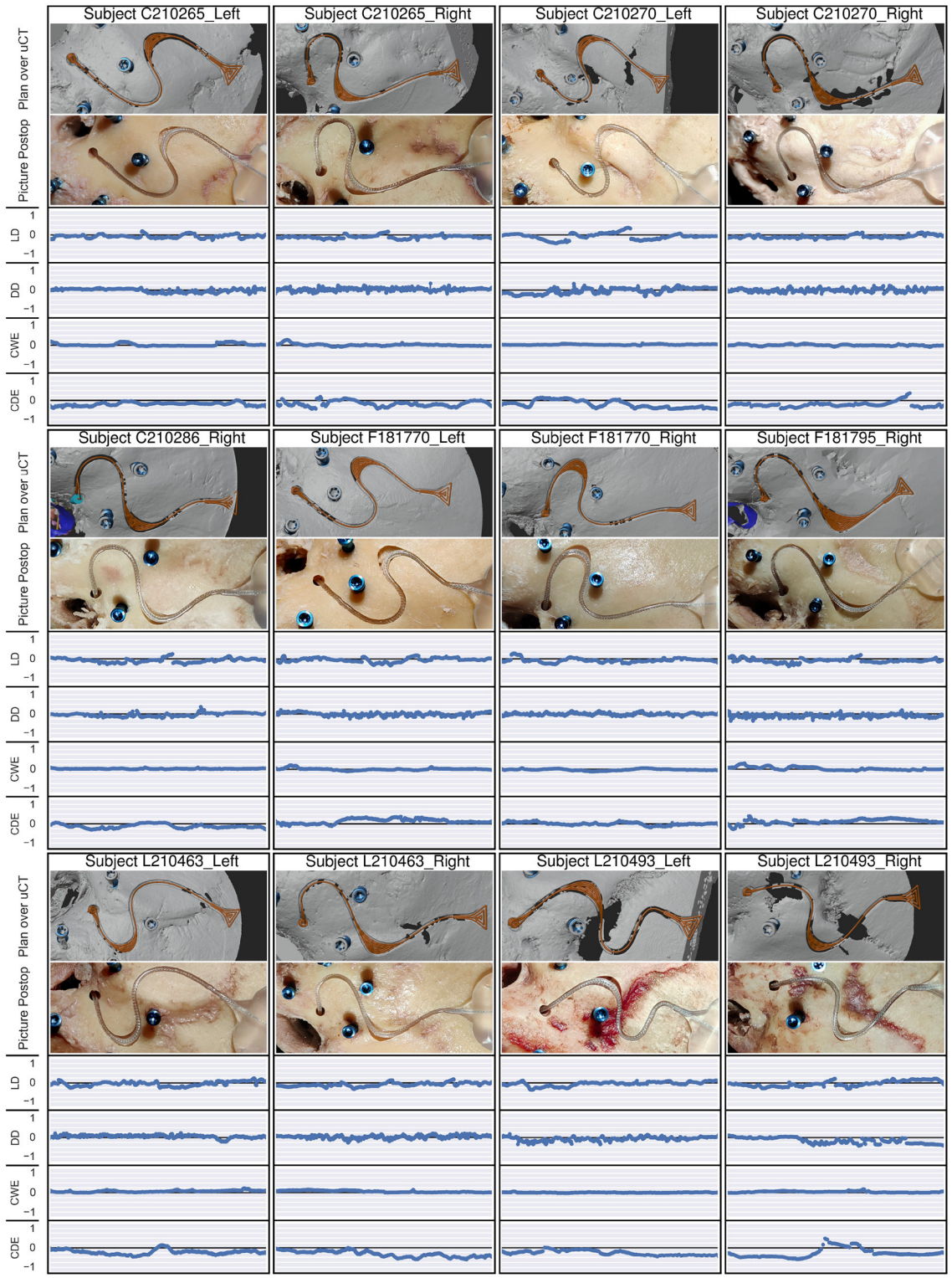

FIGURE 6 | For each subject, the top image depicts the planned path (orange) over the reconstructed temporal bone surface from the micro-CT (uCT) scan, containing the resulting electrode lead channel. The second image is a photo of the postoperative result after electrode insertion. The four following graphs show the lateral displacement (LD), the depth displacement (DD), the channel width error (CWE), and the channel depth error (CDE), all on a scale from −1 to 1 mm, which corresponds to the chosen safety margin. The safety margins were respected in all endpoints and cases.

RESULTS

All 12 out of 12 cases were successfully and completely planned and milled (**Figure 6**). All cases were completed with successful cochlear insertions. The electrode could be placed into the milled channel without having to force it, and when embedded was held through the slight press fit of the channel walls (**Figure 7**). In three out of the 12 cases, full insertion (i.e., the tapering stopper of the electrode array was close to the round window, as planned, seen in **Figure 8**) could not be achieved by 2–3 mm. However, in all cases all electrodes were within the cochlea since there is a distance between the tapering stopper and the first electrode. Nevertheless, the measured lead length outside the resulting channel was zero in all cases, so the full length of the electrodes could be embedded within the milled channel and the widening. After electrode array insertion, the surgeon could clip the electrode into the channel at the middle ear access drill hole entrance, thus allowing manipulation of the electrode lead without the electrode array being pulled out of the cochlea.

The resulting channel never exceeded the planned safety margin in any case. The mean lateral displacement was −0.06 mm [standard deviation (SD) = 0.09] with a root mean square error (RMSE) of 0.11 mm, where the negative mean value indicates that the displacement tended toward the left in the milling direction. The maximal absolute lateral displacement was 0.35 mm. The mean depth displacement was −0.01 mm (SD = 0.08), with maximal depth displacements deeper than planned of 0.33 mm, shallower than planned of 0.29 mm, and an RMSE of 0.08 mm. The maximal combined lateral and depth error was 0.42 mm. The limit RMSE for the admissible risk (i.e., leaving the safety margin of 1.0 mm with a probability of 0.01% in a patient) would be 0.22 mm. Since both lateral and depth RMSE are below this limit, including the 99.9% confidence interval (see **Table 1**), it can be stated that the channel for a cochlear implant electrode lead could be robotically milled such that it remained within a planned safety margin of 1.0 mm, while the risk of leaving that safety margin is smaller than one case in 10,000 (**Figure 9**).

The electrode leads could be embedded within the channels and were immobilized by the slightly narrower channel as compared to the electrode diameter. The mean channel width was 1.22 mm (SD = 0.04), where the planned channel width and tool diameter was 1.20 mm and the electrode diameter was 1.30 mm. The mean channel depth was 2.20 mm (SD = 0.16) with a RMSE of 0.19 mm, and the planned channel depth was 2.30 mm. The minimal depth was 1.82 mm, still great enough to contain the full 1.30 mm diameter of the electrode used for the experiments. The limit RMSE for the admissible risk (i.e., leaving the safety margin of 1.0 mm with a probability of 1% in a patient) for these two efficacy endpoints is 0.28 mm, and thus higher than the measured error including the confidence interval.

The individual steps of the proposed electrode lead channel management were timed (**Figure 10**). The additional step of virtualizing the structures of the surgical site (i.e., the receiver-stimulator mockup, the tripod attachment for the patient marker, the skin border) took about 3 min on average. Using the custom-developed planning software for robotic electrode channel milling, the planning time from case loading to the exported milling path ranged from 9 to 35 min with an average of 19. The time intervals from start to stop of the milling motor were between 3 and 6 min. During the experiments, milling forces usually ranged between 2 and 8 N with a maximal force of 10 N. Spindle torques were recorded between 1 and 7 mNm with a maximal torque of 8 mNm. An explanatory video showing the process from planning to robotic execution is provided as **Supplementary Material**.

FIGURE 7 | Cross section of the resulting channel with an embedded electrode lead cut for visualization. The electrode lead lies completely below the surface of the temporal bone and is held in place through the slight press fit between the channel walls.

DISCUSSION

In this paper, we have proposed a method for electrode fixation for robotic cochlear implantation. A possible clinical workflow was described, and an experimental study investigating safety and efficacy on *ex-vivo* human specimens was conducted using a custom-developed planning software and a modified commercial robotic surgery system. It could be shown that channels for cochlear implant electrode leads can be robotically milled such that they remain within safety margins of 1.0 mm. Also, the full length of the electrode leads could be embedded within the channels in all cases. The measured resulting channel width of 1.22 mm (SD = 0.04) with a tool of diameter 1.20 mm showed that this channel will create a slight press fit along most of the channel length, prohibiting micro-movements. Furthermore, the milled channel was never shallower than the full electrode diameter of 1.30 mm, with a minimal depth of 1.82 mm. With a channel depth of 2.30 mm and a safety margin of 1.0 mm, it was possible to plan a channel in all 12 cases by choosing a path in areas with sufficiently thick bone. Therefore, this approach could provide for a channel that could be planned and executed such that the depth was always greater than the electrode diameter, and that immobilizes the electrode lead and protects it from trauma.

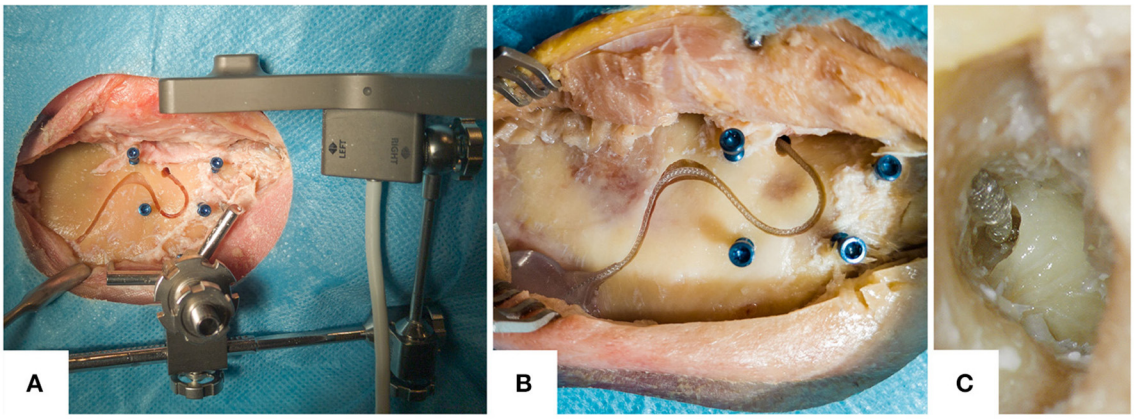

FIGURE 8 | Example photos of the resulting electrode lead management. **(A)** The resulting electrode channel with the attached patient marker on the tripod attachment. **(B)** Close-up of the electrode lead embedded within the resulting channel, in another specimen. **(C)** A microscope image through the external auditory canal after the elevation of the tympanomeatal flap. It shows the tapered neck of the electrode array, which is being inserted into the cochlea at the round window.

The probability that the safety margins would be violated in safety endpoints was smaller than 0.01% or one in 10,000 ($p < 0.001$), and for efficacy endpoints smaller than 1% or one in 100 ($p < 0.001$). Thus, the procedure was shown to be safe in this *ex-vivo* model. Based on the new data, the safety margins could even be decreased to keep the same probabilities of going beyond the safety margins of 1% for the efficacy endpoints, and 0.01% for the safety endpoints. In that case, the margin for the safety endpoints could theoretically be as low as 0.7 mm, and 0.8 mm for the efficacy endpoints, thus enabling an increased possible patient population especially with thin skull thicknesses, or small anatomies.

Past research often stated that the presented surgical systems work well, but further questions would need to be answered to introduce them into routine care, such as sterilization, transportation from storage to operating room or space requirements (55, 56, 58). The experimental work in this study was conducted using a commercially available task-specific robotic device (HEARO, CASCINATION AG, Bern, Switzerland) that has fulfilled all necessary regulatory requirements.

In agreement with previous work, we have confirmed spindle speeds of 30,000 RPM to be sufficient for robotic milling (53, 56). However, in our work the specimens cannot be rigidly fixated for clinical reasons (e.g., in a metal skull holder with screw pins), but are held in place with air-pressure cushions, thus the feed-forward rate set to 2 mm/s was decreased by the force-based velocity control to below 1 mm/s on average.

To secure the electrode lead, Leinung and Loth et al. proposed a circular groove of 3 mm length with a diameter of 1.1 ± 0.05 mm with an opening of 0.9 ± 0.05 mm, which provides holding forces equivalent to the technique using a titanium clip on the posterior buttress (18, 19). We hypothesize that the press fit rectangular channel as used in this paper with a similar width (i.e., 1.2 mm channel width) over a much longer length of (i.e., more than 30 mm) on the temporal bone surface combined with the constrained space in the 1.8 mm drill hole to the round window entrance into the cochlea will provide a similar fixation and resulting decrease in electrode migrations. While techniques with small press fit channels have been used, it is yet to be studied if the slight press fit along the longer channel will cause any damage to the electrode.

The electrode is proposed to be placed in a slight press fit into the milled electrode channel, for short-term stability until the healing processes have completed. Studies have shown that a receiver-stimulator in a subperiosteal pocket without milled bone recess will still spontaneously form one after some time through osteoclasts, assumably because of the applied pressure (66–68). It stands to reason that the press fit would also apply pressure on the channel walls, and thus the channel might widen up underneath the surface. At the same time, it has been reported that the implants become encased in fibrotic tissue with intense contact with the underlying bone, holding them in place, and potentially providing long-term stability (6).

The channel depth errors were slightly biased toward shallow channels, with a mean deviation from the planned channel depth of 0.10 mm. However, the errors are greater than what is observed in the depth displacement, where the accuracy in depth was 0.01 mm. Further analysis revealed that the bias of about 0.1 mm stemmed from a difference in temporal bone segmentation, where in most cases the reconstructed surface mesh from the planning CBCT was elevated with respect to the postoperative surface from the micro-CT. Possible explanations are the tendency to over-segment (i.e., include more voxels to the volume) to avoid holes in the planning surface, and the fact that the periosteum was not yet removed at the time when the planning CBCT was taken.

During the milling, the temperatures of the surrounding bone should not exceed 47°C degrees for more than 1 min such as not to cause thermal osteonecrosis (69). This issue is seen as unproblematic in the current work since the thin and shallow channels are created in only a couple of minutes in total, the

TABLE 1 | Summary of the measured endpoints.

	Mean (mm)	Standard deviation (mm)	Root mean square error (mm) [99.9% CI]	Minimum (mm)	Maximum (mm)
Lateral displacement	−0.057	0.088	0.105 [0.096, 0.115]		0.347
Depth displacement	−0.010	0.081	0.081 [0.075, 0.089]	−0.334	0.289
Channel width error	0.019	0.044	0.048 [0.042, 0.055]	−0.095	0.236
Channel depth error	−0.104	0.161	0.191 [0.171, 0.216]	−0.480	0.387
Electrode length outside the channel	0	0	0	0	0
Resulting channel length outside the safety margin	0	0	0	0	0

For lateral displacement, the maximum is the maximal absolute deviation both to the left and right in the milling path direction.

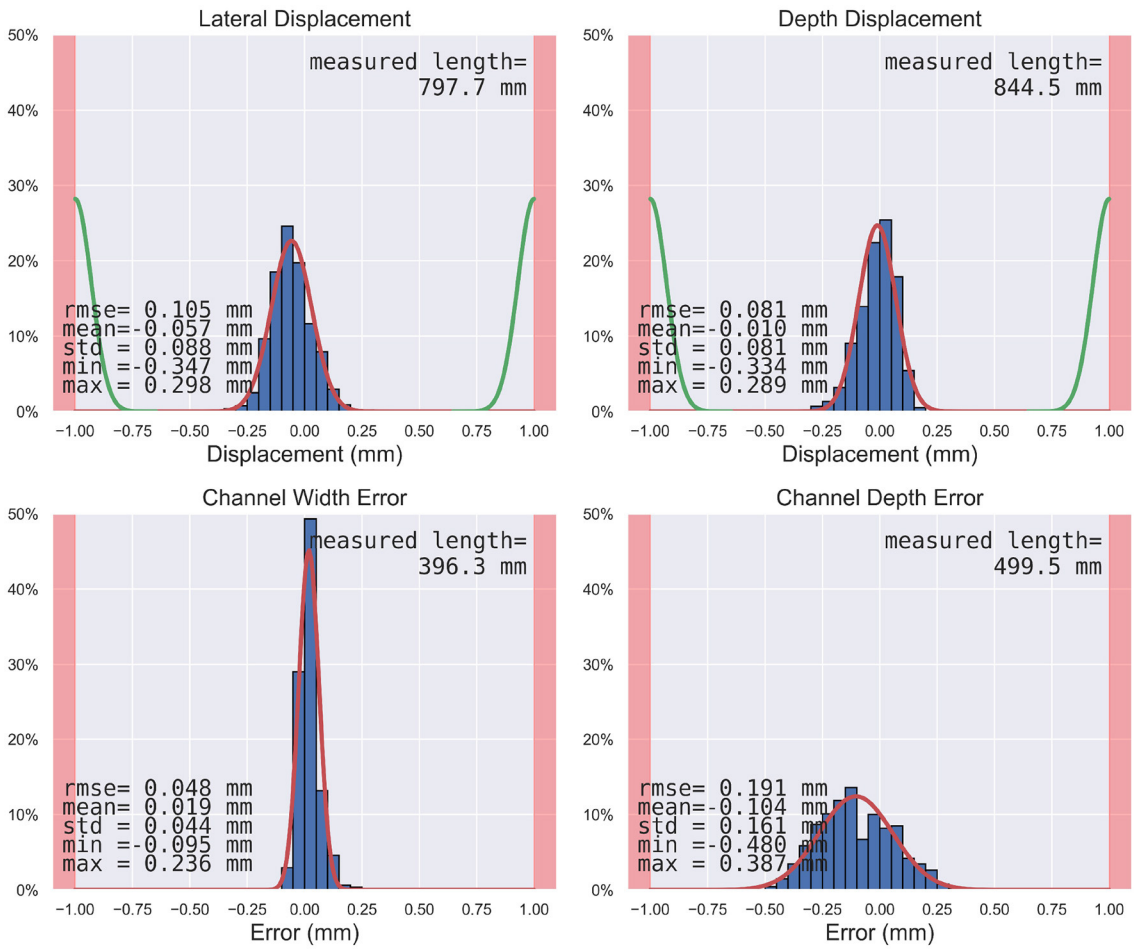

FIGURE 9 | Histograms of the measured endpoints (i.e., lateral displacement, depth displacement, channel width error, channel depth error) in blue, the estimated distribution in red, the segmentation error distribution in green (65) where applicable, and the safety margins as red zones at the sides. The measured length is the length along which the individual measurements were carried out in the resulting channel and widening.

tool is in constant motion, and the heat is conducted away by the constant irrigation. External irrigation mostly has a major impact by clearing the flutes from bone chips and, if insufficient, cooling the drill between drilling intervals could be introduced, as the heat in the bone is not dissipated quickly due to its low thermal conductivity (70).

The proposed fixation technique is only a viable option in terms of cost if the robotic system is also used for the other steps of cochlear implantation. The proposed technique here does not foresee the robotic milling of an implant bed for the receiver-stimulator, only a ramped bone recess into the channel for the fantail. However, based on the surgeon's preference the

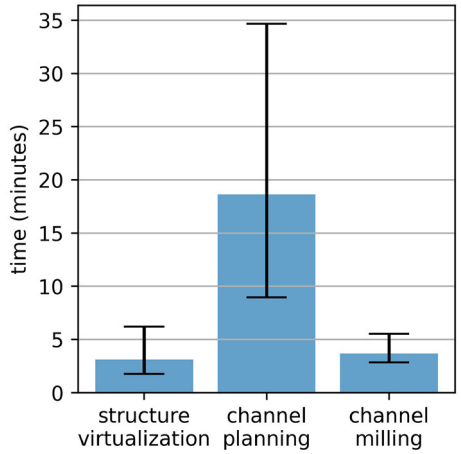

FIGURE 10 | Time spent for the electrode lead management during robotic cochlear implantation in this *ex-vivo* study.

robotic milling of the implant bed for the receiver-stimulator could be added. Right now, this would entail a bigger incision and a retraction of the periosteum, such that the robot can access that area with its milling tool close to perpendicular to the bone surface as when milling the channel. Milling at an acute angle to the bone surface, as it is done manually by the surgeon under the lifted skin flap, is difficult with the current five-axis robot arm design. This is because the tool tracking marker would then be oriented toward the patient and would hardly be visible by the tracking camera. Just as the full implant bed could be added, so could smaller recesses for the individual cochlear implant types with pedestals, pins, and screw fixations.

Surgeons have created the electrode lead channel manually in the incised and retracted skin so far during this robotic technique. With the concept presented here, the robot creates the electrode channel in the same space and thus does not need a greater skin incision. Exposed bone surface in-between drill tunnel and the electrode lead exit of the receiver-stimulator is required. If there is insufficient space for the required channel length without exceeding curvatures, or also if there is insufficient bone thickness, then the surgeon can again create the electrode lead channel manually over the whole length, or partially in the affected areas.

In this study, the cochlear implants were the same as used for the manual surgery technique. Due to the more direct path from the implant bed to the cochlea, less electrode lead length is required in the robotic technique and thus, shorter channels with smaller bends would potentially be necessary in the future if specific cochlear implants with shorter electrode leads for the robotic technique were developed.

The sharp edges created through the milling of the rectangular channel could be a potential danger to the electrode. A milling tool with a defined cutting depth of the cylindrical milling cutter and a cone-shaped design above that depth could round off the edges of the channel in passing. An additional flat stop could mechanically prevent excessive milling depth for additional safety. Furthermore, safety monitoring systems have been investigated that could detect contact of the milling cutter with the dura mater through determination of the milling condition based on sensor data (e.g., vibrations from a force-torque sensor, electrical impedance, optics) (52, 71).

In the case where full electrode array insertion into the cochlea cannot be achieved, and the insertion depth difference exceeds the length difference that the widening can accommodate, then the widening can be further enlarged manually by the surgeon, or another widening could be introduced.

The process of virtualizing the structures in the surgical site by recording specific points on either the receiver-stimulator mockup or the tripod attachment for the patient marker could be further simplified and made more precise by developing these structures with in-built reference registration points. At the same time, a specific patient marker attachment with an off-center screw design could leave more space for electrode channels.

While the custom-developed prototype planning software enabled an acceptable plan in all 12 cases, it took several iterations per case to get to the desired result. The chosen channel path varied in its shape depending on the patient anatomy, where the position of the middle ear access hole relative to the four surrounding fiducial screws had the biggest impact. The concept of using three Bézier splines with automatic curvature-optimized shapes, connected by two control points might unnecessarily limit the number of solutions of possible electrode channel paths. Future solutions should focus on allowing all possible electrode channel paths with the correct length and acceptable curvatures. The planning times between 9 and 35 min with this prototype software is mostly due to the prototype nature. A fully developed planning software should enable intraoperative planning in a couple of minutes. Since the step of virtualizing the structures of the surgical site took 3 min on average and the robotic milling execution about 4 min, the proposed electrode lead management approach, with intraoperative planning and execution, could be completed in $<$15 min.

The technology presented above for creating tight-fitting and precisely placed implant beds, with bone removal accuracies with a root mean square error of 0.1 mm and maximal errors below 0.5 mm, could potentially be applied for further hearing implantation surgeries, for example for direct acoustic cochlear stimulators, active middle ear implants, novel vestibular implants (72), or novel drug delivery devices (73). Further possible applications include the creation of access cavities (e.g., mastoidectomy, labyrinthectomy) to tumors such as vestibular schwannomas either using the middle fossa or the retrosigmoid approach. Moreover, cranial flap resection, facial nerve decompression and several neurosurgical approaches are also potentially foreseeable robotic procedures.

CONCLUSION

This study investigated robotic milling on the specific use case of surplus electrode lead management during robotic cochlear implantation in an *ex-vivo* model and verified a

proposed approach as safe and effective. The approach follows a concept of a non-intersecting electrode lead channel on the temporal bone surface, intraoperatively planned while taking the virtualized surgical site into account and executed with a high-accuracy robotic system. It is designed to provide a standardized, reproducible way of protecting the electrode lead from external trauma and mechanical fatigue due to micro-movements, and to prevent electrode migrations and iatrogenic intracochlear damage. The method of image-guided robotic bone removal in a compliant headrest presented here with average errors below 0.2 mm and maximal errors below 0.5 mm could be used for a variety of other otologic surgical procedures.

DATA AVAILABILITY STATEMENT

The raw data supporting the conclusions of this article will be made available by the authors, without undue reservation.

ETHICS STATEMENT

The studies involving human participants were reviewed and approved by KEK Bern, Switzerland, Project-ID 2018-00770. The patients/participants provided their written informed consent to participate in this study.

AUTHOR CONTRIBUTIONS

SW and JH created the study design. JH and FM developed the hardware components. JH developed the software components. JH, DS, FM, and GO'T carried out the *ex-vivo* experiments. JH analyzed the collected data and wrote the manuscript. All authors reviewed the manuscript and approved the submitted version.

FUNDING

This work was supported by the Swiss National Science Foundation SNF (Project 176007). Blackberry QNX provided an Academic Key for the QNX Software Development Platform. Funding in the form of cochlear implantation surgery equipment (e.g., Mi1250 Implant Template Ms040107, Mi1250 Silicone Mock-up Implants) was provided by MED-EL.

ACKNOWLEDGMENTS

We would like to thank the teams at CASCINATION and MED-EL for providing access to the HEARO robotic platform and laboratories for this study. Special thanks to Marco Matulic (CASCINATION AG, Bern, Switzerland), and Dr. Masoud Zoka Assadi (MED-EL GmbH, Innsbruck, Austria) for their help and insights for the study design and improvements to the manuscript. Additionally, many thanks for the contribution to the ethics committee approval by Prof. Dr. Paul Van de Heyning and Prof. Dr. Vedat Topsakal.

SUPPLEMENTARY MATERIAL

The Supplementary Material for this article can be found online at: https://www.frontiersin.org/articles/10.3389/fsurg.2021.742147/full#supplementary-material

REFERENCES

1. Weber S, Gavaghan K, Wimmer W, Williamson T, Gerber N, Anso J, et al. Instrument flight to the inner ear. *Sci Robot.* (2017) 2:eaal4916. doi: 10.1126/scirobotics.aal4916
2. Labadie RF, Balachandran R, Noble JH, Blachon GS, Mitchell JE, Reda FA, et al. Minimally invasive image-guided cochlear implantation surgery: first report of clinical implementation. *Laryngoscope.* (2014) 124:1915–22. doi: 10.1002/lary.24520
3. Khater A, El-Anwar M. Methods of hearing preservation during cochlear implantation. *Int Arch Otorhinolaryngol.* (2017) 21:297–301. doi: 10.1055/s-0036-1585094
4. Weinreich HM, Francis HW, Niparko JK, Chien WW. Techniques in cochlear implantation. *Oper Tech Otolaryngol-Head Neck Surg.* (2014) 25:312–20. doi: 10.1016/j.otot.2014.09.002
5. Friedmann DR, Jethanamest D, Roland Jr JT. Surgery for cochlear implantation: standard approach. In *Cochlear Implants: From Principles to Practice*. JP Medical Ltd. p.47–54.
6. Carlson ML, O'Connell BP, Lohse CM, Driscoll CL, Sweeney AD. Survey of the American neurotology society on cochlear implantation: part 2, surgical and device-related practice patterns. *Otol Neurotol.* (2018) 39:e20–e7. doi: 10.1097/MAO.0000000000001631
7. Cochlear Ltd. *Cochlear Nucleus CI622 cochlear implant with Slim Straight electrode-Physician's Guide*. Sydney (2020).
8. MED-EL Elektromedizinische Geräte GmbH. *Mi1250 SYNCHRONY 2-Surgical Guide*. Innsbruck.
9. Advanced Bionics AG. *Surgeon Manual for the HiRes^{TM} Ultra Cochlear Implant with the HiFocus^{TM} SlimJ and HiFocus^{TM} Mid-Scala Electrodes*. Stäfa: Advanced Bionics AG (2017).
10. Oticon Medical N. *Surgical Manual - Neuro Zti cochlear implant range*. Vallauris: Oticon Medical, Neurelec SAS (2019).
11. Yoshikawa N, Hirsch B, Telischi FF. Cochlear implant fixation and dura exposure. *Otol Neurotol.* (2010) 31:1211–4. doi: 10.1097/MAO.0b013e3181dd1400
12. Garaycochea O, Manrique-Huarte R, Vigliano M, Ferrán de la Cierva S, Manrique M. Sculpting the temporal bone: an easy reversible cochlear implant electro-array stabilization technique. *Eur Arch Oto-Rhino-Laryngology.* (2020) 277:1645–50. doi: 10.1007/s00405-020-05895-y
13. Gstoettner WK, Hamzavi J, Baumgartner WD, Czerny CC. Fixation of the electrode array with bone paté in cochlear implant surgery. *Acta Otolaryngol.* (2000) 120:369–74. doi: 10.1080/000164800750000586
14. Balkany T, Telischi FF. How I do it: otology and neurotology: fixation of the electrode cable during cochlear implantation: the split bridge technique. *Laryngoscope.* (1995) 105:217–8. doi: 10.1288/00005537-199502000-00022
15. Kawano A, Chiba H, Ueda K, Nishiyama N, Suzuki M. The modified split bridge method to prevent electrode slip-out. *Adv Otorhinolaryngol.* (2000) 57:84–6. doi: 10.1159/000059156
16. Leinung M, Helbig S, Adel Y, Stöver T, Loth AG. The effect of a bone groove against cochlear implant electrode migration. *Otol Neurotol.* (2019) 40:e511–e7. doi: 10.1097/MAO.0000000000002228
17. Loth AG, Adel Y, Weiß R, Helbig S, Stöver T, Leinung M. Evaluation of a bone groove geometry for fixation of a cochlear implant electrode. *Eur Arch Otorhinolaryngol.* (2020) 277:385–92. doi: 10.1007/s00405-019-05713-0

18. Cohen NL, Kuzma J. Titanium clip for cochlear implant electrode fixation. *Ann Otol Rhinol Laryngol.* (1995) 104:402–3.
19. Müller J, Schön F, Helms J. Reliable fixation of cochlear implant electrode mountings in children and adults - initial experiences with a new titanium clip. *Laryngorhinootologie.* (1998) 77:238–40. doi: 10.1055/s-2007-996968
20. Ribári O, Répássy G, Küstel M. New method for inserting and fixing the active electrode during cochlear implantation. *Acta Otolaryngol.* (2001) 121:194–6. doi: 10.1080/000164801300043460
21. Zawawi F, Cushing SL, James AL, Gordon KA, Papsin BC. How I do it: proximal cochlear implant electrode fixation using ned's knot. *Int J Pediatr Otorhinolaryngol.* (2021) 142:110593. doi: 10.1016/j.ijporl.2020.110593
22. Wang JT, Wang AY, Psarros C, Da Cruz M. Rates of revision and device failure in cochlear implant surgery: a 30-year experience. *Laryngoscope.* (2014) 124:2393–9. doi: 10.1002/lary.24649
23. Cullen RD, Fayad JN, Luxford WM, Buchman CA. Revision cochlear implant surgery in children. *Otol Neurotol.* (2008) 29:214–20. doi: 10.1097/MAO.0b013e3181635e9a
24. Neill GO, Tolley NS, O'Neill G, Tolley NS. Cochlear implant reliability: on the reporting of rates of revision surgery. *Indian J Otolaryngol Head Neck Surg.* (2020) 72:257–66. doi: 10.1007/s12070-020-01795-z
25. Causon A, Verschuur C, Newman TA. Trends in cochlear implant complications: implications for improving long-term outcomes. *Otol Neurotol.* (2013) 34:259–65. doi: 10.1097/MAO.0b013e31827d0943
26. Carlson ML, Archibald DJ, Dabade TS, Gifford RH, Neff BA, Beatty CW, et al. Prevalence and timing of individual cochlear implant electrode failures. *Otol Neurotol.* (2010) 31:893–8. doi: 10.1097/MAO.0b013e3181d2d697
27. Schow B, Friedland DR, Jensen J, Burg L, Runge CL. Electrode failure and device failure in adult cochlear implantation. *Cochlear Implants Int.* (2012) 13:35–40. doi: 10.1179/146701011X12962268235823
28. Goehring JL, Hughes ML, Baudhuin JL, Lusk RP. How well do cochlear implant intraoperative impedance measures predict postoperative electrode function? *Otol Neurotol.* (2013) 34:239–44. doi: 10.1097/MAO.0b013e31827c9d71
29. Newbold C, Risi F, Hollow R, Yusof Y, Dowell R. Long-term electrode impedance changes and failure prevalence in cochlear implants. *Int J Audiol.* (2015) 54:453–60. doi: 10.3109/14992027.2014.1001076
30. Terry B, Kelt RE, Jeyakumar A. Delayed complications after cochlear implantation. *JAMA Otolaryngol Head Neck Surg.* (2015) 141:1012–7. doi: 10.1001/jamaoto.2015.2154
31. Lane AP, Carrasco VN. A new technique for securing cochlear implants. *Otolaryngol Neck Surg.* (1999) 120:897–8. doi: 10.1016/S0194-5998(99)70333-5
32. Alexander NS, Caron E, Woolley AL. Fixation methods in pediatric cochlear implants: retrospective review of an evolution of 3 techniques. *Otolaryngol Head Neck Surg.* (2011) 144:427–30. doi: 10.1177/0194599810390336
33. Shelton C, Warren FM. Minimal access cochlear implant fixation: temporalis pocket with a plate. *Otol Neurotol.* (2012) 33:1530–34. doi: 10.1097/MAO.0b013e318271bb2f
34. Pamuk AE, Pamuk G, Jafarov S, Bajin MD, Saraç S, Sennaroglu L. The effect of cochlear implant bed preparation and fixation technique on the revision cochlear implantation rate. *J Laryngol Otol.* (2018) 132:534–9. doi: 10.1017/S0022215118000609
35. Boscolo-Rizzo P, Muzzi E, Barillari MR, Trabalzini F. Non-sutured fixation of the internal receiver-stimulator in cochlear implantation. *Eur Arch Oto-Rhino-Laryngology.* (2011) 268:961–5. doi: 10.1007/s00405-010-1479-5
36. Morrel WG, Jayawardena ADLL, M Amberg S, Dawant BM, Noble JH, Labadie RF. Revision surgery following minimally invasive image-guided cochlear implantation. *Laryngoscope.* (2019) 129:1458–61. doi: 10.1002/lary.27636
37. Mittmann P, Rademacher G, Mutze S, Ernst A, Todt I. Electrode migration in patients with perimodiolar cochlear implant electrodes. *Audiol Neurotol.* (2015) 20:349–53. doi: 10.1159/000435873
38. von Mitzlaff C, Dalbert A, Winklhofer S, Veraguth D, Huber A, Röösli C. Electrode migration after cochlear implantation. *Cochlear Implants Int.* (2021) 22:103–10. doi: 10.1080/14670100.2020.1833516
39. Van Der Marel KS, Verbist BM, Briaire JJ, Joemai RMS, Frijns JHM. Electrode migration in cochlear implant patients: not an exception. *Audiol Neurotol.* (2012) 17:275–81. doi: 10.1159/000338475
40. Zawawi F, Cushing SL, James AL, Gordon KA, Papsin BC. Extrusion of straight cochlear implant electrodes may be diminished by proximal fixation. *Int J Pediatr Otorhinolaryngol.* (2019) 116:164–7. doi: 10.1016/j.ijporl.2018.10.031
41. Dietz A, Wennström M, Lehtimäki A, Löppönen H, Valtonen H. Electrode migration after cochlear implant surgery: more common than expected? *Eur Arch Oto-Rhino-Laryngology.* (2016) 273:1411–8. doi: 10.1007/s00405-015-3716-4
42. Rader T, Baumann U, Stover T, Weissgerber T, Adel Y, Leinung M, et al. Management of cochlear implant electrode migration. *Otol Neurotol.* (2016) 37:e341–e8. doi: 10.1097/MAO.0000000000001065
43. Ishiyama A, Risi F, Boyd P, Ishiyama A, Risi F, Boyd P. Potential insertion complications with cochlear implant electrodes. *Cochlear Implants Int.* (2020) 21:206–19. doi: 10.1080/14670100.2020.1730066
44. Green KMJ, Bhatt YM, Saeed SR, Ramsden RT. Complications following adult cochlear implantation: experience in Manchester. *J Laryngol Otol.* (2004) 118:417–20. doi: 10.1258/002221504323219518
45. Connell SS, Balkany TJ, Hodges A V., Telischi FF, Angeli SI, Eshraghi AA. Electrode migration after cochlear implantation. *Otol Neurotol.* (2008) 29:156–9. doi: 10.1097/mao.0b013e318157f80b
46. Brown KD, Connell SS, Balkany TJ, Eshraghi AE, Telischi FF, Angeli SA. Incidence and indications for revision cochlear implant surgery in adults and children. *Laryngoscope.* (2009) 119:152–7. doi: 10.1002/lary.20012
47. Gardner PA, Shanley R, Perry BP. Failure rate in pediatric cochlear implantation and hearing results following revision surgery. *Int J Pediatr Otorhinolaryngol.* (2018) 111:13–5. doi: 10.1016/j.ijporl.2018.05.017
48. Rayamajhi P, Kurkure R, Castellino A, Kumar S, HA M, Nandhan R, et al. A clinical profile of revision cochlear implant surgery: MERF experience. *Cochlear Implants Int.* (2021) 22:61–7. doi: 10.1080/14670100.2020.1823128
49. Çelik M, Orhan KS, Öztürk E, Avci H, Polat B, Güldiken Y. Impact of routine plain X-ray on postoperative management in cochlear implantation. *J Int Adv Otol.* (2018) 14:365–9. doi: 10.5152/iao.2018.4252
50. Holder JT, Kessler DM, Noble JH, Gifford RH, Labadie RF. Prevalence of extracochlear electrodes: computerized tomography scans, cochlear implant maps, and operative reports. *Otol Neurotol.* (2018) 39:e325–e31. doi: 10.1097/MAO.0000000000001818
51. Lavinsky-Wolff M, Lavinsky L, Dall'Igna C, Lavinsky J, Setogutti E, Viletti MC. Transcanal cochleostomy in cochlear implant surgery: long-term results of a cohort study. *Braz J Otorhinolaryngol.* (2012) 78:118–23. doi: 10.1590/S1808-86942012000200018
52. Federspil PA, Geisthoff UW, Henrich D, Plinkert PK. Development of the first force-controlled robot for otoneurosurgery. *Laryngoscope.* (2003) 113:465–71. doi: 10.1097/00005537-200303000-00014
53. Federspil PA, Plinkert B, Plinkert PK. Experimental robotic milling in skull-base surgery. *Comput Aided Surg.* (2003) 8:42–8. doi: 10.3109/10929080309146102
54. Stolka PJ, Henrich D, Tretbar SH, Federspil PA. First 3D ultrasound scanning, planning, and execution of CT-free milling interventions with a surgical robot. *Conf Proc IEEE Eng Med Biol Soc.* (2008) 2008:5605–10. doi: 10.1109/IEMBS.2008.4650485
55. Korb W, Engel D, Boesecke R, Eggers G, Kotrikova B, Marmulla R, et al. Development and first patient trial of a surgical robot for complex trajectory milling. *Comput Aided Surg.* (2003) 8:247–56. doi: 10.3109/10929080309146060
56. Danilchenko A, Balachandran R, Toennies JL, Baron S, Munske B, Fitzpatrick JM, et al. Robotic mastoidectomy. *Otol Neurotol.* (2011) 32:11–6. doi: 10.1097/MAO.0b013e3181fcee9e
57. Dillon NP, Balachandran R, Michael Fitzpatrick J, Siebold MA, Labadie RF, Wanna GB, et al. A compact, bone-attached robot for mastoidectomy. *J Med Devices, Trans ASME.* (2015) 9:1–7. doi: 10.1115/1.4030083
58. Dillon NP, Balachandran R, Siebold MA, Webster RJ, Wanna GB, Labadie RF. Cadaveric testing of robot-assisted access to the internal auditory canal for vestibular schwannoma removal. *Otol Neurotol.* (2017) 38:441–7. doi: 10.1097/MAO.0000000000001324

59. Dillon NP, Kratchman LB, Dietrich MS, Labadie RF, Webster RJ, Withrow TJ. An experimental evaluation of the force requirements for robotic mastoidectomy. *Otol Neurotol.* (2013) 34:e93–e102. doi: 10.1097/MAO.0b013e318291c76b
60. Schneider D, Stenin I, Ansó J, Hermann J, Mueller F, Pereira Bom Braga G, et al. Robotic cochlear implantation: feasibility of a multiport approach in an *ex vivo* model. *Eur Arch Oto-Rhino-Laryngology.* (2019) 276:1283–9. doi: 10.1007/s00405-019-05318-7
61. Ansó J, Dür C, Apelt M, Venail F, Scheidegger O, Seidel K, et al. Prospective validation of facial nerve monitoring to prevent nerve damage during robotic drilling. *Front Surg.* (2019) 6:1–12. doi: 10.3389/fsurg.2019.00058
62. Caversaccio M, Wimmer W, Anso J, Mantokoudis G, Gerber N, Rathgeb C, et al. Robotic middle ear access for cochlear implantation: first in man. *PLoS ONE.* (2019) 14:e0220543. doi: 10.1371/journal.pone.0220543
63. Sugita N, Osa T, Mitsuishi M. Analysis and estimation of cutting-temperature distribution during end milling in relation to orthopedic surgery. *Med Eng Phys.* (2009) 31:101–7. doi: 10.1016/j.medengphy.2008.05.001
64. Hermann J, Ledergerber J, Wigger M, Schneider D, Müller FM, Weber S, et al. Towards robotic embedding of cochlear implants in the temporal bone. In: Burgert, Oliver; Hirt, Bernhard, editors. *18 Jahrestagung der Deutschen Gesellschaft für Computer- und Roboterassistierte Chirurgie e.V. (CURAC). Reutlingen. 19. - 21. September 2019.*
65. Rathgeb C, Wagner F, Wimmer W, Gerber N, Williamson T, Anschütz L, et al. The accuracy of image-based safety analysis for robotic cochlear implantation. *Int J Comput Assist Radiol Surg.* (2019) 14:83–92. doi: 10.1007/s11548-018-1834-3
66. Orhan KS, Polat B, Enver N, Çelik M, Güldiken Y, Deger K. Spontaneous bone bed formation in cochlear implantation using the subperiosteal pocket technique. *Otol Neurotol.* (2014) 35:1752–4. doi: 10.1097/MAO.0000000000000509
67. Turanoglu AK, Yigit O, Acioglu E, Okbay AM. Radiologic evidence of cochlear implant bone bed formation following the subperiosteal temporal pocket technique. *Otolaryngol Head Neck Surg.* (2016) 154:702–6. doi: 10.1177/0194599816628456
68. Marks DR, Jackler RK, Bates GJ, Greenberg S. Pediatric cochlear implantation: strategies to accommodate for head growth. *Otolaryngol-Head Neck Surg.* (1989) 101:38–46. doi: 10.1177/019459988910100108
69. Augustin G, Davila S, Mihoci K, Udiljak T, Vedrina DS, Antabak A. Thermal osteonecrosis and bone drilling parameters revisited. *Arch Orthop Trauma Surg.* (2007) 128:71–7. doi: 10.1007/s00402-007-0427-3
70. Feldmann A, Wandel J, Zysset P. Reducing temperature elevation of robotic bone drilling. *Med Eng Phys.* (2016) 38:1495–504. doi: 10.1016/j.medengphy.2016.10.001
71. Dai Y, Xue Y, Zhang J. Vibration-based milling condition monitoring in robot-assisted spine surgery. *IEEE/ASME Trans Mechatronics.* (2015) 20:3028–39. doi: 10.1109/TMECH.2015.2414177
72. Guyot J-P, Perez Fornos A. Milestones in the development of a vestibular implant. *Curr Opin Neurol.* (2019) 32:145–53. doi: 10.1097/WCO.0000000000000639
73. Piu F, Bishop KM. Local drug delivery for the treatment of neurotology disorders. *Front Cell Neurosci.* (2019) 13:238. doi: 10.3389/fncel.2019.00238

Conflict of Interest: SW is cofounder, shareholder, and chief executive officer of CASCINATION AG (Bern, Switzerland), which commercializes the robotic cochlear implantation technology.

The remaining authors declare that the research was conducted in the absence of any commercial or financial relationships that could be construed as a potential conflict of interest.

Publisher's Note: All claims expressed in this article are solely those of the authors and do not necessarily represent those of their affiliated organizations, or those of the publisher, the editors and the reviewers. Any product that may be evaluated in this article, or claim that may be made by its manufacturer, is not guaranteed or endorsed by the publisher.

frontiers in Surgery

ORIGINAL RESEARCH
published: 19 November 2021
doi: 10.3389/fsurg.2021.742160

Continuous Feature-Based Tracking of the Inner Ear for Robot-Assisted Microsurgery

Christian Marzi[1], *Tom Prinzen*[2], *Julia Haag*[1], *Thomas Klenzner*[2]* *and Franziska Mathis-Ullrich*[1]*

[1] Health Robotics and Automation, Institute for Anthropomatics and Robotics, Karlsruhe Institute of Technology, Karlsruhe, Germany, [2] Department of Otorhinolaryngology, Head & Neck Surgery, University-Hospital Düsseldorf, Düsseldorf, Germany

OPEN ACCESS

Edited by:
Vincent Van Rompaey,
University of Antwerp, Belgium

Reviewed by:
AB Zulkiflee,
University Malaya Medical Centre, Malaysia
Yann Nguyen,
Sorbonne Universités, France

***Correspondence:**
Franziska Mathis-Ullrich
franziska.ullrich@kit.edu
Thomas Klenzner
thomas.klenzner@med.uni-duesseldorf.de

Specialty section:
This article was submitted to Otorhinolaryngology - Head and Neck Surgery, a section of the journal Frontiers in Surgery

Received: 15 July 2021
Accepted: 21 October 2021
Published: 19 November 2021

Citation:
Marzi C, Prinzen T, Haag J, Klenzner T and Mathis-Ullrich F (2021) Continuous Feature-Based Tracking of the Inner Ear for Robot-Assisted Microsurgery. Front. Surg. 8:742160. doi: 10.3389/fsurg.2021.742160

Robotic systems for surgery of the inner ear must enable highly precise movement in relation to the patient. To allow for a suitable collaboration between surgeon and robot, these systems should not interrupt the surgical workflow and integrate well in existing processes. As the surgical microscope is a standard tool, present in almost every microsurgical intervention and due to it being in close proximity to the situs, it is predestined to be extended by assistive robotic systems. For instance, a microscope-mounted laser for ablation. As both, patient and microscope are subject to movements during surgery, a well-integrated robotic system must be able to comply with these movements. To solve the problem of on-line registration of an assistance system to the situs, the standard of care often utilizes marker-based technologies, which require markers being rigidly attached to the patient. This not only requires time for preparation but also increases invasiveness of the procedure and the line of sight of the tracking system may not be obstructed. This work aims at utilizing the existing imaging system for detection of relative movements between the surgical microscope and the patient. The resulting data allows for maintaining registration. Hereby, no artificial markers or landmarks are considered but an approach for feature-based tracking with respect to the surgical environment in otology is presented. The images for tracking are obtained by a two-dimensional RGB stream of a surgical microscope. Due to the bony structure of the surgical site, the recorded cochleostomy scene moves nearly rigidly. The goal of the tracking algorithm is to estimate motion only from the given image stream. After preprocessing, features are detected in two subsequent images and their affine transformation is computed by a random sample consensus (RANSAC) algorithm. The proposed method can provide movement feedback with up to 93.2 μm precision without the need for any additional hardware in the operating room or attachment of fiducials to the situs. In long term tracking, an accumulative error occurs.

Keywords: tracking, feature-based, microscope, image-processing, inner ear, robotic surgery, cochlea implantation

1. INTRODUCTION

Otologic microsurgery requires the surgeon to work at the limit of their visuo-tactile feedback and dexterity. The procedure of a cochlea implantation, for example, consists traditionally of a manually drilled, nearly cone-shaped access beginning on the outer surface of the skull with a diameter of around 30 mm and tapered to a 2 mm narrow opening to the middle-ear (posterior tympanotomy). After visualization of the round window, the cochlea can be opened through the round window or a cochleostomy, an artificial opening drilled by the surgeon. The surgeon then has to move a 0.3–1 mm thin electrode array through the posterior tympanotomy in the even more narrow cochlea. Robotic systems can exceed human precision in order of multiple magnitudes. Therefore, it is obvious that otologic microsurgery can highly benefit from robotic assistance.

When introducing novel technological robotic aids into surgery, space is often a critical factor. The closer to the surgical situs, the more important it is to keep the spacial obstruction to a minimum. In microsurgical interventions, a surgical microscope is always present. Therefore, mounting an assistive robotic manipulator to a microscope's optic unit poses high potential for robotic support. This allows for bringing the robot into close proximity of the situs while maintaining obstruction to the surgeon on a similar level as in regular microsurgery.

While being widely established for ablation of soft tissue (for example in ophthalmology), robotic laser surgery is gaining increasing interest in ablation of bone. In otologic surgery different kind of handheld lasers are used to penetrate the footplate of the stapes and more recently robotic guided lasers for interventions in the inner ear are taken into clinical trials (1). Also ablation of larger volumes of bone tissue could be demonstrated to be ready for clinical applications as for example by AOT's recent certification of CARLO (2), a laser osteotome mounted on a collaborative robot arm. The latter is applied in craniofacial surgery and provides cleaner cuts as well as additional freedom in cut geometry. Also the research project MIRACLE (3) aims on ablation of bone. However, in this case a minimally invasive robotic approach is pursued to reduce trauma. In addition, interventions at the inner ear are in focus of laser ablation of bone (4–6). In combination with sensory feedback about residual bone tissue, laser ablation provides a precise tool for opening of the cochlea. Such robotic systems in particular, could greatly benefit from integration into a surgical microscope toward clinical translation.

However, integration into a movable microscope will pose the challenge for the robotic system to maintain precise registration to the patient. Modern microscopes provide robotic support with position encoders as well as interfaces to marker based registration systems (7). Still, registration may be interrupted or become inaccurate by small, sudden movements, which can occur due to unintended contact with the microscope or movement of the patient. Compensating for such motions will be a necessary skill for any microscope-mounted robotic system manipulating tissue.

Modern surgical microscopes provide a magnified image of the surgical scene and integrate cameras or adapters for camera attachment. Often, the recorded images can be streamed to monitors in the operation room (OR) by standardized interfaces. Thus, the magnified image provides information available at no additional cost of hardware. Utilizing these images to derive movement information for a robotic system would thus be integrateable without increased efforts. In addition, such an image based tracking system would gain precision from the microscopes magnification.

State of the art for tracking the surgical microscope (and other tools or the patient) remain retro-reflective markers detected optically by infrared (IR) cameras in combination with IR-LED (7). Recent works have focused on using features based tracking in microscopes images for augmentation and registration of preoperative data. For example in (8), the pose of the cochlea is augmented for navigation support. Here, *Speeded Up Robust Features* (SURF) were used for maintaining the augmented images registered. In (9), the tips of the instruments for microsurgical intervention had to be colored green to allow for pose estimation through the microscope's image.

Extending the modification of tools or introduction of fiducials, this work aims on processing the microscope images based on natural features to gather information of the relative movement between the microscope and the patient. These tracking information can then be made available to enable robotic assistance. Cochleostomy is used as an example for a common and standardized intervention with high potential for automation.

2. MATERIALS AND METHODS

2.1. Imaging Setup

The investigated method aims on interfering as little as possible with the existing surgical workflow. This also means no additional hardware should be introduced into the operating room or, in particular, in proximity to the patient. Therefore, the existing imaging capabilities of commercial surgical microscopes should be utilized. To record microscope images, most conventional microscopes are equipped with standardized flanges to attach a camera as it is often used for documentation in current practice. Here, a computer with a frame grabber (DeckLink Recorder Mini 4K, Blackmagic Design Pty Ltd, Victoria, Australia) is used to gain access to the image frames. The processing computer is equipped with an Intel(R) Core(TM) i7-8086K CPU and GeForce GTX 1080 Ti GPU. These components are the only additional hardware, which could be easily positioned outside of the OR.

2.2. Image Processing Pipeline

2.2.1. Framework

To facilitate data exchange and enable a connection to a future robotic system the Robot Operation System (ROS, Distribution *Noetic*) is used as a software framework. A ROS driver for the frame grabber was developed to provide the images from the microscope to ROS. The raw frames are submitted to the image processing node on a ROS topic. For representation of pose information, ROS' dedicated data structure called *TF-Three* is

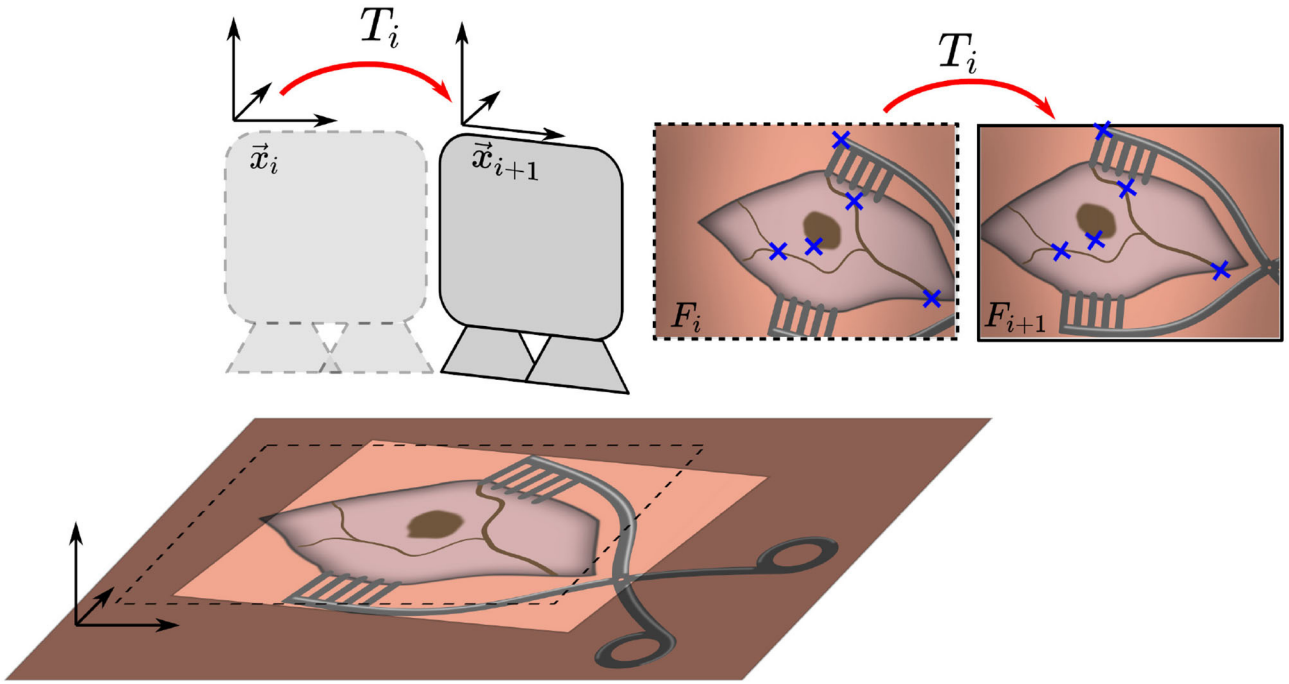

FIGURE 1 | Overview of the proposed method. Two consecutive microscope image frames F_i and F_{i+1} are processed to identify features, which are used to estimate the transformation T_i and maintain an initial registration by updating position x_i to x_{i+1}.

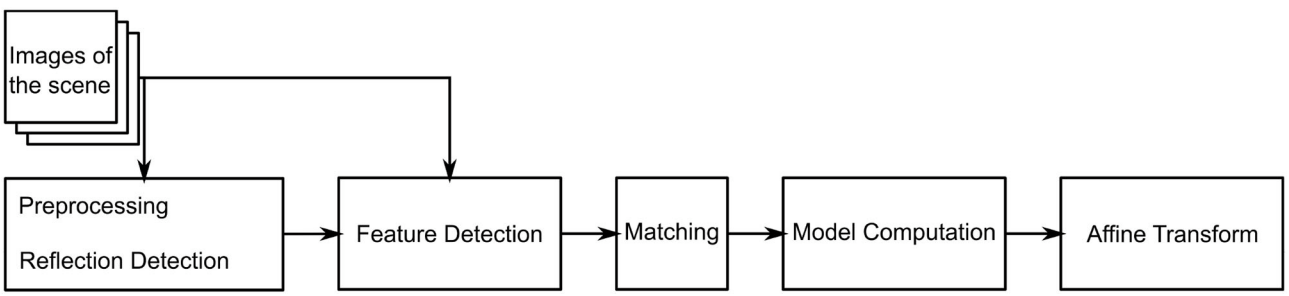

FIGURE 2 | UML diagram of the proposed algorithm.

used. It represents pose information in a hierarchical structure and is easily expandable and accessible in a network.

$$T = \begin{bmatrix} a_{00} & a_{01} & b_0 \\ a_{10} & a_{11} & b_1 \\ 0 & 0 & 1 \end{bmatrix} \quad (1)$$

2.2.2. Scene Tracking

Due to the bony structure of the surgical site, the cochleostomy scene is assumed to move rigidly and tissue deformations can be neglected. Movement is tracked in 2D in the microscope image plane, as illustrated in **Figure 1**. The proposed tracking algorithm provides an estimate of the relative motion between the surgical situs and microscope, given only the microscope's image stream and no further information. Motivated by microscope mounted robotic systems, this information would be sufficient to allow for compensation of unintended motion of either patient or microscope. In the proposed method, two subsequent images are compared and their affine transformation is estimated. The algorithm consists of three main steps. The flowchart in **Figure 2** outlines the algorithm. First, a feature detection algorithm (see section 2.2.4) identifies distinct natural landmarks. Second, the identified features are matched. An example of these identified features is displayed in **Figure 3**. Third, a transformation model between the established matches is estimated. Additional preprocessing to detect reflection artifacts in the images can increase tracking robustness for some surgical scenes. Here, thresholding is used to confine illumination artifacts in the field of view. The full image processing pipeline is illustrated in **Figure 2**.

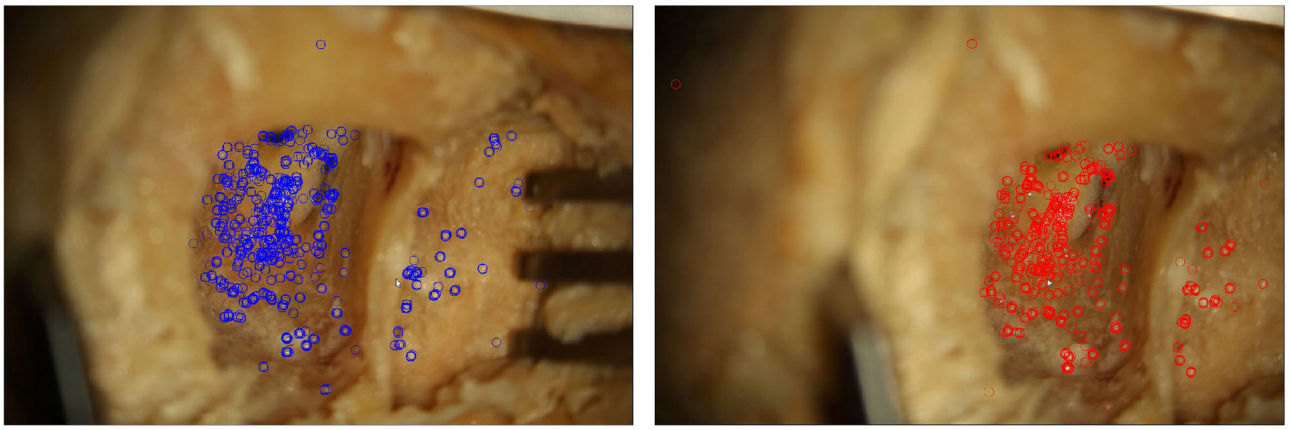

FIGURE 3 | Two microscope images of a moving situs. In each frame, features detected by the proposed algorithm are marked.

2.2.3. Image Preprocessing

Lighting-dependent artifacts appear as pixels with distinctively high color values in the microscope image. This delimits the affected points from their neighboring points. Accordingly, thresholding is a reasonable approach for reflection detection (10). As reflections are often prone to wrongly serving as detected features, thresholding is conducted before feature detection. It is conducted for each pixel comprising a saturation S and intensity I. If the statement in Equation (2) holds true, the pixel is added to the mask.

$$I < \tau_1 \cdot I_{\max} \cup S > \tau_2 \cdot S_{\max} \tag{2}$$

Here, $I_{\max}$ is the image's maximum intensity and $S_{\max}$ the image's maximum saturation. Parameters τ_1 and τ_2 are the respective thresholds, which were iteratively identified and evaluated. Sufficiently suitable values are given by $\tau_1 = 0.8$ and $\tau_2 = 0.2$. Preprocessing generates a mask, which excludes part of the images from further processing.

2.2.4. Feature Detection

The masked image is used to detect features utilizing the *Oriented FAST and Rotated BRIEF* (ORB) algorithm first presented by (11). It was developed as an alternative to the patented *Scale Invariant Feature Transform* (SIFT) algorithm (12). ORB is faster than SIFT and other alternatives like SURF, while being more sensitive to movements and more robust (13). The ORB feature detector is invariant to translation, rotation and scaling of the image, as well as robust against illumination changes and noise. The first step of the ORB algorithm is the detection of keypoints. These are generated by the *Features from Accelerated Segment Test* (FAST), which are combined with an orientation measure. For all keypoints found, a Binary Robust Independent Elementary Features (BRIEF) descriptor is computed. The number k of desired keypoints depends on the size of the obtained images. For 1080p images, k is suggested to be set to 2,000 according to the results by (14). Here, the ORB algorithm is implemented in Python using the image processing library OpenCV (15).

2.2.5. Transformation Model

Natural landmark detection results in a set of keypoints and their descriptors. Given two such sets obtained from images that share image features, the next step in our tracking algorithm is to find the corresponding matches between two images based on the detected features. The found matches are then used to estimate the affine transformation between these scenes. Since surgical scenes do not vary significantly in color or features it is likely that many keypoints are matched incorrectly despite the computed descriptors. Thus, a model estimation algorithm that is robust against a high ratio of mismatches (outliers) is required. The Random Sample Consensus (RANSAC) algorithm (16) estimates a model's parameters based on a set of data D which contains more points than are required for model description.

The desired model is the affine transformation T (see Equation 1). The set D is formed by tuples of ORB features with matching BRIEF descriptor in two subsequent images. The model is estimated to approximate the best affine transformation with respect to the translations of the features. For the developed image processing software, the implementation of RANSAC from the Python library *scikit-images* (17) was used. The affine transformations T_n of each iteration n can be cascaded to form an accumulated position $\vec{x}_n$ and the measured trajectory (formed by all $x_i \in \{1, \ldots, n\}$) of the relative movement of situs and microscope.

$$\vec{x}_n = (\prod^{n} T_n) \begin{pmatrix} 0 \\ 0 \\ 1 \end{pmatrix} \tag{3}$$

The evaluated position is passed to the TF-tree in ROS to easily be accessible by any connected robotic system.

2.3. Experimental Evaluation

For evaluation of the proposed algorithm, a robot is used to create a precise reference movements of a specimen. The trajectories are captured through the microscope and the image processing pipeline estimates the movement. Comparing

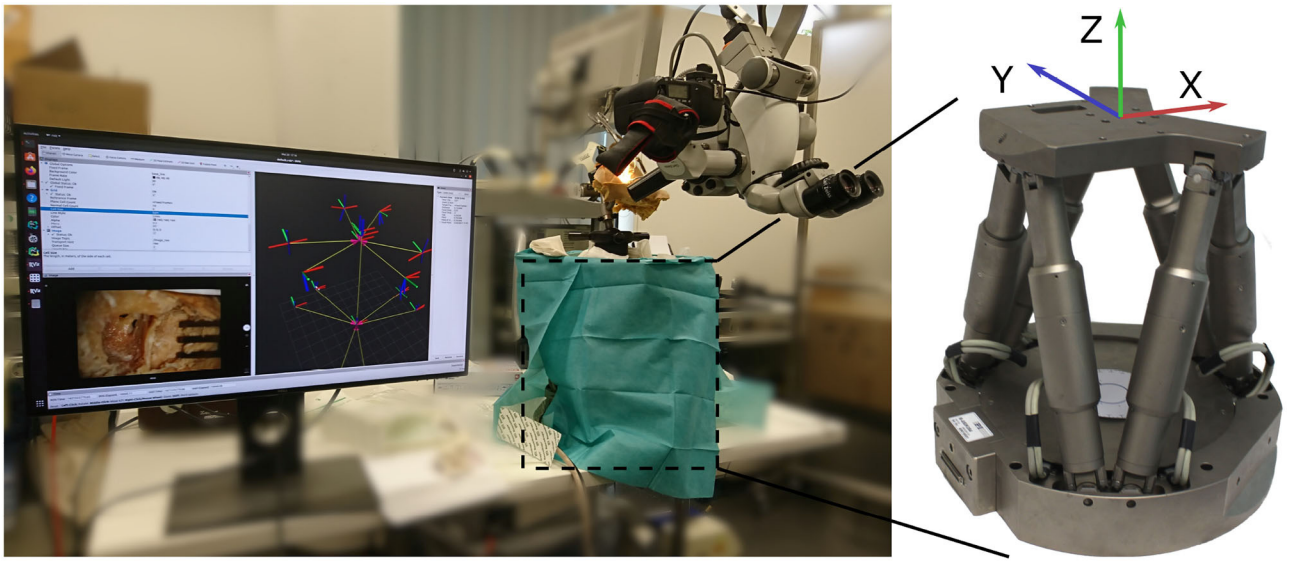

FIGURE 4 | Overview of the evaluation setup. A camera is attached to the side port of a surgical microscope. Below, the phantom is attached to a Stewart platform (covered by drapes). The robot is used for generating precise reference movement data.

estimated movement and reference movement allows for determination of a tracking error.

The setup for evaluation consist of a commercial surgical microscope (OPMI Pro Magis/S8, Carl Zeiss AG, Oberkochen, Germany). A camera (Canon EOS 100D) is attached to the side port of the microscope, recording a video stream. The video stream is captured by the frame grabber card in the processing computer. Below the microscope the surgical scene is set up on a Stewart platform (M-850, Physik Instrumente GmbH, Karlsruhe, Germany) that allows for defined control of precise reference movement with a repeatability of 2μm. The robot is controlled by the processing computer using ROS. The complete experimental setup is depicted in **Figure 4**.

To evaluate the presented tracking pipeline on several levels of realism and allow for comparison between different domains, three specimens are evaluated:

1. A temporal bone phantom **(TBP)** (PHACON GmbH, Leipzig, Germany) comprising only of bone-like material (see **Figure 5A**)
2. A temporal bone phantom comprising of bone-like material covered with multilayered skin-like material **(TBPs)** (PHACON GmbH, Leipzig, Germany). The skin incision is held apart by self-retaining retractors to facilitate good visualization (see **Figure 5B)**
3. A cadaveric temporal bone **(CTP)**. The skin incision is held apart by self-retaining retractors to facilitate good visualization (see **Figure 5C**).

All models and phantoms have been prepared to represent the last surgical phase before opening the cochlea. Therefore, a skin incision, mastoidectomy and posterior tympanotomy have been previously performed. The microscope is set up to provide a view similar to visualization during a surgical intervention.

The Stewart platform provides 6 degrees of freedom motion, however only translation movement along its x- and y-axes are used for reference motion (compare **Figure 4**). For data recording, the x-axis and y-axis of the robot are aligned manually to the image axes.

Motion of the patient is then simulated by driving the robot along a predefined trajectory. First, linear translational movement in x- and y-directions are evaluated. To also cover combinations of x- and y-motion in the 2D image space, we additionally evaluated spiral motion of the robot. The processing of the image data, as well as the control of the robot and sampling of reference data were conducted on the same computer to allow for data synchronization. The data was recorded for later evaluation as *rosbag*, ROS' data recording format. Equations (4) and (5) define the waypoints for the chosen trajectories. As soon as one waypoint was reached by the robot, the next one was passed to the robot's controller. In between the waypoints, the used controller interpolates a linear trajectory. The robot conducted the movement with its maximum speed of 2 mm/s. Linear translations in x- and y-directions (i.e., cross-shape) are defined by the waypoints

$$\vec{c}_{lin,n} \in \left\{ \begin{pmatrix} 0 \\ 0 \end{pmatrix}, \begin{pmatrix} 0 \\ 10 \end{pmatrix}, \begin{pmatrix} 0 \\ -10 \end{pmatrix}, \begin{pmatrix} 0 \\ 0 \end{pmatrix}, \begin{pmatrix} 10 \\ 0 \end{pmatrix}, \begin{pmatrix} -10 \\ 0 \end{pmatrix}, \begin{pmatrix} 0 \\ 0 \end{pmatrix} \right\}. \tag{4}$$

The spiral trajectory is defined by the waypoints

$$\vec{c}_{spir,n} = \begin{pmatrix} 10\frac{n}{50} \sin\left(4 \cdot 2\pi \frac{n}{50}\right) \\ 10\frac{n}{50} \cos\left(4 \cdot 2\pi \frac{n}{50}\right) \end{pmatrix} \Big|_{\forall} \; n = [0, 25] \in \mathbb{N}. \tag{5}$$

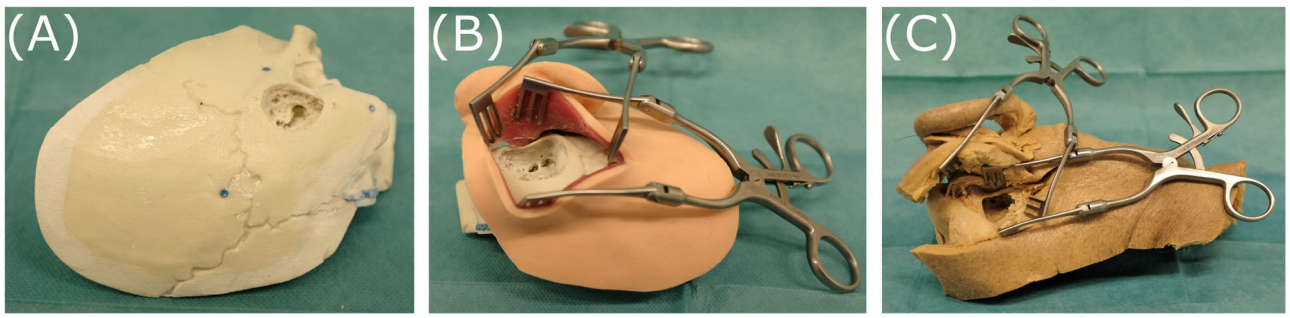

FIGURE 5 | The three specimens evaluated, representing different levels of realism: **(A)** temporal bone phantom (TBP), **(B)** temporal bone phantom with skin-like material (TBPs), **(C)** cadaveric temporal bone (CTP).

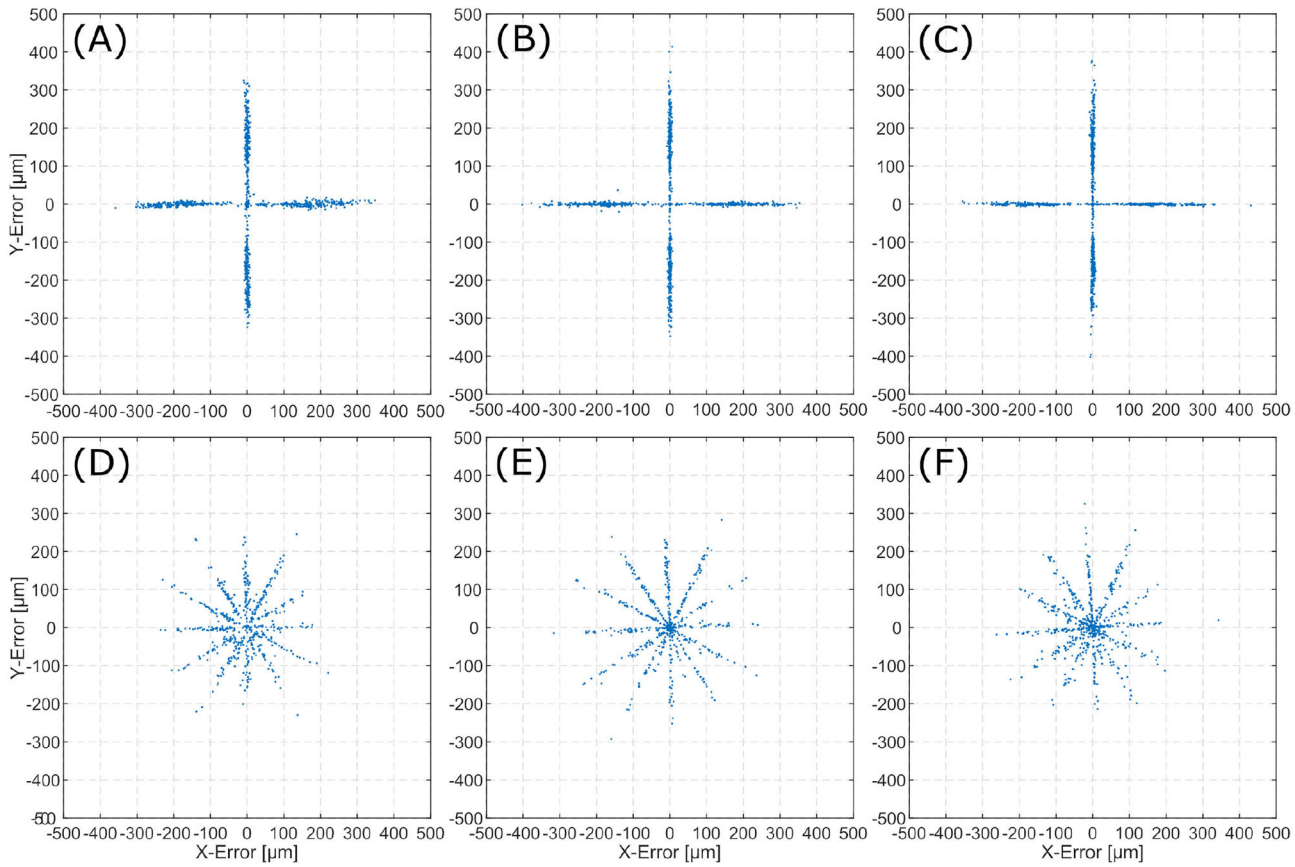

FIGURE 6 | Error ($\vec{E}$) distribution for the evaluated scenes. The top row displays 2D-errors for the linear trajectories on TBP **(A)**, TBPs **(B)**, and CTP **(C)**. The bottom row displays 2D-errors for the spiral trajectories on TBP **(D)**, TBPs **(E)**, and CTP **(F)**.

3. RESULTS

3.1. Frame to Frame Precision

To evaluate the precision of the algorithm, for two consecutive frames the estimated affine transformations is compared to the reference transformation of the robot. For the evaluated trajectories the translation error $\vec{E}$ is calculated by Equation (6) from the translations given from the algorithm $\Delta\vec{x}_{\text{ORB}}$ and reference from robot $\Delta\vec{x}_{\text{robot}}$.

$$\vec{E} = \Delta\vec{x}_{\text{ORB}} - \Delta\vec{x}_{\text{robot}} \tag{6}$$

For each trajectory (linear and spiral), $\vec{E}$ is calculated for all two consecutive frames. This results in an error distribution, which is plotted for each inner ear model. Error distributions are presented for the linear trajectories (**Figures 6A–C**), and spiral trajectories (**Figures 6D,E**).

The mean absolute error distance μ is derived from the n sets of consecutive frames by

$$\mu = \frac{1}{n}\sum^{n} \|\vec{E}_n\|. \quad (7)$$

Table 1 summarizes the mean errors of the tracked motion and their standard deviations for each specimen.

Error distributions in **Figure 6** show that the x and y locations of the error correlate with the number of trajectory sections with a constant orientation. Execution of linear trajectories in x- and y-directions results in error aggregation around $x = 0$ and $y = 0$. The spiral trajectories result in error aggregation along distinct angles.

TABLE 1 | Summary of the tracking precision results.

	TBP		TBPs		CTP	
	Mean	**Std**	**Mean**	**Std**	**Mean**	**Std**
Linear	93.9	118.4	135.8	114.3	110.1	112.6
Spiral	98.7	79.0	97.2	85.9	93.2	80.0

For each sample and each tested trajectory the mean error for the tracking error of two consecutive frames and their standard deviation are presented (all values in μm).

3.2. Trajectories

A set of affine transformation is estimated from the image stream. Cascading these transformations and applying them to the initial pose, results in an estimation of the current pose. The translational information of these poses can be displayed as the scenes full trajectory. This trajectory allows for comparison to the reference trajectories as executed by the Stewart platform. **Figures 7A–C** show reference trajectories (blue) and the image based trace of motion (red) for linear trajectories for each inner ear model (i.e., TBP, TBPs, and CTP). **Figures 7D–F** show reference trajectories and the image based trace of motion for the spiral trajectories for each scene.

The tracked linear trajectories (i.e., cross-shape) display an offset to the reference path but returns to its original starting point for all three models. For the spiral trajectories the accumulating pose error results in a total error of the final position.

3.3. Performance

The average duration of each algorithmic step in the process is listed in **Table 2**. These values refer to the runtime per image

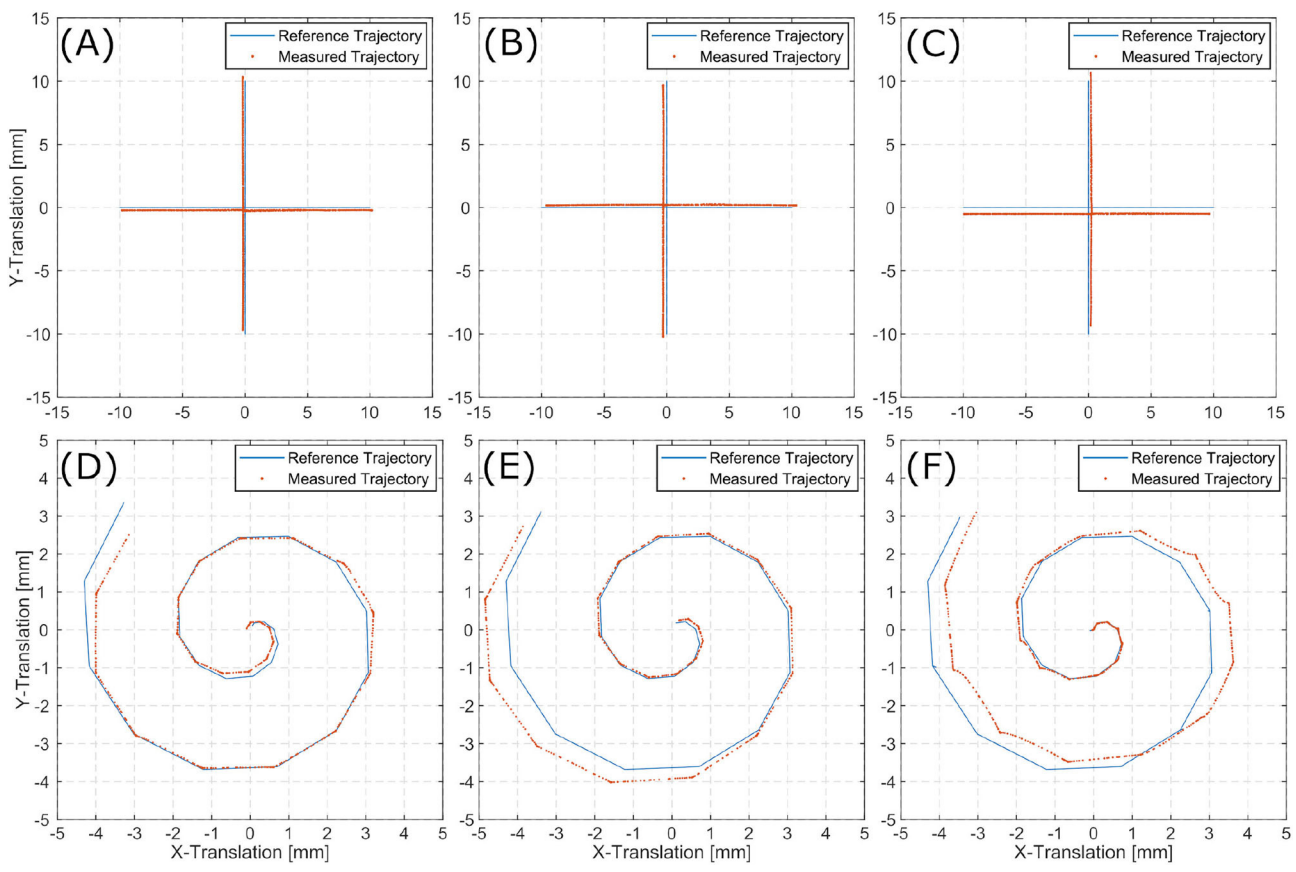

FIGURE 7 | Linear **(A–C)** and spiral **(D–F)** trajectories for TBP **(A,D)**, TBPs **(B,E)**, and CTP **(C,F)**.

TABLE 2 | Results of performance evaluation.

Step	Runtime mean ± standard deviation in ms	
	1,920×1,080	960×540
Feature detection	74 ± 9	18 ± 1
Matching	16 ± 3	12 ± 8
Model estimation	246 ± 77	234 ± 11
Preprocessing	36 ± 9	17 ± 5
Approximate total time	327	281

Runtime for 1,920×1,080 (Full HD) and 960×540 images are compared.

for images of size 1,920×1,080 and 960×540 px. The runtime is measured using 30 random images of the surgical site. The total runtime is listed for the implemented algorithm using scikit's RANSAC implementation, which was used for model estimation in this work.

4. DISCUSSION

The precision result exhibit few deviations between the phantoms (TBP, TBPs) and the human model (CTP). This leads to the conclusion, that the proposed method is well-suited for application in surgery independent of the specific domain.

The smallest tissue manipulation necessary for the intervention of cochlea implantation is the 2,000 μm opening to the middle-ear. The average translational error for all trajectories and scenarios (93.2–135.8μm) is more then one magnitudes below. Therefore, the frame to frame tracking proves suitable for supporting the localization of an assistive robotic system.

In the error distribution diagrams in **Figure 6** a strong correlation between the error and the direction of movement can be observed. For the linear trajectories erroneous motion only occurred along the x- and y-axes. The respective error distributions exhibit errors along the x- and y-axes. This leads to the conclusion, that the presented algorithm can determine the direction of a translation with significantly higher precision than the magnitude of the same translation. For the spiral trajectories the errors are distributed more evenly. The observation of aggregation along distinct angles (i.e., creating the star-like error distribution), can also be explained by the conclusion of higher angular precision. As the spiral trajectory is interpolated by linear sections, translation occurs section-wise linearly and for each section errors aggregate in the respective direction of translation.

The presented algorithm for reconstruction of the trajectory incrementally traces the current relative pose of microscope to patient. Position information only relies on the last increment of the pose as it is derived from the last two consecutive images. Therefore, it suffers from typical loss in precision over time as errors accumulate. For linear trajectories along x- and y-directions this effect is sufficiently small. However, when combining translation in multiple directions in the spiral trajectories, the accumulated error increases over time. The latter displays an accumulating overall position error in all three inner ear models. Presumably, this observation is caused by the aforementioned uncertainty in distance exceeding the angular uncertainty.

Despite the relatively high pose error after conduction of the spiral trajectories, the proposed method is suitable for extension by initial registration of the scene, which may be marker based or manually conducted. The trajectories evaluated in this work have a longer duration (44 s for the linear, 30 s for the spiral) compared to a shock caused by unintended motion in the OR. Thus, more iterations evaluated, which increase the accumulative error, in contrast to a real surgical scenario. In a robotic intervention such as motivated in section 1, global registration is likely to be considered a necessary prerequisite anyway. As an example, we envision a manual registration of an ablation laser spot before the ablation process. This could for example be conducted by manual input through a joystick. Extending this with the presented method represents a reliable safety measure against short unintended motion of patient or microscope.

The current algorithm and used hardware allows for processing of the microscope images in real-time with approximately 3 Hz. The major limitation is given by the RANSAC algorithm. Here scikit's implementation was used as it offers greater flexibility in implementation however in preliminary studies also an openCV implementation's runtime was evaluated and resulted in a significant reduction in the exection of RANSAC from an average of 246 ms down to 4 ms. This demonstrates the high potential software as well as hardware optimization offers for increasing the frame rates.

The presented method is limited to tracking an initially conducted registration and compensate for small errors occurring over short periods of time. The initial registration is outside the scope of this work as several methods have previously been presented. Initial registration methodologies strongly depend on the intervention and the applied robotic system. The presented method is prone to long term drifts of the pose due to accumulation of errors. As the scene can be expected to display only small and fast changes in pose. A suggested improvement may be to compare the current frame not only to the most recent one but also to past image data like a user defined initial frame or images captured multiple iterations earlier. The estimated transform from these frames can be used to correct a global drift of the tracked pose.

For appropriate integration to a robotic system, a frame rate suitable to the robotics kinematics needs to be reached by optimizing hardware, image resolution and implementation. For high speed (short term) tracking of relative pose changes, the here presented method could be extended by the use of inertial measurement units. However, these would require integration into the robotic system as well as attachment to the patient.

The presented method has been evaluated for feature-based tracking of inner ear models in two dimensions only. Here, we assume planar motion of surgical situs in the microscope image. To extend this method to covering full 6D pose estimation, i.e., three translations and three rotations, the estimated model needs to be expanded to a 3D-Transformation, as in

$$T_3 = \begin{bmatrix} a_{00} & a_{01} & a_{02} & b_0 \\ a_{10} & a_{11} & a_{12} & b_1 \\ a_{20} & a_{21} & a_{22} & b_2 \\ 0 & 0 & 0 & 1 \end{bmatrix} \quad (8)$$

For application in clinical intervention the surgical scene might become less rigid for example due to moving instruments (robotic or manual). The same issue is likely to occur for manipulations of the surgical field, obstructions by blood or residual tissue from drilling. If these artifacts only cover small areas of the field of view they are likely to be filtered by the RANSAC algorithm. Future work could investigate the robustness of the presented algorithm against such artifacts. Further approaches could research the masking of instruments and residual tissue in the image before feature detection to avoid falsely using features on the tools instead of the situs for tracking. This challenge could be solved by semantic segmentation of the instruments prior to executing the tracking algorithm, as demonstrated in Bodenstedt et al. (18) for laparoscopic scenes. With sufficient training data, typical instruments are masked from the scene and only the situs' image information are utilized for tracking.

5. CONCLUSION

A method for feature-based tracking of the inner ear for compensation of unintended motion was proposed. It is motivated by its use as safety feature enabling microscope mounted medical robotic assistance. Aiming for application in various fields of microsurgery, the application in cochlea implantation was regarded exemplary. Images from a surgical microscope are processed to derive pose changes between patient and microscope. These information can serve as input for compensating motion of a microscope mounted robotic system. Two consecutive images are analyzed for ORB features, which are matched and an affine transformation is estimated by a RANSAC algorithm. The transform is published in the Robot Operating System for integration into robotic systems. Making use of existing hardware in the OR during microsurgery, the microscope image stream is available for processing without introduction of additional hardware. This potentially allows for simple clinical translation of the proposed method. Evaluation showed sub-millimeter accuracy for frame to frame pose changes but revealed increasing offset in absolute pose due to accumulating errors. Application as shock countermeasure seems promising, however, clinical translation will require extension to 3D tracking and optimized performance.

DATA AVAILABILITY STATEMENT

The original contributions presented in the study are included in the article/supplementary material, further inquiries can be directed to the corresponding author/s.

ETHICS STATEMENT

The studies involving human participants were reviewed and approved by Ethikkommission an der Med. Fakultät der HHU Düsseldorf Moorenstr. 5 D-40225 Düsseldorf FWA-Nr.: 00000829 HHS IRB Registration Nr.: IRB00001579. The patients/participants provided their written informed consent to participate in this study.

AUTHOR CONTRIBUTIONS

CM and JH conceived and implemented the algorithm. CM, TP, and JH conceived, designed, and executed the experimental study. CM, TP, TK, and FM-U analyzed and involved in interpretation of data and made final approval of the version to be published. CM, TP, and FM-U drafted the article. All authors contributed to the article and approved the submitted version.

REFERENCES

1. Vittoria S, Lahlou G, Torres R, Daoudi H, Mosnier I, Mazalaigue S, et al. Robot-based assistance in middle ear surgery and cochlear implantation: first clinical report. *Eur Arch Otorhinolaryngol*. (2021) 278:77–85. doi: 10.1007/s00405-020-06070-z
2. Ureel M, Augello M, Holzinger D, Wilken T, Berg BI, Zeilhofer HF, et al. Cold ablation robot-guided laser osteotome (Carloa®): from bench to bedside. *J Clin Med*. (2021) 10:450. doi: 10.3390/jcm10030450
3. Rauter G. The miracle. In: Stobinger S, Klompfl F, Schmidt M, Zeilhofer HF, editors. *Lasers in Oral and Maxillofacial Surgery*. Cham: Springer Nature (2020). p. 247–53. doi: 10.1007/978-3-030-29604-9_19
4. Zhang Y, Pfeiffer T, Weller M, Wieser W, Huber R, Raczkowsky J, et al. Optical coherence tomography guided laser cochleostomy: towards the accuracy on tens of micrometer scale. *Biomed Res Int*. (2014) 2014:251814. doi: 10.1155/2014/251814
5. Zhang Y. *Optical Coherence Tomography Guided Laser-Cochleostomy*. Chichester: Scientific Publishing (2015).
6. Kahrs LA, Burgner J, Klenzner T, Raczkowsky J, Schipper J, Wörn H. Planning and simulation of microsurgical laser bone ablation. *Int J Comput Assist Radiol Surg*. (2010) 5:155–62. doi: 10.1007/s11548-009-0303-4
7. Ma L, Fei B. Comprehensive review of surgical microscopes: technology development and medical applications. *J BiomedOptics*. (2021) 26:1–74. doi: 10.1117/1.JBO.26.1.010901
8. Hussain R, Lalande A, Berihu Girum K, Guigou C, Grayeli AB. Augmented reality for inner ear procedures: visualization of the cochlear central axis in microscopic videos. *Int J Comput Assist Radiol Surg*. (2020) 15:1703–11. doi: 10.1007/s11548-020-02240-w
9. Giraldez JG, Talib H, Caversaccio M, Ballester MAG. Multimodal augmented reality system for surgical microscopy. In: Cleary KR, Robert L Galloway J, editors. *Medical Imaging 2006: Visualization, Image-Guided Procedures, and Display*. San Diego, CA: International Society for Optics and Photonics. SPIE (2006). p. 537–44.
10. Groeger M, Sepp W, Ortmaier T, Hirzinger G. Reconstruction of image structure in presence of specular reflections. In: Radig B, Florczyk S, editors. *Pattern Recognition*. Berlin; Heidelberg: Springer (2001). p. 53–60. doi: 10.1007/3-540-45404-7_8
11. Rublee E, Rabaud V, Konolige K, Bradski G. ORB: an efficient alternative to SIFT or SURF. In: *2011 International Conference on Computer Vision*. Barcelona (2011). p. 2564–71. doi: 10.1109/ICCV.2011.6126544
12. Lowe DG. Distinctive image features from scale-invariant keypoints. *Int J Comput Vision*. (2004) 60:91–110. doi: 10.1023/B:VISI.0000029664.99615.94

13. Karami E, Prasad S, Shehata MS. Image matching using SIFT, SURF, BRIEF and ORB: performance comparison for distorted images. *arXiv [Preprint]. arXiv:1710.02726.* (2017).
14. Mur-Artal R, Montiel JMM, Tardas JD. ORB-SLAM: a versatile and accurate monocular SLAM system. *IEEE Trans Robot*. (2015) 31:1147–63. doi: 10.1109/TRO.2015.2463671
15. Bradski G. The OpenCV library. *Dobbs J Softw Tools*. (2000) 120:122–5.
16. Fischler MA, Bolles RC. Random sample consensus: a paradigm for model fitting with applications to image analysis and automated cartography. *Commun ACM*. (1981) 24:381–95. doi: 10.1145/358669.358692
17. Van der Walt S, Schönberger JL, Nunez-Iglesias J, Boulogne F, Warner JD, Yager N, et al. scikit-image: image processing in Python. *PeerJ*. (2014) 2:e453. doi: 10.7717/peerj.453
18. Bodenstedt S, Allan M, Agustinos A, Du X, Garcia-Peraza-Herrera L, Kenngott H, et al. Comparative evaluation of instrument segmentation and tracking methods in minimally invasive surgery. *arXiv [Preprint]. arXiv:1805.02475.* (2018).

Conflict of Interest: The authors declare that the research was conducted in the absence of any commercial or financial relationships that could be construed as a potential conflict of interest.

frontiers in Surgery

ORIGINAL RESEARCH
published: 25 November 2021
doi: 10.3389/fsurg.2021.761217

Image-Based Planning of Minimally Traumatic Inner Ear Access for Robotic Cochlear Implantation

Fabian Mueller[1], Jan Hermann[1], Stefan Weber[1], Gabriela O'Toole Bom Braga[1] and Vedat Topsakal[2,3]*

[1] ARTORG Center for Biomedical Engineering Research, University of Bern, Bern, Switzerland, [2] Department of Otorhinolaryngology, Head and Neck Surgery, Vrije Universiteit Brussel, Brussels, Belgium, [3] Department of Otorhinolaryngology, Head and Neck Surgery, University Hospital UZ Brussel, Vrije Universiteit Brussel, Brussels, Belgium

Objective: During robotic cochlear implantation, an image-guided robotic system provides keyhole access to the scala tympani of the cochlea to allow insertion of the cochlear implant array. To standardize minimally traumatic robotic access to the cochlea, additional hard and soft constraints for inner ear access were proposed during trajectory planning. This extension of the planning strategy aims to provide a trajectory that preserves the anatomical and functional integrity of critical intra-cochlear structures during robotic execution and allows implantation with minimal insertion angles and risk of scala deviation.

Methods: The OpenEar dataset consists of a library with eight three-dimensional models of the human temporal bone based on computed tomography and micro-slicing. Soft constraints for inner ear access planning were introduced that aim to minimize the angle of cochlear approach, minimize the risk of scala deviation and maximize the distance to critical intra-cochlear structures such as the osseous spiral lamina. For all cases, a solution space of Pareto-optimal trajectories to the round window was generated. The trajectories satisfy the hard constraints, specifically the anatomical safety margins, and optimize the aforementioned soft constraints. With user-defined priorities, a trajectory was parameterized and analyzed in a virtual surgical procedure.

Results: In seven out of eight cases, a solution space was found with the trajectories safely passing through the facial recess. The solution space was Pareto-optimal with respect to the soft constraints of the inner ear access. In one case, the facial recess was too narrow to plan a trajectory that would pass the nerves at a sufficient distance with the intended drill diameter. With the soft constraints introduced, the optimal target region was determined to be in the antero-inferior region of the round window membrane.

Conclusion: A trend could be identified that a position between the antero-inferior border and the center of the round window membrane appears to be a favorable target position for cochlear tunnel-based access through the facial recess. The planning

OPEN ACCESS

Edited by:
Georgios Psychogios, University Hospital of Ioannina, Greece

Reviewed by:
Yann Nguyen, Sorbonne Universités, France
AB Zulkiflee, University Malaya Medical Center, Malaysia

****Correspondence:***
Fabian Mueller
fabian.mueller@artorg.unibe.ch

Specialty section:
This article was submitted to Otorhinolaryngology - Head and Neck Surgery, a section of the journal Frontiers in Surgery

Received: *19 August 2021*
Accepted: *02 November 2021*
Published: *25 November 2021*

Citation:
Mueller F, Hermann J, Weber S, O'Toole Bom Braga G and Topsakal V (2021) Image-Based Planning of Minimally Traumatic Inner Ear Access for Robotic Cochlear Implantation. Front. Surg. 8:761217. doi: 10.3389/fsurg.2021.761217

concept presented and the results obtained therewith have implications for planning strategies for robotic surgical procedures to the inner ear that aim for minimally traumatic cochlear access and electrode array implantation.

Keywords: sensorineural hearing loss, task-autonomous robotics, computer-assisted surgery, image-guided surgery, cochlear implantation, patient-specific planning

INTRODUCTION

Robotic cochlear implantation is emerging with the objective to standardize surgical outcomes for patients with sensorineural hearing loss. It is designed to conduct cochlear access relying on image-based accurate surgical planning and activity using a sensor- and image-guided robotic system (1–5). The keyhole access to the cochlea (*cochlea*) is obtained through a robotically drilled tunnel from the lateral surface of the mastoid through the facial recess (*sinus facialis*) to the round window (*fenestra cochleae*) (RW) of the cochlea. This robotic activity is considered task autonomous, according to the definition of autonomy levels for medical robotics as introduced by Yang et al. (6). The objective of the robotic task presented herein is to standardize minimally traumatic access to the cochlea. In this context, a procedure is considered minimally traumatic if no mechanical trauma occurs during robotic activity; a condition that is met if the anatomical and functional integrity of critical structures of the middle ear (*auris media*) and inner ear (*auris interna*) remain preserved. The importance of protecting critical intra-cochlear structures for residual hearing preservation during inner ear access and electrode array insertion is a widely discussed research topic. There are high expectations that a robotic approach could reduce trauma to the cochlea. However, it remains to be proven whether this is a sufficient condition for preserving residual hearing; biological factors also need to be investigated.

For cochlear implantation surgery, it is critical to have a precise anatomical knowledge of the region of the RW including its anatomical microenvironment. The RW niche (*fossula fenestrae cochleae*), is an open cave-like area with an overhanging oblique ridge from the promontory consisting of a posterior pillar (*postis posterior*), a tegmen (*tegmen*) and an anterior pillar (*postis anterior*). The superior part, which resembles a canopy and covers the round window membrane (*membrana tympani secundaria*) (RWM), is referred to as the canonus (*canonus fossulae fenestrae cochleae*) (7–9). The RWM which is embedded in the RW niche, covers the entrance to the scala tympani and has a complex variable conical shape with a posterior portion close to the osseous spiral lamina (10). This distance increases from about 0.1 mm to about 1 mm, as does the width and height of the scala tympani as one moves anteriorly and inferiorly to the center of the RW (11). The scala tympani, the favored intra-cochlear lumen for implant placement, can be accessed through a RW or extended RW approach or a RW-related cochleostomy (12, 13). A favorable trajectory directed into the scala tympani, without targeting the osseous spiral lamina and the lateral wall of the basal portion, must pass through the canonus of the niche (14). Removal of the canonus (canonectomy) or creation of an opening in the canonus (canonostomy) may cause trauma to the hook region, where the osseous spiral lamina, the spiral ligament and the basilar membrane fuse (10). To avoid damage to the basilar membrane and mitigate a reduction of the hair cell and nerve fiber population, it is important to anatomically preserve the osseous spiral lamina (15).

In conventional cochlear implantation surgery, the surgeon removes the complete superior part (canonectomy) to create a visual exposure of the RWM for orientation during insertion of the cochlear implant electrode. This procedure is conducted at the limit of human tactile feedback and sensory capabilities (16). Therefore, trauma may result from direct mechanical damage to the anatomy caused by the hand-guided tool or indirectly from the high induced sound pressure within the cochlea (17). Efforts have been made to provide a more consistent approach minimizing induced trauma on the hearing organ with the use of a force guided controlled tool or a robotic system (18–24). All of these developed approaches aimed for robust controlled penetration of the outer bone shell of the cochlea without penetration of the RWM. With the robotic approach, the opening of the canonus could be reduced to a circle with a diameter of 1.0 mm (canonostomy), allowing the electrode array to be passed through the drilled tunnel without visual exposure of the entire RWM (5). This surgical technique allows removal of drill debris prior to electrode insertion and minimizes induced disturbance and sound pressure on the cochlea (17, 25, 26). Regardless of the method, it is generally concluded, that the RWM must be preserved during the canonectomy or canonostomy to minimize trauma to the cochlea (13, 27). Additionally, it is concluded, that the ideal insertion trajectory should align with the centerline of the scala tympani to prevent damage to intra-cochlear structures during electrode array insertion (23, 28). While there is consensus on the optimal position for accessing the RW in conventional cochlear implantation surgery, this has not been adequately studied in tunnel-based robotic cochlear implantation (13).

There are several factors affecting the optimal target position and trajectory orientation in robotic cochlear implantation. This includes the size and shape of the facial recess, the variable anatomy of the RW including the basal portion of the cochlea, and the size and orientation of the scala tympani (29, 30). In addition, the dimensions of the surgical tools and the accuracy of the robotic system have an important role in limiting the direction of entry into the scala tympani and the size of the feasible target region (31). Recent research suggested a target position central or inferiorly to the center of the RWM with the optimal trajectory defined to minimize the cochlear in- and out

plane angle (13, 23). The in- plane angle is the offset between the optimal and the ideal trajectory that delineates alongside the lateral wall of the basal turn for a given target position. However, this definition of an optimal target position does not take into account the complex anatomy of the RW and the intra-cochlear hook region in intra-operative planning, and aims only for reliable electrode insertion within the scala tympani. Due to limited clinical imaging modalities, the RW and the bony cochlear wall remain the only consistent landmarks in intra-operative planning. To standardize trajectory planning, more precise planning parameters and criteria for inner ear access need to be introduced. Ideally these are expressed in terms of anatomical and structural properties of the RW and the bony cochlear wall to allow a consistent and accurate characterization of an optimal trajectory with clinical imaging modalities.

The aim of this work was to evaluate an optimal trajectory to the inner ear in tunnel based robotic cochlear implantation taking into account the complex RW anatomy and its anatomical microenvironment. A set of complementary hard and soft constraints for middle ear and inner ear access were proposed to calculate an optimal trajectory solution space. The hard constraints ensure, that the trajectory passes through the facial recess and maintains a safe distance to critical middle ear and intra-cochlear structures. In parallel, the soft constraints for the inner ear access aim to minimize the angle of cochlear approach, minimize the risk of scala deviation and maximize the distance to critical intra-cochlear structures. This approach of trajectory planning is defined as a multi-criteria constraint optimization problem. The solution space was evaluated to derive possible implications for tunnel-based robotic access to the inner ear.

MATERIALS AND METHODS

Adaption of the OpenEar Library

The planning analysis conducted in this study was based on the OpenEar library consisting of the data set of eight human temporal bones (five right side, three left side) (32). Each dataset is based on a combination of multimodal imaging including cone beam computed tomography and micro-slicing with the corresponding segmentation of inner ear compartments, middle ear bones, tympanic membrane, relevant nerve structures, blood vessels, and the temporal bone (33). For this study, the segmentation of the dataset was extended to include relevant inner ear structures that were discernible by the micro-slicing reconstruction method, these include the RWM, osseous spiral lamina, inferior cochlear vein, and the cochlear aqueduct. Due to the limited image quality available, the osseous spiral lamina, the basilar membrane, and the secondary spiral lamina could not be reliably separated during segmentation and were combined in the model of the osseous spiral lamina (15). All segmentations were carried out with 3D Slicer, an open source software platform for medical image informatics, image processing, and three-dimensional visualization (http://www.slicer.org) (34). The final output was a library consisting of eight datasets with the aforementioned extension made to the model (**Figure 1**). For comparability, the naming of the cases in this work was adopted from the OpenEar library.

Hard Constraints for Trajectory Planning

An approach was developed to automatically plan a trajectory to the RW that fulfills anatomical safety margin constraints and aims to optimize the soft constraints for inner ear access. For safety related considerations, hard constraints were introduced to maintain a safe predefined distance to all structures at risk (**Table 1**). The anatomical safety margins were adopted from the otological planning software OTOPLAN (Version 1.5.0, CASCINATION AG, Switzerland). These are to be understood as the minimum accepted distances from the anatomy at risk to the surgical drill. In this study, the tool set of the HEARO robotic system (CASCINATION AG, Switzerland) consisting of the HEARO Step Drill Bit 1.8 mm for middle ear access (∅ 1.8–2.5 mm) and the HEARO Diamond Burr for inner ear access (∅ 1.0 mm) were used to calculate the safety margins. For this particular robotic system, the safety margins are fulfilled if the tool has a minimum distance of 0.4 mm to the facial nerve and 0.3 mm to the chorda tympani and all other structures at risk (**Table 1**) (35, 36). There are no reference values available for safe distance to intra-cochlear structures. In this work, the safety margin to intra-cochlear structures was constrained to 0.2 mm. This value was concluded to be adequate based on the current reported accuracy of the robotic system (0.15 mm, $SD = 0.08$) (2). However, an additional soft constraint as introduced later, aimed to increase this intra-cochlear safety margin.

Target Region and Candidate Trajectories

The RW approach is considered the best approach for minimally traumatic access to the scala tympani. Therefore, the lateral RWM area was defined as the potential target region for trajectory planning. In a first step, the RWM target region was sampled and constrained by potential target positions that have a sufficient distance to all relevant intra-cochlear structures. A distance of 0.7 mm was determined based on the diameter of the burr (∅ 1.0 mm) together with the constrained distance of 0.2 mm to the structures. Therefore, all target positions on the RWM not fulfilling a minimum distance of 0.7 mm to the closest intra-cochlear structure were excluded from the target region. In a further step, all possible and reasonable trajectory orientations for the remaining target region were generated in a uniformly sampled volume. These trajectories were further decimated by the trajectories that did not meet the hard constraints for access to the middle ear and inner ear (**Table 1**). The remaining trajectories were designated as candidate trajectories and considered for further investigation.

Soft Constraints for Inner ear Access

The following soft constraints were introduced based on the current knowledge of the anatomy, experience, and findings in planning and execution of robotic inner ear access (**Figure 2**).

Minimum Angle Between the Trajectory and the Scala Tympani

The angle of cochlear approach φ is the minimum angle in three-dimensional space between the candidate trajectory and the linear approximation of the scala

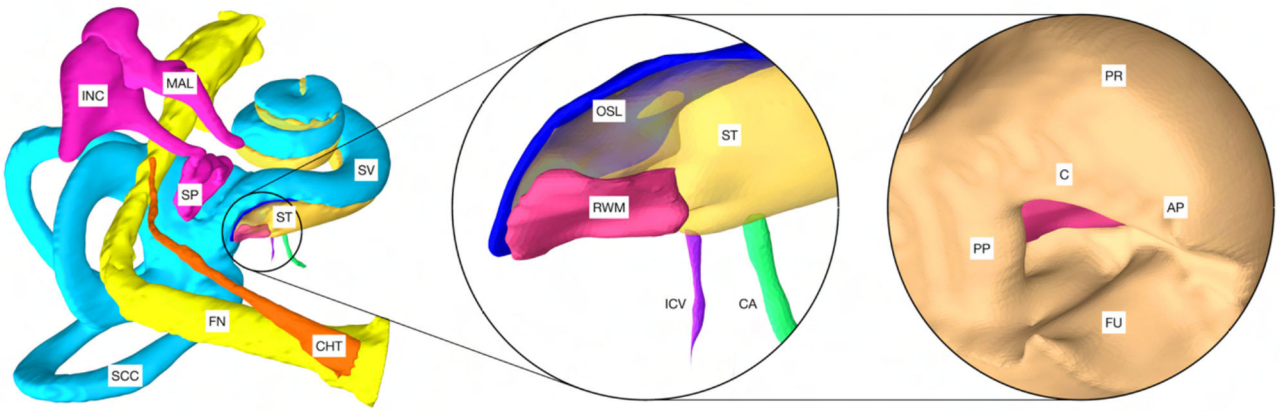

FIGURE 1 | Model of a cochlea of the right human ear based on the OpenEar dataset. CHT, chorda tympani; FN, facial nerve; SCC, semicircular canals; MAL, malleus; INC, incus; SP, stapes; ST, scala tympani; SV, scala vestibule. The magnification in the center shows the extensions made to the model: RWM, round window membrane; OSL, osseous spiral lamina; ICV, inferior cochlear vein; CA, cochlear aqueduct. Right: PP, posterior pillar; C, canonus; AP, anterior pillar; FU, fustis; PR, promontory. Note: For visualization purposes, the model of the external ear canal (*meatus acusticus externus*) was excluded.

TABLE 1 | Middle ear and inner ear access hard and soft constraints.

Hard constraints	**Access**	**Anatomy**	**Constrained value**	**Priority**
Safety margin	Middle ear	Facial nerve	0.4 mm	-
		Chorda tympani	0.3 mm	
		Incus		
		Malleus		
		Stapes		
		External auditory canal		
	Inner ear	Osseous spiral lamina	0.2 mm	
		Inferior cochlear vein		
		Cochlear aqueduct		
Soft constraints	**Access**	**Anatomy**	**Objective**	**Priority**
Angle of cochlear approach φ	Inner ear	–	Minimize φ	20%
RWM coverage ratio r		Round window membrane	Maximize r	60%
Intra-cochlear distance d		Osseous spiral lamina	Maximize d	20%
		Inferior cochlear vein		
		Cochlear aqueduct		

tympani centerline in the RW periphery (**Figure 2A**). This angle can be further decomposed in the in-plane and the out-plane angle as commonly used in literature to depict deviations from the ideal trajectory in two planes (13, 23).

Maximum RWM Coverage Ratio

The coverage ratio *r* is the maximum ratio between the cross-sectional area of the electrode projected onto the RWM along the candidate trajectory and the electrode cross-sectional area (**Figure 2B**). This soft constraint accounts for the offset of the trajectory from the centerline of the scala tympani and is an indicator of proximity to the RW antero-inferior border, where in most cases the sharp bony crest of the RW (*crista fenestrae cochleae*) is localized. This crest of the RW is a potential obstacle for adequate access to the scala tympani (10, 37, 38) .

Maximum Distance to Critical Intra-Cochlear Structures

The distance *d* is the maximum Euclidean distance from the tool to the closest critical intra-cochlear structure for the candidate trajectory (**Figure 2C**). This allows the hard-constrained minimal safety distance of 0.2 mm to be increased in order to reduce the risk of potential mechanical trauma to intra-cochlear structures, especially considering the accuracy of the robotic system.

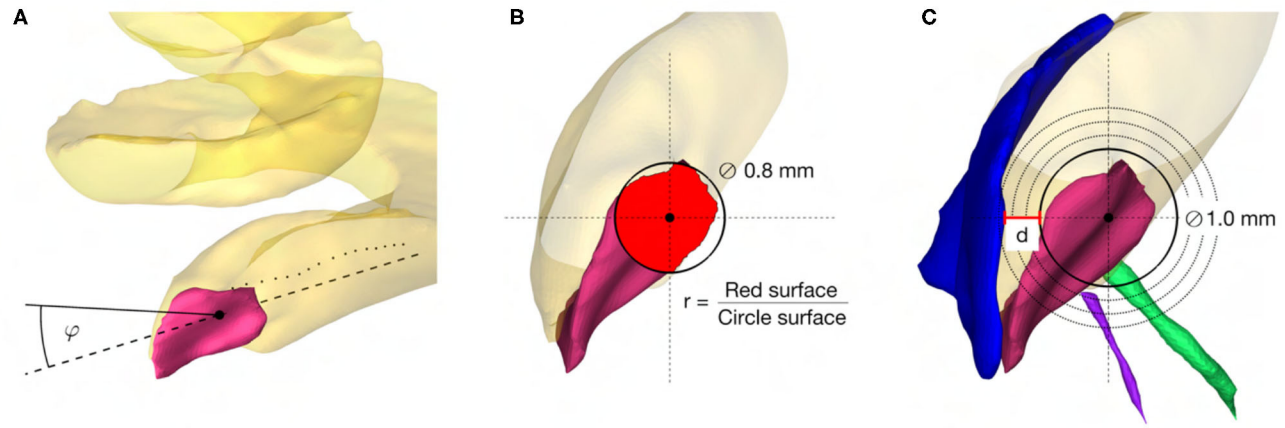

FIGURE 2 | (A) Angle of cochlear approach constraint minimizing the angle φ in three-dimensional space between the linear approximation (– –) of the scala tympani centerline (··) and the candidate trajectory (–). **(B)** RWM coverage ratio constraint maximizing the ratio r between the projection of the electrode (⌀ 0.8mm) on the RWM (red area) and the electrode cross-sectional area. **(C)** Intra-cochlear structure distance constraint maximizing the distance d to the closest intra-cochlear structure, here the osseous spiral lamina.

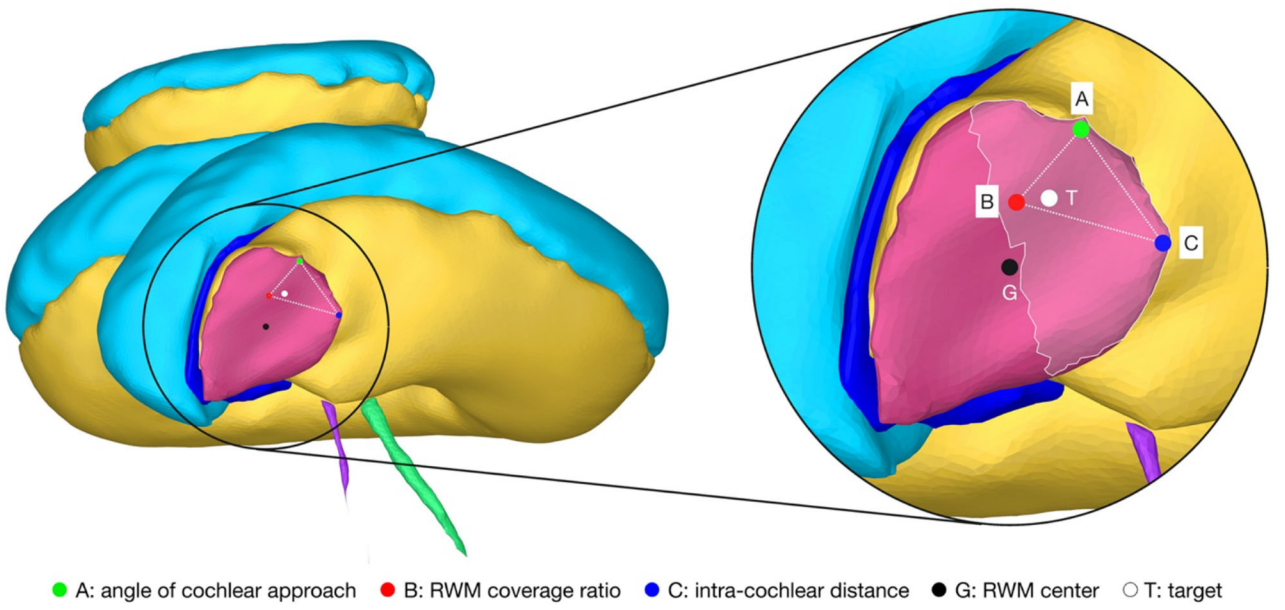

FIGURE 3 | Cochlea of the right ear as seen along the line from the center of the RWM (G) to the apex of the cochlea that is parallel to the cochlear plane. The magnification on the right shows the target region (highlighted area) and the Pareto-optimal target solution space (··) on the RWM. The optimal solution space is spanned by the individual best solutions A, B and C of each soft constraint. T, optimal target position with user-defined priorities; G, geometric center of the RWM.

Target and Trajectory Solution Space

For the introduced hard and soft constraints an optimal solution space of target positions on the RWM with the corresponding trajectory orientation was calculated with the set of candidate trajectories. The optimal target solution space is spanned by the optimal solutions of the three soft constraints, termed the basic solutions (**Figure 3**). All solutions in the target position solution space on the RWM are Pareto-optimal. A Pareto optimum is a state in which it is not possible to improve one soft constraint without at the same time having to worsen another. An optimal trajectory orientation was assigned to each individual target position. In addition to the Pareto optimal solution space, a final trajectory was calculated with the user-defined priorities listed in **Table 1**. The algorithms and the computations were implemented and conducted in MATLAB 2019b using the Parallel Computing Toolbox (39).

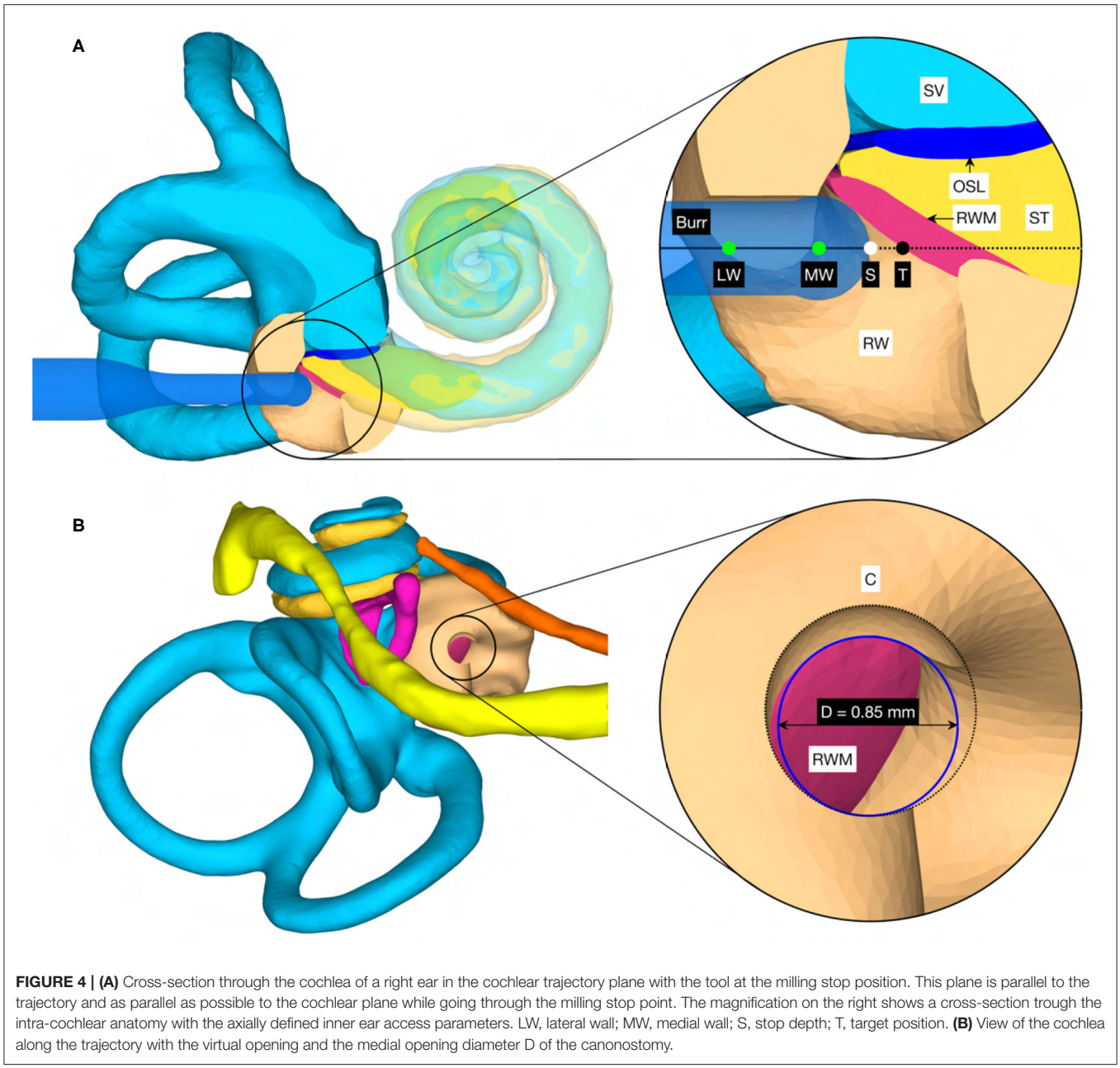

FIGURE 4 | (A) Cross-section through the cochlea of a right ear in the cochlear trajectory plane with the tool at the milling stop position. This plane is parallel to the trajectory and as parallel as possible to the cochlear plane while going through the milling stop point. The magnification on the right shows a cross-section trough the intra-cochlear anatomy with the axially defined inner ear access parameters. LW, lateral wall; MW, medial wall; S, stop depth; T, target position. **(B)** View of the cochlea along the trajectory with the virtual opening and the medial opening diameter D of the canonostomy.

Inner Ear Access Parameterization and Virtual Canonostomy

In addition to the target position and orientation of the trajectory, parameters were also defined axially along the trajectory to define the surgical procedure of the canonostomy in the RW niche. These parameters include the lateral and medial wall of the canonus and the milling stop depth. The lateral wall was defined as the position where the tool first contacts the canonus when approaching laterally along the trajectory, while the medial wall was defined as the posterior border of the RWM. The milling stop depth was defined as the position where the tool first contacts the RWM laterally (**Figure 4A**). According to this definition, the lateral wall and the milling stop depth depend on the geometric shape of the burr. The tip of the milling burr is composed of a diamond-coated hemisphere with a cylindrical extension and has a total cutting length of 4 mm with a diameter of 1 mm. A virtual canonostomy was created through a Boolean subtraction of the milling burr from the canonus, with the milling burr positioned co-axial to the trajectory at the depth of the milling stop depth (**Figure 4B**). The maximum opening diameter of the virtual canonostomy was defined by the maximum circle size that

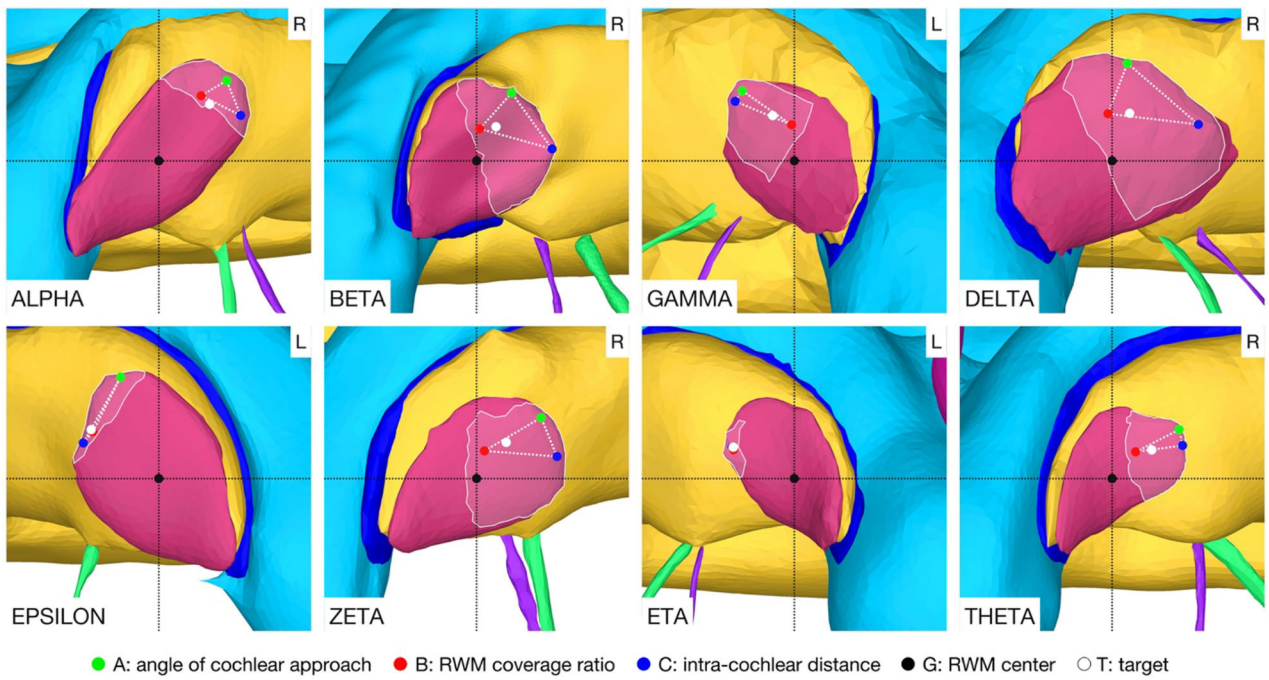

FIGURE 5 | Feasible target region (highlighted area) and the optimal target solution space (··) on the RWM. The optimal solution space is spanned by the individual best solutions A, B, and C of each soft constraint. L, left side cochlea; R, right side cochlea.

fits axially projected into the opening of the medial wall of the canonus.

RESULTS

Target and Trajectory Solution Space

A target and trajectory solution space was successfully calculated for each case based on the introduced middle ear and inner ear access constraints. The feasible target region on the RWM includes all target positions for which a trajectory exists that satisfies the hard constraints. This domain was further confined by the optimal target solution space wherein all solutions are Pareto-optimal with respect to the soft constraints (**Figure 5**). Additionally, a target position was calculated based on the user-defined priorities. In most cases, with the exception of the cases EPSILON and ETA, the target position was close to, and approximately halfway along the line directed from the antero-inferior border to the center of the RWM. It was observed that the best target position for maximizing the angle of cochlear approach constraint was the antero-inferior border of the RWM, while for the intra-cochlear structure distance constraint, this position was more inferior. As expected from the geometric arrangement of the RWM and the trajectory orientation, the best position to maximize the RWM coverage ratio constraint was closer to the center of the RWM. The size of the feasible target region ranged from 0.066 to 1.566 mm^2 with an average area of 0.604 mm^2 ($SD = 0.485$). The cases EPSILON and ETA had a very limited feasible target region and consequently only a local concentrated region for optimal target positions.

In the case THETA, a facial recess trajectory orientation could not be calculated as the facial recess was too narrow and a collision with the facial nerve or the chorda tympani would have been inevitable (**Figure 6**). In all other cases, the trajectory calculated with the user-defined priorities fulfilled all safety margins for access to the middle ear and inner ear (**Figure 7**). The distances to the facial nerve were very close to the constrained safety margin and ranged from 0.405 to 0.503 mm with an average value of 0.443 mm ($SD = 0.034$), excluding the case THETA. In all cases, the shortest distance to the intra-cochlear structures was the distance to the osseous spiral lamina and ranged from 0.251 to 0.516 mm with an average value of 0.350 mm ($SD = 0.092$). In general, with a larger feasible target region, mainly related to a wider facial recess, a higher optimality of the soft constraint values was achieved. In particular, for the cases EPSILON and ETA, which had a limited feasible target region, only a low optimization value was obtained for the angle of cochlear approach φ and the RWM coverage ratio r.

Inner Ear Access Parameterization and Virtual Canonostomy

The virtual surgical procedure of creating an access hole in the canonus based on the aforementioned inner ear access parameterization was performed for all cases (**Figure 8**). It could be observed that a safe distance to the osseous spiral

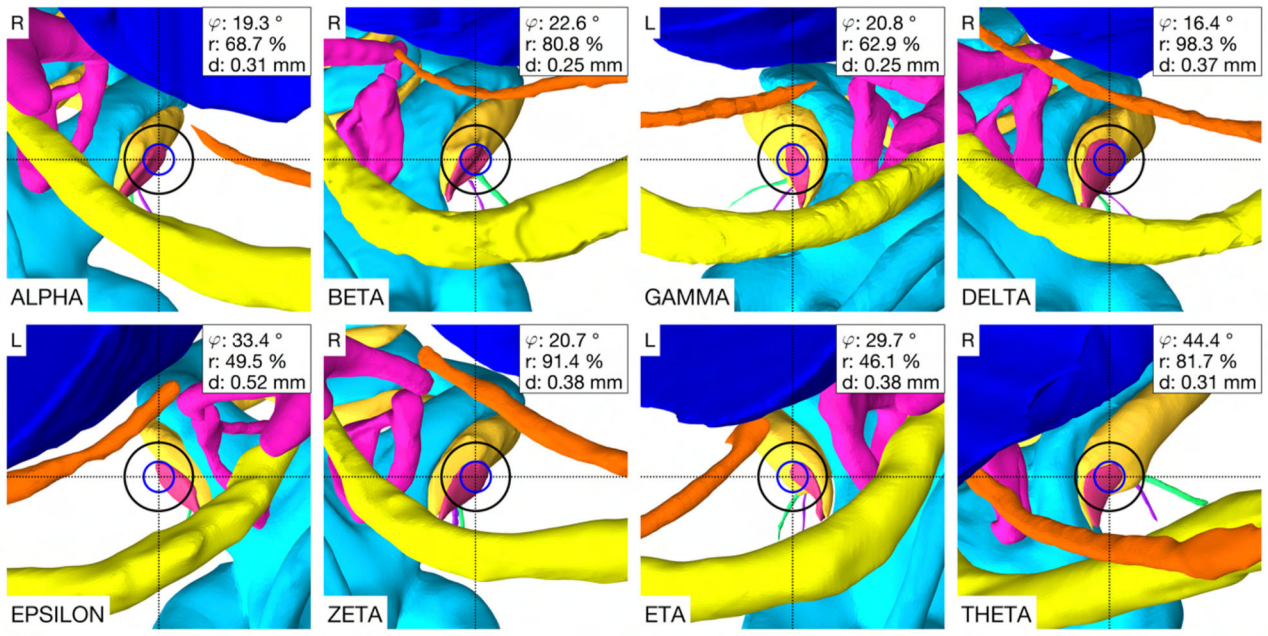

FIGURE 6 | Optimal trajectory with the user-defined priorities. Each case shows the view along the trajectory to the RWM with the corresponding soft constraint optimization value φ, r and d. Blue circle, diameter of the electrode (⌀ 0.8 mm), black circle, tool diameter at the depth of the facial recess (⌀ 1.8 mm), L, left side cochlea; R, right side cochlea.

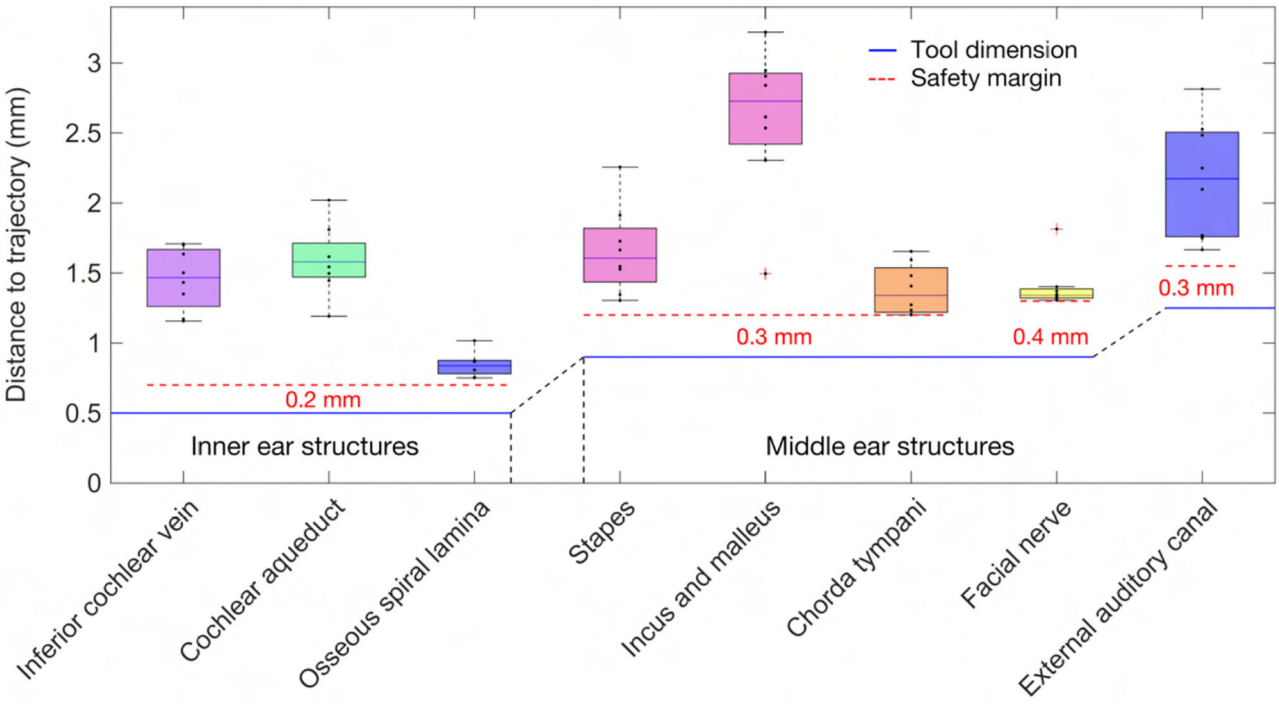

FIGURE 7 | Distance of the anatomy to the trajectory together with the dimension of the tool and the constrained safety margins to the critical middle ear and inner ear structures.

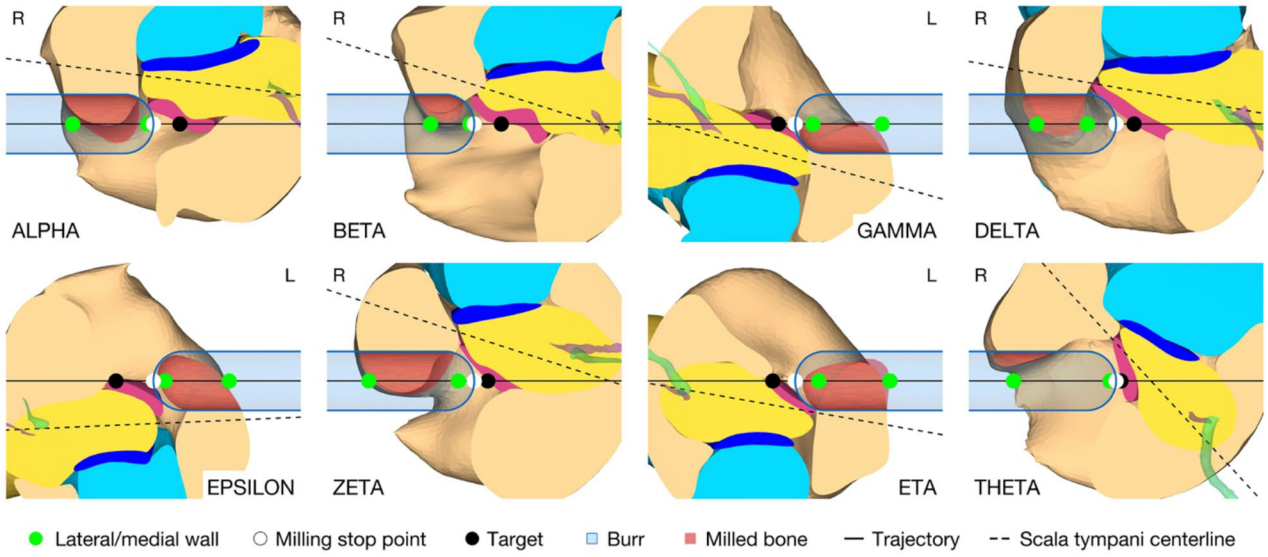

FIGURE 8 | Cross-section through the RW along the cochlear trajectory plane showing the intra-cochlear structures, the burr at its milling stop position, and the surgical parametrization of the canonostomy. L, left side cochlea; R, right side cochlea.

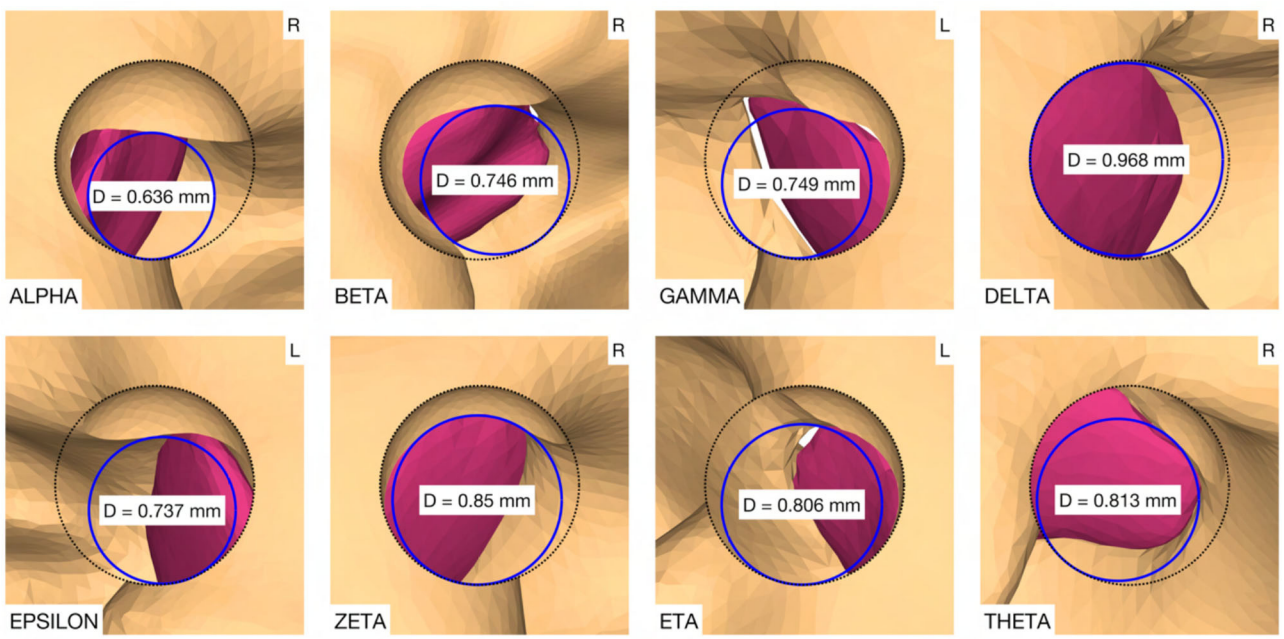

FIGURE 9 | Canonostomy from a trajectory view. D, medial opening diameter of the canonus. L, left side cochlea; R, right side cochlea.

lamina was maintained and that the RWM was not perforated as expected according to the definition of the milling stop depth. Therefore, the intra-cochlear structures were not in contact with the milling burr during the virtual canonostomy. In addition to the angle of cochlear approach, a lateral offset of the trajectory from the scala tympani centerline was observed in most cases. The measured circular opening diameter at the medial wall of the canonus ranged from 0.636 to 0.968 mm with an average value of 0.788 mm ($SD = 0.097$) (**Figure 9**).

DISCUSSION

In conventional cochlear implantation surgery, there is consensus that an electrode insertion vector from postero-superior to antero-inferior to the RWM potentially avoids scala

deviation and preserves the osseous spiral lamina and the basilar membrane (30, 40). In recent robotic cochlear implantation, the target position was placed in the center of the RW and planning of a trajectory through the facial recess with minimal cochlear in- and out plane angles was considered as an optimal insertion trajectory (13, 23). This definition did not take into account the close proximity to intra-cochlear structures during planning due to insufficient clinical imaging modalities and primarily aimed for a reliable electrode insertion within the scala tympani. During image-based clinical planning, intra-cochlear structures cannot be identified and segmented, therefore their position and shape must be estimated based on their local relationship to the RW and the bony cochlear wall, the only consistent landmarks.

This work introduced additional inner ear access constraints for trajectory planning and used high resolution anatomical models to account for the imaging limitations of the clinical approach. The soft constraints were defined based on in-depth knowledge of the anatomy, experience and findings regarding planning and execution of robotic inner ear access and manual electrode insertion. Due to the definition of multiple criteria and the nature of the spatial relationship between the anatomical structures, there was no unique solution for an optimal target position and trajectory orientation. Rather, there was an entire solution space of optimal trajectories that could be explored with the adaption of priorities that affect the individual soft constraints of the inner ear access. The results showed that the size and shape of the feasible target region was highly variable. This could be explained with the high variability of the shape and size of the RW and the spatial relationship between the basal turn and the facial recess (38, 41, 42). The size of the facial recess directly limits the possible orientations of the trajectory and thus the accessibility to the scala tympani. Therefore, cases with a narrow facial recess had either no solution or minimal freedom in target and trajectory optimization, as observed in the cases EPSILON and ETA. This problem could be addressed by using surgical tools with a smaller diameter, for example ∅ 1.4 mm instead of ∅ 1.8 mm at the level of the facial recess. The difficulty here, however, would be the development of electrode guide tubes that could be placed in smaller diameter tunnels, which are mostly needed as insertion aid to avoid kinking in the usually highly aerated mastoid bone (mastoid antrum, mastoid cells; *antrum mastoideum*, *cellulae mastoideae*) (4).

The results of this work showed, that there is a clear tendency that a position between the antero-inferior border and the center of the RWM may prove to be the optimal position for cochlear tunnel based access. This target position would potentially avoid damage to critical inner ear and middle ear structures while providing minimal insertion angles and a sufficient cochlear opening for electrode insertion. In some analyzed cases, the measured diameter of the medial opening of the canonus was slightly smaller than the diameter of most existing implants at the depth of the RW (∅ 0.8 mm). However, it is assumed that the thin layer of remaining bone shell could be easily removed by the surgeon during the opening of the RWM and may also contribute to a better fixation of the electrode in the RW niche. An extremely small or narrow shaped RW with a diameter smaller than the diameter of the cochlear implant array could make a minimally traumatic access difficult because an enlarged RW approach would be required. In addition, the sharp bony crest of the RW could be a potential obstacle for soft insertion of the electrode array. The corresponding trajectory orientation could result in bending of the electrode array at the antero-inferior margin of the RW niche and the bony crest could damage the electrode array during insertion or over time. Additional removal of bone in this area to allow adjustment of the insertion vector and to reduce mechanical resistance during insertion should be avoided, as the close proximity to the hook region could potentially traumatize the cochlea and result in loss of residual hearing (38). Therefore, the implications of the proposed target position and trajectory orientation for minimally traumatic electrode array insertion need to be investigated experimentally. It would also be conceivable that patient-specific access priorities could be introduced in clinics. In patients with profound hearing loss, it would be less important to preserve specific inner ear structures. Planning priorities could be adjusted to focus on depth and placement quality of the electrode, and only in a patient seeking preservation of residual hearing, priorities could be set on the minimally traumatic approach.

The planning concept presented in this work was not based on image data available in routine clinical practice as the current computed tomography technology used in clinics does not provide the necessary image resolution to detect intra-cochlear structures. Consideration must also be given to the fact that the calculation of the entire trajectory solution space is computationally expensive and time consuming, and therefore is not an ideal approach for intra-operative planning. Despite these considerations, the planning concept introduced and the information obtained therewith are helpful and guiding for the planning strategies in future implementations. Current otological planning software is already capable of intra-operatively segmenting the bony anatomy of the RW and modeling the RWM. Moreover, it could be concluded from the results that the calculation of the optimal trajectory solution space can be limited to the antero-inferior region of the RWM. Therefore, it might be possible to already implement planning strategies that allow for potentially less traumatic robotic access to the cochlea. However, the applicability of the planning concept in clinical image-based planning and the efficacy of the corresponding surgical approach for minimally traumatic cochlear access need to be investigated in further studies.

CONCLUSION

Incorporating the introduced hard and soft constraints for the inner ear access during trajectory planning, a tendency could be identified that a position between the antero-inferior border and the center of the RWM could be a favorable target position for tunnel-based cochlear access. The planned trajectories were compatible with the middle ear access, would potentially avoid damage of critical intra-cochlear structures during robotic execution, and would allow implantation with minimal insertion angles and risk of scala deviation. The planning concept presented, as well as the findings obtained therewith, have

implications for planning strategies for tunnel-based robotic surgical procedures to the inner ear that aim for minimally traumatic cochlear access and electrode array implantation.

DATA AVAILABILITY STATEMENT

The raw data supporting the conclusions of this article will be made available by the authors, without undue reservation.

AUTHOR CONTRIBUTIONS

FM created the OpenEar library extension, developed and evaluated the planning concept, and is the primary author of the manuscript. VT, JH, GO'T, and SW contributed with their scientific advice. All authors reviewed the manuscript and approved the submitted version.

FUNDING

This work was supported by the Swiss National Science Foundation SNF (Project 176007).

ACKNOWLEDGMENTS

The authors would like to thank Marco Matulic (CASCINATION AG, Bern, Switzerland), Dr. Masoud Zoka Assadi (MED-EL GmbH, Innsbruck, Austria), and Dr. Daniel Schneider (AOT AG, Basel, Switzerland) for their support and scientific advice.

REFERENCES

1. Bell B, Williamson T, Gerber N, Gavaghan K, Wimmer W, Kompis M, et al. An image-guided robot system for direct cochlear access. *Cochlear Implants Int.* (2014) 15:S11–3. doi: 10.1179/1467010014Z.000000000192
2. Weber S, Gavaghan K, Wimmer W, Williamson T, Gerber N, Anso J, et al. Instrument flight to the inner ear. *Sci Robot.* (2017) 2. doi: 10.1126/scirobotics.aal4916
3. Caversaccio M, Gavaghan K, Wimmer W, Williamson T, Anso J, Mantokoudis G, et al. Robotic cochlear implantation: surgical procedure and first clinical experience. *Acta Otolaryngol.* (2017) 137:447–54. doi: 10.1080/00016489.2017.1278573
4. Caversaccio M, Wimmer W, Anso J, Mantokoudis G, Gerber N, Rathgeb C, et al. Robotic middle ear access for cochlear implantation: First in man. *PLoS ONE.* (2019) 14:e0220543. doi: 10.1371/journal.pone.0220543
5. Schneider D, Stenin I, Anso J, Hermann J, Mueller FG, Braga PB, et al. Robotic cochlear implantation: feasibility of a multiport approach in an ex vivo model. *Eur Arch Otorhinolaryngol.* (2019) 276:1283–9. doi: 10.1007/s00405-019-05318-7
6. Yang GZ, Cambias J, Cleary K, Daimler E, Drake J, Dupont PE, et al. Medical robotics-Regulatory, ethical, and legal considerations for increasing levels of autonomy. *Sci Robot.* (2017) 2. doi: 10.1126/scirobotics.aam8638
7. Proctor B, Bollobas B, Niparko JK. *Anatomy of the round window niche. Ann Otol Rhinol Laryngol.* (1986) 95:444–6. doi: 10.1177/000348948609500502
8. Marchioni D, Alicandri-Ciufelli M, Pothier D, Rubini A, Presutti L. The round window region and contiguous areas: endoscopic anatomy and surgical implications. *Eur Arch Otorhinolaryngol.* (2014) 272:1103–12. doi: 10.1007/s00405-014-2923-8
9. Topsakal V, Kachlik D, Bahşi I, Carlson M, Isaacson B, Broman J, et al. Relevant temporal bone anatomy for robotic cochlear implantation: An updated terminology combined with anatomical and clinical terms. *Transl Res Anat.* (2021) 25:100138. doi: 10.1016/j.tria.2021.100138
10. Franz BK, Clark GM, Bloom DM. Surgical anatomy of the round window with special reference to cochlear implantation. *J Laryngol Otol.* (1987) 101:97–102. doi: 10.1017/S0022215100101343
11. Li PM, Wang H, Northrop C, Merchant SN, Nadol JBJr. Anatomy of the round window and hook region of the cochlea with implications for cochlear implantation and other endocochlear surgical procedures. *Otol Neurotol.* (2007) 28:641–8. doi: 10.1097/mao.0b013e3180577949
12. Adunka OF, Dillon MT, Adunka MC, King ER, Pillsbury HC, Buchman CA. Cochleostomy versus round window insertions: influence on functional outcomes in electric-acoustic stimulation of the auditory system. *Otol Neurotol.* (2014) 35:613–8. doi: 10.1097/MAO.0000000000000269
13. Topsakal V, Matulic M, Assadi MZ, Mertens G, Rompaey VV, Van de Heyning P. Comparison of the surgical techniques and robotic techniques for cochlear implantation in terms of the trajectories toward the inner ear. *J Int Adv Otol.* (2020) 16:3–7. doi: 10.5152/iao.2020.8113
14. Pringle MB, Konieczny KM. Anatomy of the round window region with relation to selection of entry site into the scala tympani. *Laryngoscope.* (2021) 131:E598–604. doi: 10.1002/lary.28738
15. Agrawal S, Schart-Moren N, Liu W, Ladak HM, Rask-Andersen H, Li H. The secondary spiral lamina and its relevance in cochlear implant surgery, in Ups. *J Med Sci.* (2018) 9–18. doi: 10.1080/03009734.2018.1443983
16. Coulson CJ, Reid AP, Proops DW, Brett PN. ENT challenges at the small scale. *Int J Med Robot.* (2007) 3:91–6. doi: 10.1002/rcs.132
17. Khater A, El-Anwar MW. Methods of Hearing Preservation during Cochlear Implantation. *Int Arch Otorhinolaryngol.* (2017) 21:297–301. doi: 10.1055/s-0036-1585094
18. Brett PN, Taylor RP, Proops D, Coulson C, Reid A, Griffiths MV. A surgical robot for cochleostomy. *Annu Int Conf IEEE Eng Med Biol Soc.* (2007) 2007:1229–32. doi: 10.1109/IEMBS.2007.4352519
19. Coulson CJ, Taylor RP, Reid AP, Griffiths MV, Proops DW, Brett PN. An autonomous surgical robot for drilling a cochleostomy: preliminary porcine trial. *Clin Otolaryngol.* (2008) 33:343–7. doi: 10.1111/j.1749-4486.2008.01703.x
20. Du X, Assadi MZ, Jowitt F, Brett PN, Henshaw S, Dalton J, et al. Robustness analysis of a smart surgical drill for cochleostomy. *Int J Med Robot.* (2013) 9:119–26. doi: 10.1002/rcs.1462
21. Brett P, Du X, Zoka-Assadi M, Coulson C, Reid A, Proops D. Feasibility study of a hand guided robotic drill for cochleostomy. *Biomed Res Int.* (2014) 2014:656325. doi: 10.1155/2014/656325
22. Williamson T, Du X, Bell B, Coulson C, Caversaccio M, Proops D, et al. Mechatronic feasibility of minimally invasive, atraumatic cochleostomy. *Biomed Res Int.* (2014) 2014:181624. doi: 10.1155/2014/181624
23. Wimmer W, Venail F, Williamson T, Akkari M, Gerber N, Weber S, et al. Semiautomatic cochleostomy target and insertion trajectory planning for minimally invasive cochlear implantation. *Biomed Res Int.* (2014) 2014:596498. doi: 10.1155/2014/596498
24. Du X, Brett PN, Zhang Y, Begg P, Mitchell-Innes A, Coulson C, et al. A hand-guided robotic drill for cochleostomy on human cadavers. *Robot Surg.* (2018) 5:13–8. doi: 10.2147/RSRR.S142562
25. Assadi MZ, Du X, Dalton J, Henshaw S, Coulson CJ, Reid AP, et al. Comparison on intracochlear disturbances between drilling a manual and robotic cochleostomy. *Proc Inst Mech Eng H.* (2013) 227:1002–8. doi: 10.1177/0954411913488507
26. Coulson CJ, Assadi MZ, Taylor RP, Du X, Brett PN, Reid AP, et al. A smart micro-drill for cochleostomy formation: a comparison of cochlear disturbances with manual drilling and a human trial. *Cochlear Implants Int.* (2013) 14:98–106. doi: 10.1179/1754762811Y.0000000018
27. Lehnhardt E. [Intracochlear placement of cochlear implant electrodes in soft surgery technique]. *HNO.* (1993) 41:356–9.
28. Meshik X, Holden TA, Chole RA, Hullar TE. Optimal cochlear implant insertion vectors. *Otol Neurotol.* (2010) 31:58–63. doi: 10.1097/MAO.0b013e3181b76bb8

29. Avci E, Nauwelaers T, Lenarz T, Hamacher V, Kral A. Variations in microanatomy of the human cochlea. *J Comp Neurol.* (2014) 522:3245–61. doi: 10.1002/cne.23594
30. Luers JC, Huttenbrink KB, Beutner D. Surgical anatomy of the round window-Implications for cochlear implantation. *Clin Otolaryngol.* (2018) 43:417–24. doi: 10.1111/coa.13048
31. Rau TS, Kreul D, Lexow J, Hugl S, Zuniga MG, Lenarz T, et al. Characterizing the size of the target region for atraumatic opening of the cochlea through the facial recess. *Comput Med Imaging Graph.* (2019) 77:101655. doi: 10.1016/j.compmedimag.2019.101655
32. *Sieber DM,* Erfurt P, John S, Santos GRD, Schurzig D, Sorensen MS, et al. The OpenEar library of 3D models of the human temporal bone based on computed tomography and micro-slicing. *Zenodo.* 6 (2018) doi: 10.5281/zenodo.1473724
33. Sieber D, Erfurt P, John S, Santos GRD, Schurzig D, Sorensen MS, Lenarz T. The OpenEar library of 3D models of the human temporal bone based on computed tomography and micro-slicing. *Sci Data*. (2019) 6:180297. doi: 10.1038/sdata.2018.297
34. Fedorov A, Beichel R, Kalpathy-Cramer J, Finet J, Fillion-Robin JC, Pujol S, et al. 3D Slicer as an image computing platform for the Quantitative Imaging Network. *Magn Reson Imaging.* (2012) 30:1323–41. doi: 10.1016/j.mri.2012.05.001
35. Bell B, Gerber N, Williamson T, Gavaghan K, Wimmer W, Caversaccio M, et al. In vitro accuracy evaluation of image-guided robot system for direct cochlear access. *Otol Neurotol.* (2013) 34:1284–90. doi: 10.1097/MAO.0b013e318295 61b6
36. Williamson T, Gavaghan K, Gerber N, Weder S, Anschuetz L, Wagner F, et al. Population statistics approach for safety assessment in robotic cochlear implantation. *Otol Neurotol.* (2017) 38:759–64. doi: 10.1097/MAO.0000000000001357
37. Angeli RD, Lavinsky J, Setogutti ET, Lavinsky L. The crista fenestra and its impact on the surgical approach to the scala tympani during cochlear implantation. *Audiol Neurootol.* (2017) 22:50–5. doi: 10.1159/000471840
38. Mehanna AM, Abdelnaby MM, Eid M. The anatomy and anatomical variations of the round window prechamber and their implications on cochlear implantation: an anatomical, imaging, surgical study. *Int Arch.* (2020) 24:e288–98. doi: 10.1055/s-0039-1698783
39. *MATLAB version 9.7.0.1296695 (R2019b) Update 4*. The Mathworks, Inc.
40. Badr A, Shabana Y, Mokbel K, Elsharabasy A, Ghonim M, Sanna M. Atraumatic Scala Tympani Cochleostomy; Resolution of the Dilemma. *J Int Adv Otol.* (2018) 14:190–6. doi: 10.5152/iao.2018.4974
41. Atturo F, Barbara M, Rask-Andersen H. Is the human round window really round? An anatomic study with surgical implications. *Otol Neurotol.* (2014) 35:1354–60. doi: 10.1097/MAO.0000000000000332
42. Jain S, Gaurkar S, Deshmukh PT, Khatri M, Kalambe S, Lakhotia P, et al. Applied anatomy of round window and adjacent structures of tympanum related to cochlear implantation. *Braz J Otorhinolaryngol.* (2019) 85:435–46. doi: 10.1016/j.bjorl.2018.03.009

Conflict of Interest: SW is cofounder, shareholder, and chief executive officer of CASCINATION AG (Bern, Switzerland), a spin-off company from our university that commercializes the robotic cochlear implantation technology.

The remaining authors declare that the research was conducted in the absence of any commercial or financial relationships that could be construed as a potential conflict of interest.

Publisher's Note: All claims expressed in this article are solely those of the authors and do not necessarily represent those of their affiliated organizations, or those of the publisher, the editors and the reviewers. Any product that may be evaluated in this article, or claim that may be made by its manufacturer, is not guaranteed or endorsed by the publisher.

frontiers in Neurology

CLINICAL TRIAL
published: 21 March 2022
doi: 10.3389/fneur.2022.804507

First Study in Men Evaluating a Surgical Robotic Tool Providing Autonomous Inner Ear Access for Cochlear Implantation

Vedat Topsakal[1], Emilie Heuninck[1], Marco Matulic[2], Ahmet M. Tekin[1,3], Griet Mertens[4], Vincent Van Rompaey[4], Pablo Galeazzi[5], Masoud Zoka-Assadi[5] and Paul van de Heyning[4]*

[1] Department of Otorhinolaryngology Head and Neck Surgery, University Hospital UZ Brussel, Vrije Universiteit Brussel, Brussels, Belgium, [2] CASCINATION AG, Bern, Switzerland, [3] Department of Otorhinolaryngology, Klinikum Bad Salzungen, Bad Salzungen, Germany, [4] Department of Otorhinolaryngology, Head and Neck Surgery, Department of Translational Neurosciences, Faculty of Medicine and Health Sciences, Antwerp University Hospital, University of Antwerp, Antwerp, Belgium, [5] MED-EL Medical Electronics, Innsbruck, Austria

OPEN ACCESS

Edited by:
Louis Murray Hofmeyr, Stellenbosch University, South Africa

Reviewed by:
Hong Ju Park, University of Ulsan, South Korea
AB Zulkiflee, University Malaya Medical Centre, Malaysia

***Correspondence:**
Vedat Topsakal
Vedat.Topsakal@uzbrussel.be

Specialty section:
This article was submitted to Neuro-Otology, a section of the journal Frontiers in Neurology

Received: *29 October 2021*
Accepted: *10 February 2022*
Published: *21 March 2022*

Citation:
Topsakal V, Heuninck E, Matulic M, Tekin AM, Mertens G, Van Rompaey V, Galeazzi P, Zoka-Assadi M and van de Heyning P (2022) First Study in Men Evaluating a Surgical Robotic Tool Providing Autonomous Inner Ear Access for Cochlear Implantation. Front. Neurol. 13:804507. doi: 10.3389/fneur.2022.804507

Image-guided and robot-assisted surgeries have found their applications in skullbase surgery. Technological improvements in terms of accuracy also opened new opportunities for robotically-assisted cochlear implantation surgery (RACIS). The HEARO® robotic system is an otological next-generation surgical robot to assist the surgeon. It first provides software-defined spatial boundaries for orientation and reference information to anatomical structures during otological and neurosurgical procedures. Second, it executes a preplanned drill trajectory through the temporal bone. Here, we report how safe the HEARO procedure can provide an autonomous minimally invasive inner ear access and the efficiency of this access to subsequently insert the electrode array during cochlear implantation. In 22 out of 25 included patients, the surgeon was able to complete the HEARO® procedure. The dedicated planning software (OTOPLAN®) allowed the surgeon to reconstruct a three-dimensional representation of all the relevant anatomical structures, designate the target on the cochlea, i.e., the round window, and plan the safest trajectory to reach it. This trajectory accommodated the safety distance to the critical structures while minimizing the insertion angles. A minimal distance of 0.4 and 0.3 mm was planned to facial nerve and chorda tympani, respectively. Intraoperative cone-beam CT supported safe passage for the 22 HEARO® procedures. The intraoperative accuracy analysis reported the following mean errors: 0.182 mm to target, 0.117 mm to facial nerve, and 0.107 mm to chorda tympani. This study demonstrates that microsurgical robotic technology can be used in different anatomical variations, even including a case of inner ear anomalies, with the geometrically correct keyhole to access to the inner ear. Future perspectives in RACIS may focus on improving intraoperative imaging, automated segmentation and trajectory, robotic insertion with controlled speed, and haptic feedback. This study [Experimental Antwerp robotic research otological surgery (EAR2OS) and Antwerp Robotic cochlear

implantation (25 refers to 25 cases) (ARCI25)] was registered at clinicalTrials.gov under identifier NCT03746613 and NCT04102215.

Clinical Trial Registration: https://www.clinicaltrials.gov, Identifier: NCT04102215.

Keywords: sensorineural hearing loss (SNHL), cochlear implantation, image-guided surgery, robotically-assisted cochlear implantation surgery, HEARO procedure

INTRODUCTION

Since the introduction of direct electrical stimulation of the human auditory system more than 60 years ago, cochlear implants (CIs) are now widely regarded as one of the most successful neural prostheses in the modern world of otology (1). Thanks to the advances made in the field of biomedical engineering, the implants that are on the market today are able to bypass the damaged sensory hair cells in the cochlea of patients with severe-to-profound sensorineural hearing loss (SNHL). By exciting subpopulations of the auditory nerve directly with electrical pulses, CIs have restored hearing in more than 600,000 patients (2)[1] The CI indication field is expected to expand significantly together with the growing and aging world population. Since an increased number of studies have showed a link between hearing loss and cognitive decline (3), hearing restoration will become increasingly important for people's health and well-being (4, 5). Moreover, the CI market is driven by an established history of successful technological innovation. Most innovations related to the reliability of the device (6), the design of the implant and electrode array (7), the miniaturized digital processing chips, and the speech coding strategies (8). Less research and, therefore, fewer modifications were made on the side of the surgical implantation techniques. In 1976, House first described the essential surgical steps for CI, including opening the skin flap, preparing the subperiosteal pocket, drilling the mastoidectomy and the facial recess approach (also called posterior tympanotomy), opening the scala tympani, inserting the electrode array, and fixating the implant (9). Until today, the facial recess approach is considered the golden standard, with a consistent rate of <1% of facial nerve (FN) injury. These cases most frequently are partial weaknesses of short duration or delayed-onset pareses, which resolve over time. In the past, alternative techniques to the facial recess approach have been suggested, such as the Veria (10), the suprameatal (11), and the pericanal approach (12). Although these approaches will reduce drilling near the FN, they have their own set of disadvantages such as difficult and traumatic insertion angles for the array, perforation of the tympanic membrane, and postoperative infection (13). Most subsequent innovations were concentrated on techniques to approach the scala tympani (14), adjusted techniques for the (partially) ossified cochlea (15) or dysplasia (16), techniques for hearing and structure preservation (17), intraoperative guiding recordings (18), and the use of corticosteroids (19).

The development of robotically-assisted cochlear implantation surgery (RACIS), therefore, has been evaluated in preclinical studies in the last decade and Labadie et al. succeeded in a clinical study for the first time (20–22). A new milestone was reached when Caversaccio et al. achieved the facial recess approach using the self-developed OtoBot with its own navigation (23). Robotic-assisted techniques have found their way to otological and neurosurgical procedures, which offer new possibilities for minimally invasive keyhole CI surgery. These techniques enable a tool position and orientation based on image data and virtual anatomical models to be calculated and visualized by the surgeon. Stereotactic navigation or the use of an image-based template was initially investigated in the context of CI surgery with the premise of replacing the traditional mastoidectomy in favor of a small tunnel drilled in a predetermined location with the aid of a navigation system (24, 25). In these early studies, researchers hypothesized that high navigation accuracies (tool positioning), typically <0.5 mm (26), were necessary to safely preserve critical anatomical structures [FN, chorda tympani (ChT), and ossicles]. Probably to adequately target specific areas of the cochlea [round window (RW)] for electrode insertion, even a higher accuracy is necessary. Ultimately, stereotaxy alone was unable to achieve sufficient control of the tool position relative to anatomical locations due to insufficient accuracy of the navigation system itself and lack of a mechanical tool positioning method to overcome the limitations of human dexterity. Further research sought to develop the use of mechanical positioning devices such as patient-specific templates (27, 28) and robotic manipulators (29, 30). Each of the previous designs possessed insufficient accuracy; thus, no stereotactic aid has been routinely used in otological surgery.

The OtoBot robotic system was developed to achieve the goal of a tunnel-based direct robotic middle ear access (31). The feasibility of the robotic middle ear access through the facial recess was successfully demonstrated in 6 patients using the OtoBot system at Insel Hospital, Bern in Switzerland (ClinicalTrials.gov Identifier: NCT02641795). However, the surgeon created the inner ear access manually through the ear canal after lifting the tympanomeatal flap. The electrode array insertion was also performed manually into the cochlea through cochleostomy (31). When middle ear access is not perfectly aligned with inner ear access, it is surgically very challenging to insert a flexible array, since there is little space for manipulations. Aligned in this sense means literally the continuation of the inner ear access in the same line as the middle ear access. Therefore, the next phase of the development of robotic workflow focused on the robotic inner ear access

[1] http://www.earfoundation.org.uk/files/download/1221

thought the already gained keyhole access through mastoid. This step also implies a significant contribution toward structure and hearing preservation. Although this is a different aim and involves also a biological factor that cannot be controlled, robotic approaches aim to control the reduction of mechanical and noise-induced trauma and rupture of the RW membrane. Future robotic insertion should aim to avoid intracochlear pressure disturbances causing damage and possibly hearing deterioration.

The current RACIS given by the HEARO procedure also meets the demand for more accuracy and provides a new robotic inner ear diamond burr that is an equivalent of conventional microdrills (30–32). For the middle ear access, a 1.8-mm drill needs to pass through the facial recess that has an average size of 2.54 ± 0.5 mm (23), which is already very demanding for a systems accuracy in terms of safety. In inner ear access, there is even less room for inaccuracy because the 1.0 mm diameter diamond burr needs to be rather perfectly aligned with the RW membrane with a crucial diameter of 1.31 ± 0.31 mm (33). RACIS needs to provide even more accuracy in terms of successful insertion in the scala tympani aligned with the basilar membrane (34, 37).

The main objectives of this first-in-man clinical trial using the HEARO were:

- To evaluate the intraoperative accuracy of robotic middle ear and inner ear access with regard to the distance to critical anatomical structures (such as the ChT and FN) and the designated target (i.e., opening the bony overhang of the round window niche or *canonus* and targeting the center of the round window membrane).
- To evaluate whether full manual insertion of the electrode array could be achieved through the drilled tunnel.

MATERIALS AND METHODS

Study Design

We performed an interventional clinical trial in two stages. First, a pilot study for the feasibility of RACIS including access to the inner ear was completed for the first time in men. This study (EAR2OS) was registered at clinicalTrials.gov under identifier NCT03746613 and the HEARO device exemption number 80M0763 from the Belgium Competent Authority [Federal Agency for Medicines and Health Products (FAMHP)]. The approval of the Antwerp University Hospital ethics committee was granted with number B300201837507. In a second stage, a follow-up pivotal study (ARCI25) was also performed involving the effectiveness of RACIS and registered under identifier NCT04102215. The approval of the Antwerp University Hospital ethics committee was granted with number B300201941457 and the HEARO device exemption 80M0793. Adult (18 years or older) patients, running for cochlear implantation according to local reimbursement and candidacy criteria, were clinically and radiologically screened for eligibility. All the participants gave a written informed consent to the same ear, nose, and throat (ENT) surgeon counseling them and performing all the surgeries (VT). The inclusion criteria comprised adult CI candidates with suitable anatomy opting for a Medical Electronics (MED-EL) device. Patients for instance with previous temporal bone surgery, e.g., radical cavities were excluded. Exclusion criteria consisted of pregnancy, the vulnerability of the patient (not able to consent), and withdrawn or invalid informed consent. Radiological exclusion criteria were defined by a planned trajectory on the routine clinical high-resolution CT (HRCT) scan often using 0.3 mm slice thickness: a distance to FN <0.4 mm and <0.3 mm to ChT were excluded from this study.

HEARO Procedure

The HEARO® robotic system (CASCINATION AG, Bern, Switzerland) is an assistive otological next-generation surgical robot (**Figure 1**). It integrates a set of sensors, actuators, and core functionalities to allow the surgeon to perform image-guided surgery with a robotic arm. The HEARO procedure for CI surgery is described below and comprises three main stages followed by postoperative analyses (**Figure 2**). Today, the current HEARO system is "conformité européenne (CE)" marked for clinical use in adults and requires a minimal planned distance of 0.4 mm to the FN (26). In preoperative analyses of patients, it is possible to estimate the cochlear duct lengths (CDLs) for tailored and complete cochlear coverage for an optimal audiological outcome (36). In this study, patients were inserted with a 28-mm (96%) and a 20-mm (4%) electrode array (MED-EL, Innsbruck, Austria). Both the electrodes have a diameter of 0.8 mm and allow, therefore, passage to middle ear by the 1.8 mm tunnel and access to inner ear by the 1.0 mm diameter diamond burr.

A commercially available mobile cone-beam CT (CBCT) with 0.1 mm spatial resolution (XCAT XL, Xoran Ltd, Ann Arbor, Michigan, USA) acquired radiological images for preoperative planning, checking the partially drilled trajectory, and for postoperatively checking the array placement in the cochlea. Visual inspection of the cochlear entrance site was assured by a conventional microscope for stereoscopic viewing through the ear canal allowing the surgeon to work with both the hands or an endoscope that could view closer to the target, but always occupied one surgical hand. This step may become obsolete in future protocols, but in this study visual inspection served as a safety control. Also, commercially available multichannel endoscopes with a diameter of 1.3 mm (Carl Storz, Denzlingen, Germany) allowed the surgeon for visual inspection, irrigation, and suction through the drilled tunnel when desired.

Preparations and Planning

The patients were prepared for surgery and the head was non-invasively immobilized into a customized head clamp in slight hyperextension of the neck and rotation to the contralateral side. After a retroauricular incision, five fiducial screws (four for image to patient registration and one for patient marker attachment) were placed on the mastoid cortex, as artificial landmarks before the preoperative imaging were required for subsequent navigation. Then, the patient's head was scanned with the mobile CBCT (0.1 mm resolution) and the images were imported to the dedicated planning software (OTOPLAN®, CASCINATION AG, Bern, Switzerland). The surgeon three-dimensionally reconstructs all the relevant anatomical structures

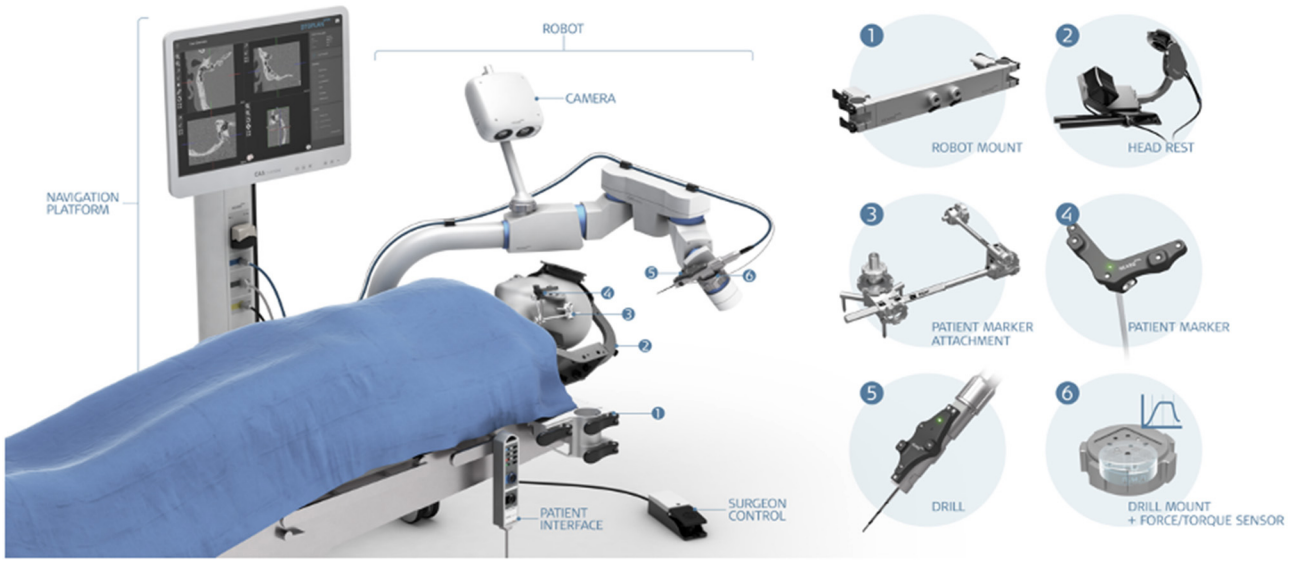

FIGURE 1 | The HEARO® robotic system. **(1)** Robot mount, **(2)** headrest, **(3)** patient marker attachment, **(4)** patient marker, **(5)** drill, and **(6)** drill mount with force/torque sensor.

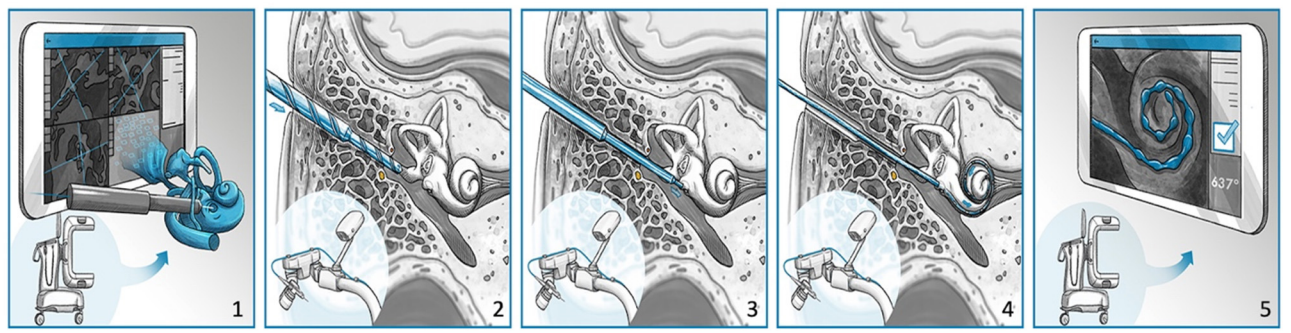

FIGURE 2 | The HEARO procedure for cochlear implantation surgery. **(1)** Scanning and planning, **(2)** performing middle ear access with cutting bur, **(3)** performing inner ear access with diamond bur, **(4)** placement of array through a removable insertion tube, and **(5)** postoperative scanning and quality analysis.

of the FN, the ChT, the ossicles, and the external auditory canal. The surgeon then manually sets the target point at the level of the RW membrane and adjusts the ideal trajectory line based on the patient's specific anatomy and in-plane and out-plane angels, as previously described by Wimmer et al. (34). Sufficient safety distances and individualized inner ear access are optimized. The surgical plan is exported from OTOPLAN to the HEARO. The HEARO software automatically renders, if the planned trajectory is executable within the safety margins to the FN. The surgeon performs a patient-to-image registration to enable the navigation of the robot. Possible planning out of the reach of the robot arm or possible collision with fiducials are signaled to the surgeon by the system.

Performing Robotic Drilling

In this stage, the robotic arm executes the surgical plan. With a custom-made helical step drill of 1.8 mm diameter, the first access is drilled into the middle ear, which is decomposed in three phases:

(i) Drilling from the cortex of mastoid bone until 3 mm before the level of the FN.

(ii) Drilling through the facial recess.

(iii) Drilling mastoid cells further than FN to complete the middle ear access.

After completion of phase (i), a titanium rod is placed in the partially drilled tunnel by the surgeon and intraoperative imaging was performed in every case. The rod enhances the contrast of the drilling tunnel in the image. The image is loaded into the planning software allowing the surgeon to the assessment of the safety margins between the drilling trajectory and the anatomy as well as for the measurement of the drilling accuracy. Upon confirmation of the safe trajectory (not compromising FN), the drilling can be continued through the facial recess at phase

(ii). Here, multipolar FN stimulation would be performed five times at 0.5 mm intervals providing diverse and from navigation independent means to verify the safe distances to the FN. Phase (iii) is usually swiftly performed because it is beyond FN and not near middle ear structures. In some cases, there is also very little bone left here to drill. Throughout cortical drilling toward the middle ear, the robotic drilling is performed in pecking cycles. The drill bit needs to come out of the trajectory for automatic irrigation to clean the helix of the drill bit. It also allows the surgeon to clean the drilled tunnel and check for possible bleeding tendencies. The cleanness of the drill bit is necessary to avoid extensive heat to FN during drilling (26).

Inner Ear Access

After completion of the middle ear access, a 1.0-mm tungsten-carbide diamond burr with fine diamond coating needs to be correctly mounted for milling a canonostomy, which is a hole in the bony overhang of the round window (37). The inner ear access is achieved by combining preoperative and intraoperative parameters. The canonus thickness was predicted preoperatively and milling forces from the six-axis force-torque sensor of the arm (Mini-40, SI-20-1 calibration, ATI, USA) and intraoperative depth of the drill in the trajectory was intraoperatively determined from the navigation of the system. As the milling starts, the surgeon observes and follows the force graph on the robot interface to determine the relative position of the diamond burr in respect of the canonus (38, 39). The tunnel approach for millimetric keyhole surgery limits the visual feedback for the surgeon during the drilling of the canonus. Particularly, the depth of the burr tip cannot be continuously assessed by vision. Therefore, the surgeon has to mainly rely on the information provided by the system graphical user interface (GUI) instead of visual feedback. This situation without surgical view is out of the surgeon's comfort zone. It is important to note that the surgeon can stop the milling at any point and visually inspect the access either through the drilled keyhole exposition with endoscope or with the microscope through the ear canal by lifting the eardrum. An example of an endoscopic view over the partial canonostomy is shown in **Figure 3**. This maneuver of lifting the eardrum is also necessary for electrode insertion later on and is a rather standardized procedure for a trained otologist. After a stop, the system allows it to continue according to surgical plan or to further mill a selectable distance. To avoid damage to the inner structures of the cochlea, drilling cannot be further than the target point. If a surgeon suspects a target point was set wrongly, it is even possible to abort from RACIS and continue manually. **Figure 4** illustrates the inner ear access algorithm of the newest generation RACIS with the HEARO.

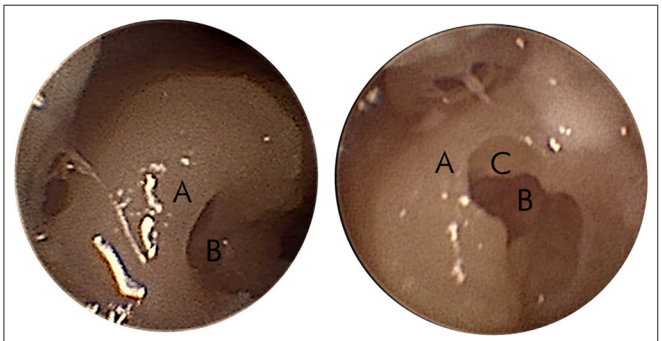

FIGURE 3 | Endoscopic view of the partial canonostomy. An example of the endoscopic view of the canonus **(A)** and the round window (RW) niche **(B)** on the left side. The right side shows a partial canonectomy **(C)** during intraoperative surgical check.

Canonostomy can be divided into four phases depending on the location of the diamond burr.

Phase I: The diamond burr reaches the lateral wall (LW) of the canonus and the force profile starts increasing with a steep gradient: **the touchdown phase**. The depth of the LW of the canonus predicted in the preoperative planning is used as an estimation depth at which the contact should occur. In an ideal case, phase I shall start exactly at the estimated LW point in the preoperative planning. However, the surgeon needs to verify this, so the inner ear algorithm is not starting prematurely. If the force profile rises before or after the estimated LW point, the surgeon can shift the preset LW line. This would automatically shift the medial wall (MW) line to maintain predicted bone thickness of canonus.

Phase II: The diamond burr is fully in the canonus: **the plateau phase**. If the canonus is sufficiently thick and approached rather perpendicularly, as simulated in **Figure 4**, the force profile stabilizes. Perpendicular angles on canonus are likely to have a plateau phase, whereas more tangential angles may not. The latter represent a grazing shot on canonus. There is automated feedback between the milling speed and feedforward rate. When a force threshold of 2.0 N is applied by the system and when this force is reached, the system automatically adjusts the feed rate to reduce the milling force.

Phase III: The diamond burr just reached the MW of canonus**: the breakthrough phase.** As bone in front of the drill becomes very thin, it begins to deform locally resulting in a drop of force. The MW selected in the preoperative planning is used as an estimation at which the breakthrough occurs, but again the surgeon is observing the force graph and must confirm this moment.

Phase IV: The diamond burr is in the RW niche: **the enlarging phase**. The diameter of the CI array used here is 0.8 mm. For a frictionless passage, the minimum required size of the canonostomy is 0.9 mm. Since the diameter of the drill burr is 1 mm, a further 0.3 mm milling after the MW is required to achieve this. The system automatically stops the milling process at the predicted target depth. The surgeon needs to verify, if this predicted target is correct and if an insertion is possible. When a larger canonostomy is desired, the surgeon also needs to verify that there is enough distance between the MW of canonus and the RW membrane in the RW niche for that specific trajectory.

Placing the Array and Postoperative Analyses

The next step is the most critical for the aim of this study, but also for the aim of the surgery: correct placement of the array

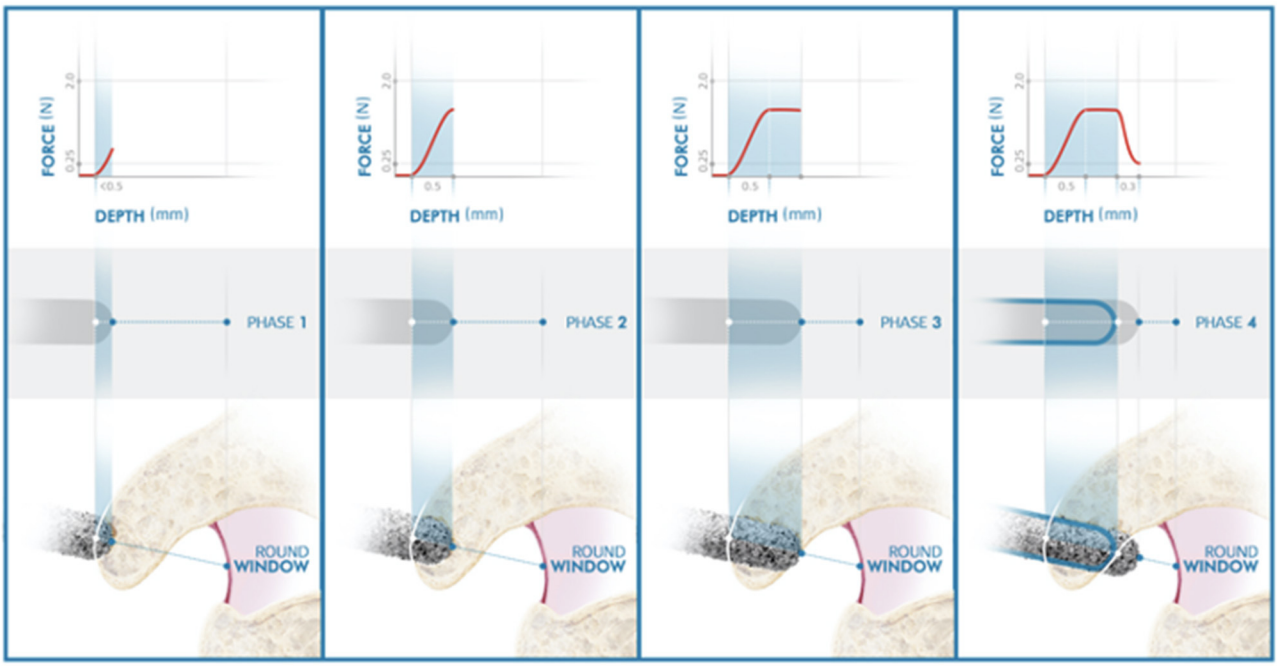

FIGURE 4 | Illustration of the inner ear access of the HEARO. The distance between point lateral wall (LW) and medial wall (MW) represents the bone thickness of the inner ear access point. The red rectangle under the graph also represents the thickness of the bony wall. The white solid line on the graph defines the target point set by the user at the preoperative planning stage. The filled blue line represents the force transients and the exact force at each specific point and is also displayed inside the burr illustration under the graph. The dashed white line represents the estimated point at which the size of 0.9 mm for the opening is achieved.

will determine the success of the surgery for the patient. Since the surgeon now has to take over from the robotic system, a visual exposure through the ear canal becomes indispensable. An insertion tube, consisting of two half-pipes, has to be placed in the drilled trajectory to avoid a false route of the array into aerated mastoid cells in the temporal bone. The insertion tube consists of two pieces, allowing for its removal from the drilled tunnel alongside the array after insertion and leaving the array in place. Furthermore, the insertion tube has been designed with a step to avoid overinsertion and the surgeon decides how far it may be inserted by selecting a target. The two composing pieces are of different lengths, allowing the surgeon to see how the array slides through toward the inner ear. The shorter piece has to be oriented toward the visualizing modality, either an endoscope or a microscope through the ear canal. Before insertion, the surgeon will have to perform classical steps of CI surgery according to local or personal habits. The surgeon will make an implant bed or will use other fixation methods: as such for the PIN implants that require a tight periosteal pocket and two pin holes drilled in the cortex of the temporal bone. The surgeon needs to position his or her hands to manually open the RW membrane, insert the electrode array, and take the insertion tube out the keyhole trajectory in two pieces without manipulating the array. Some standard surgical steps have to be performed as well: such as suturing the skin, sealing the RW area depending on the surgeon's preferences, and sinking the complete array into a cortical bone channel to protect against trauma. All these steps require some training for the surgeon to get acquainted with the view and the handlings.

A postoperative radiological CBCT image after the final stage of the procedure is performed to analyze the electrode's insertion status into the inner ear. Also, the planning software has postoperative analysis features that can even provide a processing strategy for the implant. Usually, electrophysiological tests can also confirm correct placement by registering impedance and currents of the implant to verify its functioning. The ultimate proof of a good placement is of course testing the hearing function and a symmetric smile on the patient.

Surgical follow-up included an overnight stay and evaluation of possible clinical complications in short term, but also in the long term with almost 1-year follow-up for all the participants. The primary aim of this study was to evaluate the effectiveness in terms of how many insertions were possible (and to what depth) with this protocol for RACIS and second to evaluate the safety in terms of the relative risk for FN damage or other complications.

RESULTS

Demographics, Preparations, and Planning

All the eligible patients indicated for CI between December 2018 and July 2020 were checked for eligibility and 32 preoperative HRCT scans were screened. In three cases, the trajectory planning did not allow a safe trajectory because the distance to FN was smaller than 0.4 mm; in two cases, the surgeon

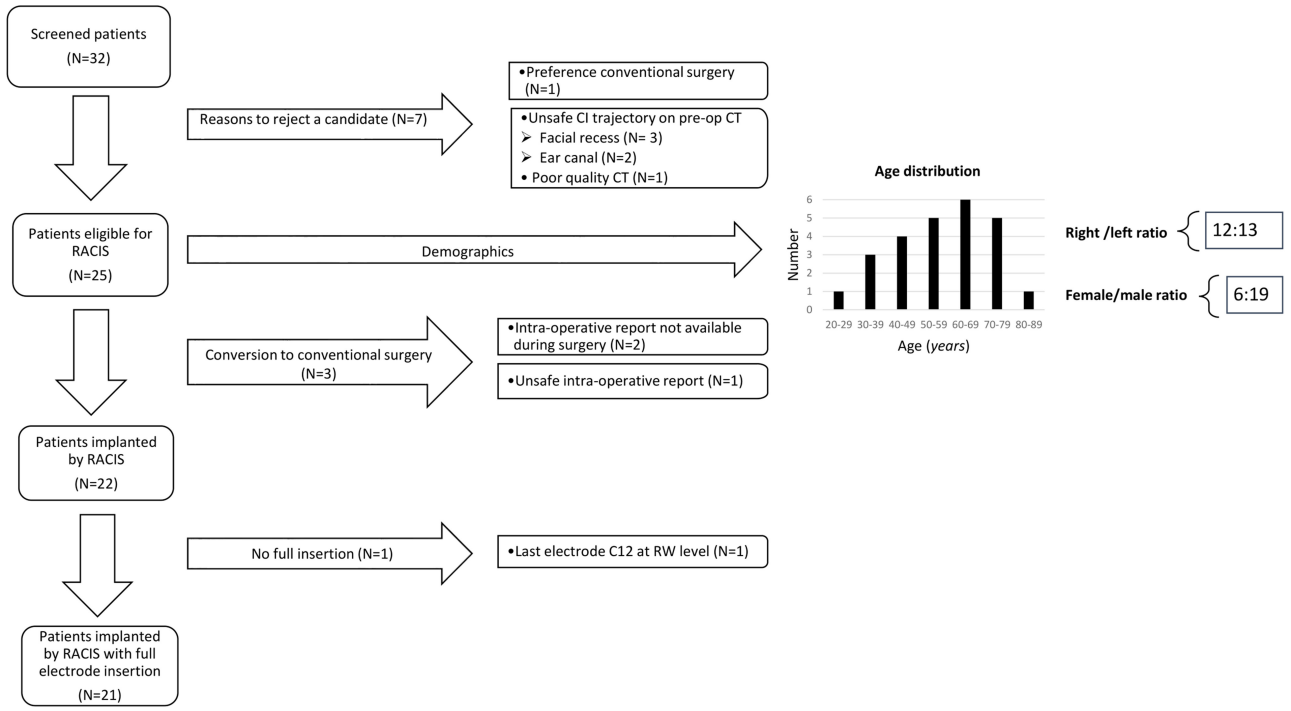

FIGURE 5 | Patient selection and demographics.

decided that the distance to the ear canal is too and in one case, the ChT was not visible due to low soft-tissue contrast in the image. Thus, 26 segmented trajectories were safe according to this study protocol for RACIS. In total, 25 patients gave an informed consent and only one candidate chose to have the surgery in a conventional manner. The same surgeon did all the 25 cases. In 22 cases, the HEARO procedure was completed and in 3 cases, it had to be converted to conventional surgery and every patient indicated for CI received a CI (**Figure 5**). The age of the 25 participants ranged from 28 to 83 years; the study population consisted of 6 women (24%) and 19 men (76%) and the left-right ratio was 12:13. Evaluation of the inner ear anatomy of 21 patients showed normal CT scans. Three patients had ossification anomalies: one patient had a postmeningitis ossification, one patient had far advanced otosclerosis causing also (de)calcifications, and one patient with Cogan syndrome had an intracochlear calcification. One patient had an inborn genetic error and showed an incomplete partition type III (IP-III) anomaly of the inner ear (40). **Table 1** shows a complete overview of the other etiologies of SNHL. When the etiology is marked as unknown, it usually involved progressive SNHL and table reports the onset of the hearing loss, but also the duration of hearing loss.

In the initial EAR2OS trial, it took longer to prepare the surgical field with sterile draping and the incisions may have been more posterior. As more patients underwent the surgery, the scrub nurse and surgeon worked out a faster workflow to drape the patients and the incision was reduced to a standard

FIGURE 6 | Retroauricular incision. Left side is one of the first 3 cases (initial EAR2OS trial) and right side all other more recent cases (ARCI25 trial).

retroauricular incision (**Figure 6**). The software for segmenting the anatomy and planning trajectories worked well as well as the patient-to-image registration. The signaled collisions of the robot or trajectories beyond the reach of the robot arm could be resolved by adjusting the patient and robot positioning or by repositioning the patient marker.

Performing the Drilling

In three cases of the 25, RACIS was converted to conventional surgery because of the safety protocol for middle ear access. Therefore, the inner ear access in these cases was not even performed with assistance of the system. Although in all the cases, the electrophysiological safety checks for the FN respected

TABLE 1 | Subjects' demographics.

Subjects	Etiology	Implantation ear (R, right; L, left)	Age at implantation (years)	Age of hearing loss onset (years)	Inactive electrodes
EAROS_1	Unknown	R	47	40	/
EAROS_2	Unknown	L	61	47	/
EAROS_3	*DFNA9*	R	56	49	/
ARCI25_1	Unknown	R	62	47	/
ARCI25_2	IP-III	R	71	46	/
ARCI25_3	Meningitis	L	56	6	/
ARCI25_4	Sudden SSD	L	47	45	/
ARCI25_5	(Neuro) Sarcoidosis	L	39	34	/
ARCI25_6	Usher	R	58	0	/
ARCI25_7	Sudden deafness	L	83	72	/
ARCI25_8	*DFNA9*	L	53	39	/
ARCI25_9	Unknown	R	42	39	/
ARCI25_10	*OPA1* mutation	R	38	12	/
ARCI25_11	*DFNA9*	R	68	40	/
ARCI25_12	Far advanced otosclerosis	L	56	39	/
ARCI25_13	Unknown	L	40	15	/
ARCI25_14	Unknown	R	76	71	e12
ARCI25_15	Unknown	L	75	12	/
ARCI25_16	Chronic middle ear infection	R	68	62	/
ARCI25_17	Unknown	L	70	50	/
ARCI25_18	Unknown	L	67	62	/
ARCI25_19	Unknown	L	64	53	/
ARCI25_20	Unknown	R	28	0	/
ARCI25_21	MELAS	R	62	50	/
ARCI25_22	Cogan syndrome	L	31	28	/
ARCI25_23	Unknown	R	78	58	/

our safety protocol. The reason of aborting RACIS was the intraoperative CT scan. In two cases, the intraoperative accuracy of the drilling trajectory could not be confirmed by OTOPLAN due to metal artifact or insufficient image contrast resolution and the procedure was converted to conventional. When the intraoperative scan was evaluated later on another computer, it demonstrated accuracy within safe margins for one case. In another case, where the software worked fine, the surgery was converted because intraoperative accuracy predicted a trajectory that was closer than 0.4 mm to FN. Concerning middle ear access, the accuracy of the RACIS procedures has been safe to our protocol in 22 out of 25 cases. In none of the cases the facial monitor gave a warning and there was no postoperative facial weakness or facial palsy (**Table 2**).

The inner ear access was completed in all the 22 cases according to protocol. It proved to have a steep learning curve for the surgeon to follow and rely on the information provided by the system GUI instead of visual feedback. In some cases, with suitable anatomy, the canonostomy performed by RACIS was filmed through the ear canal by a microscope or even an endoscope just to have visual feedback. The manipulations of the eardrum have led to an eardrum perforation in case ARCI25_11, due to the obligatory lifting of it for exposure in RACIS protocol and because of a desire for maximum visual inspection. It was immediately supported with temporalis muscle fascia in underlay and it showed uncomplicated healing in the follow-up. In three cases, a cochleostomy was planned from the beginning of RACIS. The reasons for cochleostomy were ossification of the RW in case ARCI25_3 and ARCI25_12 and better gusher management *via* cochleostomy through the ear canal in case ARCI25_2. This case, with an inner ear malformation, is reported in more details elsewhere by Tekin et al. (40). In case ARCI25_14, the smallest RW membrane measured 0.5 mm (on the screening CT) and an enlarged RW approach was drilled robotically.

Placement of the Array and Postoperative Analyses

The insertion tube proved very efficient in all the 22 cases after inner ear access was created successfully. It proved not only to be useful, but also easy to remove after insertion and removal did not affect the array once inserted. In 3 cases, the insertion of the array was not possible in the first effort. In case ARCI25_22, affected by Cogan syndrome, an intracochlear ossification hindered the first attempt. Full insertion, in this case, was only possible after a so-called Rambo technique (41) by widening the inner ear space with an insertion test device (ITD). In the case of ARCI25_5 and ARCI25_14, correct insertion of all the electrodes was also not possible in the first attempt. There was little space through the ear canal, but, moreover the angle to manipulate the array in a non-traumatic manner was very challenging. It was decided to robotically drill an enlarged RW approach in both the cases. Hereafter, full insertion was achieved for case ARCI25_5, but for case ARCI25_14, the angle of insertion still remained problematic and contact C12 could not be inserted further than where the RW membrane was. This was the only contact that remained outside in the complete series of 22 cases (**Figure 5**). Although the patient had an auditory sensation on this contact, it was switched off. The audiological results are not within the aim of this study and will be reported elsewhere. However, there was not a single electrode damaged in the complete study population including the converted cases. The insertion depth of electrodes is shown in **Figure 7**.

The postoperative CBCT not only allowed evaluation of the angular insertion depth, but confirmed placements in the scala tympani in all the 22 patients. Moreover, no tip fold-over could be identified on imaging. In 18 out of 22 cases, these scans also allowed to visualize the implant house handling in terms of fixation (PIN holes) and arrays embedded in channels. The distance from the keyhole access to the implant house was 35.1 mm (SD 8.4 mm) allowing a comfortable wearing of the processor.

Clinical results were evaluated 1 day, 2 weeks, and 1 month later from surgery. The postoperative follow-up clinically did not show any adverse events. Some cases showed pressure spots because of the head fixation with pressured air pumps. In the first case, the EAR2OS case, this even led to local alopecia that recovered spontaneously after a few months. Case ARCI25_1 suffered from lower back pain at the recovery ward. Although this was a known condition, the length and positioning of RACIS are likely to have provoked this. Again, the lower back pain recovered, but the patient was given additional pain therapy. Case ARCI25_17 suffered from pain on the resolved where the occlusion cuff was placed to register the blood pressure. Again, with an additional painkiller, the patient recovered without permanent injury.

TABLE 2 | Intraoperative accuracy.

Variable	Mean (SD)	Median
Stapes (mm)	0.183 (0.265)	0.078
Incus and malleus (mm)	0.097 (0.68)	0.096
External auditory canal (mm)	0.127 (0.110)	0.091
Facial nerve (mm)	0.117 (0.109)	0.091
Chorda tympani (mm)	0.107 (0.103)	0.082
In-plane (°)	0.239 (0.173)	0.225
Out-plane (°)	0.182 (0.159)	0.146
Entrance (mm)	0.127 (0.067)	0.124
Target (mm)	0.182 (0.124)	0.157

	Insertion Angle [deg] Mean (SD)	Centre Freq. [Hz] Mean (SD in %)
C1	571 (65)	276 (7.6%)
C2	500 (72)	427 (7.0%)
C3	424 (66)	659 (5.8%)
C4	355 (50)	976 (4.2%)
C5	305 (38)	1324 (3.3%)
C6	261 (33)	1758 (2.9%)
C7	219 (32)	2336 (2.8%)
C8	177 (30)	3114 (2.6%)
C9	135 (28)	4250 (2.6%)
C10	95 (27)	5845 (2.6%)
C11	60 (24)	7963 (2.4%)
C12	29 (16)	10715 (1.7%)

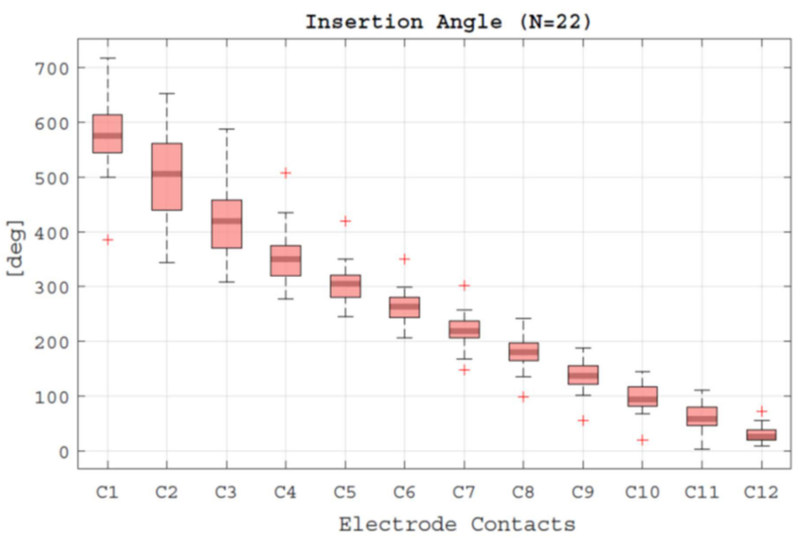

FIGURE 7 | Insertion status.

DISCUSSION

Robotically-assisted cochlear implantation surgery described here enables a surgeon to gain inner ear access in the most standardized fashion. This addresses the main objectives of this first-in-man clinical trial using the HEARO were:

- This system delivers the required intraoperative accuracy of robotic cochlear implantation.
- This system facilitates full manual insertion of the electrode array through the drilled tunnel.

This assistive tool is not designed or it can ever replace a surgeon. It is currently, however, the most autonomous otological tool for CI that meets the true definition of a surgical robot in contrast to many telemanipulators in otology. Parameterization of the anatomy and a radiologically predefined trajectory describing keyhole access with RACIS for CI placement proved safe and efficient in this study. However, this robotic procedure is still highly experimental surgery. Although the device has CE marking, many aspects are susceptible to improvement. The HEARO procedures cover more aspects than can be seen or expected at a first glance. Therefore, it is called a procedure and not a technique. Every aspect in the procedure is an accumulation of knowledge gained by engineered design tested against clinical application and to close the circular learning, it is again evaluated for improvement.

The most essential aspect is safety and pioneering studies have focused on safety and more specifically on not damaging the FN. In 2017, Weber at al. reported the safety of an instrument flight to the "inner ear," whereas this study actually concentrated on accessing the middle ear starting a voyage toward the inner ear (42). In this series of 6 patients, Caversaccio et al. reported safe access to the middle ear (31) without harm to the FN. From these 6 cases, at least three had an incomplete insertion of the CI in the inner ear. This study never specifically aimed at complete insertion, but rather safe passage through the facial recess. Once the hurdle of facial recess was passed, the surgeon took over manually for the inner ear access and insertion. The surgeon had to create access toward the inner ear through the ear canal with little space. In cases with favorable anatomy, this inner ear access (presumably cochleostomy) could be aligned with the drilled middle ear trajectory. Alignment here refers literally to the inner ear access being on the same line as the middle access, which leads to a straight track. However, it is likely that the manual inner ear access is not aligned and poses major challenges to the surgeons to manipulate the electrode from one track to the other track. The CI array now needs to be manipulated in an S-shaped curve changing from the middle ear trajectory to the manually created inner ear track. There is little room and poor exposure for surgical manipulation, but, moreover, it is highly undesirable because electrodes can easily be damaged due to excessive manipulation. In this study, we did not encounter this problem because the aim of this study was also to drill the inner ear access through the keyhole middle ear access. Consequently, by definition, middle ear and inner ear access tracks were automatically in the same line in continuation of each other. Of course, this required even higher accuracy of the system. Aligning inner ear access with a 1.0-mm diamond burr to enter a 0.8-mm array parallel with the basal turn is less forgiving for inaccuracy as for middle ear access where a 1.8-mm drill diameter needs to pass through a facial recess that is 2.5 mm on average. With only three procedures converted to conventional surgery because of intraoperative inaccuracy, the HEARO system makes a strong claim to provide the required accuracy. It is actually accurate enough to safely warrant middle ear access in 22 from 25 screened cases. Noteworthy, in all these 25 cases, the electrophysiological measurements and estimations have met the safety measurements. It needs further study to reveal, if the radiological safety measures with a required distance of 0.4 mm to the FN are too strict or the electrophysiological measurements need to be stricter.

The inner ear access strategy is an important parameter in personalized inner ear access. Soft surgery principles, one of these strategies, have been discussed and popularized, since 1993 for CI (43). Surgeons are able to perform tissue-preserving approaches, thanks to the widespread hybrid electroacoustic stimulation, thus aiming to preserve hearing. In relation to that, the strategy of access the inner ear affects the angles of cochlear approach (ACA). The ACA affects contact or crash factors regardless of stiffness or stiffness in the sidewall of the basal turn (35). Torres et al. report the "presence of optimal scale axis," indicating that the semiautomated robot-based system reduces the margin of error in the placement axis (44). In this study, in which Topsakal et al. compared different posterior tympanotomy modalities, they reported that mathematically calculated approaches for RACIS provide the most optimal ACA in an array and a non-crash trajectory that provides easy access to the surgeon (35). The mean in-plane angle in this study is 6.5° and the out-plane angle in this study is 19.0°. Even though angles close to zero might be in favor for electrode placement, the proximity to the FN prevents this ideal trajectory. In other words, 0° angles would pass through the FN or stapes (34). These predetermined "ideal" trajectories cannot be applied clinically because they would pass through the FN (35). In this study, the ideal trajectory to the basal turn is defined as a straight line. This line should be coaxial with the current central axis of the scala tympani to minimize intracochlear damage.

Nevertheless, using the same drilled middle ear access keyhole for inner ear access, it probably explains why all the patients in this study benefited from full insertions of their CI arrays, except for one. Actually, it would be fair to evaluate accuracy not in millimetric distances that deviate from the set target, but in terms of efficiency. With direct linear inner ear access on the same line as middle ear access, the challenge lies more in overcoming the deviations from target perhaps better stated with inaccuracy rather than accuracy. The more we deviate from target, assuming we placed the target in the most ideal spot, the more difficult it will become to insert either with or without manipulations.

In 20 of the 22 cases, RACIS provided efficient inner ear access allowing swift insertions that did not require surgical manipulations. A device that just pushes with a preset force and speed actually could have performed this procedure. In fact, that device will become yet another development in RACIS. In two cases of the performed 22 cases, the provided inner ear

access did not allow a swift, correct array placement. Surgical manipulations could not recover the submillimetric inaccuracy in alignment and a manual enlarged RW approach was required for satisfactory insertion.

The reason for not being able to insert could also have been that the target was set wrong. In another case, the diameter of the round window itself was just too small.

Nevertheless, the inability to insert swiftly is inevitably related to the planned trajectory and, therefore, within the responsibilities of the surgeon. Although a surgeon may have been trained in RACIS as a technique, he or she will lack the clinical experience to oversee such problems already in the planning phase. Therefore, it is only fair to consider RACIS an experimental surgery until this knowledge is available and can be shared with trained CI surgeons.

An important aspect of the HEARO procedure is that it facilitates individualized surgery. The dedicated software can screen preoperative scans for eligibility for RACIS. Furthermore, based on patients' individual cochlear parameters, it can estimate the frequency and angle allocation for an individualized selection of the electrode array (36). Individualized surgery proved to be important, especially in anatomically challenging cases. Optimizing such millimetric adjustments requires extensive surgical skill and experience in traditional CI surgery (45). In addition, angle and direction estimation may not be accurate, even by experienced surgeons (46). In a cochlea with an IP-III anomaly, especially the standardized angles of insertion proved important for correct placement. Challenges in this type of case, such as liquor cerebrospinal gusher and electrode misplacement in the internal auditory canal, are well-described in the literature (47, 48). We chose to opt for a cochleostomy rather than a RW approach and even for a shorter array (20 mm) for this patient (case ARCI25_2) because of these shared surgical experiences in literature. In addition, ossifications (postmeningitis case ARCI25_3) and bony alterations around RW because of far advanced otosclerosis (ARCI25_12) are always challenging for conventional surgery because the surgeon needs to rely on experience to find the right angle and to access to the inner ear. Actually, the features to customize insertion angles and target depth encourage us to utilize these aspects of RACIS for the benefit of the patient and surgeon. As a result of measuring the cochlea and the CDL in these patients with RACIS, intervening after determining the anatomical variant of the patient and selecting an appropriate short electrode array reduce the possibility of an incorrect electrode placement. In addition, the insertion of ACA is provided accurately and securely with RACIS. RACIS provides us with the optimum insertion angle by using preoperative planning, intraoperative imaging, anatomical landmarks in malformed anatomical structures, and sometimes using data beyond human perception to guarantee safety and accuracy. In this study, RACIS helped for the planning of the most appropriate cochlear access according to the optimum insertion angles in the patient with IP-III anomaly. Successful application of RACIS to a patient with a cochlear anatomical anomaly for the first time in the literature paved the way for the application of RACIS to patients with different anatomical variations in the future.

The HEARO procedure, which was successfully completed in 22 patients in this study, applies important steps in minimally invasive RACIS. This includes possibilities such as planning the trajectory on the cochlea and personalized inner ear access by configuring the relevant anatomical structures three-dimensionally before surgery. Establishing an autonomous system in the surgical field requires different technologies for the same purpose. But yet, robots can never replace surgeons and there is no such application purpose. Robots are auxiliary surgical instruments that increase the quality and reliability of the surgery. The more complex and diverse tasks a robot has to perform, the more difficult it is to optimize it. Besides that, the more autonomous steps a robot can take in a surgical procedure, the more standard the surgical result can become and the margin of error will be minimized. For this reason, robotic developments in the field of otology have always been followed with amazement and interest by otologists, as it is of great importance to establish submillimetric calculated accuracy and precision. As a result, the robot is superior to a surgeon's dexterity, consistency ability, and surgical acuity. Besides that, anatomical differences and anomalies are difficult areas of robotic surgery for programmers and designers. In addition, intraoperative adverse events, such as unexpected bleeding or unwanted patient movement during anesthesia, cannot be handled by robotic surgery alone nor can the full medicolegal responsibility that comes with surgery be attributed to a robotic device.

We argue that with a newly developed system of robotically-assisted and image-guided approach and FN monitoring, this idea of robotic surgery pushed everyone to develop a complete set of new technologies. This is a turning point because now we are able to do this without any complications in inner ear anomaly patients to get to the precision. Besides, it is not a threat to the surgeon at all. It is like an electric bike or an electric boot: if you do not pedal as a cyclist, it is not going to move forward. Surgeons should reach out to this technology to standardize surgical outcomes in anatomical anomaly and potentially difficult cases and to serve their patients.

LIMITATIONS

There is an obvious learning curve for surgeons, engineers, and nurses performing these surgeries. Therefore, the duration of surgeries was not considered relevant. Time loss occurred due to problems with sterile draping, software hick-ups, poor image resolutions, and absence of routine.

CONCLUSION

This study demonstrated the feasibility of RACIS by the HEARO procedure in a clinical study. The accuracy of performing a robotic workflow, more specifically the robotic inner ear access, is reported to meet the current criteria for insertion. In 22 out of 25 patients, a surgeon could complete the HEARO procedure with a full insertion in all the cases, except one where the last electrode was deactivated because it was positioned at the spot of the round window. Future generations of RACIS may focus on improving intraoperative imaging, automated segmentation and trajectory,

robotic insertion with controlled speed, and haptic feedback. In addition, smaller tunnels can be developed for smaller electrodes consequently leading to less invasive surgery and more likelihood of preservation of residual hearing levels.

DATA AVAILABILITY STATEMENT

The raw data supporting the conclusions of this article will be made available by the authors, without undue reservation.

ETHICS STATEMENT

The studies involving human participants were reviewed and approved by Antwerp University Hospital Ethics Committee (EAR2OS: B300201837507 and ARCI25: B300201941457). The patients/participants provided their written informed consent to participate in this study.

AUTHOR CONTRIBUTIONS

VT and PH contributed to the conception and design of the study. VT, EH, and AT wrote the first draft of the manuscript. MM and MZ-A codesigned concept and helped with data collection. PG contributed to the data analysis. VV and GM were involved in inclusion and postoperative evaluation of participants. All the authors contributed to manuscript revision and read and approved the submitted version of the manuscript.

FUNDING

This study was funded by Department of Otorhinolaryngology Head and Neck Surgery, Antwerp University Hospital receives an unrestrictive grant from MED-EL. VT holds a national FWO FKM senior researcher grant number 18B2222N.

REFERENCES

1. Djourno A, Eyries C. Auditory prosthesis by means of a distant electrical stimulation of the sensory nerve with the use of an indwelt coiling. *Presse Med.* (1957) 65:1417.
2. Ear Foundation. *Cochlear Implants Information Sheet*. (2016). Available online at: http://www.earfoundation.org.uk/files/download/1221 (accessed October 29, 2021).
3. Livingston G, Huntley J, Sommerlad A, Ames D, Ballard C, Banerjee S, et al. Dementia prevention, intervention, and care: 2020 report of the lancet commission. *Lancet.* (2020) 396:413–46. doi: 10.1016/S0140-6736(20)30367-6
4. Mertens G, Andries E, Claes AJ, Topsakal V, Van de Heyning P, Van Rompaey V, et al. Cognitive improvement after cochlear implantation in older adults with severe or profound hearing impairment: a prospective, longitudinal, controlled, multicenter study. *Ear Hear.* (2020) 42:606–14. doi: 10.1097/AUD.0000000000000962
5. Claes AJ, Mertens G, Gilles A, Hofkens-Van den Brandt A, Fransen E, Van Rompaey V, et al. The repeatable battery for the assessment of neuropsychological status for hearing impaired individuals (RBANS-H) before and after cochlear implantation: a protocol for a prospective, longitudinal cohort study. *Front Neurosci.* (2016) 10:512. doi: 10.3389/fnins.2016.00512
6. Van de Heyning P, Atlas M, Baumgartner W-D, Caversaccio M, Gavilan J, Godey B. et al. The reliability of hearing implants: report on the type and incidence of cochlear implant failures. *Cochlear Implants Int.* (2020) 21:228–37. doi: 10.1080/14670100.2020.1735678
7. Dhanasingh A. Jolly C. An overview of cochlear implant electrode array designs. *Hear Res.* (2017) 356:93–103. doi: 10.1016/j.heares.2017.10.005
8. Wouters J, McDermott HJ, Francart T. Sound coding in cochlear implants: from electric pulses to hearing. *IEEE Signal Process Mag.* (2015) 32:67–80. doi: 10.1109/MSP.2014.2371671
9. House WF. Cochlear implants. *Ann Otol Rhinol Laryngol.* (1976) 85:1–93. doi: 10.1177/00034894760850S301
10. Kiratzidis T, Arnold W, Iliades T. Veria operation updated. I The transcanal wall cochlear implantation. *ORL J Otorhinolaryngol Relat Spec.* (2002) 64:406–12. doi: 10.1159/000067578
11. Kronenberg J, Migirov L. Dagan T. Suprameatal approach: new surgical approach for cochlear implantation. *J Laryngol Otol.* (2001) 115:283–5. doi: 10.1258/0022215011907451
12. Häusler R. Cochlear implantation without mastoidectomy: the pericanal electrode insertion technique. *Acta Otolaryngol.* (2002) 122:715–9. doi: 10.1080/00016480260349773
13. Bruijnzeel H, Ziylan F, Cattani G, Grolman W. Topsakal V. Retrospective complication rate comparison between surgical techniques in paediatric cochlear implantation. *Clin Otolaryngol.* (2016) 41:666–72. doi: 10.1111/coa.12582
14. Havenith S, Lammers MJW, Tange RA, Trabalzini F, della Volpe A, van der Heijden GJMG, et al. Hearing preservation surgery: cochleostomy or round window approach? a systematic review. *Otol Neurotol.* (2013) 34:667–74. doi: 10.1097/MAO.0b013e318288643e
15. Vashishth A, Fulcheri A, Prasad SC, Bassi M, Rossi G, Caruso A. et al. Cochlear implantation in cochlear ossification: retrospective review of etiologies, surgical considerations, and auditory outcomes. *Otol Neurotol.* (2018) 39:17–28. doi: 10.1097/MAO.0000000000001613
16. Sennaroglu L. Cochlear implantation in inner ear malformations-a review article. *Cochlear Implants Int.* (2010) 11:4–41. doi: 10.1002/cii.416
17. Miranda PC, Sampaio AL, Lopes RA, Ramos Venosa A, de Oliveira CA. Hearing preservation in cochlear implant surgery. *Int J Otolaryngol.* (2014) 2014:468515. doi: 10.1155/2014/468515
18. Dalbert A, Pfiffner F, Hoesli M, Koka K, Veraguth D, Roosli C, et al. Assessment of cochlear function during cochlear implantation by extra- and intracochlear electrocochleography. *Front Neurosci.* (2018) 12:18. doi: 10.3389/fnins.2018.00018
19. Paasche G, Bockel F, Tasche C, Lesinski-Schiedat A, Lenarz T. Changes of postoperative impedances in cochlear implant patients: the short-term effects of modified electrode surfaces and intracochlear corticosteroids. *Otol Neurotol.* (2006) 27:639–47. doi: 10.1097/01.mao.0000227662.88840.61
20. Majdani O, Rau TS, Baron S, Eilers H, Baier C, Heimann B, et al. A robot-guided minimally invasive approach for cochlear implant surgery: preliminary results of a temporal bone study. *Int J Comput Assist Radiol Surg.* (2009) 4:475–86. doi: 10.1007/s11548-009-0360-8
21. Müller S, Kahrs LA, Gaa J, Tauscher S, Kluge M, John S. et al. Workflow assessment as a preclinical development tool: Surgical process models of three techniques for minimally invasive cochlear implantation. *Int J Comput Assist Radiol Surg.* (2019) 14:1389–401. doi: 10.1007/s11548-019-02002-3
22. Labadie RF, Balachandran R, Noble JH, Blachon GS, Mitchell JE, Reda FA, et al. Minimally invasive image-guided cochlear implantation surgery: first report of clinical implementation. *Laryngoscope.* (2014) 124:1915–22. doi: 10.1002/lary.24520
23. Caversaccio M, Gavaghan K, Wimmer W, Williamson T, Ansò J, Mantokoudis G, et al. Robotic cochlear implantation: surgical procedure and first clinical experience. *Acta Otolaryngol.* (2017) 137:447–54. doi: 10.1080/00016489.2017.1278573
24. Labadie RF, Chodhury P, Cetinkaya E, Balachandran R, Haynes DS, Fenlon MR, et al. Minimally invasive, image-guided, facial-recess approach to the middle ear: demonstration of the concept of percutaneous cochlear access *in vitro*. *Otol Neurotol.* (2005) 26:557–62. doi: 10.1097/01.mao.0000178117.61537.5b

25. Schipper J, Klenzner T, Aschendorff A, Arapakis I, Ridder GJ, Laszig R. Navigiert-kontrollierte Kochleostomie. Ist eine Verbesserung der Ergebnisqualität in der Kochleaimplantatchirurgie möglich? [Navigation-controlled cochleostomy Is an improvement in the quality of results for cochlear implant surgery possible?]. *HNO.* (2004) 52:329–35. doi: 10.1007/s00106-004-1057-5
26. Ansó J, Dür C, Apelt M, Venail F, Scheidegger O, Seidel K, et al. Prospective validation of facial nerve monitoring to prevent nerve damage during robotic drilling. *Front Surg.* (2019) 6:58. doi: 10.3389/fsurg.2019.00058
27. Labadie RF, Balachandran R, Mitchell JE, Noble JH, Majdani O, Haynes DS, et al. Clinical validation study of percutaneous cochlear access using patient-customized microstereotactic frames. *Otol Neurotol.* (2010) 31:94–9. doi: 10.1097/MAO.0b013e3181c2f81a
28. Warren FM, Balachandran R, Fitzpatrick JM, Labadie RF. Percutaneous cochlear access using bone-mounted, customized drill guides: demonstration of concept *in vitro*. *Otol Neurotol.* (2007) 28:325–9. doi: 10.1097/01.mao.0000253287.86737.2e
29. Baron S, Eilers H, Munske B, Toennies JL, Balachandran R, Labadie RF, et al. Percutaneous inner-ear access *via* an image-guided industrial robot system. *Proc Inst Mech Eng H.* (2010) 224:633–49. doi: 10.1243/09544119JEIM781
30. Klenzner T, Ngan CC, Knapp FB, Knoop H, Kromeier J, Aschendorff A, et al. New strategies for high precision surgery of the temporal bone using a robotic approach for cochlear implantation. *Eur Arch Otorhinolaryngol.* (2009) 266:955–60. doi: 10.1007/s00405-008-0825-3
31. Caversaccio M, Wimmer W, Anso J, Mantokoudis G, Gerber N, Rathgeb C, et al. Robotic middle ear access for cochlear implantation: First in man. *PLoS ONE.* (2019)14:e0220543. doi: 10.1371/journal.pone.0220543
32. Coulson CJ, Assadi MZ, Taylor RP, Du X, Brett PN, Reid AP, et al. A smart micro-drill for cochleostomy formation: a comparison of cochlear disturbances with manual drilling and a human trial. *Cochlear Implants Int.* (2013) 14:98–106. doi: 10.1179/1754762811Y.0000000018
33. Atturo F, Barbara M, Rask-Andersen H. Is the human round window really round? an anatomic study with surgical implications. *Otol Neurotol.* (2014) 35:1354–60. doi: 10.1097/MAO.0000000000000332
34. Wimmer W, Venail F, Williamson T, Akkari M, Gerber N, Weber S, et al. Semiautomatic cochleostomy target and insertion trajectory planning for minimally invasive cochlear implantation. *Biomed Res Int.* (2014) 2014:596498. doi: 10.1155/2014/596498
35. Topsakal V, Matulic M, Assadi MZ, Mertens G, Rompaey VV, Van de Heyning P. Comparison of the surgical techniques and robotic techniques for cochlear implantation in terms of the trajectories toward the inner ear. *J Int Adv Otol.* (2020) 16:3–7. doi: 10.5152/iao.2020.8113
36. Mertens G, Van Rompaey V, Van de Heyning P, Gorris E, Topsakal V. Prediction of the cochlear implant electrode insertion depth: clinical applicability of two analytical cochlear models. *Sci Rep.* (2020) 10:3340. doi: 10.1038/s41598-020-58648-6
37. Donkelaar HJT, Elliott KL, Fritzsch B, Kachlik D, Carlson M, Isaacson B. An updated terminology for the internal ear with combined anatomical and clinical terms. *J Phonet Audiol.* (2020) 6:147. doi: 10.35248/2471-9455.20.6.147
38. Ten Donkelaar HJ, Kachlík D, Tubbs RS. *An Illustrated Terminologia Neuroanatomica*. Cham: Springer International Publishing (2018).
39. Topsakal V, Kachlik D, Bahşi I, Carlson M, Isaacson B, Broman J, et al. Relevant temporal bone anatomy for robotic cochlear implantation: an updated terminology combined with anatomical and clinical terms. *Transl Res Anat.* (2021) 25:100138. doi: 10.1016/j.tria.2021.100138
40. Tekin AM, Matulic M, Wuyts W, Assadi MZ, Mertens G, Rompaey VV, et al. A new pathogenic variant in POU3F4 causing deafness due to an incomplete partition of the cochlea paved the way for innovative surgery. *Genes.* (2021) 12:613. doi: 10.3390/genes12050613
41. Meyerhoff WL, Stringer SP, Roland PS. Rambo procedure: modification and application. *Laryngoscope.* (1988) 98:795–6. doi: 10.1288/00005537-198807000-00025
42. Weber S, Gavaghan K, Wimmer W, Williamson T, Gerber N, Anso J, et al. Instrument flight to the inner ear. *Sci Robot.* (2017) 2:eaal4916. doi: 10.1126/scirobotics.aal4916
43. Lehnhardt E. Intrakochleäre Plazierung der Cochlear-Implant-Elektroden in soft surgery technique [Intracochlear placement of cochlear implant electrodes in soft surgery technique]. *HNO.* (1993) 41:356–9.
44. Torres R, Kazmitcheff G, De Seta D, Ferrary E, Sterkers O, Nguyen Y. Improvement of the insertion axis for cochlear implantation with a robot-based system. *Eur Arch Otorhinolaryngol.* (2017) 274:715–21. doi: 10.1007/s00405-016-4329-2
45. Incesulu A, Adapinar B, Kecik C. Cochlear implantation in cases with incomplete partition type III (X-linked anomaly). *Eur Arch Otorhinolaryngol.* (2008) 265:1425–30. doi: 10.1007/s00405-008-0614-z
46. Torres R, Kazmitcheff G, Bernardeschi D, De Seta D, Bensimon JL, Ferrary E, et al. Variability of the mental representation of the cochlear anatomy during cochlear implantation. *Eur Arch Otorhinolaryngol.* (2016) 273:2009–18. doi: 10.1007/s00405-015-3763-x
47. Sennaroglu L, Bajin MD. Incomplete partition type III: a rare and difficult cochlear implant surgical indication. *Auris Nasus Larynx.* (2018) 45:26–32. doi: 10.1016/j.anl.2017.02.006
48. Saeed H, Powell HRF, Saeed SR. Cochlear implantation in X-linked deafness - how to manage the surgical challenges. *Cochlear Implants Int.* (2016) 17:178–83. doi: 10.1080/14670100.2016.1180018

Conflict of Interest: MM was an employee and shareholder of CASCINATION AG. MZ-A and PG were employees of MED-EL Medical Electronics.

The remaining authors declare that the research was conducted in the absence of any commercial or financial relationships that could be construed as a potential conflict of interest.

Publisher's Note: All claims expressed in this article are solely those of the authors and do not necessarily represent those of their affiliated organizations, or those of the publisher, the editors and the reviewers. Any product that may be evaluated in this article, or claim that may be made by its manufacturer, is not guaranteed or endorsed by the publisher.

frontiers in Surgery

SYSTEMATIC REVIEW
published: 24 March 2022
doi: 10.3389/fsurg.2022.823219

Suitable Electrode Choice for Robotic-Assisted Cochlear Implant Surgery: A Systematic Literature Review of Manual Electrode Insertion Adverse Events

Paul Van de Heyning[1,2], Peter Roland[3], Luis Lassaletta[4], Sumit Agrawal[5], Marcus Atlas[6], Wolf-Dieter Baumgartner[7], Kevin Brown[8], Marco Caversaccio[9], Stefan Dazert[10], Wolfgang Gstoettner[7], Rudolf Hagen[11], Abdulrahman Hagr[12], Greg Eigner Jablonski[13,14], Mohan Kameswaran[15], Vladislav Kuzovkov[16], Martin Leinung[17], Yongxin Li[18,19], Andreas Loth[17], Astrid Magele[20], Robert Mlynski[21], Joachim Mueller[22], Lorne Parnes[5], Andreas Radeloff[23], Chris Raine[24], Gunesh Rajan[25], Joachim Schmutzhard[26], Henryk Skarzynski[27], Piotr H. Skarzynski[27], Georg Sprinzl[20], Hinrich Staecker[28], Timo Stöver[17], Dayse Tavora-Viera[29], Vedat Topsakal[30], Shin-Ichi Usami[31], Vincent Van Rompaey[1,2], Nora M. Weiss[10], Wilhelm Wimmer[9], Mario Zernotti[32] and Javier Gavilan[4]*

[1] Department of Otorhinolaryngology Head and Neck Surgery, Antwerp University Hospital, University of Antwerp, Antwerp, Belgium, [2] Department of Translational Neurosciences, University of Antwerp, Antwerp, Belgium, [3] Department of Otolaryngology, Head & Neck Surgery, University of Texas Southwestern Medical Center, Dallas, TX, United States, [4] Hospital Universitario La Paz, Institute for Health Research (IdiPAZ), Madrid, Spain, [5] Department of Otolaryngology-Head and Neck Surgery, Western University, London, ON, Canada, [6] Ear Sciences Institute Australia, Lions Hearing Clinic, Perth, WA, Australia, [7] Vienna Medical University-General Hospital AKH, Vienna, Austria, [8] UNC Ear and Hearing Center at Chapel Hill School of Medicine, Chapel Hill, NC, United States, [9] Department for ENT, Head and Neck Surgery, Bern University Hospital, Bern, Switzerland, [10] Department of Otorhinolaryngology-Head and Neck Surgery, Ruhr-University Bochum, St. Elisabeth University Hospital Bochum, Bochum, Germany, [11] Würzburg ENT University Hospital, Würzburg, Germany, [12] King Abdullah Ear Specialist Center, King Saud University Medical City, King Saud University, Riyadh, Saudi Arabia, [13] Institute of Clinical Medicine, University of Oslo, Oslo, Norway, [14] Department of Otorhinolaryngology & Head and Neck Surgery, Oslo University Hospital, Rikshospitalet, Oslo, Norway, [15] Madras ENT Research Foundation (Pvt) Ltd., Chennai, India, [16] St. Petersburg ENT and Speech Research Institute, St. Petersburg, Russia, [17] Department of Otolaryngology, Head and Neck Surgery, University Hospital Frankfurt, Frankfurt am Main, Germany, [18] Department of Otorhinolaryngology Head and Neck Surgery, Beijing Tongren Hospital, Capital Medical University, Beijing, China, [19] Key Laboratory of Otolaryngology Head and Neck Surgery (Capital Medical University), Ministry of Education, Beijing, China, [20] Ear, Nose and Throat Department, University Clinic St. Poelten, Karl Landsteiner Private University, St. Poelten, Austria, [21] Department of Otorhinolaryngology, Head and Neck Surgery, "Otto Körner" Rostock University Medical Center, Rostock, Germany, [22] Klinik und Poliklinik für Hals-, Nasen- und Ohrenheilkunde, Ludwig-Maximilians-Universitat Munchen, Munchen, Germany, [23] Division of Oto-Rhino-Laryngology, Evangelisches Krankenhaus Oldenburg, Research Center of Neurosensory Sciences, University Oldenburg, Oldenburg, Germany, [24] Bradford Royal Infirmary Yorkshire Auditory Implant Center, Bradford, United Kingdom, [25] Department of Otolaryngology, Head and Neck Surgery, Luzerner Kantonsspital, Luzern, Medical Sciences Department of Health Sciences and Medicine. University of Lucerne, Luzern, Switzerland. Otolaryngology, Head & Neck Surgery, Medical School University of Western Australia, Perth, WA, Australia, [26] Department of Otorhinolaryngology, Medical University of Innsbruck, Innsbruck, Austria, [27] Department of Teleaudiology and Screening, World Hearing Center of the Institute of Physiology and Pathology of Hearing, Kajetany, Poland, [28] Kansas University Center for Hearing and Balance Disorders, Kansas City, KS, United States, [29] Fiona Stanley Fremantle Hospitals Group, Perth, WA, Australia, [30] Department of ENT HNS, University Hospital Brussels, Brussels, Belgium, [31] Department of Hearing Implant Sciences, Shinshu University School of Medicine, Nagano, Japan, [32] Catholic University of Córdoba and National University of Córdoba, Córdoba, Argentina

Background and Objective: The cochlear implant (CI) electrode insertion process is a key step in CI surgery. One of the aims of advances in robotic-assisted CI surgery (RACIS) is to realize better cochlear structure preservation and to precisely control insertion. The aim of this literature review is to gain insight into electrode selection for RACIS by

OPEN ACCESS

Edited by:
Ingo Todt,
Bielefeld University, Germany

Reviewed by:
Hans Thomeer,
University Medical Center Utrecht, Netherlands
A. B. Zulkiflee,
University Malaya Medical Centre, Malaysia

***Correspondence:**
Paul Van de Heyning
paul.vandeheyning@uza.be

Specialty section:
This article was submitted to Otorhinolaryngology – Head and Neck Surgery, a section of the journal Frontiers in Surgery

Received: *26 November 2021*
Accepted: *09 February 2022*
Published: *24 March 2022*

Citation:
Van de Heyning P, Roland P, Lassaletta L, Agrawal S, Atlas M, Baumgartner W-D, Brown K, Caversaccio M, Dazert S, Gstoettner W, Hagen R, Hagr A, Jablonski GE, Kameswaran M, Kuzovkov V, Leinung M, Li Y, Loth A, Magele A, Mlynski R, Mueller J, Parnes L, Radeloff A, Raine C, Rajan G, Schmutzhard J, Skarzynski H, Skarzynski PH, Sprinzl G, Staecker H, Stöver T, Tavora-Viera D, Topsakal V, Usami S-I, Van Rompaey V, Weiss NM, Wimmer W, Zernotti M and Gavilan J (2022) Suitable Electrode Choice for Robotic-Assisted Cochlear Implant Surgery: A Systematic Literature Review of Manual Electrode Insertion Adverse Events. Front. Surg. 9:823219. doi: 10.3389/fsurg.2022.823219

acquiring a thorough knowledge of electrode insertion and related complications from classic CI surgery involving a manual electrode insertion process.

Methods: A systematic electronic search of the literature was carried out using PubMed, Scopus, Cochrane, and Web of Science to find relevant literature on electrode tip fold over (ETFO), electrode scalar deviation (ESD), and electrode migration (EM) from both pre-shaped and straight electrode types.

Results: A total of 82 studies that include 8,603 ears implanted with a CI, i.e., pre-shaped (4,869) and straight electrodes (3,734), were evaluated. The rate of ETFO (25 studies, 2,335 ears), ESD (39 studies, 3,073 ears), and EM (18 studies, 3,195 ears) was determined. An incidence rate (±95% CI) of 5.38% (4.4–6.6%) of ETFO, 28.6% (26.6–30.6%) of ESD, and 0.53% (0.2–1.1%) of EM is associated with pre-shaped electrodes, whereas with straight electrodes it was 0.51% (0.1–1.3%), 11% (9.2–13.0%), and 3.2% (2.5–3.95%), respectively. The differences between the pre-shaped and straight electrode types are highly significant ($p < 0.001$). Laboratory experiments show evidence that robotic insertions of electrodes are less traumatic than manual insertions. The influence of round window (RW) vs. cochleostomy (Coch) was not assessed.

Conclusion: Considering the current electrode designs available and the reported incidence of insertion complications, the use of straight electrodes in RACIS and conventional CI surgery (and manual insertion) appears to be less traumatic to intracochlear structures compared with pre-shaped electrodes. However, EM of straight electrodes should be anticipated. RACIS has the potential to reduce these complications.

Keywords: robotic assisted cochlear implant surgery, pre-shaped electrode, straight electrode, tip fold-over, scalar deviation, electrode migration

INTRODUCTION

Cochlear implants (CIs) are widely accepted as the *state-of-the-art* hearing solution for *partial-to-profound* sensorineural hearing loss (SNHL) in adults (1) and children (2). The implant's stimulator-receiver is surgically placed under the skin and rests on the surface of the skull. While the electrode array is placed within the cochlea, the excess electrode lead is left coiled in the surgically drilled mastoid cavity (3). The speech processor converts the acoustical signals into electrical signals and is worn externally. The maximum benefit for patients is expected when the electrode array is optimally placed fully inside scala tympani (ST) (or even in scala vestibuli (SV) in special cases of ST ossification) without any degree of scalar deviation, so as to create an effective electrode-neural interface (4).

Intra-cochlear electrode insertion is considered one of the crucial steps of a successful CI surgery. In particular, studies have suggested that slow steady insertion (achieved more easily with robotic insertion) can reduce pressure changes within the cochlea (5, 6), reduce insertion forces (7), and increase the likelihood of an in-axis insertion into ST and improve hearing outcomes (8). Robotic-assisted cochlear implant surgery (RACIS) aims to optimize this insertion process by (1) computer control of insertion speed and by applying insertion forces more steadily and smoothly, (2) defining the angle with which the electrode is inserted into the ST, and (3) improving the estimated insertion depth to minimize trauma and provide better hearing outcomes.

Robotic-assisted cochlear implant surgery has the potential of being included in the surgical armamentarium in the future. Before RACIS can become the standard approach for cochlear implantation, aspects of clinical benefits, cost, and duration of the procedure still need to be addressed (9). Currently, there are three such systems with either Conformité Européenne (CE) or Food and Drug Administration (FDA) approval and a new system is under clinical trial. RobOtol® is a French innovation that recently received the CE mark (10) and the iotaSOFT® insertion system received the American FDA approval in October 2021 (11). These two systems offer automated electrode insertion support after manual drilling of the temporal bone to reach the round window (RW) niche. The third system is HEARO®, a Swiss innovation which drills a narrow tunnel in the mastoid bone and through the facial recess (12, 13) to reach the RW through which the electrode is inserted (14). The HEARO® system received a CE mark in the year 2020. A new robotic system called Rosa®, another French innovation that offers robotic-controlled drilling of the mastoid and electrode insertion, has been recently evaluated for safety and accuracy in live patients (15). RoboJig is a German innovation currently under development. The robot drills a narrow tunnel in the mastoid guided by a jig that is developed on-site and is based on the patient's specific anatomy. It includes an automated insertion

TABLE 1 | Search terms used in the identification of relevant literature to perform the systematic literature review.

Electrode insertion related complications	Search terms
Electrode tip fold over (ETFO)	Cochlear implant electrode tip fold over or cochlear implant electrode tip roll over.
Electrode scalar deviation (ESD)	Cochlear implant electrode scalar deviation or cochlear implant electrode scalar location or cochlear implant electrode scalar position.
Electrode migration (EM)	Cochlear implant electrode-migration

tool for the electrode (16). Recent reports in a series of patients demonstrate the clinical feasibility and effectiveness of these robotic systems in accommodating various CI electrode variants (14, 15, 17, 18).

The aim of RACIS is to eliminate or minimize intracochlear trauma during electrode insertion. Several electrode array insertion complications with a negative influence on post-operative outcomes have been reported after manual insertion. These include electrode tip fold over (ETFO) (19), electrode array scalar deviation (ESD) (20), and electrode array migration (EM) or slippage (21). A recent report on the application of RACIS also included one of the electrode-related complications mentioned above (17). Electrode variants that are currently available can be classified as either pre-shaped or straight electrode types (22). *Up-to-date* knowledge of the literature on the rate of these various electrode insertion complications by electrode type could facilitate electrode array selection for RACIS and for manual insertion. Therefore, this article is aimed to provide a systematic literature review on electrode-related insertion complications for both pre-shaped and straight electrodes.

METHODS

Study Design

Following the recommendations of the Preferred Reporting Items for Systematic Reviews and Meta-Analysis (PRISMA) (23), the literature was systematically reviewed to establish the rate of ETFO, ESD, and EM for both pre-shaped and straight electrodes.

Search Strategy and Study Selection

To perform the systematic literature review, a search for articles in PubMed, Scopus, Cochrane, and Web of Science was carried out using appropriate search terms (as listed in **Table 1**) by the first two authors PVH and PR. Articles published up to October 31, 2021 in English and German languages were considered for analysis. In addition, a manual search for relevant literature reviews and random checking of PubMed and Google Scholar were conducted using pertinent key terms. The first two authors independently screened titles and abstracts to select potential full-text articles according to the inclusion criteria. Exclusion criteria included review articles, surgical methodological studies, studies in languages other than English and German, studies using other approaches than through the posterior tympanotomy, and studies on auditory brain stem implants.

Data Extraction

A template in Microsoft Excel (www.microsoft.com/en-us/microsoft-365/excel) was created to record the extracted data, i.e., the first author of the study, study type, analyzing methods, the total number of ears implanted with CI, the number of ears implanted with each type of electrode, and, finally, the number of insertions with ETFO, ESD, and EM per electrode type.

Data Analysis and Statistics

The rate of ETFO, ESD, and EM was calculated by dividing the number of ears with the associated issue by the total number of ears implanted with a specific type of electrode. Significance was calculated with the test for the difference of 2 proportions and 95% CIs, both implemented in MiniTab® (© 2019 Minitab, LLC, State College, PA, USA).

Risk of Bias Assessment

The risk of bias was independently assessed by the third and the last authors (LL and JG). Included studies were assessed using the Risk of Bias in Non-randomized Studies of Interventions (ROBINS-I) tool (24). This tool contains seven items judging the risk of bias due to confounding, study participant selection, classification of interventions, deviations from intended intervention, missing data, measurement of outcomes, and selection of reported results. Each of the seven items in included studies was judged low, moderate, or high risk. Inner ear malformation was considered as the one of the confounding factors for ETFO, whereas electrode type was considered as the confounding factor for ESD and EM. Results of risk of bias assessment were graphically summarized using Microsoft Excel (https://www.microsoft.com/en-us/microsoft-365/excel).

RESULTS

Search Results

Figure 1 details the systematic literature review process followed in the identification of relevant articles. A total of 37 articles on ETFO, 96 articles on ESD, and 38 articles on EM were identified using the search terms. After a thorough review of the abstract for search terms, 25 articles on ETFO, 39 articles on ESD, and 18 articles on EM were included in the evaluation of incidence rate.

Risk of Bias

ROBINS-I—Risk of Bias Assessment

The risk of bias assessment using the ROBINS-I tool is summarized in **Figure 2**. The majority of the studies included had a noticeable lower risk of bias as represented by green bars. All the studies identified specifically under all three electrode insertion complications had a low risk of bias for the reported result and for deviations from the intended intervention.

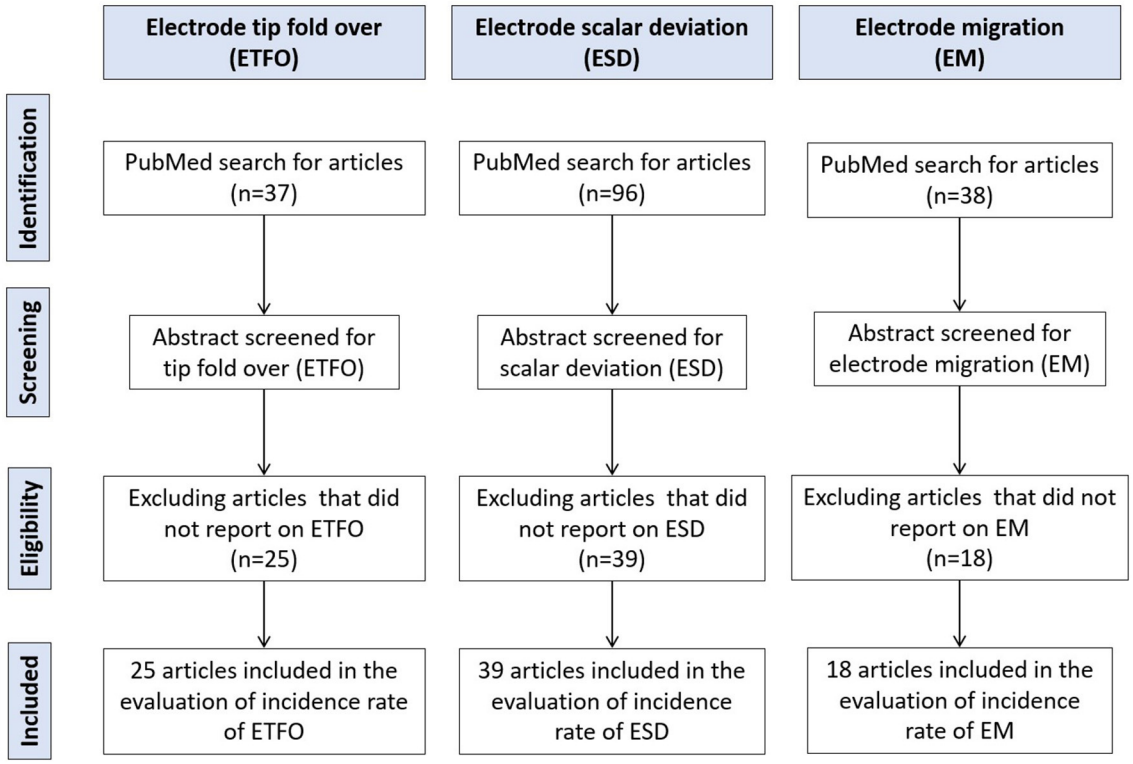

FIGURE 1 | Literature review process utilizing the Preferred Reporting Items for Systematic Reviews and Meta-Analyses (PRISMA) guidelines.

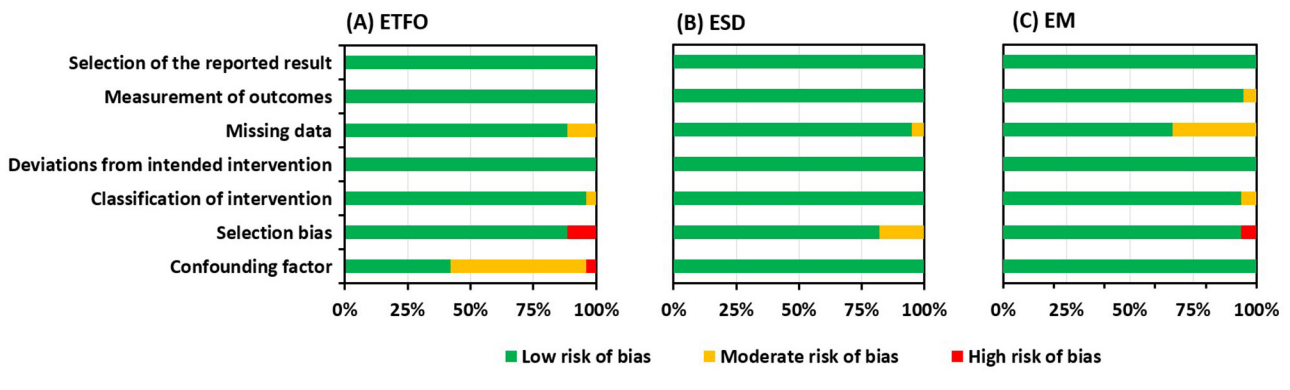

FIGURE 2 | Risk of bias graph: review authors' judgment presented as percentages across all included studies about each risk of bias item for electrode tip fold over (ETFO) **(A)**, electrode scalar deviation (ESD) **(B)**, and electrode migration (EM) **(C)**.

Confounding Bias

For the ETFO, cystic ear anatomy was considered a confounding factor, because cystic cochlear anatomy increases the chances of ETFO. Fourteen studies out of 25 did not reveal if the images of the selected patients were analyzed for any degree of anatomical deviation from the normal anatomy, suggesting those studies had a moderate risk of bias (studies 29–32, 34, 36–38, 40, 41, 43, 45, and 46). One study included the patients with the inner ear malformations and was graded with a high risk of bias (study 47).

The type of electrode was taken as the confounding factor for ESD and EM. Electrode stiffness could increase the chances for ESD, and the pre-curved shape of the electrode would hook around the modiolar wall offering a natural fixation and minimizing the chances of EM. All the studies identified within ESD and EM issues reported the electrode type, suggesting a low risk of bias. The different sites and techniques of entering the ST, e.g., Cochleostomy (Coch) or RW, were not taken into account as a confounding factor.

Selection Bias

Selection bias mainly concerns how the patients were selected in the identified studies. Case series were graded with a high risk of bias whereas patients selected for a specific electrode type within a certain time period were thought to have a low risk of bias. Three out of 25 studies (studies 19, 43, 45) and 1 out of 18 studies (study 77) within ETFO and EM issues, respectively, were graded as having a high risk of bias. Seven out of 39 studies within the ESD issue were assigned a moderate risk of bias (studies 54, 57, 65-).

Missing Data Bias

Missing data bias becomes a concern if the type of electrode used is not specified for cases with electrode complications. Three studies within ETFO (Appendix 1: studies 7, 17, and 24), two studies within ESD (Appendix 2: studies 3 and 35), and 6 studies within EM issues (Appendix 3: studies 8, 11, 13–15, and 18) did not provide clear information on the electrode type and hence were considered to have a moderate risk of bias.

Study Results

Electrode Tip Fold Over

Table 2 lists the 25 articles that reported on ETFO include the number of cases implanted and the type of electrode. Intra-operative or post-operative imaging was used in the identification of ETFO. A total of 5,042 ears were reported and after excluding the studies that did not specify the electrode type, 2,335 ears were taken for the evaluation. These 25 articles covered a total of 1,559 implantations with pre-shaped electrodes and 776 with straight electrodes. Eighty-four out of 1,559 ears implanted with a pre-shaped electrode, irrespective of CI brand, were associated with ETFO, an incidence rate (±95% CI) of 5.38% (4.4–6.6%). For the straight electrodes, irrespective of the CI brand, a rate (±95% CI) of only 0.51% (0.1–1.3%) was identified. The difference in rate between the pre-shaped and the straight electrode is highly significant ($p < 0.001$).

Electrode Scalar Deviation

Table 3 lists the 39 articles which reported ESD along with the number of ears implanted and the type of electrode. Different modalities, such as electrocochleography (EcochG), intra-operative fluoroscopy or CT, and post-operative CT imaging, were used to detect the ESD. A total of 3,073 ears (1,983 pre-shaped and 1,090 straight electrodes) were included for further analysis after excluding studies that did not specify the electrode type. Out of 1,983 ears implanted with pre-shaped electrodes, irrespective of manufacturer, ESD was reported in 567 ears yielding a rate (±95% CI) of 28.6% (26.6–30.6%). Out of 1,090 ears implanted with straight electrodes, irrespective of manufacturer, ESD was reported in 120 ears yielding a rate (±95% CI) of 11% (9.2–13.0%). The difference in rate between the pre-shaped and the straight electrode is highly significant ($p < 0.001$).

Electrode Migration

Table 4 lists the 18 articles which reported on EM. Post-operative imaging was used in the identification of EM. A total of 5,795 ears implanted with CI were identified from the literature search. After excluding those studies that did not specify the electrode type, a total of 3,195 ears were taken for analysis. Pre-shaped electrodes were implanted in 1,327 ears and straight electrodes were implanted in 1,868 ears. EM was identified in 61 ears implanted with straight electrodes, an incidence rate (±95% CI) of 3.2% (2.5–3.95%). For pre-shaped electrodes, only 7 ears were identified with EM, a rate (±95% CI) of around 0.53% (0.2–1.1%). The difference in proportion between the pre-shaped and the straight, electrode is highly significant ($p < 0.001$).

DISCUSSION

Summary of Evidence

The aim of this literature review was to determine the type of electrode best suited to minimize deleterious complications for use in RACIS and in conventional CI surgery. This systematic literature review yielded a total of 82 studies covering a total of 8,603 CI procedures, which met within the inclusion criteria. This review specifically sought to establish the incidence of ETFO, ESD, and EM for both pre-shaped and straight electrodes. A total of 4,869 ears implanted with pre-shaped and 3,734 ears implanted with straight electrodes were identified from the search. The high number of CI procedures (8,603) in total allowed us to compare the rate of electrode insertion complications between the two electrode types, which are of value for RACIS and conventional CI surgery.

Electrode Tip Fold Over

An ETFO occurs when the tip of the electrode gets stuck in the ST and, on further insertion, the tip bends back on itself as shown in **Figures 3A,B**. This could provoke short circuiting between the apical electrode contacts and can result in pitch confusion and perversion. Moreover, it may damage the basilar membrane leading afterward to fibrosis, hydrops, and ossification (93).

Electrode tip fold over is associated in most cases with varying degrees of decreased speech understanding and, in several series, co-stimulation of the facial nerve and dizziness was reported. The speech understanding may be as low as 20% with a Bamford-Kowal-Bench (BKB) speech test in quiet (38) or with hearing in noise test (HINT) (19) up to a reported case with preserved residual hearing and one with 80% speech in Quite (45). Revision operations or deselecting the involved electrodes increased in most cases the speech and solved the complaints of facial co-stimulation and dizziness (19, 41, 45). Intra-operative imaging is one possible means of detecting the ETFO during surgery in which case it can be corrected as part of the initial surgery, as it has been suggested by several clinicians (19, 28, 43).

This literature review demonstrates that ETFO is more commonly associated with pre-shaped electrodes (rate of 5.3%) than with straight electrodes (0.5%). Based on reasons cited in the literature, the higher prevalence in pre-shaped electrodes could be due to any of the following factors: the pre-mature pulling of the stylet/polymer sheath, the orientation of the electrode contacts away from the modiolar wall during insertion, variations in the size and shape of the cochlea, and variations in the length of the straight portion of the basal turn. The shape of the electrode

TABLE 2 | Twenty-five articles reporting on electrode tip fold-over.

Study/type	No. of cases taken for analysis/method	No. of electrode per type/brand			No. of cases reported tip fold-over	
		A	B	C	Pre-shaped	Straight
Högerle et al. (25)/R	378 (Post-op x-ray)	–	–	FL (378)	–	0
Klabbers et al. (26)/P	25 (Intra-operative fluoroscopy)	SM (25)	–	–	3	–
Müller et al. (27)/R	108 (Spread of excitation/Intra-operative fluoroscopy)	SM (7), CA (87), SS (14)	–	–	CA (2), SM (2),	SS (1)
Durakovic et al. (28)/R	326 (Intra-operative x-rays)	SM (326)	–	–	23	–
Shaul et al. (29)/P	120 (Intra-operative x-ray)	SM (120)	–	–	8	–
Dimak et al. (30)/R	84 (Post-op x-ray)	SM (94)	–	–	3	–
Labadie et al. (31)/R	175 (Intra-operative imaging)	No info on brand segments: Straight electrodes (86); Pre-curved electrodes (89)			4 (SM) (not included in the analysis)	
Heutink et al. (32)/P	23 (Intra-operative fluoroscopy)	SM (23)	–	–	1	–
Garaycochea et al. (33)/R	19 (Intra-operative fluoroscopy)	SM (19)	–	–	3	–
Mittmann et al. (34)/R	85 (Flat-panel CT)	SM (85)	–	–	4	-
Iso-Mustajärvi et al. (35)/R	18 (Cone beam CT)	SM (18)	–	–	0	-
McJunkin et al. (36)/R	117 (Intra-op x-ray)	SM	–	–	9	–
Friedmann et al. (37)/R	237 (Intra-op x-ray)	SM (237)	–	–	11	–
Serrano et al. (38)/R	40 (Intra/Post-op x-ray)	SM (40)	–	–	2	–
Timm et al. (39)/R	275 (Post-op CT)	–	–	275 (F28, F24, F20, F16)	–	0
Sipari et al. (40)/R	23 (Post-op CBCT)	–	MS (23)	–	2	–
Gabrielpillai et al. (41)/R	1,722 (Post-op x-ray)	No info on brand segments			CA (7), SM (6), SS (2) (not included in the analysis)	
Jia et al. (42)/R	65 (Intra-op CBCT) (Contains 3 electrodes from Oticon)	CA (12), SM (1), SS (31)	1J (2), MS (3)	F28 (13)	SM (1)	–
Sabban et al. (19)/R	2 (x-ray & CT)	–	MS	–	2	–
Garaycochea et al. (43)/R	1 (Intra-op fluoroscopy)	SM	–	–	1 (100%)	–
Aschendorff et al. (44)/R	45 (Post-op CBCT)	SM	–	–	2 cases. 1st case corrected in the same surgery. 2nd case underwent revision surgery	–
Zuniga et al. (45)/R	303 (Post-op CT)	CA, SS	MS, 1J	–	CA (3), [MS (1), SS (1) and 1J (1)]	
		No info on brand segments			(not included in the analysis)	
Fischer et al. (46)/R	63 (Post-op CBCT)	–	–	F24, F28, Std	–	1
Dirr et al. (47)/R	215 (Post-op x-ray)	CA, SS	–	Std, M, S, FL, F28	FL (2)	
		No info on brand segments			(not included in the analysis)	
Cosetti et al. (48)/R	277 (Intra-op x-ray)	CA	–	–	5	–
Total	5,042				110 (102 pre-shaped electrodes + 8 straight electrodes)	
Total, after excluding four studies that did not specify number per electrode type	2,335	Pre-shaped (1,559), Straight (776)			Pre-shaped (84), Straight (4)	

R, retrospective; P, prospective; SM, Slim-Modiolar; CA, contour advance; MS, mid-scala; SS, slim straight; Std, standard; M, medium; S, compressed; FL, FLEX SOFT, F28: FLEX^{28}; F24, FLEX^{24}; F20: FLEX^{20}; F16: FLEX^{16}; CBCT, cone-beam CT. Studies that are shaded in gray were not included in the analysis due to the non-availability of information on the CI brand.

tip (conical/pointed geometry) is another design-related factor that could influence the incidence of ETFO issues (25, 94, 95).

Once the electrode is inserted inside the ST, it follows its own path, and currently, there are no steerable electrodes available. Experimental work on cadaveric temporal bones demonstrated that robotic insertion could reduce intracochlear trauma by applying a constant insertion speed in an optimized axis (96). Hence, it is to be expected that the application of RACIS would lead to less traumatic insertions. However, there is no evidence yet that better control of insertion speed, as offered by some

TABLE 3 | Thirty-eight studies reported on electrode scalar deviation.

Study/type	No. of analyzed cases	Analyzing method	No. of electrode from type/brand			No. of cases reported with scalar deviation	
			A	B	C	Pre-shaped	Straight
Riemann et al. (49)/P	20	3T MRI	–	MS (5), SJ (5)	F28 (10)	1	0
Liebcher et al. (50)/R	255	Post-op CT	CA (99), SM (156)	–	–	32 (CA), 8 (SM)	—
Heutink et al. (51)/R	129	Post-op CT	CA (85), SS (44)	–	–	20 (CA)	SS (18)
Ketterer et al. (52)/R	201	Post-op CBCT	–	–	F24 (28), F26 (15), F28 (139), FL (19)	–	F24 (1), F28 (6), FL (5)
Lenarz et al. (53)/R	20	Post-op CBCT	–	SJ (20)	–	0	–
Durakovic et al. (28)/R	76	Post-op CT	SM (76)	–	–	5	–
Morrel et al. (54)/P	177	Post-op CBCT	SS (46)	1J/SJ (39)	F24 (8), F28 (52), Std (32)	–	39
Nassiri et al. (55)/R	24	Intra-op CT	SM (24)	–	–	1	–
Heutink et al. (32)/P	23	Post-op CT	SM (23)	–	–	8	–
Iso-Mustajärvi et al. (35)/R	18	Post-op CBCT	SM (18)	–	–	0	–
Riggs et al. (56)/P	21	Post-op CT/EcochG	–	MS (21)	–	7	–
Chakravorti et al. (57)/R	220	Post-op CT	CA (89), SS (20), ST (11)	MS (21), 1J (29)	F24 (3), F28 (22), M (1), Std (24)	45	11
Yamamoto et al. (58)/R	58	Intraoperative CT	CA/C (30), SS (12)	1 (MS)	F24 (3), F28 (12)	16	7
Shaul et al. (59)/P	110	Post-op CBCT	CA (92), SM (18)	–	–	18	–
Sipari et al. (40)/R	23	Post-op CT	–	MS (23)	–	5	–
Koka et al. (60)/P	32	Post-op CT/EcochG	–	MS (32)	–	7	–
Jia et al. (42)/R	65	Intra-op CT	CA (12), SM (1), SS (31)	1J (2), MS (3)	F28 (16),	1	–
McJunkin et al. (36)/R	23	Post-op CT	SM (23)	–	–	6	–
Ketterer et al. (61)/R	368	Post-op CBCT	CA (368)	–	–	118	–
An et al. (62)/R	26	Post-op CT	SS (5)	–	F28 (21)	–	F28 (1), SS (1)
Aschendorff et al. (44)/P	45	Post-op CBCT	SM (45)	–	–	0	–
O'Connell et al. (63)/R	48	Post-op CT	–	–	F24, F28, Std (48)	-	0
O'Connell et al. (64)/P	18	EcochG/Post-op CT	–	MS (18)	–	6	–
Mittmann et al. (65)/R	50	NRT/Post-op CT	SS (50)	–	–	-	SS (2)
Lathuilliere et al. (66)/P	24	Post-op CBCT	CA (24),	–	–	3	–
O'Connell et al. (67)/R	56	Post-op CT	CA (36), SS (20)	–	–	19	SS (2)
O' Connell et al. (68)/R	220	Post-op CT	CA (115), SS (19),	1J (21), MS (14)	F28 (28), Std (17), F24 (4) & M (2)	67	F (4)
Wanna et al. (69)/P	45	Post-op CT	CA (15)	MS (3)		5	1J and SSS (2)
			SS, 1J & F collectively (27=9 each)				
Nordfalk et al. (70)/R	39	Post-op CT	–	–	F28 (18), FL (17), F24 (4)	–	F (0)
Mittmann et al. (71)/R	23	NRT/Post-op CT	CA (23)	–	–	6	–
Mittmann et al. (71)/R	85	NRT/Post-op CT	CA (85)	–	–	16	–
Boyer et al. (72)/n/a	61	Post-op CBCT	CA (31),	–	FL, F28, F24, Std (30)	8	F (0), Std (1)
Fischer et al. (46)/R	63	Post-op CBCT	–	–	F28 (40), F24 (2), FL (7), Std (14)	–	F28 (5)
Wanna et al. (73)/P	116	Post-op CT	CA (35), MS (34)		(47) LW from all 3 CI brands (15, 15, 17)	29	All LW (5)
Dirr et al. (47)/R	215	Post-op x-ray	107		108	–	F (1)
Nordfalk et al. (74)/R	13	Post-op CT	CA (7)	1J (3)	Std (2), F24 (1)	3 (CA)	Std (1), 1J (1)
Aschendorff et al. (75)/R	223	Post-op CT	C (21), CA (202)	–	–	19 (C), 70 (CA)	–
Wanna et al. (73)/R	32	Post-op CT	20	10	2	11	F (0)
Lane et al. (76)/R	23	Post-op CT	C/CA (13)	H (1)	–	6 (C)	LW (7)
			LW electrodes from brand A (5) & B (4)				
Total (excluding Dirr et. al)	3,073		2,073	333	667	567	120
			Pre-shaped (1,983) Straight (1,090)			Pre-shaped (567) Straight (120)	

R, retrospective; P, progressive; n/a, non-availability of data; SM, Slim-Modiolar; CA, contour advance; MS, mid-scala; SS, slim straight; SJ, Slim J; Std, standard; M, medium; S, compressed; FL, FLEX SOFT, F28: FLEX^{28}; F24, FLEX^{24}; F20: FLEX^{20}; F16: FLEX^{16}; NRT, neural response telemetry; EcochG, electrocochleography. A study that is shaded in gray was not included in the analysis due to the non-availability of information on the CI brand.

TABLE 4 | Eighteen studies reported on electrode migration.

Study/type	No. of analyzed cases	Analyzing method	No. of electrode from type		No. of cases reported with electrode migration	
			Pre-shape	Straight	Pre-shaped	Straight
Ozer et al. (77)/R	149	Post-op CT	–	149	–	1
Chan et al. (78)/R	1	Post-op x-ray and CT	–	1	–	1
Mitzlaff et al. (79)/R	560	Post-op CT	414	146	–	6
Leinung et al. (80)/R	1,603	Post-op x-ray and CT	772	831	–	17
Rajan et al. (81)/R	56	Not mentioned	–	56	–	1
Celik et al. (82)/R	245	Post-op x-ray	Not specified	Not specified	–	1
Rader et al. (83)/R	270	Post-op CBCT	–	270	–	10
Patnaik et al. (84)/R	534	Post-op HRCT	Not specified	Not specified	–	2
Mittmann et al. (71)/R	54	Post-op CT	54	–	7	–
Dietz et al. (21)/R	201	Post-op CBCT	64	137	–	12
Jeppesen et al. (85)/R	308	Post-op CT	Not specified	Not specified	–	4
van der Marel et al. (86)/R	35	Post-op CT	–	35	–	10
Lavinsky-Wolff et al. (87)/R	75	Post-op X-ray	Not specified	Not specified	–	2
Brown et al. (88)/R	806	Post-op CT	Not specified	Not specified	–	4
Connell et al. (89)/R	580	Post-op CT	Not specified	Not specified	–	2
Green et al. (90)/R	239	Post-op imaging	23	216	–	3
Roland Jr et al. (91)/P	27	Post-op x-ray	–	27	–	0
de Long et al. (92)/R	52	Post-op imaging	Not specified	Not specified	–	0
Total	5,795				7	83
Excluding studies that did not specify the electrode type	3,195		1,327	1,868	7	61

R, Retrospective; P, Progressive; CBCT, Cone-Beam Computerized Tomography.

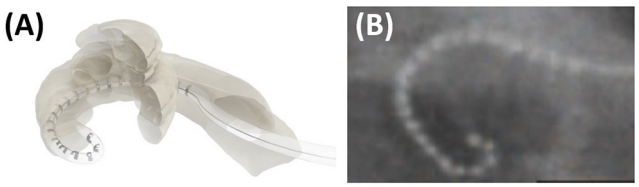

FIGURE 3 | Cartoon picture demonstrating how an electrode tip fold over would look like **(A)**. Post-operative plain film x-ray showing electrode tip fold-over in a patient case **(B)**. Reproduced by permission of Wolters Kluwer Health Inc. (Appendix 1—reference 17).

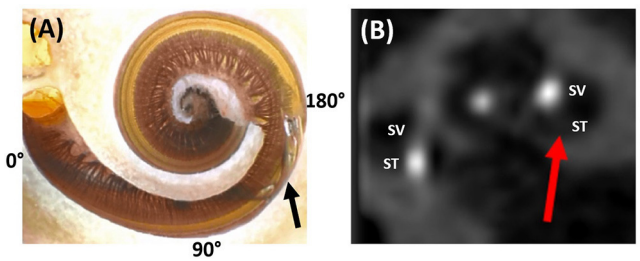

FIGURE 4 | Dissected cochlear sample showing the electrode tip of a pre-shaped electrode penetrating the spiral ligament from the scala tympani (ST) and translocating to scala vestibuli (SV) **(A)**. Image courtesy of Prof. Peter Roland from Southwestern University, TX, USA. Post-operative CT image slice showing part of the electrode in the SV as pointed by the red arrow **(B)**. Reproduced by permission of Elsevier B.V (Appendix 2—reference 2).

systems, or an insertion more axial to the basal part of ST, as offered by other robotic systems would decrease the rate of ETFO with pre-shaped electrodes. Testing in the future will determine whether the implementation of haptic pressure feedback might detect a tip getting stuck.

Electrode Scalar Deviation

Electrode scalar deviation means that the electrode which is inserted into the ST through an RW or Coch approach perforates the basilar membrane and a number of apical electrodes end up in SV. ESD is by far the most frequent serious complication. This occurs mainly between 90 and 180° of angular insertion depth, causing a scalar deviation as pointed by a black arrow in **Figure 4A** and a red arrow in **Figure 4B**.

Electrode scalar deviation is associated with fibrous tissue growth and osteo-neogenesis with the cochlea. Most importantly, ESD has been associated with irreversible degeneration of neuronal cells as detected from the histological evaluation

of cadaveric temporal bones from patients who in life had undergone CI (97). Breaching the basilar membrane and allowing the mixture of perilymph and endolymph can result in the loss of any residual hearing.

Electrode scalar deviation is associated with poorer hearing outcomes when compared to patients with no ESD (20, 67, 68). Jwair et al. through a meta-analysis on ESD identified six studies that compared post-operative speech perception scores between post-lingually adult CI recipients with and without ESD. They concluded that ESD was negatively associated with speech perception scores (weighted mean 41%) compared to full ST placement (weighted mean 55%) (20). O' Connell et al. in 2016 reported the rates of 22.4 and 55% ESD with contour advance (CA, pre-shaped) and mid-scala (MS; pre-shaped) electrodes, respectively, and the ESD was associated with a 12% decrease in consonant-nucleus-consonant (CNC) score (67). O'Connell et al. in 2016 through a literature review covering 6 studies reported that ST insertions are associated with better speech performance when compared to patients with SD. They further reported that the SD affects the low-frequency residual hearing of patients negatively (68).

Electrode scalar deviation is more frequent with pre-shaped electrodes (rate of 28.7%) than with straight electrodes (rate of 11%) in this literature review. The reasons for the higher rate might be explained as follows: (1) due to the variation in cochlear size, shape, and the length of the straight portion of the cochlear basal turn, the standard insertion depth to which the straightened pre-shaped electrode should be inserted inside the cochlea prior to stylet rod/polymer sheath removal could already be deep enough to penetrate the spiral ligament. (2) Orientation of the contact pads of the pre-shaped electrode away from the modiolus wall and facing the basilar membrane/spiral ligament may cause the pre-shaped electrode to curl upward (rather than laterally around the modiolus) when the stylet rod/polymer sheath is retracted. This would cause the tip to penetrate the osseous spiral lamina or basilar membrane. In contrast, the straight electrode has the flexibility to bend in all directions, making it far less traumatic even if the electrode contacts are oriented away from the modiolar wall (94).

The different sites and techniques of entering the ST, e.g., Coch, RW, or extended RW (ERW), approach may also have an influence on ESD. Mainly CI studies in case of residual hearing addressed this issue. Although the approach could not be analyzed as a confounding factor, it deserves special attention. The first multicenter studies that reported atraumatic electrode insertions used a Coch approach (98) and later studies with long-term follow-up could not demonstrate a difference between RW and Coch (99).

Studies focusing on ESD have demonstrated that electrode insertion through RW is associated with a lower incidence of ESD, compared to a Coch approach (46, 73). A consensus publication on atraumatic insertion strongly advocated the RW approach (2). A histopathological study by Ishiyama et al. analyzed the temporal bones of CI patients who in life underwent CI surgery with either an RW or a Coch approach revealed that although insertion through a standard promontory Coch resulted in hydrops and fibrosis in both the ST and SV in the majority of subjects, RW insertions did not (100). Hence, RACIS aims for minimal traumatic inner ear access at the level of the RW in the case of normal anatomy (101).

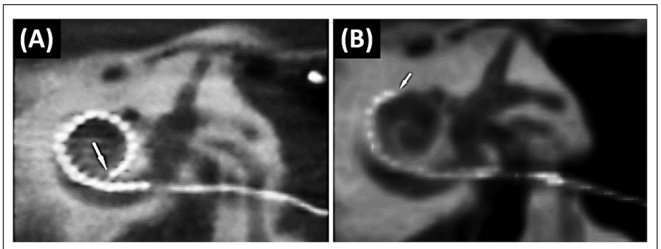

FIGURE 5 | The immediate post-operative CT scan shows a fully inserted Cochlear Slim Straight array (CI422) with an insertion angle of 390° **(A)**. The follow-up scan shows a substantially retracted electrode with six extra-cochlear electrodes and an insertion angle of 210°. The arrow points to the tip of the electrode (21) **(B)**. Reproduced by permission of Springer Nature.

Cadaveric temporal bone experiments show that, in particular, the occurrence of ESD is decreased in motorized co-axial insertion with a slow steady speed (102). Yet, even in the limited series of RACIS, ESD has been reported with pre-shaped electrodes (17). With straight electrodes, RACIS can better manage co-axial insertion into the ST, minimizing damage to the scalar walls. Indeed, studies have shown that the orientation of insertion with a robotic system reduces both the error and the variability of the alignment to a defined optimal axis that it is significantly better compared with a manual insertion, even with experienced surgeons (102, 103). The detection of premature electrode contact with the basilar membrane is expected to improve when intra-operative evoked potentials can be reliably measured (64, 104, 105) with advanced intra-operative imaging (106).

Electrode Migration

In the case of EM, the electrode retracts from its original intracochlear position. This results in the partial displacement of some electrode contacts outside the cochlea. Although, it is believed not to occur often in the opinion of several experienced surgeons, EM is underreported (21). **Figure 5A** shows a fully inserted electrode immediately post-op. A follow-up scan, however, shows that the electrode array has retracted out of the cochlea (**Figure 5B**).

Electrode migration can occur during the closing phase of surgery, immediately post-operatively or later on. EM can result in increased electrode impedances and deterioration of speech recognition scores (21). Depending on the number of extra-cochlear electrodes and the associated impact on hearing, revision surgery to reinsert the electrode into the cochlea may be undertaken. The reason for EM with a straight electrode is believed to be the spring-back force stored in the excess electrode lead coiled in the mastoid drilled cavity. Even a slight relaxation in the coiled electrode lead in the mastoid cavity due to the patient's activity or natural mastoid growth (107) could potentially pull the electrode array out of the cochlea. A possible solution is the electrode lead fixation clip, as shown in **Figure 6A**,

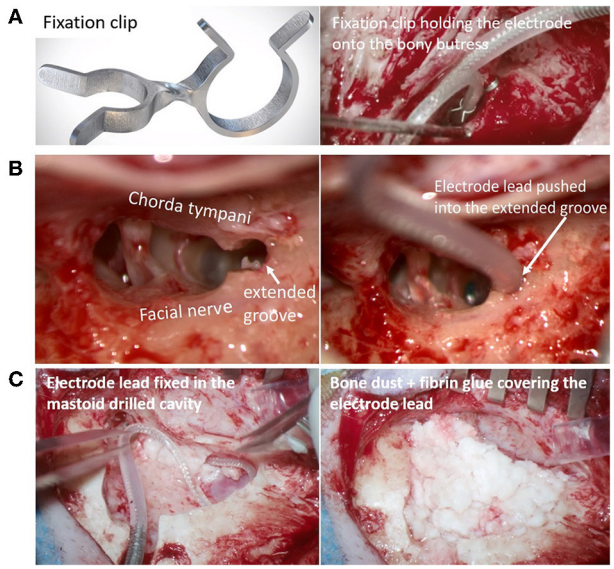

FIGURE 6 | Fixation clip holding the electrode lead onto the bony-buttress of the middle ear space [**(A)** Image courtesy of Joachim Müller, Munich, Germany]. Electrode lead pushed into the extended groove between the facial nerve and chorda tympani [**(B)** Image courtesy of Timo Stöver, Frankfurt, Germany]. The electrode lead is fixed in the posterior tympanotomy [**(C)**-left] and the excess electrode lead coil within the undercut cortex is covered with bone dust mixed with fibrin glue [**(C)**-right- Image courtesy of Paul Van de Heyning, Antwerp, Belgium].

that could minimize/prevent electrode movement and retraction (108). Alternatively, a gentle groove between the facial nerve and chorda tympani (as shown in **Figure 6B**) into which the electrode lead is placed has limited the movement of the electrode lead (109). Fixing the electrode with bone dust mixed with fibrin glue (as shown in **Figure 6C**) is advocated by some surgeons (110).

Electrode migration occurs more commonly with the straight electrodes (rate of 3.2%) than with pre-shaped electrodes (rate of 0.53%). EM out of the cochlea is usually not associated with pre-shaped electrodes because the curved electrode array acts like a hook around the modiolus which provides 5–10 times the holding force needed to extract the electrode from the cochlea compared to straight electrodes (71). Nevertheless, fixating the electrode is advocated for all types of electrodes and not only to prevent EM but also to reduce fatigue electrode wire breakage due to electrode micromovements.

Robotic systems, such as RobOtol® and iotaSOFT®, that insert the electrode through the classic CI approach with an open mastoid and posterior tympanotomy have the same options as that of manual electrode insertion in stabilizing the electrode regardless of the electrode types. Robotic systems, such as HEARO®, Rosa®, which drill a narrow tunnel (direct cochlear access) from the cortex to the cochlea, need an alternate solution for stabilizing the electrode. EM has not been reported in the limited series of patients operated on who have had robotic insertions (12–15, 17, 18). Although the narrow tunnel approach itself provides some stabilization and the absence of coiled excess electrode lead in the mastoid cavity minimizes the EMs, caution is needed in fixing the electrode in the tunnel, which might be accomplished, for example with bone paté.

RACIS and Electrode Type

As the main goal of RACIS is to be less traumatic, this literature review favors the use of straight electrodes due to the significantly lower incidence of ETFO and ESD. ESD often results in irreversible an intra-cochlear injury that permanently degrades hearing outcomes. ETFO and EM, however, are generally correctable and do not result in permanent cochlear damage. Therefore, minimizing the risk of scalar translocations should be a high priority, none-the-less, special care has to be taken to avoid EM when using straight electrodes. This is in line with the conclusions of Jwair et al., 'if one aims to minimize clinically relevant intracochlear trauma, lateral wall arrays would be the preferred option for cochlear implantation' (20).

It is to be hoped that RACIS could further decrease the occurrence of these complications when motorized insertion, with a slow steady speed, is combined with directional control in all three planes to realize an optimized alignment with the ST. Robotic systems have proved to be superior in controlling both speed and directionality. Doudi et al. recently reported from their clinical study comparing 40 CI patients with manual insertion with 20 CI patients with robotic insertion showed a less ESD for robotic insertion of straight electrode arrays when compared with manual insertion (111).

A study by Barriat et al. in 2021 reported complete hearing preservation with a mean loss of pure tone average for five frequencies of 13.60 ± 7.70 dB, and this was associated with a lower insertion speed of 0.88 ± 0.12 mm/s applied by RobOtol® (10). One must realize, however, that the anatomical course of the facial nerve prohibits a perfect co-axial approach to the ST. Animal studies have demonstrated that flexible electrodes are associated with less ESD, thereby, minimizing the hearing loss and intra-cochlear fibrosis (112).

These conclusions are based on a large number of cases taken for analysis from 82 studies. Due to the heterogeneous design of all these studies, a meta-analysis with a forest plot could not be made. This literature review focused on three deleterious complications affecting the hearing outcomes linked with the use of two types of electrodes. There are many factors that have an impact on the electrode choice in RACIS, such as electrode length, electrode stiffness (113), and electrode insertion path that includes both a direct tunnel approach and through posterior tympanotomy. While the electrode insertion through a posterior tympanotomy approach can handle any type of electrode, the direct tunnel approach can only handle straight electrodes. Electrode selection matching the cochlear anatomy, the cochlear duct length, and spiral ganglion cell body distribution (114–117) will prove beneficial when combined with a robotic-assisted electrode insertion and pre-planned computational insertion angles and electrode lengths of 16–34 mm.

Strengths and Limitations

This Systematic Review (SR) provides a systematic evaluation that includes the risk of bias assessment of published evidence on the topic of ETFO, ESD, and EM that are associated with manual insertion of electrodes. The possibility of reducing electrode insertion complications through electrode design is of high relevance to healthcare providers and patients. The electrode insertion complications as reported in the identified articles were confirmed by visually looking at either intra-operative or post-operative images that decrease the overall bias with measurement of outcomes. We did this systematic review strictly following the PRISMA guidelines of reporting. Limitations include the bias in the studies identified mainly due to the risk of selection and confounding bias. Most of the studies identified were retrospective in nature.

CONCLUSIONS

The design of the electrode influences the incidence of electrode insertion complications. The literature findings of the current study reveal that there is a higher incidence of ETFO and ESD associated with pre-shaped electrodes compared to straight electrodes. EM, on the other hand, occurs more often with straight lateral wall electrodes. *Ex vivo* experiments and clinical studies indicate that the application of robotic systems could optimize the electrode insertion characteristics thereby reducing the insertion-related issues. Robotic-assisted electrode insertion and manual insertion should be complemented with the straight electrode design that is associated with the least positioning complications.

DATA AVAILABILITY STATEMENT

The original contributions presented in the study are included in the article/supplementary material, further inquiries can be directed to the corresponding author/s.

AUTHOR CONTRIBUTIONS

PV and PR: study design, search for articles, review of articles, data extraction, and manuscript writing. LL and JG: quality assessment of the articles identified and manuscript writing. The remaining authors were involved in the study design, data analysis, manuscript editing, and overall discussion. All authors contributed to the article and approved the submitted version.

ACKNOWLEDGMENTS

The authors thank Dr. Anandhan Dhanasingh for editing a version of this document and Dr. Edwin Wappl-Kornherr for his assistance in the statistical analysis. The authors of the paper are members of the HEARRING group. The HEARRING Group is an independent network of world leading centers and experts dealing with all aspects of hearing disorders. We believe that advancements in the field of hearing devices are achieved through international research and the pooling of collective experience. Therefore, HEARRING members are committed to leading research in hearing device science, to advancing audiological procedures, and to developing and perfecting surgical techniques.

REFERENCES

1. Carlson ML. Cochlear implantation in adults. *N Engl J Med*. (2020) 382:1531–42. doi: 10.1056/NEJMra1904407
2. Rajan G, Tavora-Vieira D, Baumgartner WD, Godey B, Müller J, O'Driscoll M, et al. Hearing preservation cochlear implantation in children: the HEARRING Group consensus and practice guide. *Cochlear Implants Int*. (2018) 19:1–13. doi: 10.1080/14670100.2017.1379933
3. Praetorius M, Staecker H, Plinkert PK. Chirurgische Technik der Kochleaimplantation [Surgical technique in cochlear implantation]. *HNO*. (2009) 57:663–70. German. doi: 10.1007/s00106-009-1948-6
4. Berg KA, Noble JH, Dawant BM, Dwyer RT, Labadie RF, Gifford RH. Speech recognition with cochlear implants as a function of the number of channels: effects of electrode placement. *J Acoust Soc Am*. (2020) 147:3646. doi: 10.1121/10.0001316
5. Rajan GP, Kontorinis G, Kuthubutheen J. The effects of insertion speed on inner ear function during cochlear implantation: a comparison study. *Audiol Neurootol*. (2013) 18:17–22. doi: 10.1159/000342821
6. Todt I, Mittmann P, Ernst A. Intracochlear fluid pressure changes related to the insertional speed of a CI electrode. *Biomed Res Int*. (2014) 2014:507241. doi: 10.1155/2014/507241
7. Aebischer P, Mantokoudis G, Weder S, Anschuetz L, Caversaccio M, Wimmer W. *In-vitro* study of speed and alignment angle in cochlear implant electrode array insertions. *IEEE Trans Biomed Eng*. (2021) 69:129–37. doi: 10.1109/TBME.2021.3088232
8. Topsakal V, Matulic M, Assadi MZ, Mertens G, Rompaey VV, Van de Heyning P. Comparison of the surgical techniques and robotic techniques for cochlear implantation in terms of the trajectories toward the inner ear. *J Int Adv Otol*. (2020) 16:3–7. doi: 10.5152/iao.2020.8113
9. De Seta D, Daoudi H, Torres R, Ferrary E, Sterkers O, Nguyen Y. Robotics, automation, active electrode arrays, and new devices for cochlear implantation: a contemporary review. *Hear Res*. (2022) 414:108425. doi: 10.1016/j.heares.2021.108425
10. Barriat S, Peigneux N, Duran U, Camby S, Lefebvre PP. The use of a robot to insert an electrode array of cochlear implants in the cochlea: a feasibility study and preliminary results. *Audiol Neurootol*. (2021) 26:361–7. doi: 10.1159/000513509
11. Available online at: https://clinicaltrials.gov/ct2/show/NCT04577118 (accessed October 31, 2021).
12. Caversaccio M, Gavaghan K, Wimmer W, Williamson T, Ansò J, Mantokoudis G, et al. Robotic cochlear implantation: surgical procedure and first clinical experience. *Acta Otolaryngol*. (2017) 137:447–54. doi: 10.1080/00016489.2017.1278573
13. Caversaccio M, Wimmer W, Anso J, Mantokoudis G, Gerber N, Rathgeb C, et al. Robotic middle ear access for cochlear implantation: First in man. *PLoS ONE*. (2019) 14:e0220543. doi: 10.1371/journal.pone.0220543
14. Topsakal V, Heuninck E, Matulic M, Tekin AM, Mertens G, Van Rompaey V, et al. Clinical Evaluation of a surgical robotic tool providing autonomous inner ear access for cochlear implantation. *Front Neurol*. (2021).
15. Klopp-Dutote N, Lefranc M, Strunski V, Page C. Minimally invasive fully ROBOT-assisted cochlear implantation in humans: preliminary results in five consecutive patients. *Clin Otolaryngol*. (2021) 46:1326–30. doi: 10.1111/coa.13840
16. Majdani O, Rau TS, Baron S, Eilers H, Baier C, Heimann B, et al. A robot-guided minimally invasive approach for cochlear implant surgery:

preliminary results of a temporal bone study. *Int J Comput Assist Radiol Surg*. (2009) 4:475–86. doi: 10.1007/s11548-009-0360-8
17. Torres R, Daoudi H, Lahlou G, Sterkers O, Ferrary E, Mosnier I, et al. Restoration of high frequency auditory perception after robot-assisted or manual cochlear implantation in profoundly deaf adults improves speech recognition. *Front Surg*. (2021) 8:729736. doi: 10.3389/fsurg.2021.729736
18. Jia H, Pan J, Gu W, Tan H, Chen Y, Zhang Z, et al. Robot-assisted electrode array insertion becomes available in pediatric cochlear implant recipients: first report and an intra-individual study. *Front Surg*. (2021) 8:695728. doi: 10.3389/fsurg.2021.695728
19. Sabban D, Parodi M, Blanchard M, Ettienne V, Rouillon I, Loundon N. Intra-cochlear electrode tip fold-over. *Cochlear Implants Int*. (2018) 19:225–9. doi: 10.1080/14670100.2018.1427823
20. Jwair S, Prins A, Wegner I, Stokroos RJ, Versnel H, Thomeer HGXM. Scalar translocation comparison between lateral wall and perimodiolar cochlear implant arrays - a meta-analysis. *Laryngoscope*. (2021) 131:1358–68. doi: 10.1002/lary.29224
21. Dietz A, Wennström M, Lehtimäki A, Löppönen H, Valtonen H. Electrode migration after cochlear implant surgery: more common than expected? *Eur Arch Otorhinolaryngol*. (2016) 273:1411–8. doi: 10.1007/s00405-015-3716-4
22. Gibson P, Boyd P. Optimal electrode design: straight versus perimodiolar. *Eur Ann Otorhinolaryngol Head Neck Dis*. (2016) 133(Suppl. 1):S63–5. doi: 10.1016/j.anorl.2016.04.014
23. Available online at: http://www.prisma-statement.org/ (accessed October 31, 2021).
24. Sterne JA, Hernan MA, Reeves BC, Savovic J, Berkman ND, Viswanathan M, et al. ROBINS-I: a tool for assessing risk of bias in non-randomized studies of interventions *BMJ*. (2016) 355:i4919. doi: 10.1136/bmj.i4919
25. Högerle C, Englhard A, Simon F, Grüninger I, Mlynski R, Hempel JM, et al. Cochlear implant electrode tip fold-over: our experience with long and flexible electrode. *Otol Neurotol*. (2021) 43:64–71. doi: 10.1097/MAO.0000000000003362
26. Klabbers TM, Huinck WJ, Heutink F, Verbist BM, Mylanus EAM. Transimpedance Matrix (TIM) measurement for the detection of intraoperative electrode tip foldover using the slim modiolar electrode: a proof of concept study. *Otol Neurotol*. (2021) 42:e124–9. doi: 10.1097/MAO.0000000000002875
27. Müller A, Kropp MH, Mir-Salim P, Aristeidou A, Dziemba OC. Intraoperatives tip-foldover-screening mittels spread of excitation messungen. *Z Med Phys*. (2021) 31:276–88. German. doi: 10.1016/j.zemedi.2020.07.002
28. Durakovic N, Kallogjeri D, Wick CC, McJunkin JL, Buchman CA, Herzog J. Immediate and 1-year outcomes with a slim modiolar cochlear implant electrode array. *Otolaryngol Head Neck Surg*. (2020) 162:731–6. doi: 10.1177/0194599820907336
29. Shaul C, Weder S, Tari S, Gerard JM, O'Leary SJ, Briggs RJ. Slim, modiolar cochlear implant electrode: melbourne experience and comparison with the contour perimodiolar electrode. *Otol Neurotol*. (2020) 41:639–43. doi: 10.1097/MAO.0000000000002617
30. Dimak B, Nagy R, Perenyi A, Jarabin JA, Schulcz R, Csanady M, et al. Review of electrode placement with the Slim Modiolar Electrode: identification and management. *Ideggyogy Sz*. (2020) 73:53–9. doi: 10.18071/isz.73.0053
31. Labadie RF, Schefano AD, Holder JT, Dwyer RT, Rivas A, O'Malley MR, et al. Use of intraoperative CT scanning for quality control assessment of cochlear implant electrode array placement. *Acta Otolaryngol*. (2020) 140:206–11. doi: 10.1080/00016489.2019.1698768
32. Heutink F, Verbist BM, Mens LHM, Huinck WJ, Mylanus EAM. The evaluation of a slim perimodiolar electrode: surgical technique in relation to intracochlear position and cochlear implant outcomes. *Eur Arch Otorhinolaryngol*. (2020) 277:343–50. doi: 10.1007/s00405-019-05696-y
33. Garaycochea O, Manrique-Huarte R, Lazaro C, Huarte A, Prieto C, Alvarez de Linera-Alperi M, et al. Comparative study of two different perimodiolar and a straight cochlear implant electrode array: surgical and audiological outcomes. *Eur Arch Otorhinolaryngol*. (2020) 277:69–76. doi: 10.1007/s00405-019-05680-6
34. Mittmann P, Lauer G, Ernst A, Mutze S, Hassepass F, Arndt S, et al. Electrophysiological detection of electrode fold-over in perimodiolar cochlear implant electrode arrays: a multi-center study case series. *Eur Arch Otorhinolaryngol*. (2020) 277:31–5. doi: 10.1007/s00405-019-05653-9
35. Iso-Mustajärvi M, Sipari S, Löppönen H, Dietz A. Preservation of residual hearing after cochlear implant surgery with slim modiolar electrode. *Eur Arch Otorhinolaryngol*. (2020) 277:367–75. doi: 10.1007/s00405-019-05708-x
36. McJunkin JL, Durakovic N, Herzog J, Buchman CA. early outcomes with a slim, modiolar cochlear implant electrode array. *Otol Neurotol*. (2018) 39:e28–33. doi: 10.1097/MAO.0000000000001652
37. Friedmann DR, Kamen E, Choudhury B, Roland JT Jr. surgical experience and early outcomes with a slim perimodiolar electrode. *Otol Neurotol*. (2019) 40:e304–10. doi: 10.1097/MAO.0000000000002129
38. Gomez Serrano M, Patel S, Harris R, Selvadurai D. Initial surgical and clinical experience with the Nucleus CI532 slim modiolar electrode in the UK. *Cochlear Implants Int*. (2019) 20:207–16. doi: 10.1080/14670100.2019.1597461
39. Timm ME, Majdani O, Weller T, Windeler M, Lenarz T, Büchner A, et al. Patient specific selection of lateral wall cochlear implant electrodes based on anatomical indication ranges. *PLoS ONE*. (2018) 13:e0206435. doi: 10.1371/journal.pone.0206435
40. Sipari S, Iso-Mustajärvi M, Löppönen H, Dietz A. the insertion results of a mid-scala electrode assessed by MRI and CBCT image fusion. *Otol Neurotol*. (2018) 39:e1019–25. doi: 10.1097/MAO.0000000000002045
41. Gabrielpillai J, Burck I, Baumann U, Stöver T, Helbig S. Incidence for tip foldover during cochlear implantation. *Otol Neurotol*. (2018) 39:1115–21. doi: 10.1097/MAO.0000000000001915
42. Jia H, Torres R, Nguyen Y, De Seta D, Ferrary E, Wu H, et al. Intraoperative conebeam CT for assessment of intracochlear positioning of electrode arrays in adult recipients of cochlear implants. *AJNR Am J Neuroradiol*. (2018) 39:768–74. doi: 10.3174/ajnr.A5567
43. Garaycochea O, Manrique-Huarte R, Manrique M. Intra-operative radiological diagnosis of a tip roll-over electrode array displacement using fluoroscopy, when electrophysiological testing is normal: the importance of both techniques in cochlear implant surgery. *Braz J Otorhinolaryngol*. (2020) 86 (Suppl 1):38–40. doi: 10.1016/j.bjorl.2017.05.003
44. Aschendorff A, Briggs R, Brademann G, Helbig S, Hornung J, Lenarz T, et al. Clinical investigation of the Nucleus Slim Modiolar Electrode. *Audiol Neurootol*. (2017) 22:169–79. doi: 10.1159/000480345
45. Zuniga MG, Rivas A, Hedley-Williams A, Gifford RH, Dwyer R, Dawant BM, et al. Tip fold-over in cochlear implantation: case series. *Otol Neurotol*. (2017) 38:199–206. doi: 10.1097/MAO.0000000000001283
46. Fischer N, Pinggera L, Weichbold V, Dejaco D, Schmutzhard J, Widmann G. Radiologic and functional evaluation of electrode dislocation from the scala tympani to the scala vestibuli in patients with cochlear implants. *AJNR Am J Neuroradiol*. (2015) 36:372–7. doi: 10.3174/ajnr.A4189
47. Dirr F, Hempel JM, Krause E, Müller J, Berghaus A, Ertl-Wagner B, et al. Value of routine plain x-ray position checks after cochlear implantation. *Otol Neurotol*. (2013) 34:1666–9. doi: 10.1097/MAO.0b013e3182a09cc3
48. Cosetti MK, Troob SH, Latzman JM, Shapiro WH, Roland JT Jr, Waltzman SB. An evidence-based algorithm for intraoperative monitoring during cochlear implantation. *Otol Neurotol*. (2012) 33:169–76. doi: 10.1097/MAO.0b013e3182423175
49. Riemann C, Scholtz LU, Gehl HB, Schürmann M, Sudhoff H, Todt I. Evaluation of cochlear implant electrode scalar position by 3 Tesla magnet resonance imaging. *Sci Rep*. (2021) 11:21298. doi: 10.1038/s41598-021-00824-3
50. Liebscher T, Mewes A, Hoppe U, Hornung J, Brademann G, Hey M. Electrode translocations in perimodiolar cochlear implant electrodes: audiological and electrophysiological outcome. *Z Med Phys*. (2021) 31:265–75. doi: 10.1016/j.zemedi.2020.05.004
51. Heutink F, Verbist B, van der Woude W, Meulman T, Briaire J, Frijns J, et al. Factors influencing speech perception in adults with a cochlear implant. *Ear and Hear*. (2021) 42:949–60. doi: 10.1097/AUD.0000000000000988
52. Ketterer MC, Aschendorff A, Arndt S, Speck I, Rauch AK, Beck R, et al. Radiological evaluation of a new straight electrode array compared to its precursors. *Eur Arch Otorhinolaryngol*. (2021). 278:3707–14. doi: 10.1007/s00405-020-06434-5

53. Lenarz T, Buechner A, Lesinski-Schiedat A, Timm M, Salcher R. Hearing preservation with a new atraumatic lateral wall electrode. *Otol Neurotol*. (2020) 41:e993–1003. doi: 10.1097/MAO.0000000000002714
54. Morrel WG, Holder JT, Dawant BM, Noble JH, Labadie RF. Effect of scala tympani height on insertion depth of straight cochlear implant electrodes. *Otolaryngol Head Neck Surg*. (2020) 162:718–24. doi: 10.1177/0194599820904941
55. Nassiri AM, Yawn RJ, Holder JT, Dwyer RT, O'Malley MR, Bennett ML, et al. Hearing preservation outcomes using a precurved electrode array inserted with an external sheath. *Otol Neurotol*. (2020) 41:33–8. doi: 10.1097/MAO.0000000000002426
56. Riggs WJ, Dwyer RT, Holder JT, Mattingly JK, Ortmann A, Noble JH, et al. Intracochlear electrocochleography: influence of scalar position of the cochlear implant electrode on postinsertion results. *Otol Neurotol*. (2019) 40:e503–10. doi: 10.1097/MAO.0000000000002202
57. Chakravorti S, Noble JH, Gifford RH, Dawant BM, O'Connell BP, Wang J, et al. Further evidence of the relationship between cochlear implant electrode positioning and hearing outcomes. *Otol Neurotol*. (2019). 40:617–24. doi: 10.1097/MAO.0000000000002204
58. Yamamoto N, Okano T, Yamazaki H, Hiraumi H, Sakamoto T, Ito J, et al. Intraoperative evaluation of cochlear implant electrodes using mobile cone-beam computed tomography. *Otol Neurotol*. (2019). 40:177–83. doi: 10.1097/MAO.0000000000002097
59. Shaul C, Dragovic AS, Stringer AK, O'Leary SJ, Briggs RJ. Scalar localisation of peri-modiolar electrodes and speech perception outcomes. *J Laryngol Otol*. (2018) 132:1000–6. doi: 10.1017/S0022215118001871
60. Koka K, Riggs WJ, Dwyer R, Holder JT, Noble JH, Dawant BM, et al. Intracochlear electrocochleography during cochear implant electrode insertion is predictive of final scalar location. *Otol Neurotol*. (2018) 39:e654–9. doi: 10.1097/MAO.0000000000001906
61. Ketterer MC, Aschendorff A, Arndt S, Hassepass F, Wesarg T, Laszig R, et al. The influence of cochlear morphology on the final electrode array position. *Eur Arch Otorhinolaryngol*. (2018) 275:385–94. doi: 10.1007/s00405-017-4842-y
62. An SY, An CH, Lee KY, Jang JH, Choung YH, Lee SH. Diagnostic role of cone beam computed tomography for the position of straight array. *Acta Otolaryngol*. (2018) 138:375–81. doi: 10.1080/00016489.2017.1404639
63. O'Connell BP, Hunter JB, Haynes DS, Holder JT, Dedmon MM, Noble JH, et al. Insertion depth impacts speech perception and hearing preservation for lateral wall electrodes. *Laryngoscope*. (2017) 127:2352–7. doi: 10.1002/lary.26467
64. O'Connell BP, Holder JT, Dwyer RT, Gifford RH, Noble JH, Bennett ML, et al. Intra- and postoperative electrocochleography may be predictive of final electrode position and postoperative hearing preservation. *Front Neurosci*. (2017) 11:291. doi: 10.3389/fnins.2017.00291
65. Mittmann P, Todt I, Ernst A, Rademacher G, Mutze S, Göricke S, et al. Radiological and NRT-ratio-based estimation of slim straight cochlear implant electrode positions: a multicenter study. *Ann Otol Rhinol Laryngol*. (2017) 126:73–8. doi: 10.1177/0003489416675355
66. Lathuillière M, Merklen F, Piron JP, Sicard M, Villemus F, Menjot de Champfleur N, et al. Cone-beam computed tomography in children with cochlear implants: The effect of electrode array position on ECAP. *Int J Pediatr Otorhinolaryngol*. (2017) 92:27–31. doi: 10.1016/j.ijporl.2016.10.033
67. O'Connell BP, Cakir A, Hunter JB, Francis DO, Noble JH, Labadie RF, et al. Electrode location and angular insertion depth are predictors of audiologic outcomes in cochlear implantation. *Otol Neurotol*. (2016) 37:1016–23. doi: 10.1097/MAO.0000000000001125
68. O'Connell BP, Hunter JB, Wanna GB. The importance of electrode location in cochlear implantation. *Laryngosc Investig Otolaryngol*. (2016) 1:169–74. doi: 10.1002/lio2.42
69. Wanna GB, Noble JH, Gifford RH, Dietrich MS, Sweeney AD, Zhang D, et al. Impact of intrascalar electrode location, electrode type, and angular insertion depth on residual hearing in cochlear implant patients: preliminary results. *Otol Neurotol*. (2015) 36:1343–8. doi: 10.1097/MAO.0000000000000829
70. Nordfalk KF, Rasmussen K, Hopp E, Bunne M, Silvola JT, Jablonski GE. Insertion depth in cochlear implantation and outcome in residual hearing and vestibular function. *Ear Hear*. (2016) 37:e129–37. doi: 10.1097/AUD.0000000000000241
71. Mittmann P, Rademacher G, Mutze S, Ernst A, Todt I. Electrode migration in patients with perimodiolar cochlear implant electrodes. *Audiol Neurootol*. (2015) 20:349–53. doi: 10.1159/000435873
72. Boyer E, Karkas A, Attye A, Lefournier V, Escude B, Schmerber S. Scalar localization by cone-beam computed tomography of cochlear implant carriers: a comparative study between straight and periomodiolar precurved electrode arrays. *Otol Neurotol*. (2015) 36:422–9. doi: 10.1097/MAO.0000000000000705
73. Wanna GB, Noble JH, Carlson ML, Gifford RH, Dietrich MS, Haynes DS, et al. Impact of electrode design and surgical approach on scalar location and cochlear implant outcomes. *Laryngoscope*. (2014) 124(Suppl. 6):S1–7. doi: 10.1002/lary.24728
74. Nordfalk KF, Rasmussen K, Hopp E, Greisiger R, Jablonski GE. Scalar position in cochlear implant surgery and outcome in residual hearing and the vestibular system. *Int J Audiol*. (2014) 53:121–7. doi: 10.3109/14992027.2013.854413
75. Aschendorff A, Klenzner T, Arndt S, Beck R, Schild C, Röddiger L, et al. Insertionsergebnisse von Contour^{TM}- und Contour-Advance^{TM}-Elektroden: Gibt es individuelle Lernkurven? [Insertion results for Contour^{TM} and Contour Advance^{TM} electrodes: are there individual learning curves?]. *HNO*. (2011) 59:448–52. German. doi: 10.1007/s00106-011-2319-7
76. Lane JI, Witte RJ, Driscoll CL, Shallop JK, Beatty CW, Primak AN. Scalar localization of the electrode array after cochlear implantation: clinical experience using 64-slice multidetector computed tomography. *Otol Neurotol*. (2007) 28:658–62. doi: 10.1097/MAO.0b013e3180686e26
77. Ozer F, Yavuz H, Yilmaz I, Ozluoglu LN. Cochlear implant failure in the pediatric population. *J Audiol Otol*. (2021) 25:217–23. doi: 10.7874/jao.2021.00325
78. Chan CY, Wang F, Omar H, Tan HKK. Traumatic cochlear implant electrode extrusion: considerations, management, and outcome. *Case Rep Otolaryngol*. (2021) 2021:2918859. doi: 10.1155/2021/2918859
79. von Mitzlaff C, Dalbert A, Winklhofer S, Veraguth D, Huber A, Röösli C. Electrode migration after cochlear implantation. *Cochlear Implants Int*. (2021) 22:103–10. doi: 10.1080/14670100.2020.1833516
80. Leinung M, Helbig S, Adel Y, Stöver T, Loth AG. The effect of a bone groove against cochlear implant electrode migration. *Otol Neurotol*. (2019) 40:e511–7. doi: 10.1097/MAO.0000000000002228
81. Philip Rajan D, Siti Sabzah MH, Zulkiflee S, Tengku Mohamed I, Kumareysh Vijay V, Iskandar H, et al. Surgical and functional outcomes of cochlear implantation in post-lingual and cross-over patients: first 5-year review of the National Ministry of Health Malaysia cochlear implant programme. *Med J Malaysia*. (2018) 73:393–6. PMID: 30647210.
82. Çelik M, Orhan KS, Öztürk E, Avci H, Polat B, Güldiken Y. Impact of routine plain X-ray on postoperative management in cochlear implantation. *J Int Adv Otol*. (2018) 14:365–9. doi: 10.5152/iao.2018.4252
83. Rader T, Baumann U, Stöver T, Weissgerber T, Adel Y, Leinung M, et al. Management of cochlear implant electrode migration. *Otol Neurotol*. (2016) 37:e341–8. doi: 10.1097/MAO.0000000000001065
84. Patnaik U, Sikka K, Agarwal S, Kumar R, Thakar A, Sharma SC. Cochlear re-implantation: lessons learnt and the way ahead. *Acta Otolaryngol*. (2016) 136:564–7. doi: 10.3109/00016489.2015.1136430
85. Jeppesen J, Faber CE. Surgical complications following cochlear implantation in adults based on a proposed reporting consensus. *Acta Otolaryngol*. (2013) 133:1012–21. doi: 10.3109/00016489.2013.797604
86. van der Marel KS, Verbist BM, Briaire JJ, Joemai RM, Frijns JH. Electrode migration in cochlear implant patients: not an exception. *Audiol Neurootol*. (2012) 17:275–81. doi: 10.1159/000338475
87. Lavinsky-Wolff M, Lavinsky L, Dall'Igna C, Lavinsky J, Setogutti E, Viletti MC. Transcanal cochleostomy in cochlear implant surgery: long-term results of a cohort study. *Braz J Otorhinolaryngol*. (2012) 78:118–23. doi: 10.1590/S1808-86942012000200018
88. Brown KD, Connell SS, Balkany TJ, Eshraghi AE, Telischi FF, Angeli SA. Incidence and indications for revision cochlear implant surgery in adults and children. *Laryngoscope*. (2009) 119:152–7. doi: 10.1002/lary.20012

89. Connell SS, Balkany TJ, Hodges AV, Telischi FF, Angeli SI, Eshraghi AA. Electrode migration after cochlear implantation. *Otol Neurotol*. (2008) 29:156–9. doi: 10.1097/mao.0b013e318157f80b
90. Green KM, Bhatt YM, Saeed SR, Ramsden RT. Complications following adult cochlear implantation: experience in Manchester. *J Laryngol Otol*. (2004) 118:417–20. doi: 10.1258/002221504323219518
91. Roland JT Jr, Fishman AJ, Waltzman SB, Alexiades G, Hoffman RA, Cohen NL. Stability of the cochlear implant array in children. *Laryngoscope*. (1998) 108(8 Pt 1):1119–23. doi: 10.1097/00005537-199808000-00003
92. de Jong AL, Nedzelski J, Papsin BC. Surgical outcomes of paediatric cochlear implantation: the Hospital for Sick Children's experience. *J Otolaryngol*. (1998) 27:26–30.
93. Quesnel AM, Nakajima HH, Rosowski JJ, Hansen MR, Gantz BJ, Nadol JB Jr. Delayed loss of hearing after hearing preservation cochlear implantation: human temporal bone pathology and implications for etiology. *Hear Res*. (2016) 333:225–34. doi: 10.1016/j.heares.2015.08.018
94. Dhanasingh A, Jolly C. Review on cochlear implant electrode array tip fold-over and scalar deviation. *J Otol*. (2019) 14:94–100. doi: 10.1016/j.joto.2019.01.002
95. Briggs RJ, Tykocinski M, Lazsig R, Aschendorff A, Lenarz T, Stöver T, et al. Development and evaluation of the modiolar research array–multi-centre collaborative study in human temporal bones. *Cochlear Implants Int*. (2011) 12:129–39. doi: 10.1179/1754762811Y0000000007
96. Torres R, Jia H, Drouillard M, Bensimon JL, Sterkers O, Ferrary E, et al. An optimized robot-based technique for cochlear implantation to reduce array insertion trauma. *Otolaryngol Head Neck Surg*. (2018) 159:900–7. doi: 10.1177/0194599818792232
97. Kamakura T, Nadol JB Jr. Correlation between word recognition score and intracochlear new bone and fibrous tissue after cochlear implantation in the human. *Hear Res*. (2016) 339:132–41. doi: 10.1016/j.heares.2016.06.015
98. Gstoettner WK, van de Heyning P, O'Connor AF, Morera C, Sainz M, Vermeire K, et al. Electric acoustic stimulation of the auditory system: results of a multi-centre investigation. *Acta Otolaryngol*. (2008) 128:968–75. doi: 10.1080/00016480701805471
99. Helbig S, Adel Y, Rader T, Stöver T, Baumann U. Long-term hearing preservation outcomes after cochlear implantation for electric-acoustic stimulation. *Otol Neurotol*. (2016) 37:e353–9. doi: 10.1097/MAO.0000000000001066
100. Ishiyama A, Doherty J, Ishiyama G, Quesnel AM, Lopez I, Linthicum FH. Post hybrid cochlear implant hearing loss and endolymphatic hydrops. *Otol Neurotol*. (2016) 37:1516–21. doi: 10.1097/MAO.0000000000001199
101. Mueller F, Hermann J, Weber S, O'Toole Bom Braga G, Topsakal V. Image-based planning of minimally traumatic inner ear access for robotic cochlear implantation. *Front Surg*. (2021) 8:761217. doi: 10.3389/fsurg.2021.761217
102. Torres R, Kazmitcheff G, De Seta D, Ferrary E, Sterkers O, Nguyen Y. Improvement of the insertion axis for cochlear implantation with a robot-based system. *Eur Arch Otorhinolaryngol*. (2017) 274:715–21. doi: 10.1007/s00405-016-4329-2
103. Torres R, Kazmitcheff G, Bernardeschi D, De Seta D, Bensimon JL, Ferrary E, et al. Variability of the mental representation of the cochlear anatomy during cochlear implantation. *Eur Arch Otorhinolaryngol*. (2016) 273:2009–18. doi: 10.1007/s00405-015-3763-x
104. Kim JR, Tejani VD, Abbas PJ, Brown CJ. Intracochlear recordings of acoustically and electrically evoked potentials in nucleus hybrid L24 cochlear implant users and their relationship to speech perception. *Front Neurosci*. (2017) 11:216. doi: 10.3389/fnins.2017.00216
105. Lorens A, Walkowiak A, Polak M, Kowalczuk A, Furmanek M, Skarzynski H, et al. Cochlear microphonics in hearing preservation cochlear implantees. *J Int Adv Otol*. (2019) 15:345–51. doi: 10.5152/iao.2019.6334
106. Jablonski GE, Falkenberg-Jensen B, Bunne M, Iftikhar M, Greisiger R, Opheim LR, et al. Fusion of technology in cochlear implantation surgery: investigation of fluoroscopically assisted robotic electrode insertion. *Front Surg*. (2021) 8:741401. doi: 10.3389/fsurg.2021.741401
107. Almuhawas FA, Dhanasingh AE, Mitrovic D, Abdelsamad Y, Alzhrani F, Hagr A, et al. Age as a factor of growth in mastoid thickness and skull width. *Otol Neurotol*. (2020) 41:709–14. doi: 10.1097/MAO.0000000000002585
108. Müller J, Schön F, Helms J. Sichere Fixierung von Cochlear-Implant-Elektrodenträgern bei Kindern und Erwachsenen–erste Erfahrungen mit einem neuen Titan-Clip [Reliable fixation of cochlear implant electrode mountings in children and adults–initial experiences with a new titanium clip]. *Laryngorhinootologie*. (1998) 77:238–40. doi: 10.1055/s-2007-996968
109. Loth AG, Adel Y, Weiß R, Helbig S, Stöver T, Leinung M. Evaluation of a bone groove geometry for fixation of a cochlear implant electrode. *Eur Arch Otorhinolaryngol*. (2020) 277:385–92. doi: 10.1007/s00405-019-05713-0
110. Available online at: https://medel.webgate.media/en/directlink/1c9497505fe490ba/133240# (accessed October 31, 2021).
111. Daoudi H, Lahlou G, Torres R, Sterkers O, Lefeuvre V, Ferrary E, et al. Robot-assisted cochlear implant electrode array insertion in adults: a comparative study with manual insertion. *Otol Neurotol*. (2021) 42:e438–44. doi: 10.1097/MAO.0000000000003002
112. Drouillard M, Torres R, Mamelle E, De Seta D, Sterkers O, Ferrary E, et al. Influence of electrode array stiffness and diameter on hearing in cochlear implanted guinea pig. *PLoS ONE*. (2017) 12:e0183674. doi: 10.1371/journal.pone.0183674
113. Dhanasingh A, Jolly C. An overview of cochlear implant electrode array designs. *Hear Res*. (2017) 356:93–103. doi: 10.1016/j.heares.2017.10.005
114. Li H, Helpard L, Ekeroot J, Rohani SA, Zhu N, Rask-Andersen H, et al. Three-dimensional tonotopic mapping of the human cochlea based on synchrotron radiation phase-contrast imaging. *Sci Rep*. (2021) 11:4437. doi: 10.1038/s41598-021-83225-w
115. Helpard L, Li H, Rohani SA, Zhu N, Rask-Andersen H, Agrawal SK, et al. An approach for individualized cochlear frequency mapping determined from 3D synchrotron radiation phase-contrast imaging. *IEEE Trans Biomed Eng*. (2021) 68:3602–11. doi: 10.1109/TBME.2021.3080116
116. Breitsprecher T, Dhanasingh A, Schulze M, Kipp M, Dakah RA, Oberhoffner T, et al. CT imaging-based approaches to cochlear duct length estimation-a human temporal bone study. *Eur Radiol*. (2022) 32:1014–23. doi: 10.1007/s00330-021-08189-x
117. Mlynski R, Lüsebrink A, Oberhoffner T, Langner S, Weiss NM. Mapping cochlear duct length to electrically evoked compound action potentials in cochlear implantation. *Otol Neurotol*. (2021) 42:e254–60. doi: 10.1097/MAO.0000000000002957

Conflict of Interest: MK is the chief surgeon and Director of Madras ENT Research Foundation Pvt. LTD., which is the organization he founded and for which he is currently working for.

The remaining authors declare that the research was conducted in the absence of any commercial or financial relationships that could be construed as a potential conflict of interest.

Publisher's Note: All claims expressed in this article are solely those of the authors and do not necessarily represent those of their affiliated organizations, or those of the publisher, the editors and the reviewers. Any product that may be evaluated in this article, or claim that may be made by its manufacturer, is not guaranteed or endorsed by the publisher.

frontiers | Frontiers in Neurology

ORIGINAL RESEARCH
published: 25 April 2022
doi: 10.3389/fneur.2022.829478

Minimally Invasive Cochlear Implantation: First-in-Man of Patient-Specific Positioning Jigs

Rolf Salcher[1†], Samuel John[2*†], Jan Stieghorst[2], Marcel Kluge[2], Felix Repp[2], Max Fröhlich[1,3] and Thomas Lenarz[1]*

[1] Department of Otolaryngology, Hannover Medical School, Hannover, Germany, [2] OtoJig GmbH, Hannover, Germany, [3] MED-EL Research Center, Hannover, Germany

A minimally-invasive surgical (MIS) approach to cochlear implantation, if safe, practical, simple in surgical handling, and also affordable has the potential to replace the conventional surgical approaches. Our MIS approach uses patient-specific drilling templates (positioning jigs). While the most popular MIS approaches use robots, the robotic aspect is literally put aside, because our high-precision parallel kinematics is only used to individualize a positioning jig. This jig can then be mounted onto a bone-anchored mini-stereotactic frame at the patient's skull and used to create a drill-hole through the temporal bone to the patient's cochlea. We present the first clinical experience where we use sham drill bits of different diameters instead of drilling into the bone in order to demonstrate the feasibility and accuracy.

Keywords: minimally invasive, stereotactic, frame, jig, robotic, clinical trial, image-guided surgery, cochlear implant

OPEN ACCESS

Edited by:
Paul Van De Heyning, University of Antwerp, Belgium

Reviewed by:
Daniel Baumgarten, Private University for Health Sciences, Medical Informatics and Technology (UMIT), Austria
Isabelle Mosnier, Hôpitaux Universitaires Pitié Salpêtrière, France

***Correspondence:**
Rolf Salcher
salcher.rolf@mh-hannover.de
Samuel John
john.samuel@otojig.com

[†] These authors have contributed equally to this work and share first authorship

Specialty section:
This article was submitted to Neuro-Otology, a section of the journal Frontiers in Neurology

Received: *05 December 2021*
Accepted: *16 February 2022*
Published: *25 April 2022*

Citation:
Salcher R, John S, Stieghorst J, Kluge M, Repp F, Fröhlich M and Lenarz T (2022) Minimally Invasive Cochlear Implantation: First-in-Man of Patient-Specific Positioning Jigs. Front. Neurol. 13:829478. doi: 10.3389/fneur.2022.829478

1. INTRODUCTION

Cochlear implant (CI) surgery is widely regarded as a success story (1). However, while CI technology has continuously improved (2), the surgical technique used in implantation has not changed significantly in its basic approach since 1961 (3). With the goal of inserting an electrode array with a diameter of maximally 1.3 mm, a transmastoid procedure with posterior tympanotomy is usually performed (4). Because this conventional procedure requires an open surgery, which is recommended to be performed only in highly specialized clinics by CI surgeons with several years of experience and training (5), it is no surprise that clinicians and researchers have investigated automation and minimally-invasive surgical (MIS) approaches. These could have the potential to overcome the disadvantages inherent in the manual procedure (6–8).

Considering the widely-used transmastoid surgical access and following the path of the electrode array insertion, it becomes clear that there is a straight line of sight from the surface of the skull through the facial recess toward the cochlea. This straight line justifies aiming for a straight minimally-invasive access path (9). In MIS, the access path has to be defined based on radiological imaging data rather than by visually exposing anatomical landmarks during open surgery. Conceptually, the step of bringing a virtually planned access path to the patient involves an image-to-patient registration and there are high accuracy requirements (10). As all relevant landmarks are embedded within the temporal bone, the skull surface is well suited to establish such necessary registration. This is usually realized either by navigational markers attached rigidly to the skull or by directly bone-anchoring a guidance apparatus to the patient's skull. The first option

requires an active control loop to navigate a surgical drilling robot. The latter option is to use a passive bone-anchored stereotactic system that guides the surgical drill.

We have previously presented the accuracy and suitability of our passive, bone-anchored mini-stereotactic frame with patient-specific positioning jigs *in vitro* and *ex vivo* tests (11, 12). Herein, we present the first results of the clinical feasibility. The aims are to (1) confirm sufficient accuracy under the conditions in the operating theater and (2) investigate the suitability of our workflow. The aim of this trial, as agreed with the institutional ethics committee, is neither the minimally-invasive drilling of the access path nor the electrode insertion. We are using sham drill bits to check the accuracy similar to an approach suggested by Labadie et al. (13). Here, we report about our experience and the results from the first six out of 10 patients enrolled in this trial.

2. MATERIALS AND METHODS

2.1. Description of the Clinical Trial

This clinical trial was designed as a prospective, open, interventional, monocentric, research trial, conducted at the primary sponsor Medical School Hannover (MHH) in Hannover, Germany. The study was approved by the ethics committee of MHH (vote no. 9030_BO_S_2020 from 2020-06-15), registered as DRKS00025035 at DRKS with the title "Intraoperative feasibility of patient individual positioning and guiding jigs for cochlear implantation." A self-developed prototype system was used as described in section "System description."

2.2. Inclusion and Exclusion Criteria

To be included, potential participants had to be adult CI candidates (aged 18–75 years). Exclusion criteria were revision CI surgery or having had a previous illness or condition that required a mastoidectomy or acute infection in the middle ear or the mastoid.

2.3. System Description

The following components were developed and used in the trial:

- A reusable mini-stereotactic frame (frame) made of titanium (**Figure 1**). This frame has a C-shaped symmetrical design to fit posterior to left and right ears in adults. The frame consists of three pins which shall be in direct contact with the skull surface.
- A self-tapping bone screw (diameter 2.0 mm, length 6.0 mm, Synthes GmbH, Selzach, Switzerland), placed inside the triangular shaped area, spanned by the three pins, fixes the frame firmly on the skull in order to restrict any movements.
- An anchor and a mounting screw, both made of titanium.
- An X-ray marker made of a biocompatible polyphenylsulfone and containing multiple X-ray dense titanium balls, fixated at defined positions, can be mounted onto the frame. This X-ray marker can be automatically localized by our planning software in beam and/or computed tomography volume images (**Figure 1C**).
- The planning software is implemented in the Python programming language (14) as a plugin to the open source 3DSlicer imaging platform (15), mainly using the libraries NumPy (16), SciPy (17), and vtk (18). Additionally, the planning software allows automatic registration of the X-ray marker images and anatomical segmentation of the target and risk structures to be performed semi-automatically. It also allows the planning of minimally invasive access paths.
- The planned access path is then transferred to a fully automated on-site manufacturing system, which intraoperatively produces the patient-specific positioning jig. This jig receives the individual through-hole at the position and angle which corresponds exactly (12) to the already planned access path when mounted onto the frame.
- The positioning jig and the X-ray marker are mounted with three jig fasteners, which allow for simple, fast, and stable fixation. However, in case of emergency, the jig fasteners can be released quickly without any tools for full access to the sites.

Our design goal was to have the benefits from using a robot, like automation and high accuracy, without the risks of having a robot acting directly *in situ* at the patient.

2.4. Surgical Workflow

To fixate the frame onto the patient's skull, first the incision area was shaved and the position for the attachment of the frame was identified, see **Figure 2A**. The orbitomeatal line, passing through the outer canthus of the eye and the center of the EAC (19) can be used to position the frame, as depicted in **Figure 2B**. Otherwise, preoperative bone thickness measurements and planning of the optimal position with our software can further support in finding an optimal position (**Figures 2C,D**).

Once the intended position was identified and marked, the surgical site was disinfected and covered with sterile plastic foil, following the standard OR protocol. Next, the sterile titanium frame was fixated. In a first step, a 5-7 cm incision that allows the conventional approach, was performed. If the position of the frame fixation screw did not fall within this area, an additional incision of about 1 cm was performed at the location needed. The size of the incision was measured afterward with a sterile ruler. To ensure that the pins of the frame sat directly on the skull, the skin was punctured in additional positions (**Figure 3A**) and the periost was removed (**Figure 3B**). The self-tapping bone screw requires pre-drilling. This was performed with a small 1.5 mm diamond bur (**Figure 3C**) and the frame was used as a template to guide the surgeon in the pre-drilling. As described above, the bone screw fixes a small anchor onto the skull. The frame is tightly fixed onto this anchor *via* the mounting screw (**Figures 3D,F**). For optimal stabilization, both the bone screw and mounting screw are tightened to a defined range of 30–35 Ncm (**Figures 3E,G**) with a torque ratchet (Josef Ganter Feinmechanik GmbH, Germany). The surgeon manually checked that the frame was firmly fixated onto the skull by carefully attempting to manually pull and rotate the assembly.

For acquiring the imaging data and planning the patient-individual access path, the X-ray marker was mounted onto the frame and fixated with three jig fasteners (**Figure 4A**). Then, an intraoperative cone beam computed tomography (CBCT) scan was acquired on an xCAT IQ (Xoran Technologies LLC, USA)

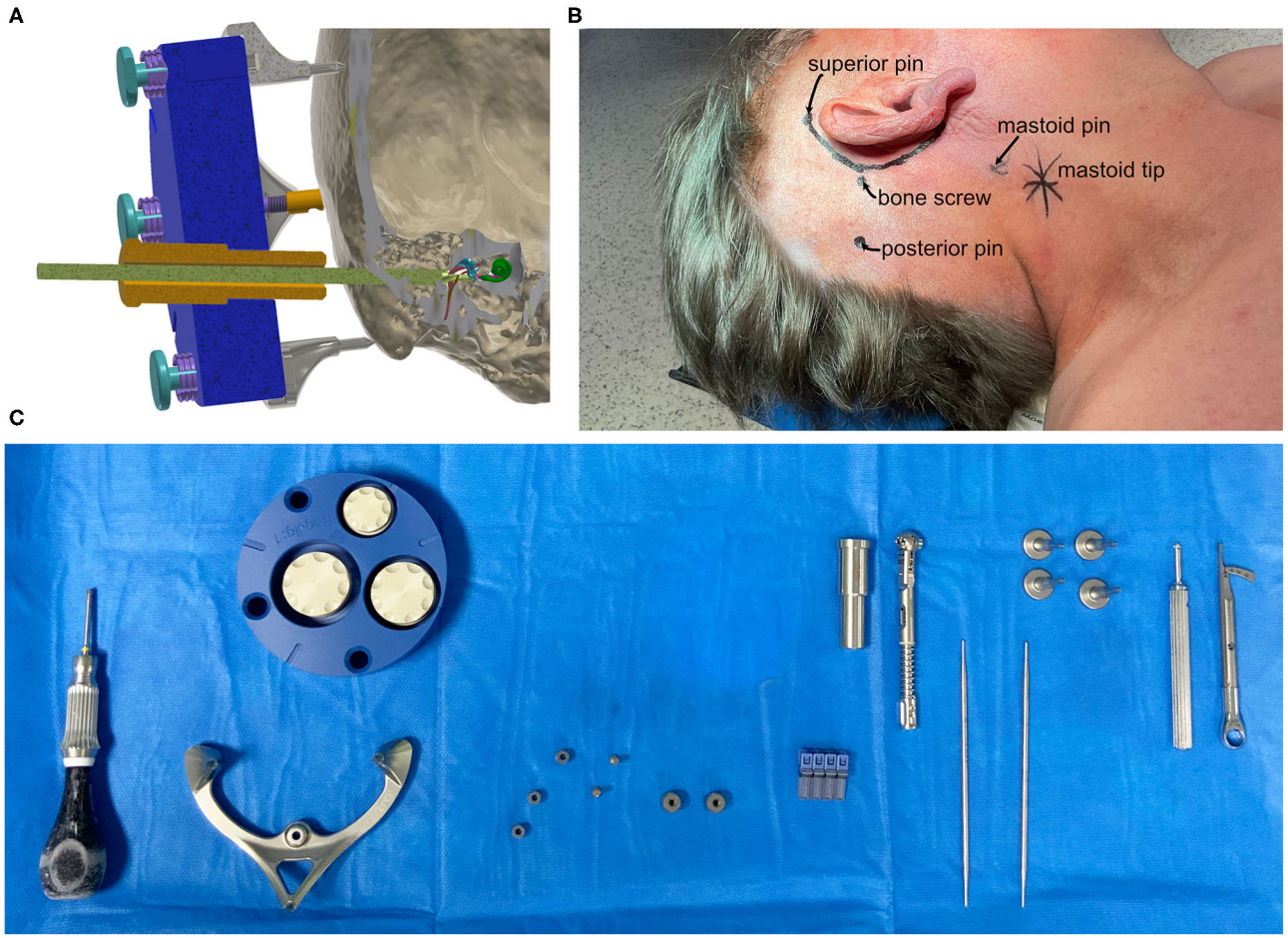

FIGURE 1 | (A) Schematic cut-plane-rendering of the proposed mini-stereotactic frame carrying a patient-specific positioning jig (blue) with a tool guide (orange) and a drill bit (green) advanced through the temporal bone toward the entry of the cochlea. The frame and the positioning jig are connected with three jig fasteners. **(B)** The positions of the pins of the mini-stereotactic frame and the position of the bone screw indicated on a patient (case 06). **(C)** From left to right, the sterilized set in the operating theater; screw driver, mini-stereotactic frame, X-ray marker, anchor, mounting screws, bone screws, tool guide, torque ratchet, and sham drill bits, jig fastener pins, screw driver, and torque limiter.

with 0.3 mm isometric voxel size (**Figure 4B**). The DICOM data were exported to a USB stick.

After importing the data into our planning software, an automated localization of the X-ray marker and semi-automatic segmentation of the target and risk structures were performed. The surgeon corrected and confirmed any segmentation suggestions presented by the planning software. The access path was semi-automatically planned by selecting its target at the round window. It was then visualized in 3D. The in-plane and off-plane insertion angles into the cochlea were visualized for the surgeon to further manipulate the access path and to plan a preferred trajectory for electrode array insertion, refer to **Figure 5A**. Furthermore, the software provided an inline view of the path to show the minimal distances to risk structures and to assess the margins. Instead of the not uniquely defined width of the facial recess, we measured the effective shortest distances from the centerline of the planned drill path to the facial nerve (FN) and the chorda tympani (CT) because those numbers can be directly compared to the radius of the drill bits (**Figure 5B**). A margin of at least 0.3 mm to the FN was aimed for. If preferred, the surgeon can further adapt the access path. Finally, the surgeon must confirm the planned access path.

To manufacture the patient-specific positioning jig based on previously-performed planning, the coordinates of the access path were wirelessly transferred to the fully automated manufacturing system. The machine consists of a high-precision hexapod, which is a parallel robot, and a linear axis with a drill unit in order to drill a through-hole into a blank jig. The position and orientation of the jig's through-hole represent the planned access path. Once the positioning jig is mounted onto the frame, this patient-specific through-hole aligns with the planning. After a production time of approximately 5 min (**Figure 6A**), the individualized positioning jig was taken out of the machine, measured with the coordinate measurement machine, disinfected, and steam sterilized. The sterilization was performed at the central sterilization facilities of the hospital in

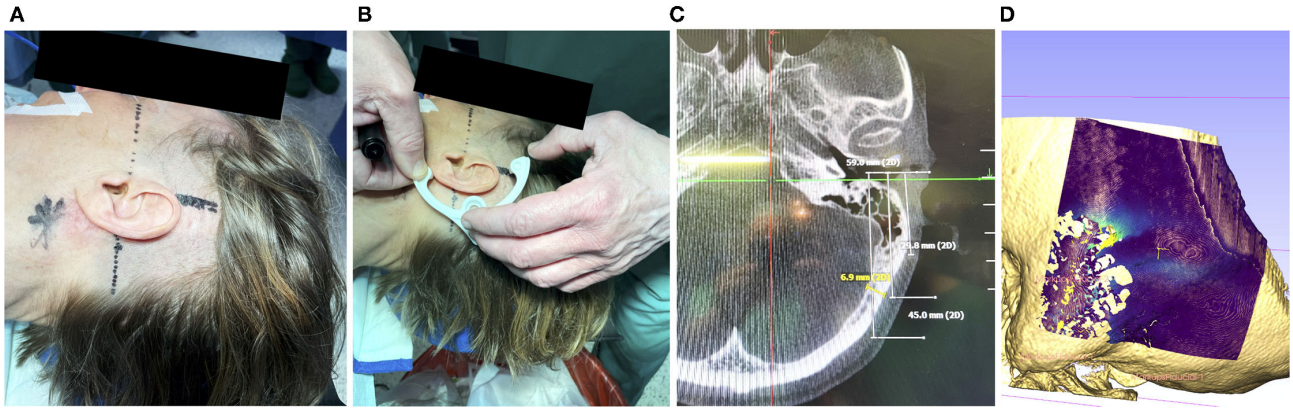

FIGURE 2 | (A) Prior to disinfection of the surgical field, marking the mastoid tip (star shaped), drawing the orbitomeatal line (dashed) and line perpendicular (solid) can help to position the frame. **(B)** A non-sterile 3d-printed dummy frame can be useful to mark the incision points and the location where the bone screw shall be placed. **(C)** Optionally, if a navigation system has been set up, the bone thickness at the designated screw position can be documented (in this case 6.9 mm). **(D)** If a preoperative scan is available, the bone thickness can be visualized. Visible are the artifacts due to the air-filled mastoid cells and the lower bone thickness at the sigmoid sinus.

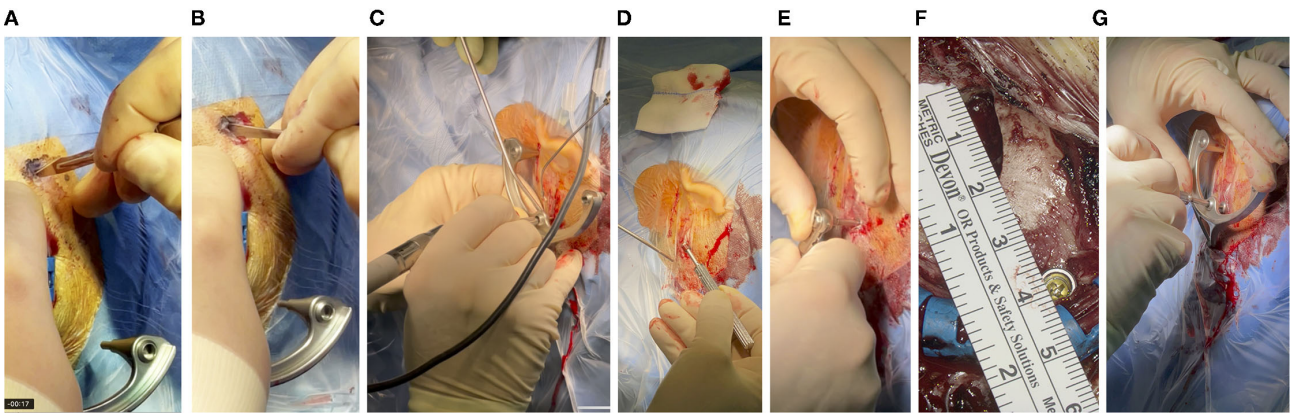

FIGURE 3 | (A) With a thin scalpel, the skin is punctured through the foil at the three marked spots for the pins of the frame, resulting in incision lengths of about 4-6 mm. **(B)** The periost is scraped so that the pin of the frame can be pressed directly onto the skull surface. **(C)** Pre-drilling and **(D)** fixation of the anchor, with a bone screw and **(E)** toque ratchet, **(F)** about 4 cm posterior to the EAC. **(G)** The same ratchet was used to attach the frame to the skull with the mounting screw, which in turn screws onto the anchor.

the routine process. After that, the individualized positioning jig was put in a sterile barrier system, labeled, and transported to the operating theater.

In the final step, the positioning jig was handed over to the surgeon, unpacked, and attached to the frame with the jig fasteners (**Figure 6B**). The tool guide was inserted into the through-hole of the positioning jig in order to guide the different sizes of sham drill bits. The sham drill bits and the tool guide were designed with a tight clearance fit (can only slide forward and backward with one degree of freedom) into the through-hole of the positioning jig. By this, they simulate different drill bits for the minimally-invasive approach for the previously planned access path. For the purpose of this trial, the mastoidectomy has already been performed in the meantime and the sham drill bits are just used to simulate the minimally-invasive access path for accuracy evaluation. For documentation reasons, the positioning jig contains two through-holes: the main through-hole, as described above, to guide the sham drill bit and an additional hole that can be used to visually inspect the situs under the positioning jig endoscopically or microscopically (**Figure 6C**).

After accuracy evaluation, our components were removed. Electrode array insertion and implant placement were performed as per our conventional techniques for CI surgery.

2.5. Evaluation Method

A conventional opening for CI implantation including mastoidectomy and posterior tympanotomy was performed while the mini-stereotactic frame was fixated on the participant's skull. In parallel, planning the access path and production of a patient-specific jig was performed. The primary outcome was a qualitative assessment of the workflow with regard to the

FIGURE 4 | (A) Mounting X-ray marker (blue). The X-ray marker has dense markers embedded, which help to localize the markers in the imaging and thereby the position of the frame can be determined. **(B)** Acquiring a cone beam computed tomography (CBCT) scan. To avoid contamination, the patient's head is covered with sterile foil.

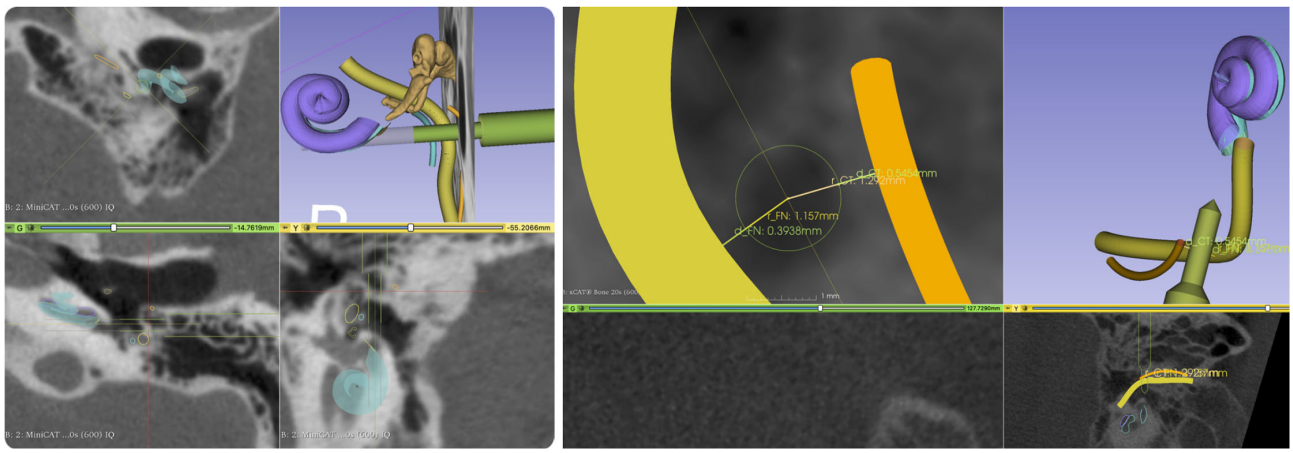

FIGURE 5 | (A) Screenshot from our planning software. An access path (green) is planned with a diameter of 1.5 mm and 3 mm through the facial recess. The facial nerve (FN) is shown in yellow and the chorda tympani (CT) in orange. **(B)** A close-up of the projection view in the direction of the planned drill path. Here, we do not measure the width of the facial recess but the effective width referred to the central axis of the planned access path. To better compare drill diameter to the facial recess width, we report two distances, one for each nerve.

planning, based on radiological image data, the production, and the attachment of the patient-specific jig to the mini-stereotactic frame. A secondary outcome was a subjective assessment of the fixation procedure and the resulting fixation strength of the mini-stereotactic frame. Instead of minimally-invasive drilling, a semi-quantitative evaluation of the overall accuracy was performed by inserting sham drill bits through a guidance through-hole in the patient-specific jigs (**Figures 1A,C**). Since the surgical site has already been completely opened and the facial recess has been exposed, we were able, with a surgical microscope or an endoscope, to assess and document the following binary properties:

- Does a sham drill bit point through the open space in the facial recess without touching any of the identified risk structures?
- What is the largest diameter of the sham drill bit that can be pointed through the facial recess?
- Does the 3 mm diameter shaft of the sham drill bit touch the external auditory canal (EAC) wall?

FIGURE 6 | (A) The (white) blank jig inside of the automated manufacturing machine, and **(B)** mounted on the frame. **(C)** A tool guide is put into the main through-hole and the sham drill bit can be inserted into the tool guide. The second through-hole can be used to inspect the path inside the conventionally opened area.

Diameters of 1.5, 1.8, 2.2, and 2.6 mm were tested. The smallest diameter was chosen to allow just enough space to insert a MED-EL Flex electrode lead with a maximal diameter of 1.3 mm. The 1.8 mm diameter was chosen because it has been reported by other research groups in this area. The accuracy of the jig manufacturing process was measured with a tactile coordinate measurement machine (8-axis FARO Quantum S / FaroArm V2, FARO Technologies, Inc.) and the effective deviations at the projected depth of the target point of the access path are computed.

2.6. Research Hypothesis

The hypothesis of this feasibility investigation: If the sham drill bit is

1. restricted in degrees of freedom along the planned path by guiding it through our patient-specific positioning jig, and
2. the tip points through the facial recess in the conventionally opened mastoid and posterior tympanotomy,

then it follows that

- the anatomical segmentations in the planning software,
- the planned path,
- the mini-stereotactic frame,
- the stability of bone fixation of the mini-stereotactic frame onto the skull,
- the accuracy of the X-ray marker and its automatic localization in the software,
- the jig manufacturing process,
- the attachment of the positioning jig to the frame, and
- the chosen diameter of said sham drill bit,

in combination, can be considered suitable for an MIS. The thickness of the bone layer above the chorda tympani and FN will be considered safe by surgeons based on the situation *in situ*.

3. RESULTS

The CI surgeries were performed by three different surgeons between April and December 2021. No adverse or serious adverse events related to the trial occurred. The surgery, including the general anesthesia, was well tolerated by all patients. Temporary wound dehiscence in patient 01 could be attributed to reasons outside of the trial.

3.1. Frame Fixation

After performing skin incisions (3x about 5 mm for the three pins and one 10 mm in length for the bone screw), it was possible to remove the periost through small skin incisions at the positions of the three pins. The procedure for fixation of the frame, including pre-drilling and tightening the self-tapping bone screw was completed in, on average, 27 min (range 14–49 min). In two cases, however, the pre-drilling was attempted without using the frame to guide the direction of pre-drilling. This resulted in a hole too wide for the 2.0 mm bone screw. The fixation then had to be performed with a bone screw of the same length but with a larger diameter of 2.4 mm. Due to this, the fixation took a maximum of 49 min. The torque to tighten the bone screw and the mounting screw for attaching the frame could both be set with the torque ratchet to the predefined 30–35 Ncm. We subjectively confirmed a rigid fixation of the frame by carefully attempting to pull, move, and rotate the frame. In all cases, the frame remained rigidly fixated throughout the surgery.

3.2. Planning

The initial position of the frame was suitable in all cases and allowed an access path within the boundaries of the yet-to-be-created positioning jig. No repositioning of the frame was required. Due to the frame's symmetrical design, it was equally appropriate for left and right ears. The planning of a suitable access path with a diameter of 1.5 mm through the facial recess toward the round window of the cochlea was possible in all cases. Furthermore, the 0.3 mm margin to the FN and a margin to the EAC wall were possible to be executed. In case 01, the position of EAC did not allow a larger distance to the FN, whereas the distance to the CT was larger (0.86 mm). **Table 1** summarizes the planned distances.

TABLE 1 | Demographics, the width of the facial recess, distances from the planning, and results of the first six patients.

Patient	01	02	03	04	05	06
Age (years)	69	61	53	32	60	72
Sex	F	F	F	M	F	M
Side	L	L	L	L	R	R
1.5 mm sham drill bit passing?	Yes	Yes	Yes	Yes	Yes	Yes
1.8 mm sham drill bit passing?	Yes	Yes	No	Yes	No	No
EAC wall touched?	No*	No	No	No	No	No
Planned distance to EAC wall	0.6	0.7	1.9	1.8	0.9	1.3
Facial recess width (d_{FN} + d_{CT})	1.04+1.61	1.16+1.29	1.06+2.28	1.33+1.08	1.08+1.60	1.11+0.95
Planned margin to FN ($m_{FN}^{1.5}$)	0.29	0.41	0.31	0.58	0.33	0.36
Planned margin to CT ($m_{CT}^{1.5}$)	0.86	0.54	1.53	0.33	0.85	0.20
Deviation in jig	0.14	0.24	0.08	0.08	0.16	0.05
Bone thickness at screw	6.9	4.6	5.6	4.8	6.2	3.7

*The width of the facial recess is reported as two numbers: d_{FN} as the shortest effective distance from the central longitudinal axis of the planned path to the segmented facial nerve (FN) canal, and d_{CT} respectively for the chorda tympani (CT). The planned margins to these nerves are denoted as $m_{FN}^{1.5}$ and $m_{CT}^{1.5}$ for the 1.5 mm diameter sham drill bit. This description of the effective width of the facial recess allows computing the margins by subtracting the radius of the drill bit for the chosen position of the path, e.g., $m_{FN}^{1.5} = 1.04\ mm - (1.5\ mm/2) = 0.29\ mm$ for case 01. The planned distance to the external auditory canal (EAC) wall is measured from the border of the 3 mm diameter part of the planned path to the end of the bony wall. All numbers (except age) are given in mm. *Additional thinning out the EAC wall was required.*

3.3. Jig Manufacturing and Sterilization

The wireless transfer of the planning data to the manufacturing system was successful in all cases. In that machine, a blank jig was mounted onto hexapod parallel kinematics. The manufacturing process of the patient-specific positioning jig is fully automated, and, as anticipated, took 5 min for each patient. The positioning jig was disinfected, sterilized, packaged in a sterile barrier system, and transported to the operating theater. Due to the large sterilizers at the clinic, the whole process of manual disinfection (5 min), sterilization (65 min), packaging (1 min), and transport (14 min) took 85 min on average. The accuracy of the manufacturing process of the patient-specific through-hole is reported in **Table 1** as "Deviation in jig", meaning the deviations projected at the target point of the access path.

3.4. Sham Drill Bits

In all six cases, microscopic or endoscopic inspection verified that the sham drill bit successfully pointed through the posterior tympanotomy (**Figure 7**). While the 1.5 mm diameter of the sham drill bit could, in all cases, be passed freely through the conventionally-opened facial recess without any contact with bone, this was only possible in 3 of 6 cases for the 1.8 mm diameter of the sham drill bit. In the remaining 3 cases, the bony layer that was left above the FN was touched. In these cases, we visually assessed that the FN itself, running inside its bony canal, would most likely not have been mechanically damaged (refer to **Table 1**). The sham drill bit increases stepwise in diameter up to 3 mm. In all cases, it was possible to advance the sham drill bit without it touching the EAC wall. In case 01, however, additional thinning of the EAC wall with a diamond bur had to be performed.

3.5. Bone Thickness for Bone Screw

The screw is designed to reach 3.6 mm into the bone. As per the intraoperative CBCT scan, the bone thickness of the skull at the position of the bone screw was in mean 5.62 mm (range 3.7–6.9 mm), see last row of **Table 1**.

4. DISCUSSION

In this article, we presented the promising results of the first six patients in this trial. These preliminary results strongly suggest that achieving high accuracy trajectories for future minimally-invasive drilling through the facial recess with this system seems both feasible and reproducible. Answering the research hypothesis this way: Any error in a) the planned access path, b) the anatomical segmentations, c) the mini-stereotactic frame and its bone fixation, d) the X-ray marker and its localization algorithm, e) the jig manufacturing process, or f) the attachment of the positioning jig would have led to not pointing through the facial recess or to directly touching risk structures by using a 1.5 mm sham drill bit.

All involved surgeons gave especially positive feedback on the fixation with a single bone screw. This is likely because it further simplifies the handling and provides a reliable bone fixation throughout the procedure. The Screw Implantation Safety Index (SISI) for 4 mm bone screws, introduced by Talon et al. (20), shows that our chosen location for the bone screw falls within the area of high safety.

In the facial recess approach to cochlear implantation, experienced surgeons almost always leave a thin layer of bone above the FN and CT. Sometimes this thin layer is even carefully removed with a diamond bur and the nerves are exposed. These aspects (exposure and thickness of the thin layer) are difficult to plan preoperatively with CT or CBCT imaging because a) only the bony structures are visible and b) the nerve has a smaller diameter than the nerve canal it runs through. For this reason, we intraoperatively compared if a drill path of a certain diameter would fit through the facial recess. Surprisingly, an access path with a diameter of 1.8 mm, which is a number often used in

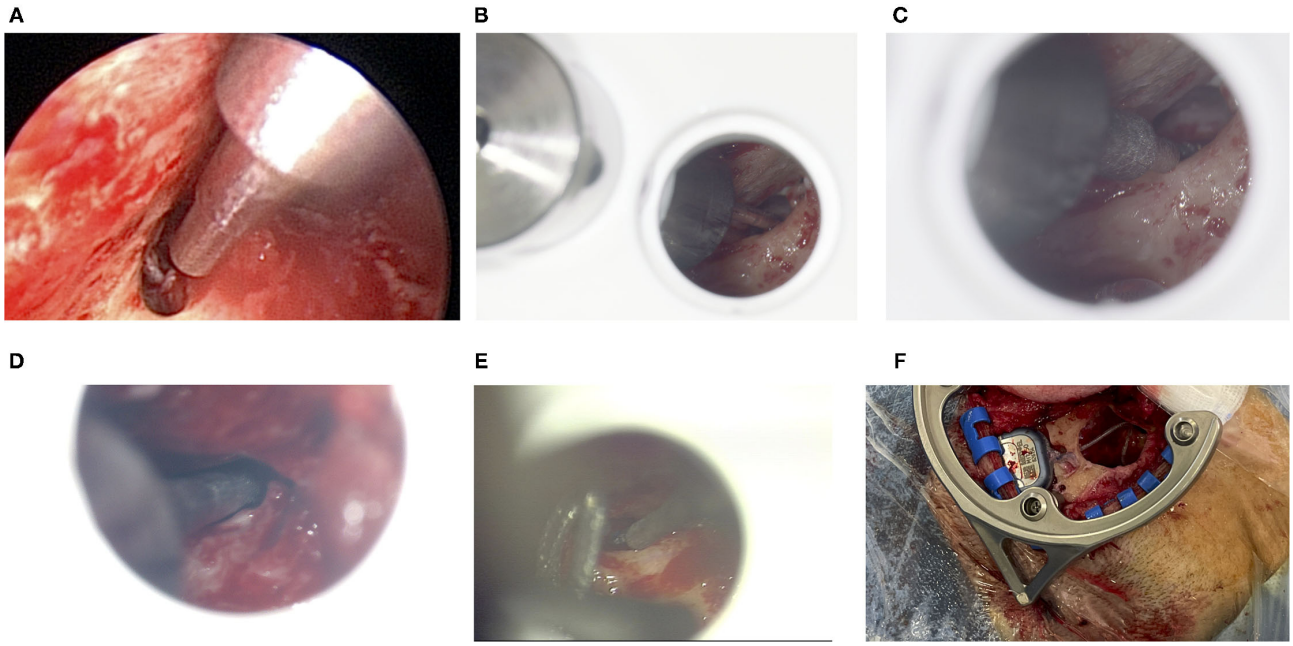

FIGURE 7 | (A) Endoscopic inspection after the facial recess has conventionally been exposed for cochlear implant (CI) surgery for patient 01. The 1.8 mm sham drill bit points through the open facial recess without collisions. The large diameter in the top right of this image is 3 mm, which - in this case - comes close to the thinned out EAC. **(B)** Microscopic view for patient 03. The 1.5 mm sham drill bit fits through, whereas **(C)** the 1.8 mm sham drill bit does touch the bony layer above the FN. **(D)** For patient 04, the 1.8 mm sham drill bit passes through. **(E)** For patient 05, only the 1.5 mm sham drill bit just passes through very tightly. **(F)** The geometry of the frame allows making the bony implant bed while the frame remains fixated.

the minimally-invasive CI literature (8, 21–23), could in three of six cases not passed through the facial recess along the access path, even if the distance to the CT would have allowed a larger diameter. One reason for this is that the EAC wall limits the planning options for the access path. A second reason is that the effective width of the facial recess in the direction of the access path is often smaller (due to the projection) than the maximum anatomical width. The latter is reported by Jain et al. (24) as "The average maximum width of the FR was 2.93 $\pm$ 0.4 mm (range 2.24 $-$ 3.45 mm) [...]" and by Bielamowicz et al. (25) as 2.61 $\pm$ 0.70 mm. The diameters of sham drill bits larger than 1.8 mm could in no case be used to pass through the facial recess, therefore, we omitted them from **Table 1**. However, all cases could have been completed using a sham drill bit with a diameter of 1.5 mm. This seems in line with recent study by Auinger et al. (26), who wrote that "up to two thirds of ears were eligible for robotic cochlear implant surgery with the standard drill bit size of 1.8 mm" and "drill bit sizes ranging from 1.0 to 1.7 mm in diameter could increase feasibility up to 100%." Labadie et al. (27) also used a smaller diameter of 1.59 mm to perform the drilling through the facial recess. Our trial, however, cannot make a statement about a possible deviation due to drilling into and through the mastoid bone because we only inserted sham drill bits. Future research, e.g., bench testing would benefit from providing this necessary evidence.

The minimally-invasive jig-based procedure described herein has the potential to reduce drilling and anesthesia time. By this, a completely new, practical, safe, and cost-effective alternative in CI care may be possible. Compared to other systems [i.e., Labadie et al. (13)], our aim was to use a stable fixation with only one single main central bone screw and to minimize the number of components that are assembled and attached to the patient. In our proposed system, the position and angular individualization are performed by drilling a through-hole in the corresponding angle into the blank jigs. We think this simplifies the surgical workflow and avoids use errors in the assembly. We propose an affordable alternative that is—compared to navigated, highly-specialized CI robotics—simpler but just as accurate.

The standardization of the operation, be it with the help of navigated robots or stereotactic frames, should allow CI implantation with greater accuracy and less variability in outcomes. CI recipients would likely benefit from the reduced trauma and a possibly shorter operation duration. This idea is becoming increasingly attractive in order to meet the rising need for "simpler" CI implantations in an aging population. In order to convince more CI candidates of the benefits of CIs use, the surgical procedure itself has to be made less invasive. A future application—where more evaluations will be required–could include difficult cases such as small or sclerotic mastoid or malposition of the FN.

DATA AVAILABILITY STATEMENT

The DICOM raw data cannot be made available due to data protection regulations. The other data presented in the study are included in the article, further inquiries can be directed to the corresponding authors.

ETHICS STATEMENT

The studies involving human participants were reviewed and approved by Ethics Committee of MHH. The patients/participants provided their written informed consent to participate in this study.

AUTHOR CONTRIBUTIONS

RS is the lead investigator responsible for the trial. RS and TL and a third surgeon from the team performed the surgeries. SJ wrote this manuscript. JS and MK supported the OR team in this trial and developed the hardware prototypes. FR supported in path planning and programming. MF revised the manuscript. All authors contributed to the article and approved the submitted version.

FUNDING

The presented study was funded in part by the Federal Ministry of Education and Research of Germany (BMBF, Grant Nos. 13GW0367A/B and 13GW0265A), and in part by European Union (EFRE) and by Lower Saxony (SER) ZW 3-85031593.

ACKNOWLEDGMENTS

We would like to express our thanks for the excellent support of Mr. Sören Brauer and his Team at MHH who helped with the sterilization concept and made the hand-in-hand collaboration beyond departments possible for this challenging on-demand sterilization. The same is true for the friendly and supportive OR staff of the ENT department at MHH. We would also like to express our gratitude toward Michael Todd (MED-EL) for helping improve the writing on a version of this manuscript.

REFERENCES

1. Wilson BS, Dorman MF. Cochlear implants: a remarkable past and a brilliant future. *Hear Res*. (2008) 242:3–21. doi: 10.1016/j.heares.2008.06.005
2. Lenarz T. Funktionsersatz des Innenohres. [Functional replacement of the inner ear]. In: *Medizintechnik Life Science Engineering*. Berlin; Heidelberg: Springer (2008).
3. Fouad YA. Advances in surgical and anesthetic techniques for cochlear implantation. In: Zanetti D, Berardino FD, editors. *Advances in Rehabilitation of Hearing Loss*. London: IntechOpen (2020).
4. Lenarz T. Cochlear implant - state of the ar t. In: *GMS Current Topics in Otorhinolaryngology - Head and Neck Surgery. German Society of Oto-Rhino-Laryngology*, Hannover: Head and Neck Surgery (2018).
5. Zahnert T. *S2k-Leitlinie: Cochlea-Implant Versorgung [S2k guidance: Cochlea implantation*]. (*AWMF-Register-Nr. 017/071)*. Dresden: Deutsche Gesellschaft für Hals-Nasen-Ohren-Heilkunde, Kopf- und Hals-Chirurgie e. V. (DGHNO-KHC) (2020).
6. Labadie RF, Chodhury P, Cetinkaya E, Balachandran R, Haynes DS, Fenlon MR, et al. Minimally invasive, image-guided, facial-recess approach to the middle ear: demonstration of the concept of percutaneous cochlear access in vitro. *Otol Neurotol*. (2005) 26:557–62. doi: 10.1097/01.mao.0000178117.61537.5b
7. Majdani O, Bartling S, Leinung M, Stöver T, Lenarz M, Dullin C, et al. A true minimally invasive approach for cochlear implantation: high accuracy in cranial base navigation through flat-panel-based volume computed tomography. *Otol Neurotol*. (2008) 29:120–3. doi: 10.1097/mao.0b013e318157f7d8
8. Caversaccio M, Gavaghan K, Wimmer W, Williamson T, Ansò J, Mantokoudis G, et al. Robotic cochlear implantation: surgical procedure and first clinical experience. *Acta otolaryngol*. (2017) 137:447–54. doi: 10.1080/00016489.2017.1278573
9. Schneider D, Stenin I, Ansó J, Hermann J, Mueller F, Pereira Bom Braga G, et al. Robotic cochlear implantation: feasibility of a multiport approach in an ex vivo model. *Eur Arch Otorhinolaryngol*. (2019) 276:1283–9. doi: 10.1007/s00405-019-05318-7
10. Schipper J, Aschendorff A, Arapakis I, Klenzner T, Teszler C, Ridder G, et al. Navigation as a quality management tool in cochlear implant surgery. *J Laryngol Otol*. (2004) 118:764–70. doi: 10.1258/0022215042450643
11. Rau TS, Timm ME, Kluge M, John S, Stieghorst J, Fröhlich M, et al. Preclinical evaluation of a micro-stereotactic surgical targeting system for minimally invasive cochlear implant surgery. In: *17th Annual Meeting of the German Society for Computer and Robot Assisted Surgery (CURAC)*. Leipzig: Thomas Neumuth and Andreas Melzer and Claire Chalopin (2018).
12. John S, Kluge M, Stieghorst J, Repp F, Fröhlich M, Lenarz T. A drill-tunnel approach for cochlear implantation: on site manufacturing of individual drilling jigs. In: *12th Asia Pacific Symposium on Ochlear Implants and Related Sciences*. Tokyo: Tatsuya Yamasoba (2019).
13. Labadie RF, Balachandran R, Mitchell JE, Noble JH, Majdani O, Haynes DS, et al. Clinical validation study of percutaneous cochlear access using patient-customized microstereotactic frames. *Otol Neurotol*. (2010) 31:94–9. doi: 10.1097/MAO.0b013e3181c2f81a
14. Van Rossum G, Drake FL. *Python 3 Reference Manual*. Scotts Valley, CA: CreateSpace (2009).
15. Fedorov A, Beichel R, Kalpathy-Cramer J, Finet J, Fillion-Robin JC, Pujol S, et al. 3D Slicer as an image computing platform for the quantitative imaging network. *Mag Reson Imaging*. (2012) 30:1323–41. doi: 10.1016/j.mri.2012.05.001
16. Harris CR, Millman KJ, van der Walt SJ, Gommers R, Virtanen P, Cournapeau D, et al. Array programming with NumPy. *Nature*. (2020) 585:357–62. doi: 10.1038/s41586-020-2649-2
17. Virtanen P, Gommers R, Oliphant TE, Haberland M, Reddy T, Cournapeau D, et al. SciPy 1.0: fundamental algorithms for scientific computing in python. *Nat Methods*. (2020) 17:261–72. doi: 10.1038/s41592-020-0772-5
18. Schroeder W, Martin K, Lorensen B. *The Visualization Toolkit. 4th* ed. Kitware (2006).
19. Hosten N, Liebig T. *CT of the Head and Spine*. (2002).
20. Talon E, Visini M, Wagner F, Caversaccio M, Wimmer W. Quantitative analysis of temporal bone density and thickness for robotic ear surgery. *Front Surg*. (2021) 8:443. doi: 10.3389/fsurg.2021.740008
21. Caversaccio M, Wimmer W, Anso J, Mantokoudis G, Gerber N, Rathgeb C, et al. Robotic middle ear access for cochlear implantation: first in man. *PLoS ONE*. (2019) 14:e0220543. doi: 10.1371/journal.pone.0220543
22. Wang J, Liu H, Ke J, Hu L, Zhang S, Yang B, et al. Image-guided cochlear access by non-invasive registration: a cadaveric feasibility study. *Sci Rep*. (2020) 10:1–13. doi: 10.1038/s41598-020-75530-7
23. Rau TS, Witte S, Uhlenbusch L, Kahrs LA, Lenarz T, Majdani O. Concept description and accuracy evaluation of a moldable surgical targeting system. *J Med Imaging*. (2021) 8:1–16. doi: 10.1117/1.JMI.8.1.015003
24. Jain S, Deshmukh P, Lakhotia P, Kalambe S, Chandravanshi D, Khatri M. Anatomical study of the facial recess with implications in round window visibility for cochlear implantation: personal observations and review of the literature. *Int Arch Otorhinolaryngol*. (2019) 23:281–91. doi: 10.1055/s-0038-1676100
25. Bielamowicz SA, Coker NJ, Jenkins HA, Igarashi M. Surgical dimensions of the facial recess in adults and children. *Arch Otolaryngol Head Neck Surg*. (1988) 114:534–7. doi: 10.1001/archotol.1988.01860170064020

26. Auinger AB, Dahm V, Liepins R, Riss D, Baumgartner WD, Arnoldner C. Robotic cochlear implant surgery: imaging-based evaluation of feasibility in clinical routine. *Front Surge*. (2021) 8:423. doi: 10.3389/fsurg.2021.742219
27. Labadie RF, Balachandran R, Noble JH, Blachon GS, Mitchell JE, Reda FA, et al. Minimally invasive image-guided cochlear implantation surgery: first report of clinical implementation. *Laryngoscope*. (2014) 124:1915–22. doi: 10.1002/lary.24520

Conflict of Interest: SJ, MK, and TL declare being limited partners of *HörSys IP GmbH* & *Co. KG* holds a financial stake in OtoJig GmbH, which is a German company that owns and further develops the described technology. SJ, FR, MK, and JS are employed by OtoJig GmbH. MF is employed at MED-EL, which holds a financial stake in OtoJig GmbH.

The remaining author declares that the research was conducted in the absence of any commercial or financial relationships that could be construed as a potential conflict of interest.

Publisher's Note: All claims expressed in this article are solely those of the authors and do not necessarily represent those of their affiliated organizations, or those of the publisher, the editors and the reviewers. Any product that may be evaluated in this article, or claim that may be made by its manufacturer, is not guaranteed or endorsed by the publisher.

Advantages of publishing in Frontiers

OPEN ACCESS
Articles are free to read for greatest visibility and readership

FAST PUBLICATION
Around 90 days from submission to decision

HIGH QUALITY PEER-REVIEW
Rigorous, collaborative, and constructive peer-review

TRANSPARENT PEER-REVIEW
Editors and reviewers acknowledged by name on published articles

Frontiers
Avenue du Tribunal-Fédéral 34
1005 Lausanne | Switzerland

Visit us: www.frontiersin.org
Contact us: frontiersin.org/about/contact

REPRODUCIBILITY OF RESEARCH
Support open data and methods to enhance research reproducibility

DIGITAL PUBLISHING
Articles designed for optimal readership across devices

FOLLOW US
@frontiersin

IMPACT METRICS
Advanced article metrics track visibility across digital media

EXTENSIVE PROMOTION
Marketing and promotion of impactful research

LOOP RESEARCH NETWORK
Our network increases your article's readership